UNIVERSITY OF LIVERPOOL

Synthesis and applications of high-sulfur polymers

Bowen Zhang, BSc, MSc

March 2022

Dr Tom Hasell

Dr Tom McDonald

Thesis submitted in accordance with the requirements of the University of Liverpool for the degree of Doctor of Philosophy

Abstract

Elemental sulfur has many applications for both commodity and specialty chemicals. However, because sulfur is a by-product of the petrochemicals industry, its supply greatly outweighs demand, causing a current global issue- the “excess sulfur problem”. Polymeric material made from pure elemental sulfur is not stable, and readily to depolymerizes to more thermodynamically stabled S_8. The recent discovery of inverse vulcanization, capping radical chain end of polymeric sulfur by dienes, allows polymeric materials with high sulfur contents (up to 90 wt.%) to be produced. High sulfur content polymers are promising materials, with potential applications in LiS batteries, IR transparent lenses and capture of heavy metals.

However, there are still several challenges of inverse vulcanisation in processing, applications and researches. In this thesis, A ternary co-polymer system of inverse vulcanisation was explored initially, which provided a potential approach for practical production. The application of inverse vulcanised polymer in mercury uptake was also discussed. Additionally, catalyst was studied in inverse vulcanisation to decrease reaction temperature, which could effectively prevent auto-acceleration. At last, thiopolymers were reacted as precursors to prepare sulfur-doped carbons and magnetic sulfur-doped carbons, showing their potential to be applied in water purification and environmental remediation.

Acknowledgments

I would like to gratefully acknowledge a large number of people who supported and accompanied with me in last four years during my PhD programme. These four years were so complex, which was full of happiness and toughness. Especially, after 2020, when pandemic, COVID-19, spread around the whole world, we had to overcome all obstacles to keep our life moving. More than 5 million people dead because of this pandemic, but far more people were survived from their own braveness and other's help. The world changes, the time flies, and both never stop, however love and encourage between people make this planet warm. Thus, I appreciated all people who loved and backed me and even who competed with me, all making me step forward.

First, I owed much gratitude to my parents, Mr. Yiqiang ZHANG, and Mrs Cuiyun SUN. Thanks for your constant supporting. It was you made all your effort to send me to this country, so, without you, I can never imagine all the achievement I completed would happen. Please forgive me that I was not able to go back China to hug you both in last two years, however, like what I said before, we should look forward and I believe we will reunite soon. To my grandparents, you all grew me up and took care of me from I was a baby. This thesis is for all of you, especially for one of my grandpas, who left me forever in last year. Please forgive me that I cannot go back home and stay with you at that tough time.

Secondly, I would like to thank my supervisor and friend, Dr. Tom Hasell, who helped me not just in academic aspect. Four years ago, when I was applying PhD position all around the world desperately, it was you throw a lifebuoy to me and saved me. I still remember the first day I started off my project, I told you I really wanted to publish a paper, and you encourage me a lot, giving me confidence. Yes, I am a guy who is lack of confidence, but it is you changed that. I think making this change is the charming of being a supervisor. In these four year, I published my first academic paper, completed my first oral presentation, attended my first entrepreneur competition, and applied my first funding. Each step of those was full of helps from you. Thank you, Tom.

Thirdly, I have to thank my fiancée, Dai Luan. Thanks for your love and patience. We met in England, a country 8000 kilometres from China. Except destiny, I cannot find

another reason to explain this love. In this country, as immigrant, we faced too many tough problems, but finally, we overcame all of them and we won. More than 6 years, we learned together, grew up together and we loved each other. I missed every city we visited together, from Aisa to Europe, I enjoyed every concert we went, from pop to classical, and I made effort to cook ever meal for you as well, from oriental to western. I think this is the life. Do not know if the rest of my life is enough to love you.

To Dr. Sam Petcher, my best friend in England. We started our PhD programme together, however, we were more like brother than colleagues. You submitted your thesis earlier, so you won this time. Before met you, I could not imagine I could have a Briton friend who can be so important in my life. How many cities we visited together? how many days and nights we stayed together? How much alcohol we had together? How many noodles we ate together? Thanks mate! We have a big future together!

To Hasell group, Peiyao, Doug, Jess, George, Liam, Haoran, Diana, Romy, Joe, Veronica, and Xi, thanks for your help, advice and laugh in my life. To people from the Department of Chemistry, Dr. Tom MacDonald, my second supervisor, thank you for your advice in my project and useful discussion in my PhD programme. To my best Chinese 'gang', Dr. Li Qie, Dr. Hui Gao, and Dr. Dingyue Hu, thank you guys for all supports provided in academic and in my personal life. Many thanks to Stephen Moss for ICP-OES service, Glyn Connolly for ICP-MS analysis Hongjun Niu for magnetic measurements, Wei Zhao for PXRD measurements, Owen Gallagher and Keith Arnold for TEM, Dr. Samantha Chong, and Dr. Lucy Clark for useful discussions.

At last, I must give a thanks to people who gave me a hand in my last year on the way of entrepreneurship. It is you made my PhD programme perfect. To Dr. Ming Liu, it is safe to say you are one of the best advisors in my PhD programme, introducing a different way in my future life. To Dr. Gareth Crapper and Dr. Andrew Spencer, thank you for the days we worked together to achieve those amazing results. We are the best team!

Thanks to all my relatives and friends both in England, in China and all around the world.

List of Contents

Publications

The worked presented in this thesis has contributed to the following publications:

(1) **Zhang, B**.; Petcher, S.; Gao, H.; Yan, P.; Cai, D.; Fleming, G.; Parker, D. J.; Chong, S. Y.; Hasell, T. Magnetic Sulfur-Doped Carbons for Mercury Adsorption. *J. Colloid Interface Sci.* **2021**, *603*, 728–737.

(2) **Zhang, B**.; Dodd, L. J.; Yan, P.; Hasell, T. Mercury Capture with an Inverse Vulcanized Polymer Formed from Garlic Oil, a Bioderived Comonomer. *React. Funct. Polym.* **2021**, *161* (February), 104865.

(3) **Zhang, B**.; Gao, H.; Yan, P.; Petcher, S.; Hasell, T. Inverse Vulcanization below the Melting Point of Sulfur. *Mater. Chem. Front.* **2020**, *4* (2), 669–675.

(4) **Zhang, B**.; Petcher, S.; Hasell, T. A Ternary System for Delayed Curing Inverse Vulcanisation. *Chem. Commun.* **2019**, *55* (72), 10681–10684.

Other work during PhD programme had been prublished in the following publications:

(1) Mann, M.; **Zhang, B**.; Tonkin, S. J.; Gibson, C. T.; Jia, Z.; Hasell, T.; Chalker, J. M. Processes for Coating Surfaces with a Copolymer Made from Sulfur and Dicyclopentadiene. *Polym. Chem.* **2021**.

(2) Petcher, S.; **Zhang, B**.; Hasell, T. Mesoporous Knitted Inverse Vulcanised Polymers. *Chem. Commun.* **2021**, *57* (41), 5059–5062.

(3) Lu, Z.; **Zhang, B**.; Gong, H.; Li, J. Fabrication of Hierarchical Porous Poly (L-Lactide) (PLLA) Fibrous Membrane by Electrospinning. *Polymer.* **2021**, *226* (March), 123797.

(4) Yan, P.; Zhao, W.; **Zhang, B**.; Jiang, L.; Petcher, S.; Smith, J. A.; Parker, D. J.; Cooper, A. I.; Lei, J.; Hasell, T. Inverse Vulcanized Polymers with Shape Memory, Enhanced Mechanical Properties, and Vitrimer Behavior. *Angew. Chemie - Int. Ed.* **2020**, *59* (32), 13371–13378.

(5) Song, J.$^{\perp}$; **Zhang, B**.$^{\perp}$; Lu, Z.; Xin, Z.; Liu, T.; Wei, W.; Zia, Q.; Pan, K.; Gong,

R. H.; Bian, L.; Li, Y.; Li, J. Hierarchical Porous Poly(L -Lactic Acid) Nanofibrous Membrane for Ultrafine Particulate Aerosol Filtration. *ACS Appl. Mater. Interfaces* **2019**, *11* (49), 46261–46268.

(6) Smith, J. A.; Green, S. J.; Petcher, S.; Parker, D. J.; **Zhang, B**.; Worthington, M. J. H.; Wu, X.; Kelly, C. A.; Baker, T.; Gibson, C. T.; Campbell, J. A.; Lewis, D. A.; Jenkins, M. J.; Willcock, H.; Chalker, J. M.; Hasell, T. Crosslinker Copolymerization for Property Control in Inverse Vulcanization. *Chem. - A Eur. J.* **2019**, 10433–10440.

(7) Wu, X.; Smith, J. A.; Petcher, S.; **Zhang, B**.; Parker, D. J.; Griffin, J. M.; Hasell, T. Catalytic Inverse Vulcanization. *Nat. Commun.* **2019**, *10* (1), 647.

Abbreviation

ASGM	Small-Scale Gold Mining
ATR	Attenuated Total Reflection
BET	Brunauer, Emmett And Teller
CDE	1,4-Cyclohexanedimethanol Divinyl Ether
CEA	2-Carboxyethyl Acrylate
COFs	Covalent Organic Frameworks
DADS	Diallyl Disulfide
DAS	Diallyl Sulfide
DATS	Diallyl Trisulfide
DCP	Dynamic Covalent Polymerization
DCPD	Dicyclopentadiene
DGP	Dried Garlic Powder
DIB	1,3-Diisopropenylbenzene
DSC	Differential Scanning Calorimetry
DVB	Divinylbenzene
EA	Elemental Analysis
EDX	Energy-Dispersive X-Ray Analysis
EGDA	Ethylene Glycol Diacetate
EGDMA	Ethylene Glycol Dimethacrylate
ENB	Ethylidene Norbornene
FTIR	Fourier Transform Infrared
GBDA	Glyoxal Bis(Diallyl Acetal)

GEO	Garlic Essential Oil
GOB	Garlic Oil Blend
GPC	Gel Permeation Chromatography
HSAB	Hard-Soft-Acid- Base
ICP	Inductively Coupled Plasma
IR	Infrared
MDI	Diphenyl-Methane 4, 4'-Diisocyanate
MMA	Methyl Methacrylate
MOFs	Metal-Organic Frameworks
MS	Mass Spectrometry
MSCs	Magnetic Sulfur-Doped Carbons
NaDTC	Sodium Diethyldithiocarbamate Trihydrate
NL-DFT	Non-Local Density Functional Theory
NMI	N-Methylimidazole
NMR	Nuclear Magnetic Resonance
OES	Optical Emission Spectrometry
ORMOCHALC	Organically Modified Chalcogenide
ORR	Oxygen Reduction Reaction
PIMs	Polymers of Intrinsic Microporosities
PMMA	Poly(Methyl Methacrylate)
PTTB	Poly(1,3,5-Tris(Thienyl)Benzene)
PXRD	Powder X-Ray Diffraction
RI	Refractive Index
ROP	Ring-Opening Polymerization
$scCO_2$	Supercritical Carbon Dioxide

SEM	Scanning Electron Microscopy
STP	Standard Temperature and Pressure
TABQ	Tetra(Allyloxy)-1,4- Benzoquinone
TEM	Transmission Electron Microscopy
$\boldsymbol{T_g}$	Glass Transition Temperatures
TGA	Thermal Gravitational Analysis
TLC	Thin Layer Chromatography
TVTCSi	1,3,5,7-Tetravinyltetramethylcyclotetrasiloxane
4VA	4-Vinylaniline

Chapter 1. Introduction

1.1 Overview

Sulfur, mostly as sulfide in minerals, is one of the most common elements in the Earth's crust. The record of using it could go back more than thousand years. In modern days, elemental sulfur is an abundant by-product of the petrochemical industry from hydrodesulfurization process to decrease the emission of SO_2 and prevent acid rain. Annually, more than 70 million tonnes elemental sulfur were produced, the majority of which were stockpiled at refining sites as industrial waste. Elemental sulfur is not toxic, but opened to the environment, it poses high risk because of flammability. Although sulfur was widely used in both commodity and specialty chemicals, such as sulfuric acid, fertilisers and rubbers, the supply of it greatly outweighed demand. Therefore, large deposits of sulfur caused a current global issue- the "excess sulfur problem". However, this situation is a two-edged sword, providing advantages, such as extremely low cost. Thus, it will be worthy to find an approach to use sulfur as a reactant in a large-scale application.

One ideal strategy is synthesising polymeric sulfur through ring-opening polymerization (ROP) of neat elemental sulfur in high tempature (above 159 °C). However, this long chain structure is not chemically stable at room temperature because of back-biting mechanism. **Inverse vulcanisation** was first coined by Pyun and co-authors in 2013 to stabilize high content sulfur materials through reactions with dienes. Inspired by this conception, different polysulfides were synthesised by different researches and applied into different areas. As a derivative of inverse vulcanisation, high content sulfur-doped carbon was produced from pyrolysis of polysulfide. Because of high affinity to heavy metals, such as mercury and gold, it was attracted increasingly attention in environmental science as well as its precursor.

Unlike most porous materials, such as metal-organic frameworks (MOFs), covalent organic frameworks (COFs), and polymers of intrinsic microporosities (PIMs), porous carbonaceous materials are much cheaper and scalable, providing an advantage to be used in multiple applications. Heteroatom doping activated carbons are used in catalysis, gas storage, gas separation, and heavy metal remediation due to its porous structure, good stability, and electron deficiency. **Sulfur-doped activated carbons** were not deeply studied compared with other elemental atom doping, such as nitrogen, hydrogen, and oxygen, because of complex synthesis process and sulfur content

limitation of carbonisation precursor. Therefore, inversed vulcanised polymer could be an appropriate precursor for sulfur-doped carbons.

Inverse vulcanised polymers and their derivatives were studied in the **heavy metal remediation.** Heavy metal pollution is a global health issue, especially in lower income and developing countries. Mercury is the third of top 10 chemicals of major public concern reviewed by the World Health Organization (WHO).[1] Mercury releases mainly from coal combustion and artisanal and small-scale gold mining (ASGM). Exposure to Hg presents a serious threat to human health, especially to the children, such as irreversible mental and nervous system damage. Thus, efficient, large scaled and low-cost materials are desperately desired for prevention or remediation of mercury pollutions. Due to high affinity of sulfur bonds and high cost efficiency, polysulfides and sulfur-doped carbon show their promising in environmental applications.

Inverse vulcanisation attracts more interest because of its versatile applications. In this introductory chapter, basic background of both inverse vulcanisation and its applications are aimed to explain and review to cover the main projects in this thesis. More specific introductions will be expanded in details in the separate projects.

1.2 Elemental sulfur

Historically called ‘brimstone’, sulfur has been recognized for thousand years. From very early use in medicine and explosives to modern industrial application in sulfuric acid (H_2SO_4) and rubber production, sulfur and sulfur content materials played important role in human activities. Interestingly, after short term of large demand in mid-19th century, unlike other raw material, sulfur has no more shortage. There are two main reasons leading to this special phenomenon. One reason is far more sulfur than consumption was produced as by-product from petrochemical industries. Another reason is that there is no industrial scale production utilising a high percentage of sulfur as reagent because of the relative complexity of sulfur’s chemical properties and the instability of polysulfides. Therefore, unfortunately, this ancient element becomes a global environmental problem in 21st century. However, the study and research about elemental sulfur never stops because of its wide availability and incredibly low price.

1.2.1 Demand and supply

Commonly, sulfur could be found in the form of sulfides or sulfate minerals in nature.[2,3] Until late 19th century, most industrial sulfur was produced from the volcanic soil of Sicily.[2] In order to satisfy increased demand for sulfur, Frasch process was devised, producing larger scale elemental sulfur with lower cost. From this time, Frasch process was widely applied and conventional sulfur mining industry developed. However, interestingly, sulfur mining industry has become almost extinct recently.

Like Sicilian method replaced by the new technology, Frasch process would not dominate sulfur production forever. In late 20th century, immense amount of sulfur was recovered from fossil fuels via Claus process. With increasing consideration of environment and human health, sulfur must be removed from hydrocarbons to avoid harmful gas emission, which could result in acid rain. Additionally, from industrial perspective, sulfur also needs to be removed, because sulfur compounds probably poison catalytic converters in downstream chemical processes. Sulfur content varies from less than 0.1% to greater than 7% in crude oil, and approximately from 1% to 5% in coal.[4] Different sulfur compounds are separated from hydrocarbons into H_2S through scrubbing step and hydrodesulfurization, followed by Claus process, from which gaseous sulfur compounds are converted to elemental sulfur. Typically, Claus process is divided into two steps as shown in Equation 1-1and Equation 1-2.

$$2H_2S + 3O_2 \rightarrow 2SO_2 + 2H_2O \qquad \textbf{Equation 1-1}$$

$$4H_2S + 2SO_2 \rightarrow \frac{3}{2}S + 4H_2O \qquad \textbf{Equation 1-2}$$

From this time, elemental sulfur has become by-product of petrochemical industry. Although increasing renewable energy has been applied to mitigate climate change, fossil fuels are still the most important energy supply, providing 80% of global primary energy.[5] Furthermore, the use of fossil fuels was predicted to increase despite more emission regulations implemented. Consequently, more and more sulfur is produced and the amount of this waste from petroleum refining has much exceeded that of conventional sulfur mining industry. It is estimated that more than 70 million tonnes sulfur is produced annually from petroleum industry. More importantly, the trending of excess sulfur will not stop but intensify because of two main reasons. The first reason is more stringent regulation to the sulfur emission of commercial fuels. Another reason is increasing high sulfur-content feed-stocks are exploited, such as tar sands and heavy oils, because traditional energy source is becoming rare. Therefore, more sulfur will be separated from per unit recovered energy source, and the "excess sulfur problem" will be worsened.[6]

Unwanted elemental sulfur powder is always stockpiled as blocks next to the refining plant to avoid flow problem. Megatons of sulfur openly stored on the ground has limited health threat to human beings but potential security problem, because elemental sulfur is flammable, implied by its ancient name. When enormous amounts of sulfur set on fire, missive SO_2 would be emitted, being harmful to human and environment, for example the sulfur fire in Iraqi in 2003.[7] Therefore, how to utilize this redundant chemical has become a global concern.

More than 80% of sulfur is consumed as H_2SO_4, and most of which is used as fertiliser or other agrochemicals.[8,9] H_2SO_4 is also used as a solvent, a dehydrating agent, a reagent, and an acid in different applications, such as petroleum refining, copper ore leaching, and paper mills.[9] However, all this demand are much less than sulfur produced annually. And also because of limited storage capabilities of sulfur producers, the price of sulfur declined again and again. For example, the price of sulfur in Tampa, Florida, fell to $10s per ton in 2001 from more than $100 per ton in 1990s. Although it recovered to $600 per ton, but because of deduction in phosphate fertilizer output, the sulfur price collapse to an incredible $0 per ton in 2009.[9]

In summary, the production of sulfur in the world significantly outweighs its consumption. Annually, more than million tons of unwanted sulfur is produced and stockpiled openly. Traditional process or application cannot consume sulfur in large scale. Therefore, how to utilize redundant sulfur become an imperative issue to address.

1.2.2 Sulfur properties

Sulfur has been known since ancient time, and the research of it has never stopped. However, it is difficult to fully understand either physical or chemical properties of elemental sulfur, because of its numerous allotropes and complex intramolecular and intermolecular allotropic conversion.

Native sulfur occurs as sulfide or sulfate minerals, such as pyrite (FeS_2), known as fool's gold, galena (PbS), cinnabar (HgS), sphalerite (ZnS), and gypsum ($CaSO_4 \cdot 2H_2O$). Elemental sulfur could be found in nature close to the hot spring and volcanic areas. Although there are more than 30 kinds of solid allotropes reported, only two of them are thermodynamically stable.[10] Orthorhombic (α) sulfur and monoclinic (β) sulfur are both consisting of cyclo-S_8 molecules, but stable at different conditions. At standard temperature and pressure (STP), α-S_8 is the only stable form and molecules crystalized in orthorhombic. When temperature increases to higher than 96 °C but lower than 119 °C, boiling point of β-S_8, monoclinic sulfur, needle-like crystals, becomes thermodynamically stable form.[11] However, the transformation from α-S_8 to β-S_8 in single crystal is not kinetically favoured, whereas β-S_8 could be crystalized from molten sulfur or its organic solution.[10,11] Another confirmed monoclinic crystals of cyclo-S_8 is γ-S_8, which is meta-stable and quickly transform to α-S_8.[10–12] α-S_8, β-S_8, and γ-S_8 are well characterized cyclo-S_8 allotropes, while other reported forms are weak characterized or doubtable, most of which are normally the mixtures of well-known forms.

Table 1.

Form	Appearance	Colour	Stable temperature / °C	Density / mg m^{-3}
Orthorhombic (α)	Rhombus	bright yellow	< 96	2.069
Monoclinic (β)	Needles	yellow	>96, <119	1.940
Monoclinic (γ)	Needles	light-yellow	/	2.190

The geometry of α-S_8, β-S_8, and γ-S_8 is similar, which is a puckered ring configuration of eight sulfur atoms (as shown in Figure 1.1). However, the bond lengths and bond angles of these allotropes are different because of crystal structure. Different forms also result in dissimilar physical properties, which are listed in Table 1. Melting point of S_8 is very complex, because of not only different allotropes but also tested form, such as single crystal and microcrystal, and other factors, like heating rates. Melting points of single crystal of α-S_8 and β-S_8 are 112.80 °C and 119.60 °C, respectively.[11] Microcrystals of α-S_8 and β-S_8 have slightly higher melting points, which are 115.11 °C and 120.40 °C, correspondingly.[2]

Although cyclo-S_8 is the most stable and studied molecular form at STP, other crystalline phases consisting of cyclic molecules have been reported, such as S_6, S_7, S_8, S_9, S_{10}, S_{11}, S_{12}, S_{13}, S_{14}, S_{15}, S_{18}, and S_{20}.[10] In liquid sulfur, more species, like S_2, S_3, S_4, and S_5, are observed. Additionally, because of polymerization, longer sulfur chains (S_n, n>20) can be extracted.[2,3,10] The dissimilar properties of different allotropes also determine that the properties of sulfur is highly content-dependent, namely influenced by presence and concentration of each allotrope. More details of polymeric sulfur would be later explained in "polysulfide" section.

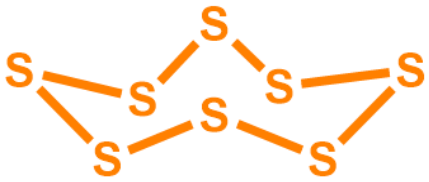

Figure 1.1. Structure of a S_8 molecule.

1.2.3 Polysulfide

1.2.3.1 Polymeric sulfur

Polymeric sulfur are referred as those forms of element sulfur consisting of long chains or large rings (n > 50). The polymerisation at 159 °C is observed as discontinuity occurred in the properties of liquid sulfur, such as density, heat capacity, dielectric constant, and, especially, viscosity.[2,13] Polymerisation of sulfur is an equilibrium reaction between small cyclic monomer molecules and long chains molecules. However, the equilibrium is not conducted only above 159 °C but also over all the temperature range. Therefore, polymeric sulfur also exists at low temperature but minority, and 159 °C is not the specific temperature that polymeric sulfur generated but more additional polymers formed.[13] The polymer content in the melt sulfur could increase up to 45% at 250–300 °C from 1% at 135°C.[10] Sulfur polymerisation starts from the sulfur ring opening by homolytic cleavage, resulting in formation of diradical ending sulfur chains, as shown in Scheme 1.1. After that, diradical chains propagate to liner chains, a reaction considered heating-rate dependent. However, polymeric sulfur is not chemical stable and favoured back to monomeric sulfur, because of backbiting. Therefore, even though polymeric sulfur could be extracted by quenching equilibrium polymerization of sulfur with CS_2, the amorphous structure rapidly converts into crystals, which are mainly S_8.

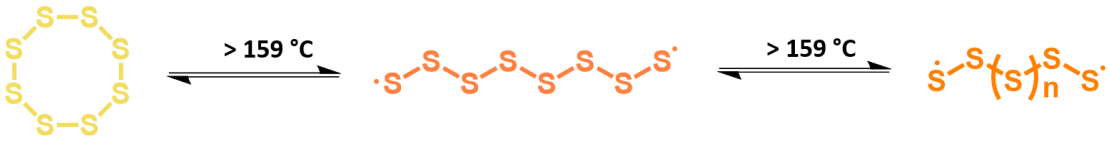

Scheme 1.1 Ring-openging reaction of elemental sulfur at high temperature, generating sulfur biridicals and the polymerisation of liner sulfur.

1.2.3.2 Polysulfides

Polysulfides were referred to the compounds of the type X-S_n-X with n > 2, including inorganic ionic compounds, such as Na_2S_4, and sulfur-rich organic compounds with repeating S-S bonds.[14–16] It was clarified by Steudel, in 2002, that polysulfides should be applied to describe ionic compounds, while polysulfanes, instead, are recommended by the IUPAC to term organic polysulfides, including polysulfide polymer, which consisting of backbones with repeating S-S units and hydrocarbons (R-S_n-R, n > 2).[14]

In recent literatures, polysulfides,[15] sulfur-containing polymers,[16] and thiopolymers[17] are referred more frequently to polysulfides polymers, however, there is no significant difference among these terms, therefore, it will not be distinguished these terms in this thesis. Unlike polymeric sulfur, polysulfides are more thermally and chemically stable, because the sulfur chains were terminated by organic substituents, improving stability. Polysulfides can be synthesized directly from S_8 through condensation, free-radical and ionic copolymerization. In terms of condensation reaction, polysulfide could be synthesized via the reaction of inorganic polysulfides, such as Na_2S_x, and halides, such as Cl-R-Cl,[18] as illustrated in Scheme 1.2. Sulfur content of polysulfide polymers through this processing was tuneable by adjusting the sulfur rank in inorganic polysulfides, which could be controlled by the amount of elemental sulfur, as shown in Scheme 1.2. These polysulfide polymers are also known as a trademarked name,

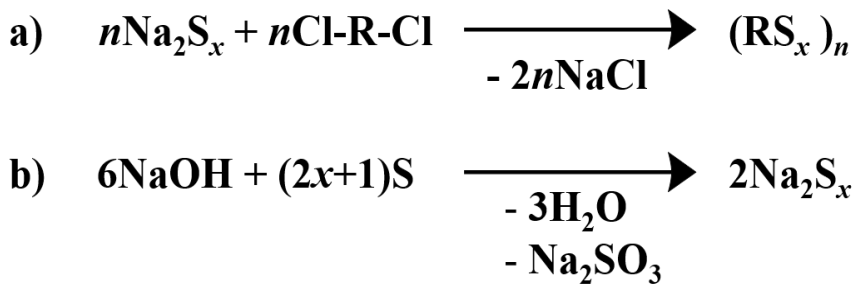

Scheme 1.2 Mechanism of condensation reaction generating polysulfide by inorganic polysulfides, prepared by elemental sulfur and alkali.

Thiokol, widely applied as adhesives and sealants.[3,15] Free-radical copolymerisation was another route investigated to generate high sulfur content polymers. Sulfur and unsaturated organic molecules were attempted to react by both solution-based and bulk copolymerisation. However, in solution based free-radical copolymerisation, synthesized polysulfides were characterised as polymers with low molecular weight. One proposed explanation for this issue was elemental sulfur act as an inhibitor, because of high rate chain transfer processes.[19] Bulk copolymerisation of sulfur and olefin was explored to circumvent low molecular weight problem, benefiting from increased reactivity ratio of monomers. One respective example of bulk copolymerisation reaction is the interaction of melt sulfur with dicyclopentadiene (DCPD) at 140 °C,[20,21] which is categorized as low temperature (up to about 140 °C) by Bateman.[22] In this condition, norbornene unsaturation in DCPD is more reactive than cyclopentene unsaturation, as norbornene unsaturation could be reacted

completely from the early stage, indicated by the vinyl peaks disappeared in nuclear magnetic resonance spectroscopy (NMR).[21] Additionally, the broadening of the peaks in NMR spectroscopy, the formation of viscous reaction system, and relatively high molecular weight (M_n > 3000) of product characterised by GPC indicated that sulfur contained polymer generated.[20,21] However, at low reaction temperature, liner polymers were more likely to be synthesized, resulting from low reactivity of cyclopentene unsaturation (Scheme 1.3). When reaction temperature was increased to 150 °C, crosslinked sulfur polymer generated, however, meanwhile generation of H_2S and depolymerisation could be observed, which became historically complex, hindering further study. However, recent study of this reaction but at higher temperature and with high ratio of S/DCPD, the process known as inverse vulcanisation, found fully crosslinked sulfur polymer synthesized and the product was chemically and thermally stable, due to complete reaction of both cyclopentene unsaturation and norbornene unsaturation, although H_2S could be still detected during the reaction.[17,23] Small sulfur-containing molecules, generated as by-products from free-radical copolymerisation between sulfur and olefins, could react with elemental sulfur under anionic conditions, which is categorized as ionically generated copolymerisation. This route provided foundation for catalytic inverse vulcanisation

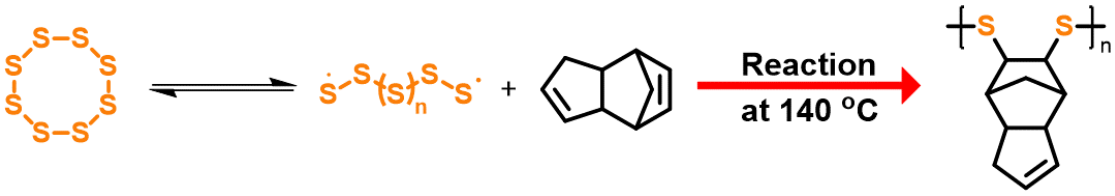

Scheme 1.3 Mechanism of copolymerisation of elemental sulfur and DCDP at low temperature to generate liner polymers.

process.

1.3 Inverse vulcanisation

High sulfur content polymers were attempted to synthesize from different strategies as mentioned from previous section, however, there is very few literature producing a stable sulfur content polymer by elemental sulfur directly before the report of inverse vulcanisation.[24] Recently, inverse vulcanization attracted significant research attention because of its facile reaction processing and high atom efficiency.[24–26] In the inverse vulcanization process, the radical ends of sulfur chains are capped by reaction with carbon = carbon double bonds. If an organic molecule contains two or more carbon = carbon double bonds, it can act as a crosslinker to sulfur biradicals to generate crosslinked high sulfur content polymers. With an appropriate ratio of sulfur and crosslinker, the degradation of polysulfides is effectively avoided and a stable, high weight percentage sulfur polymer, or inverse vulcanized polymer, is formed.

1.3.1 Conventional vulcanisation

Vulcanisation is a process of hardening natural rubber or synthetic rubbers with crosslinkers, such as, the most commonly used, sulfur. Natural rubber naturally occurs form of *cis*-1, 4- polyisoprene, refined from natural rubber latex, as shown in Figure 1.2 (a), which is a sticky and milky colloid derived from rubber trees or other plants. In order to prevent permanent deformation and to introduce elastomeric property of natural rubber (Figure 1.2 (b)), sulfur vulcanisation (Figure 1.2 (c)) was first applied to crosslink liner polymer chains by reacting with the unsaturated carbons In sulfur vulcanisation, normally, 0.5-5 parts elemental sulfur was added in hundred part of rubber under heating (~120 °C) during the shaping process.[27] After vulcanisation, molecular chain entanglements (Figure 1.2 (d)) were crosslinked into network (Figure 1.2(e)), which can reduce permanent deformation after removing force.[28] Additionally, solubility of polymers changed significantly after vulcanisation from soluble in specific solvent into non-soluble in any solvent but swelling only because of crosslinks.[27] In industry, not only sulfur but also activators and accelerators were involved in vulcanisation processing to increase the rate of the reaction. Activators were applied to break the sulfur ring and accelerators were like catalysts to form thiyl and polysulfenyl radicals during the reaction.[28]

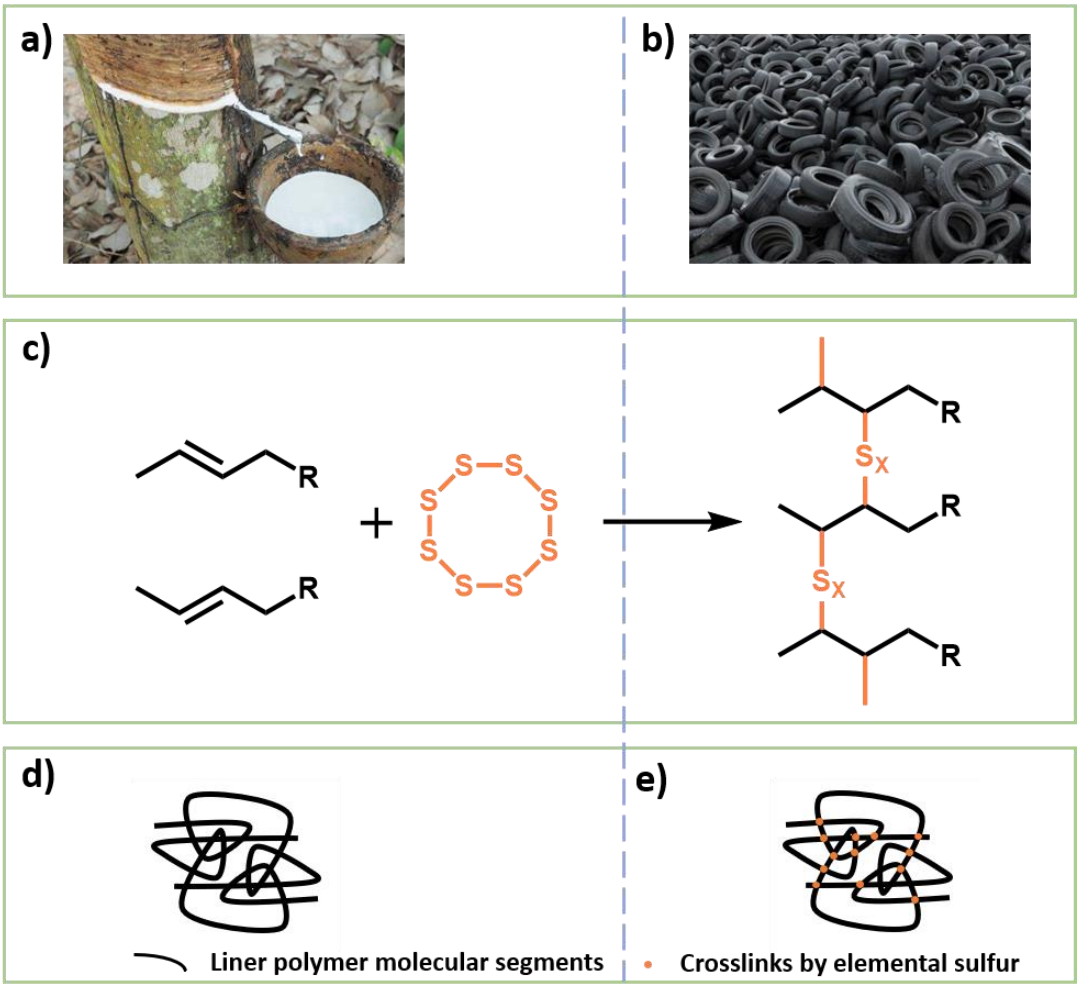

Figure 1.2 Processing of conventional vulcanisation. (a) Latex is collected from a rubber tree, a process called "tapping". (b) Tyres made by rubbers, including both natural rubber and synthetic rubber, benefitting from high elastomeric property of network structure to keep strong mechanical properties against temperature and loads. (c) Conventional vulcanisation with sulfur, generating crosslinked polymer structure. (d) Schematic diagram of the liner polymer molecules in an entanglement, before vulcanisation. (e) Schematic diagram of the network polymer structure, crosslinked by elemental sulfur.

1.3.2 Inverse vulcanisation

By contrast to the conventional vulcanisation, inverse vulcanisation crosslinks sulfur chains by small organic molecules to physically and chemically stabilise polysulfide generated, as shown in Figure 1.3. As mentioned in Section 1.2, polysulfide could be easily synthesized by further heating molten sulfur (Figure 1.3(a)) above 159 °C, which is also known as floor temperature, however, it will be able to undergo backbiting (intramolecular reaction) to revert to the more thermodynamically favourable S_8 rings as the temperature decreases. As the mechanism shown in Figure 1.4, radical sulfur chains generated from homolytic S–S bond scission initiate and promote self-polymerisation of sulfur and cross-propagation to small organic

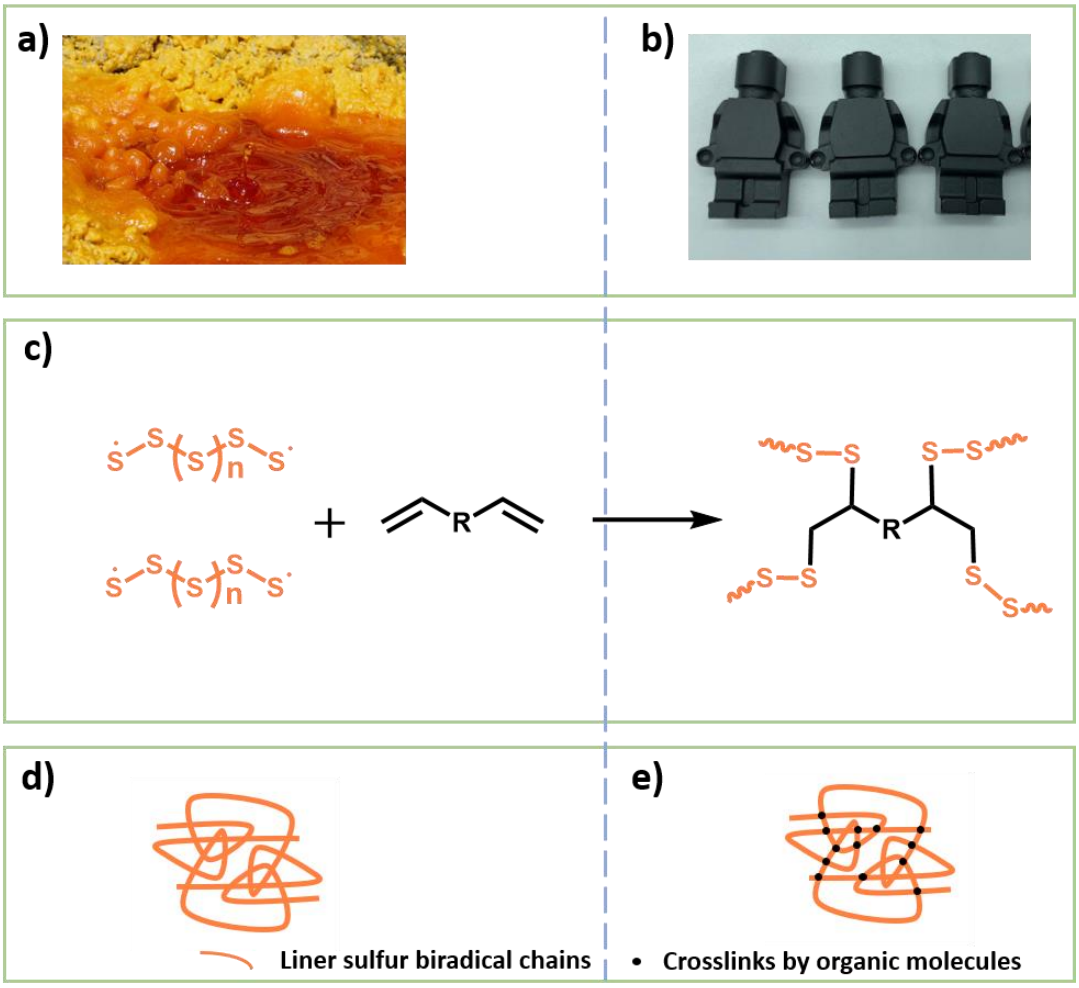

Figure 1.3 Processing of inverse vulcanisation. (a) Molten sulfur. (b) Photographs of final molded products of inverse vulcanised polymer after curing. (c) Scheme for inverse vulcanization of sulfur and small organic molecules functionalised dienes, generating crosslinked polymer structure. (d) Schematic diagram of the sulfur chains, before inverse vulcanisation. (e) Schematic diagram of the polysulfide network, crosslinked by organic molecules.

molecules functionalised with two or more carbon = carbon double bonds. Unsaturated monomers act as crosslinkers in the inverse vulcanisation, capping the radical ends of sulfur chains and preventing the degradation of polysulfides, as shown in Figure 1.3 (c)-(e). In order to explore various crosslinkers, which may have different functional groups, boiling points, miscibility with molten sulfur, and so on, some strategies to accomplish inverse vulcanisation were attempted by researchers, such as using catalyst and blend crosslinkers.

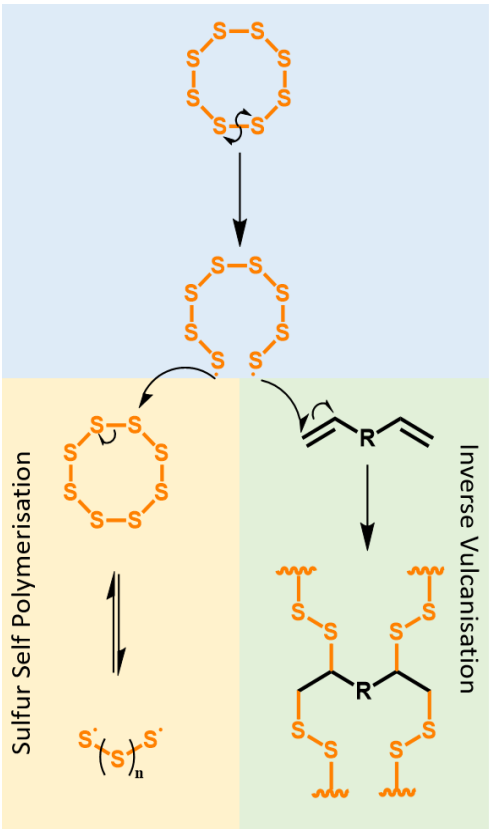

Figure 1.4 General scheme of sulfur self-polymerisation and inverse vulcanisation.

1.3.2.1 Crosslinkers

A variety of crosslinkers as shown in Figure 1.5, have been studied since 2013 when the reaction of 1,3-diisopropenylbenzene (DIB) with sulfur was reported.[24] Crosslinked by DIB, sulfur chains were stabilized and the product, poly(S-DIB), was shape persistent at room temperature. However, the DIB crosslinker is a synthetic chemical and not currently produced on large scales. Therefore, more economical or renewable crosslinkers are preferential to align with the principles of green

chemistry.[23,25,29] Limonene, a cyclic monoterpene, is a component in citrus fruit peels and is produced by the citrus industry as a by-product in a large quantities.[26] Limonene is ideal for use in inverse vulcanization, because it is a cheap, bio-derived industrial waste product. Polysulfides synthesized from sulfur and limonene were reported by Chalker and co-authors and the product demonstrated potential to detect and absorb heavy metals.[26] However, the low molecular weight and glass transition (T_g) of poly(S-limonene) are inhibitive for applications requiring rigidity. Subsequently, more renewable olefinic comonomers as crosslinkers in inverse vulcanisation were reported, including vegetable oils,[17] botryococcene,[30,31] terpinolene,[32] farnesene, farnesol, myrcene,[23] squalene, perillyl alcohol,[12] diallyl disulfide (DADS),[33–35] and garlic oil blend.[36] Moreover, industrial by-product or low cost chemicals, such as dicyclopentadiene (DCPD),[23] ethylene glycol dimethacrylate (EGDMA),[17,29,37] and ethylidene norbornene (ENB),[38] were also explored, giving it possible to scale up and commercialise high sulfur content polymer. Additionally, benefiting from the catalysts, more unreactive crosslinkers, such as 1,3,5,7-tetravinyltetramethylcyclotetrasiloxane (TVTCSi), and glyoxal bis(diallyl acetal) (GBDA), were explored to react with sulfur in inverse vulcanisation, broadening the range of possible high sulfur content polymers.[17]

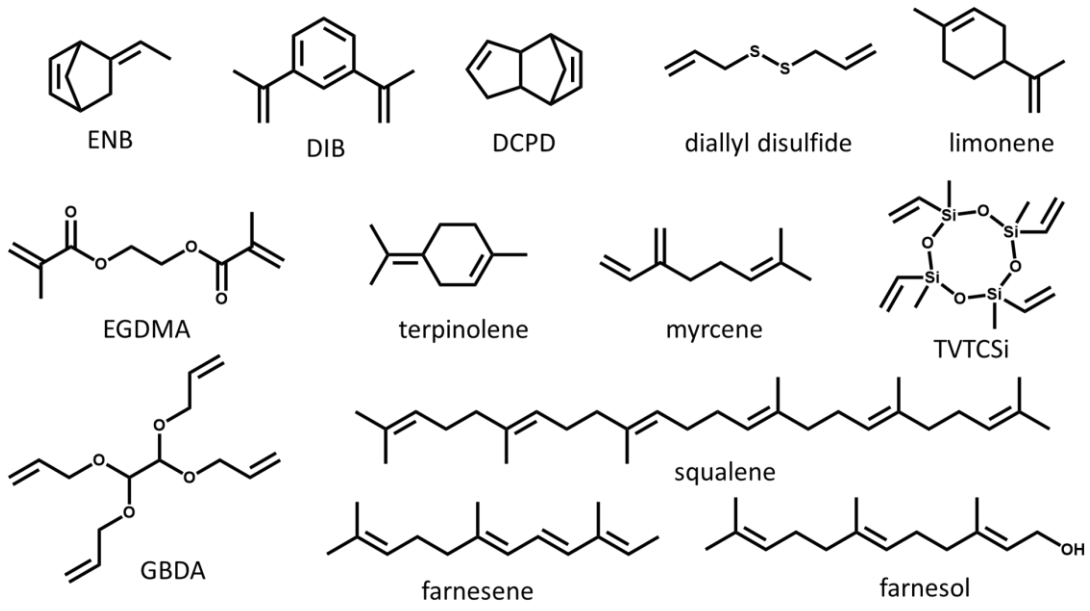

Figure 1.5 Crosslinkers studied previously in inverse vulcanisation.

1.3.2.2 Catalysts

Catalysts were widely used in conventional vulcanisation to decrease the reaction temperature. Lower reaction temperature could effectively minimize the generation of hydrogen sulfide and avoid auto-acceleration.[17] Auto-acceleration is known as the Trommsdorff–Norrish effect or the gel effect. Because inverse vulcanization is a bulk free-radical polymerisation and the reactions are exothermic, temperature increases dramatically if the dissipation of energy is poor, especially, at the end of reaction, when the viscosity rises due to the termination of free radicals. Auto-acceleration of polymerization may cause failure of the reaction vessel or, worse, explosion, as shown in Figure 1.6. Additionally, catalysts unlocked more crosslinkers, which may have poor miscibility with molten sulfur, such as EGDMA,[17] or lower boiling point than melting point of sulfur (119 °C), such as methyl methacrylate (MMA).[29]

Figure 1.6 An example of auto-acceleration in the inverse vulcanisation.

In 2019, Hasell group screened different potential catalysts, commonly used as accelerators in conventional vulcanisation, in inverse vulcanisation and discovered metal diethyldithiocarbamate complexes could effectively decrease the reaction temperature and inhibit H_2S generation. After that, Hasell and co-authors also demonstrated that the catalyst sodium diethyldithiocarbamate trihydrate allows inverse vulcanization to be conducted at low temperatures (110 °C), even below the melting point of sulfur (120 °C), therefore the inverse vulcanisation could be conducted in two phases, namely liquid crosslinkers with solid state elemental sulfur.[29] Most recently,

Hasell and co-authors investigate more about the function of catalysts in inverse vulcanisation and postulated that nucleophilic activation would be a potential mechanism.[29,39] Conventionally, inverse vulcanization has been performed at a temperature higher than 135 °C to induce cleavage of sulfur rings and generate disulfur radicals. However, in the reaction at lower temperature, it was supposed that the cleavage of S−S bonds was initiated by nucleophilic activators.

W. J. Chung *et al.* reported organic accelerators, for instance 4-vinylaniline (4VA) and N-methylimidazole (NMI), could expressively enhance the reaction rate and provide possibility to copolymerise with other crosslinkers at relatively low temperature ($\geqslant$ 60 °C). It was proposed that because of the lower bond dissociation energy, 4VA or NMI would react with sulfur by nucleophilic opening of the sulfur rings heterogeneously instead of homogeneously cleavage, which generating sulfur diradicals.[40,41] Generated prepolymers via this processing could be used as accelerator in further inverse vulcanisation, resulting from dynamic S-S bonds, a process which was termed as dynamic covalent polymerization (DCP). Similarly, Jenkins and co-authors reported a pre-polymer synthesized by elemental sulfur and divinylbenzene (DVB) could initiate inverse vulcanisation of elemental sulfur and 1,4-cyclohexanedimethanol divinyl ether (CDE) at as low as 90 °C.[42] Dynamic S-S bonds can be observed not only during the DCP but also in fully crosslinked polysulfides, resulting in a vitrimer property of these polymers.[43]

1.3.2.3 Post treatment and morphology of inverse vulcanised polymers

Sulfur polymers were discovered in different applications, therefore, to achieve a better performance in a given application, different post treatment strategies and morphologies of sulfur polymers were studied. Further curing sulfur polymers from liquid phase prepolymers in the patterned mould was one of the most common and convenient way to demonstrate the shape-persistency and mechanical properties of generated materials.[24,26] Electrospinning was performed by Theato and co-authors to fabricate a sulfur polymer nanofiber, which were demonstrated high adsorption capacity of mercury.[44] Coating sulfur polymers onto substrates or particles was conducted by different research groups to enlarge the surface area of sulfur polymers.[17,45] Additionally, porous inverse vulcanised polymers were prepared through different strategies, such as foaming the inverse vulcanised polymer with

supercritical CO_2,[46] and generating microporous sulfur polymer by salt templating.[47] Moreover, carbonisation is an important post treatment of thiopolymers generated via inverse vulcanisation to synthesise sulfur doped activated carbon. After carbonisation, the sulfur content would be decrease dramatically to ~15 wt% but with much higher specific surface areas (up to 2200 m^2 g^{-1}), which will be discussed in details in Section 1.4.1.[48–51]

1.3.3 Application of inverse vulcanised polymers

Since 2013, coined by Pyun, inverse vulcanised polymer has been applied into different areas, as shown in Figure 1.7, because of its unique physical and chemical properties. Depending upon the chemical and mechanical properties of these materials, inverse vulcanized polymers were applied in heavy metal uptake,[23,26,52,53] IR transparent lenses,[54–56] fertilizer release,[57] adhesive application,[33,58] repairable materials,[29,58] Li–S batteries,[30,34,59,60] oil–water separation,[61] sustainable and recyclable composites,[62,63] and antibacterial materials.[64]

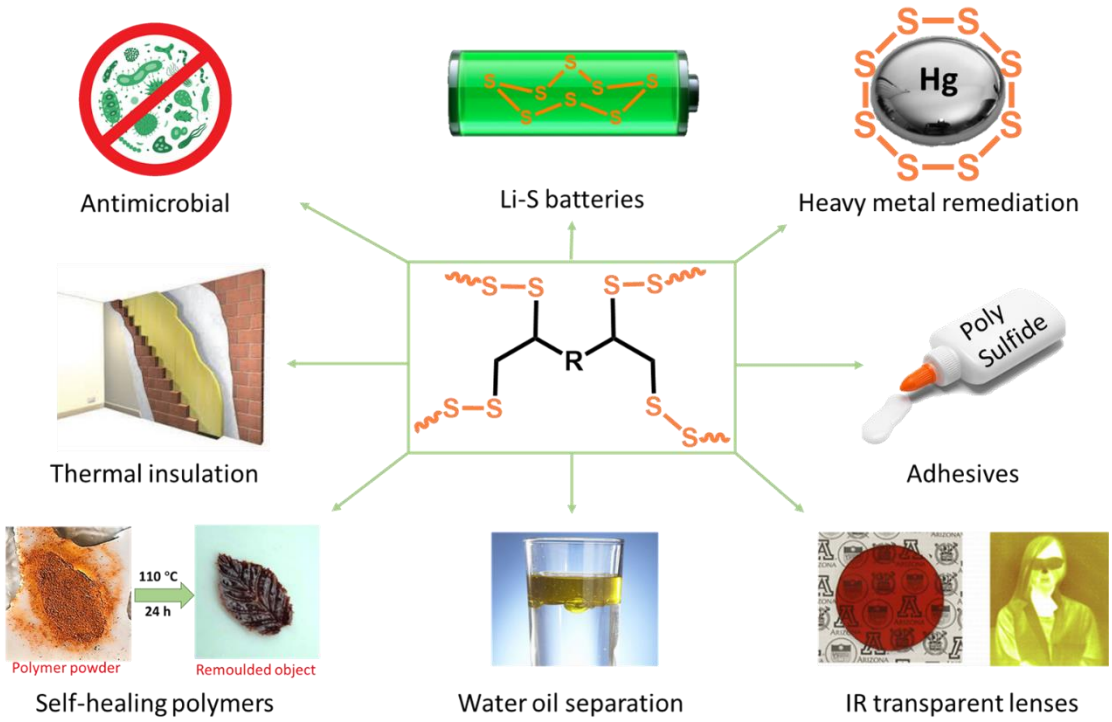

Figure 1.7 Different potential applications of inverse vulcanised polymers.

1.3.3.1 Li–S batteries

As the energy demand increased to support our high-speed developing society, renewable source energy is desperately needed as supplement of and, finally, replacement of fossil fuels. No matter for electric vehicles or mobile facilities, good performance battery is essential in nowadays. Lithium-ion batteries have been developed and widely used in many aspects, however, they almost touch their theoretical energy density limits (200– 250 Wh/kg as the technology developing.[65] Compared lithium-ion batteries, lithium-sulfur battery has much higher theoretical specific energy, which is up to 2600 Wh/kg.[66] Furthermore, the low cost and abundant resources of sulfur provide remarkable advantages as well. Nevertheless, the researches of Li-S batteries are still in baby stage with many problems, such as shuttle effect and lithium dendrite growth. Inverse vulcanised polymers and their derivates are studied in Li-S batteries recently to provide more candidate materials for cathode.[24,25,34] The first thiopolymer reported as a cathode in Li-S batteries is poly(S-DIB) by Pyun and co-authors.[24] Because of high sulfur content, poly(S-DIB) exhibited similar electrochemical behaviour in application of Li-S batteries, resulting in high capacity (1,100 mA h g^{-1}), however, suffer from capacity loss to 823 mA h g^{-1} after 100 cycles because of polysulfide shuttling effect, irreversible transfer of suffer polymer dissolved in electrolyte to lithium sulfide. After the report of poly(S-DIB) being applied as cathodes, more thiopolymers were synthesized by different monomers via inverse vulcanisation and utilised in Li–S battery, such as diallyl disulfide,[34] styrene,[60] bismaleimide,[67] vinyl phosphonic acid,[68] terpenes,[34] limonene,[59] and tetra(allyloxy)-1,4- benzoquinone (TABQ)[69]. Among these inversed vulcanised polymers, poly(S-tetra(allyloxy)-1,4-benxoquinone) demonstrated superior performance in cycling capability (833 mA h g^{-1}) at high cycling rate (10 C). Sulfur polymer applied as cathodes also benefit from the facile processing of inverse vulcanisation and potential of large scale product.[70]

1.3.3.2 IR transparent lenses

Unlike conventional polymers, some sulfur polymers synthesized through inverse vulcanisation have relatively high refractive index (RI, *n*) and infrared (IR) transparency because of S-S bonds. Therefore, sulfur polymers were researched as IR transparent lenses to substitute traditional inorganic materials, such as germanium. Traditional IR optics possess high RI, which is in the range of 2 - 4, but suffer from

high cost.[70,71] Conventional polymers possess RI typically from 1.30 - 1.70, and the material with *n* greater than 1.5 could be considered as high refractive index polymers (HRIPs). However, thiopolymers exhibit higher *n* (1.75-1.86) than conventional polymers, because of significant polarizable sulfur unit involved in the material. Additionally, RI of thiopolymers could be easily adjusted by the ratio of monomer and elemental sulfur.[72]

Poly (sulfur-selenium- diisopropenylbenzene) (poly (S-Se-*r*-DIB)), and Poly (sulfur-random-tetravinyltin (TVSn)) (poly(S-*r*-TVSn)), termed as organically modified chalcogenide (ORMOCHALC), were reported by Boyd and co-workers polymer as sulfur polymer applied in IR optics.[73,74] Moreover, 1,3,5-triisopropenylbenzene (TIB),[75] 1,3-diisopropenylbenzene (DIB),[76] and a dimer of norbornadiene (NBD) (NBD2)[55] were directly reacted with elemental sulfur to prepare as IR transparent lenses. More recently, elastic IR transmissive lens, which is stretchable and could adjust the shape of reflected images, prepared by elemental sulfur, squalene, and *β*-myrcene, were studied by Kanbara *et al.*[31] Considered the high cost of conventional inorganic IR transparent lenses, more and more thiopolymers were developed from different research group lately.

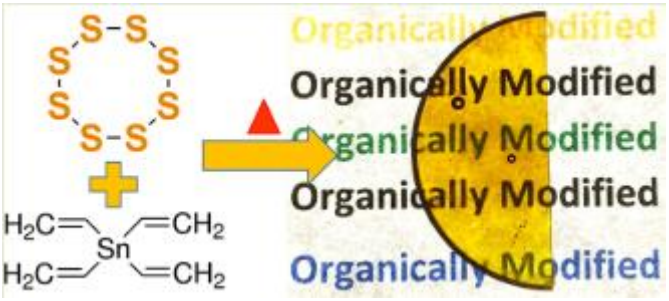

Figure 1.8 Scheme of generating poly(S-*r*-TVSn) and digital camera image of ORMOCHALC. Reproduced from ref.[74]

1.3.3.3 Heavy metal uptake

Sulfur containing polymers were found possessing high affinity for mercury, even demonstrating better performance than elemental sulfur.[23] Limonene was first reported by Chalker and co-authors. as renewable crosslinker to prepare inverse vulcanised polymers.[26] A distinct application of poly(S-limonene) is to selectively indicate mercury, a discovery that may find use in sensing applications. However, limonene is

a bio-derived renewable with low cost, but the mechanical properties of final product are very poor, resulting in a limitation in practical application. Dicyclopentadiene (DCPD) is low cost and readily available in large quantities as a by-product in petrochemicals industry. Crosslinked and stabilised poly(S-DCPD) were initially synthesised through inverse vulcanisation at 160 °C by Hasell and co-authors.[23] Then several materials characterisations and heavy metal capture capacity were investigated. It can be concluded from the result of solubility test and differential scanning calorimetry (DSC) that the new materials are fully crosslinked high sulfur contained polymer with high glass transition temperature (T_g) up to 115 °C. From the uptake test, poly(S-DCPD) could take up much more Hg than either elemental sulfur or other inverse vulcanized sulfur-containing polymers (poly(S-limonene) and poly(S-DIB)). The cost of these superior materials would not be prohibitive in comparison to activated carbon. Poly(sulfur-dicyclopentadiene) is produced solely from sulfur (~£100/tonne) and dicyclopentadiene (~£600/tonne), with no solvents required. Furthermore, more renewable small molecules were explored as monomer to make thiopolymers more economical and greener. Myrcene,[23] farnesene,[23] squalene,[12] perillyl alcohol,[12] canola oil, and garlic oil,[36] were reported in later studies for mercury remediation or water purification. Later research by Chung *et al.* demonstrated that

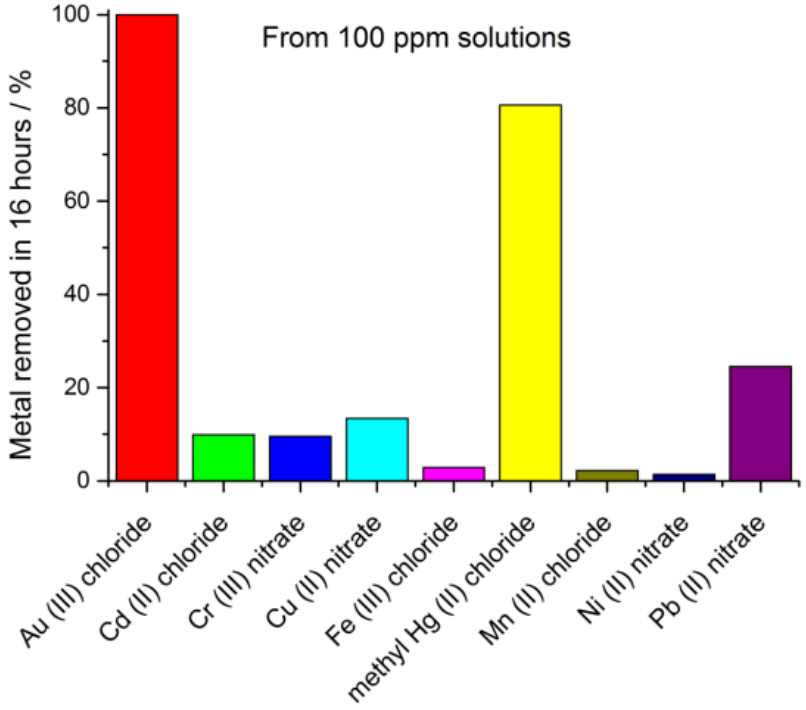

Figure 1.9 Selectivity test of poly(S-limonene) coated silica gel, showing that thiopolymers possessed high selectivity to mercury over other mixed metals. Reproduced from ref.[17]

poly (S-2-carboxyethyl acrylate) (poly (S-CEA) prepared by inverse vulcanisation had relative high capacity to mercury ($q_{e/m}$ = 989 mg g^{-1}) over other thiopolymers.[53] Besides high capacity of mercury over to elementary sulfur, thiopolymers also have high selectivity to mercury, as shown in even from mixed-ion solution, as shown in Figure 1.9.[17,53]

1.3.3.4 Self-healing polymers

Conventional polymers are normally divided as thermoplastic and thermosets.[27] Linear polymers are typically thermoplastic, which can be re-processed by melting and finally recycled. However, thermoset polymers were crosslinked polymers, which cannot be dissolved or melted, therefore it was little chance to be recycled. Recently, a new class of crosslinked polymer, named as 'Vitrimers', attracted increasingly attention.[77] 'Vitrimers' were crosslinked polymer, but unlike conventional thermoset crosslinked polymer, it can be re-processed by break thermoactivated bond, which is reversible or dynamic. It was reported that inversed vulcanised polymer exhibits similar properties to vitrimers.[12,78] Poly(S-*r*-DIB) was first reported as healable thiopolymer for IR applications by Pyun and co-authors.[78] Because of the dynamic nature of S-S bonds, Poly(S-*r*-DIB) can be healed at high temperature and reprocessed as IR lens after being scratched. Synthesized by renewable crosslinkers, poly(S-squalene) and poly(S-perillyl alcohol) were also demonstrated vitrimers behaviours, as shown in Figure 1.10.[12] More recently, a fully crosslinked ternary inverse vulcanised polymer, consisting of elemental sulfur, Span 80 and diphenyl-methane 4, 4'-diisocyanate (MDI), was also demonstrated to be reshaped and recycled, a vitrimer-like property.[43]

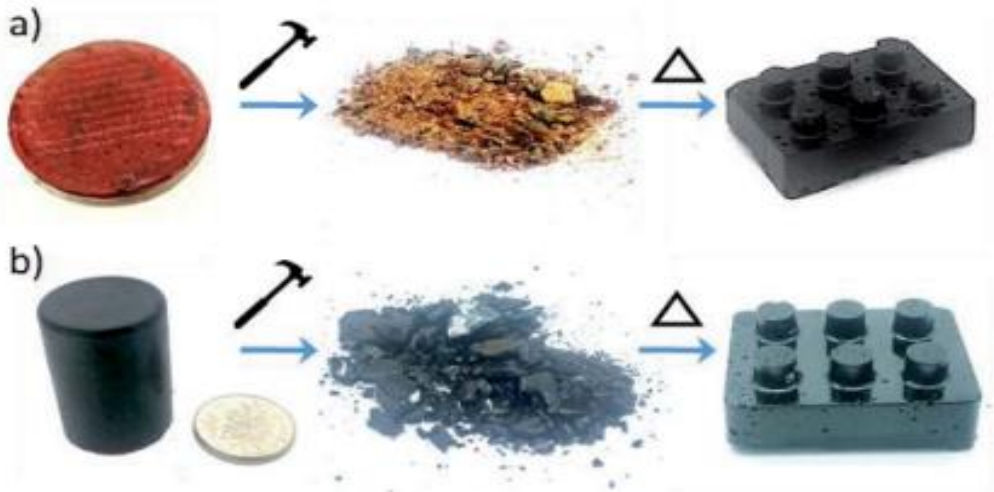

Figure 1.10 samples were reshaped after smashing. (a) Poly (S-perillyl alcohol) (b) poly(S-squalene). Reproduced from ref.[12]

1.4 Porous materials

Porous materials have attracted great interest because of high specific surface areas and pore volumes.[50,79–82] Porous materials are widely used in many applications, such as carbon dioxide capture,[83] gas separation,[50,84] catalysis,[85,86] supercapacitor electrodes,[87] removal of hazardous materials,[80,88–91] and energy conversion.[92] A variety of porous materials, for example, Metal Organic Frameworks (MOFs),[80,85,86,93] Covalent Organic Frameworks (COFs),[82] and Polymers of Intrinsic Microporosities (PIMs),[81,84,88] have been proposed, but most of them suffer from a high cost or low productive capacity. Compared with them, porous carbonaceous materials are widely used in multiple applications due to their highly porous texture and high cost effectiveness.[94]

1.4.1 Porous carbons

Activated carbons are very common and play an important role in industry, due in part to the variety of natural and synthetic materials that can be used as precursors, with preparation processes that are simple and scalable.

There are two different processes to prepare activated carbon, namely, the physical and the chemical activation.[95–99] The main difference between is the addition of chemical activation agent like $ZnCl_2$, KOH, and H_3PO_4. In the physical route, precursors were pyrolyzed in the absence of air and with no other chemicals, followed by gasification. Steam, carbon dioxide, and air are the most common agents used in gasification to selectively remove reactive carbon atoms generating porosity. On the other hand, in chemical activation, precursors are impregnated or physically mixed with a chemical agent and, then, carbonised without air or in the nitrogen gas flow. Once carbonisation process finished, the residual activating agents and impurities from activation would be washed out in order to reveal the blocked pores and interstices.

The advantage of chemical activation is that, because of the effect of chemical agents, the process generally takes place at a lower temperature, and has higher carbon yields than the physical activation. Phosphoric acid, zinc chloride, and alkaline metal compounds are the most common activating agents reported and applied. It has been shown that KOH is among one of the most successful activating agents. The porosity generated partly because of reactions shown below and partly because of the evolution

of gaseous products via these reactions and further decompositions. The surface areas of KOH activated carbon can be more than 3000 m^2/g.[98] The mechanism of $ZnCl_2$ in activating is not understood clearly, but it is regarded as dehydrating agent that help carbonisation and inhibit the formation of tar. It is reported by Watkinson *et al*. that the activation can be observed below 600 °C, almost 200 °C lower than alkali metal compounds.[96] However, the disadvantage of $ZnCl_2$ applied in the processing is as well as the common drawbacks of chemical activation. After activation, carbonaceous materials have to be washed with acid/base solutions and distilled water. Although $ZnCl_2$ is very soluble in water, with excess water, zinc oxychlorides will be formed, mixing with porous carbons or blocking the pores and interstices.

In order to optimize the application of activated carbon, as well as increasing the specific surface area of materials, incorporation of functional groups onto the carbon surface is another strategy.[100–102] Considering the improvement of adsorptive abilities and unique electronic features, heteroatom dopants were one of the most effective approaches incorporated into activated carbons.[101,103] The most abundantly investigated heteroatom is nitrogen. N-doped carbons were used widely in supercapacitors and as a catalyst in Oxygen Reduction Reaction (ORR).[104,105] Boron was studied as well to dope in carbon or synergistically co-doping with nitrogen in carbon.[104,105] Sulfur-doped carbonaceous materials with firmly and covalently bound sulfur-carbon structures were synthesized from carbonizing thienyl-contained block polymers by Schmidt *et al*.[104,105] Considering its high sulfur content and microporous structure that could introduce instinct porosity in carbons, microporous conjugated poly(1,3,5-tris(thienyl)benzene) (PTTB) network was chosen as precursor (shown in Figure 1.11). Precursors were annealed in an argon atmosphere at different temperature from 600 to 1000 °C. Homogeneous black solids with different sulfur contents (from 5.6 to 23.2 %) were yielded. All carbonised materials were porous,

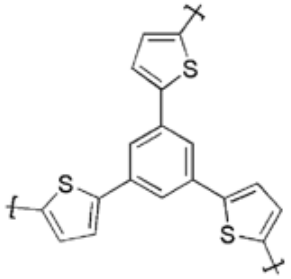

Figure 1.11 Structure of poly(1,3,5-tris(thienyl)benzene)

confirmed by nitrogen sorption isotherms. Porosity of the carbonaceous materials were depended on the carbonisation temperature with BET surface areas of up to 711 m^2 g^{-1}. A drawback of this carbon is pointed out was that the precursor, PTTB, is not very easy to synthesis, hindering scale-up. Another method was proposed by Spange *et al.* that selectively removal of template, which was coated with sulfur content polymer, in carbonised materials to generate size controlled porous sulfur-doped carbon.[73]

In 2016, the first example of porous carbons prepared from high-sulfur inverse vulcanized polymer were reported by Hasell and co-authors.[51] Poly(S-DIB) and Poly(S-limonene) were carbonised individually. The products showed microporosity and potential for gas selectivity. However, because this method lacked porogens or activators, the pore size distributions are relatively narrow. Well defined and remarkably narrow pore distribution (no pore widths higher than 2 nm in diameter in high proportion DIB sample) gave an advantage in gas adsorption, especially for CO_2. However, it was also a drawback that hindered more applications, as it was too narrow to heavy metal uptakes. Thus, they used poly(S-DCPD) as precursor and one equivalent of KOH as an activator to prepare high surface areas and broad pore size distributed sulfur doped carbons in 2017.[50] Commercial activated carbon has a surface area typically between 500 and 1000 m^2 g^{-1}, but that of highly porous S-doped carbons activated by KOH has already surpassed 2200 m^2 g^{-1}. Because of high surface area, porous S-doped carbons performed better than other reported materials in CO_2 uptake. CH_4 and H_2 uptakes were improved as well compared with previously reported carbonised inverse vulcanised polymers. Additionally, due to activating by KOH, much more mesopores (pore widths in range of 2-50 nm) were created, generating a hierarchical structure. Compared with some high surface area activated carbons without heteroatom doping, whose surface areas can be up to ~3000 m^2 g^{-1} or higher,[95,98,99] these S-doped carbons had lower surface areas, but with the advantage of high sulfur loading, this microporous S-doped carbon provided a possibility to absorb trace heavy metals from solutions. In low mercury concentration, porous S-doped carbons showed much better uptake capacity than activated carbon. At an equilibrium Hg concentration of ~10 ppm, porous S-doped carbons absorbed over 15 times more Hg than the activated carbon control.[50] The application of porous S-doped carbons was also attempted for gold recovery from lixiviants. Because of high surface areas and specific affinity of the incorporated sulfur for Au, this S-doped carbon can

adsorb up to one and a half times its weight in gold from $HAuCl_4$ solutions, three times the capacity for conventional activated carbon.

1.4.2 Gas adsorption

Gas adsorption is generally defined as the phenomenon by which adsorbate molecules (a gaseous or liquid component) are attracted to the surface of adsorbent (a solid).[106–108] Adsorption can be divided in physisorption and chemisorption. In the case of chemisorption, the intermolecular forces are mainly because of chemical bonds formed in the reaction. In physisorption, the interaction is normally because of molecular forces, such as van der Waal's forces, permanent dipole, and induced dipole. Gas adsorption depends on not only the conditions but also the material and structure and shape of that. Therefore, either external or internal morphology influence the capability of adsorption. Different categories or structures of pores are illustrated in Figure 1.12. In comparison with close pores (B), open pores (C and D) affect adsorption processing of a specific adsorbent (A).

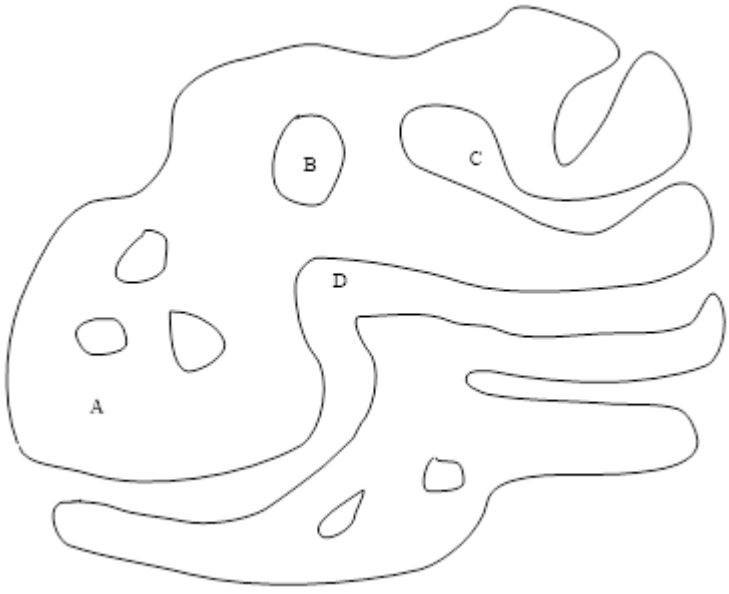

Figure 1.12 Schematic cross-section of a porous solid

According to the IUPAC recommendation[108], pores can be classified from their sizes (Figure 1.13):

Macropores: Pores with widths lager than 50 nm

Mesopores: Pores with widths between 2 nm and 50 nm

Micropores: Pores with widths smaller than 2 nm

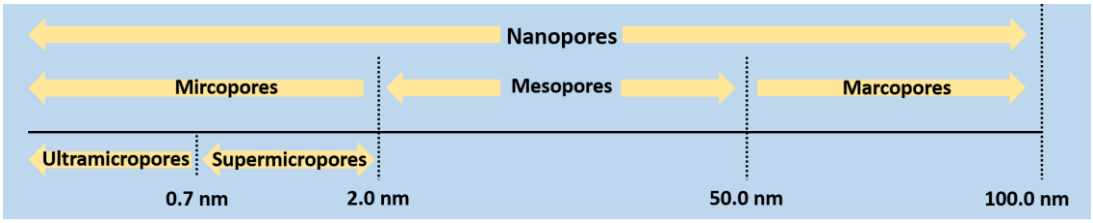

Figure 1.13 Classification of pore sizes

It is more often than not to distinguish ultramicropores (with widths smaller than 0.7 nm) and supermicropores (with widths between 0.7 nm and 2 nm). Nanopore is a term used to embrace all above mentioned pores, but with an upper limit 100 nm.

Adsorption isotherm is a quantitative relationship between the amount of adsorption and the pressure or concentration of adsorbate above the surface at equilibrium. There are experimentally six types of adsorption isotherms identified by IUPAC.[106,107] The proposed classification of physisorption isotherms is shown in Figure 1-4.[106,107]

Reversible Type I isotherms are representative of Langmuir isotherm, given by microporous solids with small external surfaces, such as activated carbons and molecular sieve zeolites. Type II isotherms are typically Brunauer, Emmett and Teller (BET) isotherm, namely multilayer physisorption, observed from the adsorption of most gases on nonporous or macroporous adsorbents. Type III, V isotherms are relatively rare, showing a weak adsorbate-adsorbent interaction. Type IV isotherms are given by adsorption onto mesoporous solid, always accompanied by a hysteresis loop. The last one Type VI are identified as Layer-by-layer adsorption on a uniform surface.

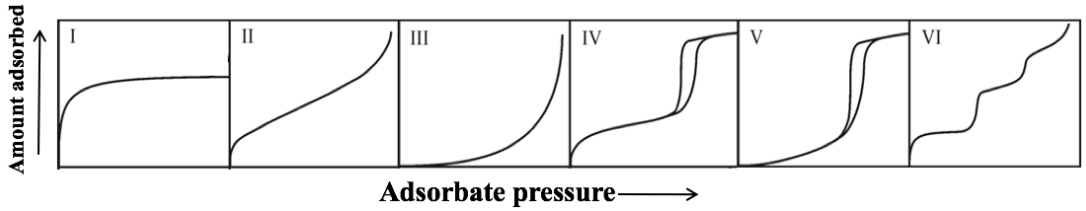

Figure 1.14 Classification of physisorption isotherms.[106,107]

1.5 Objectives

Inverse vulcanised polymers and their derivatives were studied by chemists from 2013, however, there are still several challenges of inverse vulcanisation in processing, applications and researches. Therefore, the main objectives of this thesis were including the optimisation of inverse vulcanisation processing to avoid auto-acceleration, the exploration of relevant catalysts to decrease reaction temperature in inverse vulcanisation, and the improvement of the performance of sulfur polymers and theris derivatives as sorbents in mercury uptake application. Additionally, more specific aims of each project could be checked in individual chapter.

1.6 Reference

(1) RoyChowdhury, A.; Datta, R.; Sarkar, D. *Heavy Metal Pollution and Remediation*; Elsevier Inc., 2018.

(2) Meyer, B. Elemental Sulfur. *Chem. Rev.* **1976**, *76* (3), 367–388.

(3) Griebel, J. J.; Glass, R. S.; Char, K.; Pyun, J. Polymerizations with Elemental Sulfur: A Novel Route to High Sulfur Content Polymers for Sustainability, Energy and Defense. *Prog. Polym. Sci.* **2016**, *58*, 90–125.

(4) Soleimani, M.; Bassi, A.; Margaritis, A. Biodesulfurization of Refractory Organic Sulfur Compounds in Fossil Fuels. *Biotechnol. Adv.* **2007**, *25* (6), 570–596.

(5) Gustavsson, L.; Haus, S.; Lundblad, M.; Lundström, A.; Ortiz, C. A.; Sathre, R.; Truong, N. Le; Wikberg, P.-E. Climate Change Effects of Forestry and Substitution of Carbon-Intensive Materials and Fossil Fuels. *Renew. Sustain. Energy Rev.* **2017**, *67*, 612–624.

(6) Rappold, T. A.; Lackner, K. S. Large Scale Disposal of Waste Sulfur: From Sulfide Fuels to Sulfate Sequestration. *Energy* **2010**, *35* (3), 1368–1380.

(7) Carn, S. A.; Krueger, A. J.; Krotkov, N. A.; Gray, M. A. Fire at Iraqi Sulfur Plant Emits SO2 Clouds Detected by Earth Probe TOMS. *Geophys. Res. Lett.* **2004**, *31* (19), 2–5.

(8) Ober, J. A. Materials Flow of Sulfur, Open-File Report 02–298. *Dep. Inter. U.S.*

Geol. Surv. **2003**.

(9) Sun, Y. J. *Handbook of Industrial Chemistry and Biotechnology*; Kent, J. A., Bommaraju, T. V., Barnicki, S. D., Eds.; Springer International Publishing: Cham, 2017; Vol. 34.

(10) Steudel, R.; Eckert, B. Solid Sulfur Allotropes; 2012; pp 1–80.

(11) O Mohamed, A. M.; El Gamal, M. M.; Onsy, A.-M. *SULFUR CONCRETE FOR THE CONSTRUCTION INDUSTRY A Sustainable Development Approach*; 2010; Vol. 1.

(12) Parker, D. J.; Chong, S. T.; Hasell, T. Sustainable Inverse-Vulcanised Sulfur Polymers. *RSC Adv.* **2018**, *8* (49), 27892–27899.

(13) Steudel, R. Liquid Sulfur Liquid Sulfur; 2012; pp 81–116.

(14) Steudel, R. The Chemistry of Organic Polysulfanes R-Sn-R (n > 2). *Chem. Rev.* **2002**, *102* (11), 3905–3945.

(15) Park, K. W.; Leitao, E. M. The Link to Polysulfides and Their Applications. *Chem. Commun.* **2021**, *57* (26), 3190–3202.

(16) Zhang, Y.; Glass, R. S.; Char, K.; Pyun, J. Recent Advances in the Polymerization of Elemental Sulphur, Inverse Vulcanization and Methods to Obtain Functional Chalcogenide Hybrid Inorganic/Organic Polymers (CHIPs). *Polym. Chem.* **2019**, *10* (30), 4078–4105.

(17) Wu, X.; Smith, J. A.; Petcher, S.; Zhang, B.; Parker, D. J.; Griffin, J. M.; Hasell, T. Catalytic Inverse Vulcanization. *Nat. Commun.* **2019**, *10* (1), 647.

(18) Patrick, J. C. The Formation of High Polymers by Condensation between Metallic Polysulfides and Dihalogenated Hydrocarbons and Ethers. *Rubber Chem. Technol.* **1936**, *9* (3), 373–382.

(19) Bartlett, P. D. Journal of the Chemical Society. *J. Chem. Soc. C Org.* **1970**, X001.

(20) Blight, L.; Currell, B. R.; Nash, B. J.; Scott, R. A. M.; Stillo, C. Preparation and Properties of Modified Sulfur Systems. *Adv. Chem. Ser.* **1978**, No. 165, 13–30.

(21) Bordoloi, B. K.; Pearce, E. L. I. M. Plastic Sulfur Stabilization by Copolymerization. *Adv. Chem. Ser.* **1978**, *165*, 31–53.

(22) *Reactions of Sulfur With Olefins.* Bateman, L.; Moore, C. G.; Pergamon Press Inc., 1961.

(23) Parker, D. J.; Jones, H. A.; Petcher, S.; Cervini, L.; Griffin, J. M.; Akhtar, R.; Hasell, T. Low Cost and Renewable Sulfur-Polymers by Inverse Vulcanisation, and Their Potential for Mercury Capture. *J. Mater. Chem. A* **2017**, *5* (23), 11682–11692.

(24) Chung, W. J.; Griebel, J. J.; Kim, E. T.; Yoon, H.; Simmonds, A. G.; Ji, H. J.; Dirlam, P. T.; Glass, R. S.; Wie, J. J.; Nguyen, N. A.; Guralnick, B. W.; Park, J.; Somogyi, Á.; Theato, P.; Mackay, M. E.; Sung, Y.; Char, K.; Pyun, J. The Use of Elemental Sulfur as an Alternative Feedstock for Polymeric Materials. *Nat. Chem.* **2013**, *5* (6), 518–524.

(25) Worthington, M. J. H.; Kucera, R. L.; Chalker, J. M. Green Chemistry and Polymers Made from Sulfur. *Green Chem.* **2017**, *19* (12), 2748–2761.

(26) Crockett, M. P.; Evans, A. M.; Worthington, M. J. H.; Albuquerque, I. S.; Slattery, A. D.; Gibson, C. T.; Campbell, J. A.; Lewis, D. A.; Bernardes, G. J. L.; Chalker, J. M. Sulfur-Limonene Polysulfide: A Material Synthesized Entirely from Industrial By-Products and Its Use in Removing Toxic Metals from Water and Soil. *Angew. Chemie Int. Ed.* **2016**, *55* (5), 1714–1718.

(27) *Introduction to Polymers.* Young, R. J.; Lovell, P. A., CRC Press; 2011.

(28) *Science and Technology of Rubber (Third Edition).* James E. Mark, B. E. and Frederick R. E.; 2013.

(29) Zhang, B.; Gao, H.; Yan, P.; Petcher, S.; Hasell, T. Inverse Vulcanization below the Melting Point of Sulfur. *Mater. Chem. Front.* **2020**, *4* (2), 669–675.

(30) Oishi, S.; Oi, K.; Kuwabara, J.; Omoda, R.; Aihara, Y.; Fukuda, T.; Takahashi, T.; Choi, J.-C.; Watanabe, M.; Kanbara, T. Synthesis and Characterization of Sulfur-Based Polymers from Elemental Sulfur and Algae Oil. *ACS Appl. Polym. Mater.* **2019**, *1* (5), 1195–1202.

(31) Kuwabara, J.; Oi, K.; Watanabe, M. M.; Fukuda, T.; Kanbara, T. Algae-Inspired, Sulfur-Based Polymer with Infrared Transmission and Elastic Function. *ACS Appl. Polym. Mater.* **2020**.

(32) Smith, J. A.; Green, S. J.; Petcher, S.; Parker, D. J.; Zhang, B.; Worthington, M. J. H.; Wu, X.; Kelly, C. A.; Baker, T.; Gibson, C. T.; Campbell, J. A.; Lewis, D. A.; Jenkins, M. J.; Willcock, H.; Chalker, J. M.; Hasell, T. Crosslinker Copolymerization for Property Control in Inverse Vulcanization. *Chem. - A Eur. J.* **2019**, 10433–10440.

(33) Herrera, C.; Ysinga, K. J.; Jenkins, C. L. Polysulfides Synthesized from Renewable Garlic Components and Repurposed Sulfur Form Environmentally Friendly Adhesives. *ACS Appl. Mater. Interfaces* **2019**, *11* (38), 35312–35318.

(34) Gomez, I.; Leonet, O.; Blazquez, J. A.; Mecerreyes, D. Inverse Vulcanization of Sulfur Using Natural Dienes as Sustainable Materials for Lithium–Sulfur Batteries. *ChemSusChem* **2016**, *9* (24), 3419–3425.

(35) Khawaja, S. Z.; Vijay Kumar, S.; Jena, K. K.; Alhassan, S. M. Flexible Sulfur Film from Inverse Vulcanization Technique. *Mater. Lett.* **2017**, *203*, 58–61.

(36) Zhang, B.; Dodd, L. J.; Yan, P.; Hasell, T. Mercury Capture with an Inverse Vulcanized Polymer Formed from Garlic Oil, a Bioderived Comonomer. *React. Funct. Polym.* **2021**, *161* (February), 104865.

(37) Zhang, B.; Petcher, S.; Hasell, T. A Ternary System for Delayed Curing Inverse Vulcanisation. *Chem. Commun.* **2019**, *55* (72), 10681–10684.

(38) Smith, J. A.; Wu, X.; Berry, N. G.; Hasell, T. High Sulfur Content Polymers: The Effect of Crosslinker Structure on Inverse Vulcanization. *J. Polym. Sci. Part A Polym. Chem.* **2018**, *56* (16), 1777–1781.

(39) Dodd, L. J.; Omar, Ö.; Wu, X.; Hasell, T. Investigating the Role and Scope of Catalysts in Inverse Vulcanization. *ACS Catal.* **2021**, *11* (8), 4441–4455.

(40) Zhang, Y.; Konopka, K. M.; Glass, R. S.; Char, K.; Pyun, J. Chalcogenide Hybrid Inorganic/Organic Polymers (CHIPs) via Inverse Vulcanization and Dynamic Covalent Polymerizations. *Polym. Chem.* **2017**, *8* (34), 5167–5173.

(41) Zhang, Y.; Pavlopoulos, N. G.; Kleine, T. S.; Karayilan, M.; Glass, R. S.; Char, K.; Pyun, J. Nucleophilic Activation of Elemental Sulfur for Inverse Vulcanization and Dynamic Covalent Polymerizations. *J. Polym. Sci. Part A Polym. Chem.* **2019**, *57* (1), 7–12.

(42) Westerman, C. R.; Jenkins, C. L. Dynamic Sulfur Bonds Initiate Polymerization of Vinyl and Allyl Ethers at Mild Temperatures. *Macromolecules* **2018**, *51* (18), 7233–7238.

(43) Yan, P.; Zhao, W.; Zhang, B.; Jiang, L.; Petcher, S.; Smith, J. A.; Parker, D. J.; Cooper, A. I.; Lei, J.; Hasell, T. Inverse Vulcanized Polymers with Shape Memory, Enhanced Mechanical Properties, and Vitrimer Behavior. *Angew. Chemie - Int. Ed.* **2020**, *59* (32), 13371–13378.

(44) Thielke, M.; Bultema, L.; Brauer, D.; Richter, B.; Fischer, M.; Theato, P. Rapid Mercury(II) Removal by Electrospun Sulfur Copolymers. *Polymers (Basel).* **2016**, *8* (7), 266.

(45) Scheiger, J. M.; Direksilp, C.; Falkenstein, P.; Welle, A.; Koenig, M.; Heissler, S.; Matysik, J.; Levkin, P. A.; Theato, P. Inverse Vulcanization of Styrylethyltrimethoxysilane–Coated Surfaces, Particles, and Crosslinked Materials. *Angew. Chemie - Int. Ed.* **2020**, *59* (42), 18639–18645.

(46) Hasell, T.; Parker, D. J.; Jones, H. A.; McAllister, T.; Howdle, S. M. Porous Inverse Vulcanised Polymers for Mercury Capture. *Chem. Commun.* **2016**, *52* (31), 5383–5386.

(47) Petcher, S.; Parker, D. J.; Hasell, T. Macroporous Sulfur Polymers from a Sodium Chloride Porogen - A Low Cost, Versatile Remediation Material. *Environ. Sci. Water Res. Technol.* **2019**, *5* (12), 2142–2149.

(48) Zhang, B.; Petcher, S.; Gao, H.; Yan, P.; Cai, D.; Fleming, G.; Parker, D. J.; Chong, S. Y.; Hasell, T. Magnetic Sulfur-Doped Carbons for Mercury Adsorption. *J. Colloid Interface Sci.* **2021**, *603*, 728–737.

(49) Mann, M.; Luo, X.; Tikoalu, A. D.; Gibson, C. T.; Yin, Y.; Al-Attabi, R.; Andersson, G. G.; Raston, C. L.; Henderson, L. C.; Pring, A.; Hasell, T.; Chalker, J. M. Carbonisation of a Polymer Made from Sulfur and Canola Oil.

Chem. Commun. **2021**, *57* (51), 6296–6299.

(50) Lee, J. S. M.; Parker, D. J.; Cooper, A. I.; Hasell, T. High Surface Area Sulfur-Doped Microporous Carbons from Inverse Vulcanised Polymers. *J. Mater. Chem. A* **2017**, *5* (35), 18603–18609.

(51) Bear, J. C.; McGettrick, J. D.; Parkin, I. P.; Dunnill, C. W.; Hasell, T. Porous Carbons from Inverse Vulcanised Polymers. *Microporous Mesoporous Mater.* **2016**, *232*, 189–195.

(52) Lin, H. K.; Lai, Y. S.; Liu, Y. L. Cross-Linkable and Self-Foaming Polysulfide Materials for Repairable and Mercury Capture Applications. *ACS Sustain. Chem. Eng.* **2019**, *7* (4), 4515–4522.

(53) Limjuco, L. A.; Fissaha, H. T.; Kim, H.; Nisola, G. M.; Chung, W.-J. Sulfur Copolymerization with Hydrophilic Comonomers as Polysulfides in Microbeads for Highly Efficient Hg 2+ Removal from Wastewater . *ACS Appl. Polym. Mater.* **2020**.

(54) Anderson, L. E.; Kleine, T. S.; Zhang, Y.; Phan, D. D.; Namnabat, S.; LaVilla, E. A.; Konopka, K. M.; Ruiz Diaz, L.; Manchester, M. S.; Schwiegerling, J.; Glass, R. S.; Mackay, M. E.; Char, K.; Norwood, R. A.; Pyun, J. Chalcogenide Hybrid Inorganic/Organic Polymers: Ultrahigh Refractive Index Polymers for Infrared Imaging. *ACS Macro Lett.* **2017**, *6* (5), 500–504.

(55) Kleine, T. S.; Lee, T.; Carothers, K. J.; Hamilton, M. O.; Anderson, L. E.; Ruiz Diaz, L.; Lyons, N. P.; Coasey, K. R.; Parker, W. O.; Borghi, L.; Mackay, M. E.; Char, K.; Glass, R. S.; Lichtenberger, D. L.; Norwood, R. A.; Pyun, J. Infrared Fingerprint Engineering: A Molecular-Design Approach to Long-Wave Infrared Transparency with Polymeric Materials. *Angew. Chemie - Int. Ed.* **2019**, *58* (49), 17656–17660.

(56) Griebel, J. J.; Nguyen, N. A.; Namnabat, S.; Anderson, L. E.; Glass, R. S.; Norwood, R. A.; Mackay, M. E.; Char, K.; Pyun, J. Dynamic Covalent Polymers via Inverse Vulcanization of Elemental Sulfur for Healable Infrared Optical Materials. *ACS Macro Lett.* **2015**, *4* (9), 862–866.

(57) Mann, M.; Kruger, J. E.; Andari, F.; McErlean, J.; Gascooke, J. R.; Smith, J. A.;

Worthington, M. J. H.; McKinley, C. C. C.; Campbell, J. A.; Lewis, D. A.; Hasell, T.; Perkins, M. V.; Chalker, J. M. Sulfur Polymer Composites as Controlled-Release Fertilisers. *Org. Biomol. Chem.* **2019**, *17* (7), 1929–1936.

(58) Tonkin, S. J.; Gibson, C. T.; Campbell, J. A.; Lewis, D. A.; Karton, A.; Hasell, T.; Chalker, J. M. Chemically Induced Repair, Adhesion, and Recycling of Polymers Made by Inverse Vulcanization. *Chem. Sci.* **2020**, *11* (21), 5537–5546.

(59) Wu, F.; Chen, S.; Srot, V.; Huang, Y.; Sinha, S. K.; van Aken, P. A.; Maier, J.; Yu, Y. A Sulfur-Limonene-Based Electrode for Lithium-Sulfur Batteries: High-Performance by Self-Protection. *Adv. Mater.* **2017**, *1706643*, 1–8.

(60) Zhang, Y.; Griebel, J. J.; Dirlam, P. T.; Nguyen, N. A.; Glass, R. S.; Mackay, M. E.; Char, K.; Pyun, J. Inverse Vulcanization of Elemental Sulfur and Styrene for Polymeric Cathodes in Li-S Batteries. *J. Polym. Sci. Part A Polym. Chem.* **2017**, *55* (1), 107–116.

(61) Worthington, M. J. H.; Shearer, C. J.; Esdaile, L. J.; Campbell, J. A.; Gibson, C. T.; Legg, S. K.; Yin, Y.; Lundquist, N. A.; Gascooke, J. R.; Albuquerque, I. S.; Shapter, J. G.; Andersson, G. G.; Lewis, D. A.; Bernardes, G. J. L.; Chalker, J. M. Sustainable Polysulfides for Oil Spill Remediation: Repurposing Industrial Waste for Environmental Benefit. *Adv. Sustain. Syst.* **2018**, *2* (6), 1800024.

(62) Karunarathna, M. S.; Lauer, M. K.; Thiounn, T.; Smith, R. C.; Tennyson, A. G. Valorisation of Waste to Yield Recyclable Composites of Elemental Sulfur and Lignin. *J. Mater. Chem. A* **2019**, *7* (26), 15683–15690.

(63) Lundquist, N. A.; Tikoalu, A. D.; Worthington, M. J. H.; Shapter, R.; Tonkin, S. J.; Stojcevski, F.; Mann, M.; Gibson, C. T.; Gascooke, J. R.; Karton, A.; Henderson, L. C.; Esdaile, L. J.; Chalker, J. M. Reactive Compression Molding Post-Inverse Vulcanization: A Method to Assemble, Recycle, and Repurpose Sulfur Polymers and Composites. *Chem. - A Eur. J.* **2020**, *26* (44), 10035–10044.

(64) Deng, Z.; Hoefling, A.; Théato, P.; Lienkamp, K. Surface Properties and Antimicrobial Activity of Poly(Sulfur- Co -1,3-Diisopropenylbenzene) Copolymers. *Macromol. Chem. Phys.* **2018**, *219* (5), 1700497.

(65) Fotouhi, A.; Auger, D. J.; Propp, K.; Longo, S.; Wild, M. A Review on Electric Vehicle Battery Modelling: From Lithium-Ion toward Lithium-Sulphur. *Renew. Sustain. Energy Rev.* **2016**, *56*, 1008–1021.

(66) Hou, T. Z.; Xu, W. T.; Chen, X.; Peng, H. J.; Huang, J. Q.; Zhang, Q. Lithium Bond Chemistry in Lithium–Sulfur Batteries. *Angew. Chemie - Int. Ed.* **2017**, *56* (28), 8178–8182.

(67) Arslan, M.; Kiskan, B.; Cengiz, E. C.; Demir-Cakan, R.; Yagci, Y. Inverse Vulcanization of Bismaleimide and Divinylbenzene by Elemental Sulfur for Lithium Sulfur Batteries. *Eur. Polym. J.* **2016**, *80*, 70–77.

(68) Kang, H.; Park, M. J. Thirty-Minute Synthesis of Hierarchically Ordered Sulfur Particles Enables High-Energy, Flexible Lithium-Sulfur Batteries. *Nano Energy* **2021**, *89* (PB), 106459.

(69) Kang, H.; Kim, H.; Park, M. J. Sulfur-Rich Polymers with Functional Linkers for High-Capacity and Fast-Charging Lithium–Sulfur Batteries. *Adv. Energy Mater.* **2018**, *8* (32).

(70) Lee, T.; Dirlam, P. T.; Njardarson, J. T.; Glass, R. S.; Pyun, J. Polymerizations with Elemental Sulfur: From Petroleum Refining to Polymeric Materials. *J. Am. Chem. Soc.* **2021**.

(71) Liu, J. G.; Ueda, M. High Refractive Index Polymers: Fundamental Research and Practical Applications. *J. Mater. Chem.* **2009**, *19* (47), 8907–8919.

(72) Kleine, T. S.; Glass, R. S.; Lichtenberger, D. L.; Mackay, M. E.; Char, K.; Norwood, R. A.; Pyun, J. 100th Anniversary of Macromolecular Science Viewpoint: High Refractive Index Polymers from Elemental Sulfur for Infrared Thermal Imaging and Optics. *ACS Macro Lett.* **2020**, *9* (2), 245–259.

(73) Boyd, D. A.; Baker, C. C.; Myers, J. D.; Nguyen, V. Q.; Drake, G. A.; McClain, C. C.; Kung, F. H.; Bowman, S. R.; Kim, W.; Sanghera, J. S. ORMOCHALCs: Organically Modified Chalcogenide Polymers for Infrared Optics. *Chem. Commun.* **2017**, *53* (1), 259–262.

(74) Boyd, D. A.; Nguyen, V. Q.; McClain, C. C.; Kung, F. H.; Baker, C. C.; Myers, J. D.; Hunt, M. P.; Kim, W.; Sanghera, J. S. Optical Properties of a Sulfur-Rich

Organically Modified Chalcogenide Polymer Synthesized via Inverse Vulcanization and Containing an Organometallic Comonomer. *ACS Macro Lett.* **2019**, *8* (2), 113–116.

(75) Kleine, T. S.; Nguyen, N. A.; Anderson, L. E.; Namnabat, S.; Lavilla, E. A.; Showghi, S. A.; Dirlam, P. T.; Arrington, C. B.; Manchester, M. S.; Schwiegerling, J.; Glass, R. S.; Char, K.; Norwood, R. A.; Mackay, M. E.; Pyun, J. High Refractive Index Copolymers with Improved Thermomechanical Properties via the Inverse Vulcanization of Sulfur and 1,3,5-Triisopropenylbenzene. *ACS Macro Lett.* **2016**, *5* (10), 1152–1156.

(76) Griebel, J. J.; Namnabat, S.; Kim, E. T.; Himmelhuber, R.; Moronta, D. H.; Chung, W. J.; Simmonds, A. G.; Kim, K. J.; Van Der Laan, J.; Nguyen, N. A.; Dereniak, E. L.; MacKay, M. E.; Char, K.; Glass, R. S.; Norwood, R. A.; Pyun, J. New Infrared Transmitting Material via Inverse Vulcanization of Elemental Sulfur to Prepare High Refractive Index Polymers. *Adv. Mater.* **2014**, *26* (19), 3014–3018.

(77) Denissen, W.; Winne, J. M.; Du Prez, F. E. Vitrimers: Permanent Organic Networks with Glass-like Fluidity. *Chem. Sci.* **2016**, *7* (1), 30–38.

(78) Griebel, J. J.; Nguyen, N. A.; Namnabat, S.; Anderson, L. E.; Glass, R. S.; Norwood, R. A.; Mackay, M. E.; Char, K.; Pyun, J. Dynamic Covalent Polymers via Inverse Vulcanization of Elemental Sulfur for Healable Infrared Optical Materials. *ACS Macro Lett.* **2015**, *4* (9), 862–866.

(79) Cote, A. P. Porous, Crystalline, Covalent Organic Frameworks. *Science (80-.).* **2005**, *310* (5751), 1166–1170.

(80) Khan, N. A.; Hasan, Z.; Jhung, S. H. Adsorptive Removal of Hazardous Materials Using Metal-Organic Frameworks (MOFs): A Review. *J. Hazard. Mater.* **2013**, *244–245*, 444–456.

(81) McKeown, N. B.; Budd, P. M. Polymers of Intrinsic Microporosity (PIMs): Organic Materials for Membrane Separations, Heterogeneous Catalysis and Hydrogen Storage. *Chem. Soc. Rev.* **2006**, *35* (8), 675–683.

(82) Feng, X.; Ding, X.; Jiang, D. Covalent Organic Frameworks. *Chem. Soc. Rev.*

2012, *41* (18), 6010.

(83) Lee, J. S. M.; Briggs, M. E.; Hasell, T.; Cooper, A. I. Hyperporous Carbons from Hypercrosslinked Polymers. *Adv. Mater.* **2016**, *28* (44), 9804–9810.

(84) McKeown, N. B.; Budd, P. M.; Msayib, K. J.; Ghanem, B. S.; Kingston, H. J.; Tattershall, C. E.; Makhseed, S.; Reynolds, K. J.; Fritsch, D. Polymers of Intrinsic Microporosity (PIMs): Bridging the Void between Microporous and Polymeric Materials. *Chem. - A Eur. J.* **2005**, *11* (9), 2610–2620.

(85) Rogge, S. M. J.; Bavykina, A.; Hajek, J.; Garcia, H.; Olivos-Suarez, A. I.; Sepúlveda-Escribano, A.; Vimont, A.; Clet, G.; Bazin, P.; Kapteijn, F.; Daturi, M.; Ramos-Fernandez, E. V.; Llabrés Xamena, F. X. I.; Van Speybroeck, V.; Gascon, J. Metal-Organic and Covalent Organic Frameworks as Single-Site Catalysts. *Chem. Soc. Rev.* **2017**, *46* (11), 3134–3184.

(86) Yang, Q.; Xu, Q.; Jiang, H. L. Metal-Organic Frameworks Meet Metal Nanoparticles: Synergistic Effect for Enhanced Catalysis. *Chem. Soc. Rev.* **2017**, *46* (15), 4774–4808.

(87) Qie, L.; Chen, W.; Xu, H.; Xiong, X.; Jiang, Y.; Zou, F.; Hu, X.; Xin, Y.; Zhang, Z.; Huang, Y. Synthesis of Functionalized 3D Hierarchical Porous Carbon for High-Performance Supercapacitors. *Energy Environ. Sci.* **2013**, *6* (8), 2497–2504.

(88) Jimenez-Solomon, M. F.; Song, Q.; Jelfs, K. E.; Munoz-Ibanez, M.; Livingston, A. G. Polymer Nanofilms with Enhanced Microporosity by Interfacial Polymerization. *Nat. Mater.* **2016**, *15* (7), 760–767.

(89) Crini, G. Non-Conventional Low-Cost Adsorbents for Dye Removal: A Review. *Bioresour. Technol.* **2006**, *97* (9), 1061–1085.

(90) Liu, P. S.; Chen, G. F. General Introduction to Porous Materials. In *Porous Materials*; Elsevier, 2014; pp 1–20.

(91) Oliveira, L. C. A.; Rios, R. V. R. A.; Fabris, J. D.; Garg, V.; Sapag, K.; Lago, R. M. Activated Carbon/Iron Oxide Magnetic Composites for the Adsorption of Contaminants in Water. *Carbon N. Y.* **2002**, *40* (12), 2177–2183.

(92) Wang, H.; Zhu, Q. L.; Zou, R.; Xu, Q. Metal-Organic Frameworks for Energy Applications. *Chem* **2017**, *2* (1), 52–80.

(93) Stock, N.; Biswas, S. Synthesis of Metal-Organic Frameworks (MOFs): Routes to Various MOF Topologies, Morphologies, and Composites. *Chem. Rev.* **2012**, *112* (2), 933–969.

(94) Stein, A.; Wang, Z.; Fierke, M. A. Functionalization of Porous Carbon Materials with Designed Pore Architecture. *Adv. Mater.* **2009**, *21* (3), 265–293.

(95) Caturla, F.; Molina-Sabio, M.; Rodríguez-Reinoso, F. Preparation of Activated Carbon by Chemical Activation with ZnCl2. *Carbon N. Y.* **1991**, *29* (7), 999–1007.

(96) Hayashi, J.; Kazehaya, A.; Muroyama, K.; Watkinson, A. P. Preparation of Activated Carbon from Lignin by Chemical Activation. *Carbon N. Y.* **2000**, *38* (13), 1873–1878.

(97) Ahmadpour, A.; Do, D. D. The Preparation of Activated Carbon from Macadamia Nutshell by Chemical Activation. *Carbon N. Y.* **1997**, *35* (12), 1723–1732.

(98) Lillo-Ródenas, M. .; Lozano-Castelló, D.; Cazorla-Amorós, D.; Linares-Solano, A. Preparation of Activated Carbons from Spanish Anthracite I. Activation by KOH. *Carbon N. Y.* **2001**, *39* (5), 751–759.

(99) Lozano-Castelló, D.; Lillo-Ródenas, M. A.; Cazorla-Amorós, D.; Linares-Solano, A. Preparation of Activated Carbons from Spanish Anthracite II. Activation by NaOH. *Carbon N. Y.* **2001**, *39* (5), 741–749.

(100) Huang, H.; Xia, L.; Cao, R. R.; Niu, Z.; Chen, H.; Liu, Q.; Li, T.; Shi, X.; Asiri, A. M.; Sun, X. A Biomass-Derived Carbon-Based Electrocatalyst for Efficient N 2 Fixation to NH 3 under Ambient Conditions. *Chem. - A Eur. J.* **2019**, *25* (8), 1914–1917.

(101) Xia, L.; Wu, X.; Wang, Y.; Niu, Z.; Liu, Q.; Li, T.; Shi, X.; Asiri, A. M.; Sun, X. S-Doped Carbon Nanospheres: An Efficient Electrocatalyst toward Artificial N2 Fixation to NH3. *Small Methods* **2019**, *3* (6), 2–6.

(102) Wu, T.; Li, X.; Zhu, X.; Mou, S.; Luo, Y.; Shi, X.; Asiri, A. M.; Zhang, Y.; Zheng, B.; Zhao, H.; Sun, X. P-Doped Graphene toward Enhanced Electrocatalytic N2 Reduction. *Chem. Commun.* **2020**, *56* (12), 1831–1834.

(103) Guo, J.; Huo, J.; Liu, Y.; Wu, W.; Wang, Y.; Wu, M.; Liu, H.; Wang, G. Nitrogen-Doped Porous Carbon Supported Nonprecious Metal Single-Atom Electrocatalysts: From Synthesis to Application. *Small Methods* **2019**, *3* (9), 1–33.

(104) Schmidt, J.; Weber, J.; Epping, J. D.; Antonietti, M.; Thomas, A. Microporous Conjugated Poly(Thienylene Arylene) Networks. *Adv. Mater.* **2009**, *21* (6), 702–705.

(105) Paraknowitsch, J. P.; Thomas, A.; Schmidt, J. Microporous Sulfur-Doped Carbon from Thienyl-Based Polymer Network Precursors. *Chem. Commun.* **2011**, *47* (29), 8283–8285.

(106) Thomas, W. J.; Crittenden, B. 3 - Fundamentals of Adsorption Equilibria. In *Adsorption Technology & Design*; Thomas, W. J., Crittenden, B., Eds.; Butterworth-Heinemann: Oxford, 1998; pp 31–65.

(107) Thommes, M.; Kaneko, K.; Neimark, A. V.; Olivier, J. P.; Rodriguez-Reinoso, F.; Rouquerol, J.; Sing, K. S. W. Physisorption of Gases, with Special Reference to the Evaluation of Surface Area and Pore Size Distribution (IUPAC Technical Report). *Pure Appl. Chem.* **2015**, *87* (9–10), 1051–1069.

(108) Rouquerolt, J.; Avnir, D.; Fairbridge, C. W.; Everett, D. H.; Haynes, J. H.; Pernicone, N.; Ramsay, J. D. F.; Sing, K. S. W.; Unger, K. K. Recommendations for the Characterization of Porous Solids. *Pure Appl. Chem.* **1994**, *66* (8), 1739–1758.

Chapter 2. A ternary system for delayed curing inverse vulcanisation

2.1 Context

2.1.1 Abstract

Completion of inverse vulcanisation reactions leads to a crosslinked insoluble polymer, but insufficient reaction allows phase separation of the sulfur and organic crosslinkers. A ternary co-polymer system allows delayed curing to be used, keeping the pre-polymer stable, homogeneous, and ready to be set into its final form when and where needed, allows greater opportunities for practical production.

2.1.2 Publication

Bowen Zhang, Samuel Petcher, Tom Hasell. A ternary system for delayed curing inverse vulcanisation. *Chemical Communication*, 2019, **55**, 10681

2.1.3 Author contributions

Bowen Zhang: Conceptualization, Methodology, Investigation, Formal analysis, Writing - original draft, Writing - review & editing. **Samuel Petcher**: Investigation, Formal analysis, Writing - review & editing. **Tom Hasell**: Resources, Writing - review & editing, Supervision, Project administration, Funding acquisition.

2.2 Introduction

Elemental sulfur has applications in both commodity and specialty chemicals.[1] However, as sulfur is also a by-product of the petrochemicals industry, supply outweighs demand, causing a current global issue- the "excess sulfur problem".[2–4] Using this sulfur to form polymeric materials would be an ideal solution, but polymers made from pure elemental sulfur are not stable, and readily to depolymerize to more stable S_8.[2] The recent discovery of inverse vulcanization by Pyun and co-authors. in 2013, capping radical chain end of polymeric sulfur by dienes, allows polymeric materials with high sulfur contents (up to 90 wt.%) to be produced.[3,5–7] Following this work further investigation revealed it was possible to apply this method to a range of crosslinkers, such as diisopropylbenzene (DIB),[5] limonene,[6] ethylene glycol dimethylacrylate (EGDMA),[8] diallyl disulfide,[9] dicyclopentadiene (DCPD),[10] perillyl alcohol,[11] and ethylidene norbornene (ENB).[12] High sulfur content polymers are promising materials, with potential applications in: LiS batteries,[5,9,13] IR transparent lenses,[14,15] construction materials,[16] antimicrobial materials,[17] controlled-release fertilisers,[18] the stabilization of metal nanoparticles,[19] oil-water separation,[20] water purification,[6,21–25] and capture of heavy metals.[3,8,10–12] However, due to the nature of the synthetic procedure processing is difficult. The reaction is commonly taken to completion on a hot-plate or moved directly into an oven for curing. If stirring is removed early in the reaction, the molten sulfur and organic crosslinkers phase separate back out to two layers. If heating is removed prematurely from an incomplete reaction, sulfur readily crystallises from the oligomer or pre-polymer as the mixture cooled (Figure 2.1). The reaction is a bulk free-radical polymerisation and any un-stabilised radical chains will be able to undergo backbiting (intramolecular reaction) to revert to the more thermodynamically favourable S_8 rings as temperature decreases. Precipitation and phase separation of sulfur results in inhomogeneity in the final polymer and introduces imperfections, affecting chemical stability and mechanical properties. Additionally, during the curing process, bubbles can form in the final polymer, resulting from auto-acceleration.[26] For most crosslinkers reported for inverse vulcanisation, complete polymerisation with sulfur results in highly crosslinked, insoluble solids. Therefore, if functional objects are intended to be produced from these polymers, it is convenient to form the polymer into its final shape during the synthesis itself, rather than re-processing it, in a manner comparable to reactive

injection moulding. What makes this problematic, is the phase separation of the sulfur and crosslinker that occurs in the absence of heating and stirring. This report sets out a method to form homogeneous, pre-polymer solution that can kept for long periods of time and is stable at room temperature. When desired, a final curing stage gives solidification of the material. It can therefore be seen as analogous to widely used current industrial systems like phenolic resins and epoxides where a lower viscosity liquid can be molded or composited before a final cure to thermoset crosslinked material.

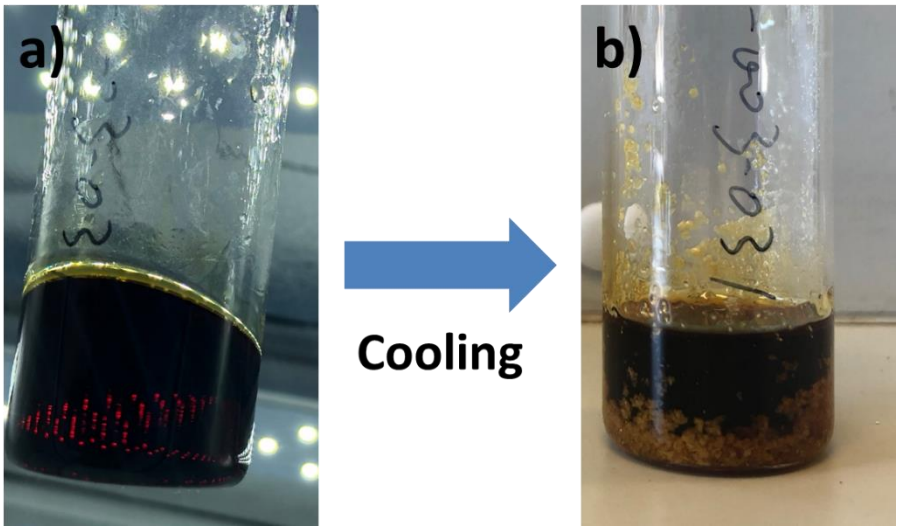

Figure 2.1 (a) Incomplete inverse vulcanisation of sulfur and DCPD taken directly from the heated and stirred reaction. The solution is homogeneous. (b) After cooling for ~ 1 hour a solid yellow precipitate can be seen

2.3 Aims

1. Investigate ternary system, consisting of S_8, DCPD, and EGDMA, in inverse vulcanisation reaction.
2. Investigate the possibility of delayed curing processing, in which prepolymer could be cured after 28 days, in inverse vulcanisation.
3. Investigate the stability of delayed cured thiopolymers.

2.4 Results and discussion

A ternary system, consisting of S_8, DCPD, and EGDMA,[27] was designed as model reaction to optimise inverse vulcanisation processing (Figure 2.2). Ternary co-polymers are often used in modern materials as a way to control and modulate properties. One of the most used ternary systems is ABS, a mixture of acrylonitrile, butadiene and styrene copolymerised to form a highly durable polymeric material. Previously, dynamic covalent polymerisation was reported by Pyun and co-authors. to prepare a terpolymer in two stages,[28,29] preparation of one polymer first and externally addition of another monomer. Additionally, dynamic covalent bonds have also been used to thermally repair damaged thiopolymers,[11,30] demonstrating that S-S bonds exhibit dynamic behaviour at high temperature. The reactivity of different crosslinkers varies.[12] DCPD and EGDMA were chosen as the former is known from previous work to have a higher reactivity with sulfur than the latter,[8] thereby giving potential for a two stage process. Thus, DCPD can be reacted with sulfur initially to generate oligomeric prepolymer chains. These can be reserved at low temperature and later activated thermally to generate radicals for further reaction. These prepolymer chains had enhanced reactivity, and were able to effectively form a crosslinked polymer with EGDMA. It was found that the reaction could be stopped after 8 minutes, stored and the reaction finished at a later date. This enhances the processability of the reaction. The pre-polymer could be preserved in sample vials or transferred to different moulds or containers. After curing at different temperatures and times, all polymers had no crystalline sulfur left and were shape persistent. This process allows for the creation of a resin that may be thermally cured without stirring to complete the polymerisation.

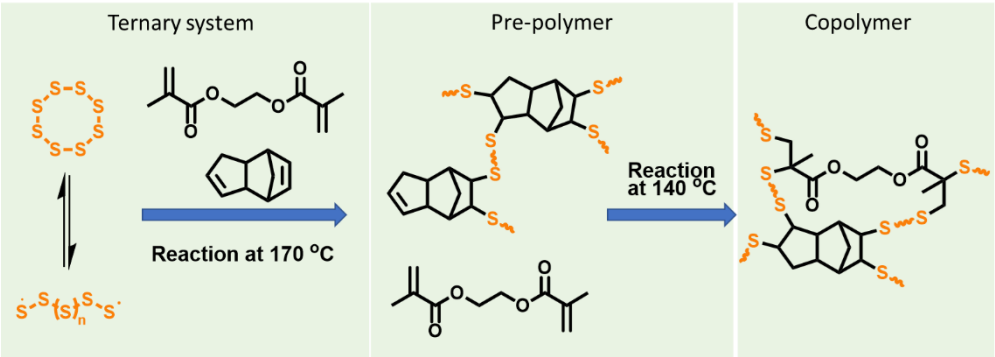

Figure 2.2 The reaction and curing stage of the ternary system consisting of sulfur, DCPD, and EGDMA

A 1:1 weight ratio of DCPD to EGDMA was used as co-crosslinkers in the ternary system with varied sulfur from 50 – 80 wt%. We found that if the weight ratio of sulfur is higher than 70%, sulfur crystals would be precipitated from pre-polymers (shown in Figure 2.3). In order to analyse the reaction much easier, in this paper, we used 1:1:2 (DCPD:EGDMA:S) system. Polymerisations were carried out in open round bottom flasks in aluminium heating blocks set to 170 °C, with stirring provided by 12 mm crossed magnetic stirrer bars. After 8 min a colour transition from brown to black was observed, at this point the reaction was cooled with stirring. (Figure 2.4) Pre-polymers were divided into 5 different sample vials to be cured later (Figure 2.5). The prepolymer was allowed to stand for different times before being cured. In this process

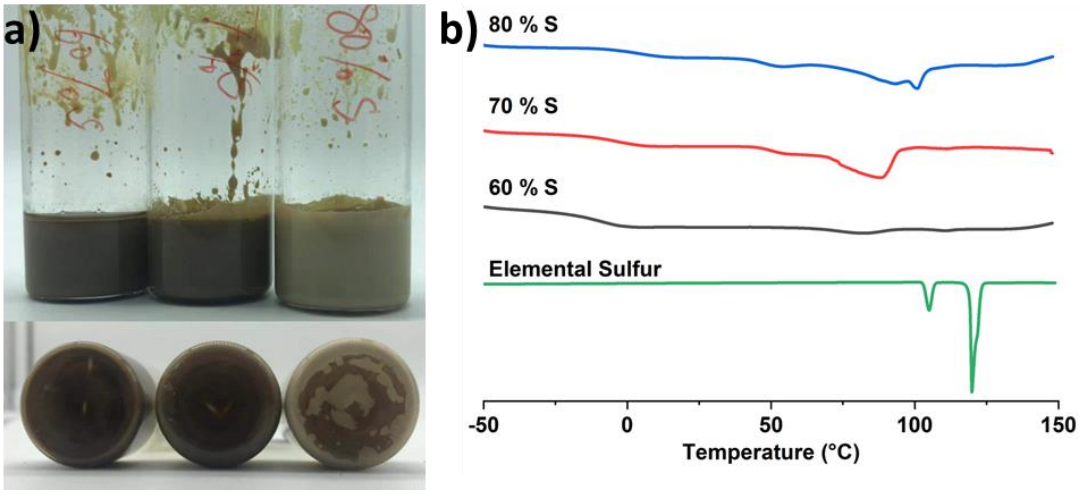

Figure 2.3 (a) photographs of vials of prepolymer: From left to right, prepolymers with 60 wt.%, 70 wt.%, and 80 wt.% sulfur respectively were preserved in room temperature for 7 days. Visibly, phase separation could be observed from the prepolymer with 80% sulfur. (b), DSC traces of these prepolymers and elemental sulfur. Melting peak can be observed in DSC trace of elemental sulfur above 100 °C. A first order transition could also be detected from 70 and 80 wt.% sulfur content prepolymers. At 60 wt.% S content the prepolymer has a clear T_g but no other transition

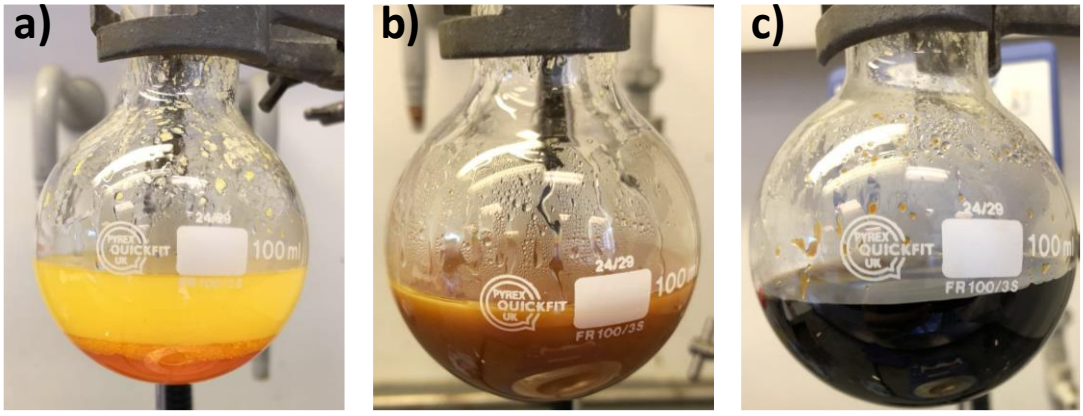

Figure 2.4 (a) Reaction at 3 minutes. (b) Reaction at 5 minutes. (c) Reaction at 8 minutes. The reaction was initially two phases, but transitted to homogeneous after 8 minutes and the coulour of product changed to black.

the sample was reheated and further cured in the oven at 140 °C (Figure 2.6). In the curing stage, once the brown viscous liquid became a black liquid again (in 1-2 minutes), it was transferred to a silicone mould and cured in the oven overnight. In order to compare the effect of comonomer, negative control samples (pre-polymer of poly(S-DCPD) without EGDMA) were synthesized as previously described.[10] Here, the pre-polymer of sulfur, DCPD, and EGDMA was referred as Pre-S-D-E-X, where X is how many days the pre-polymer was reserved and cured after first step reaction; the cured copolymer of corresponding Pre-S-D-E-X was referred as S-D-E-X. Similar, Pre-S-D and S-D were used to refer the pre-polymer and cured polymer of sulfur and DCPD individually.

Figure 2.5 Reserved prepolymers ready for delayed curing

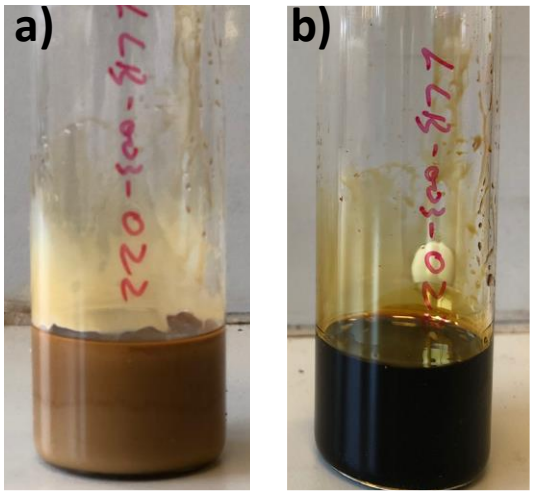

Figure 2.6 (a) Reserved pre-polymer Pre-S-D-E-14. (b) Reheated prepolymer Pre-S-D-E-14.

The stability of pre-polymers prepared from different systems was investigated. It could be observed visually that sulfur crystals had precipitated from the cooled down binary system, Pre-S-D, however, compared with that, on cooling the pre-polymer of the ternary system, Pre-S-D-E-0, became opaque, but remained as one phase, without precipitation of a separate solid sulfur phase. With further investigations conducted by

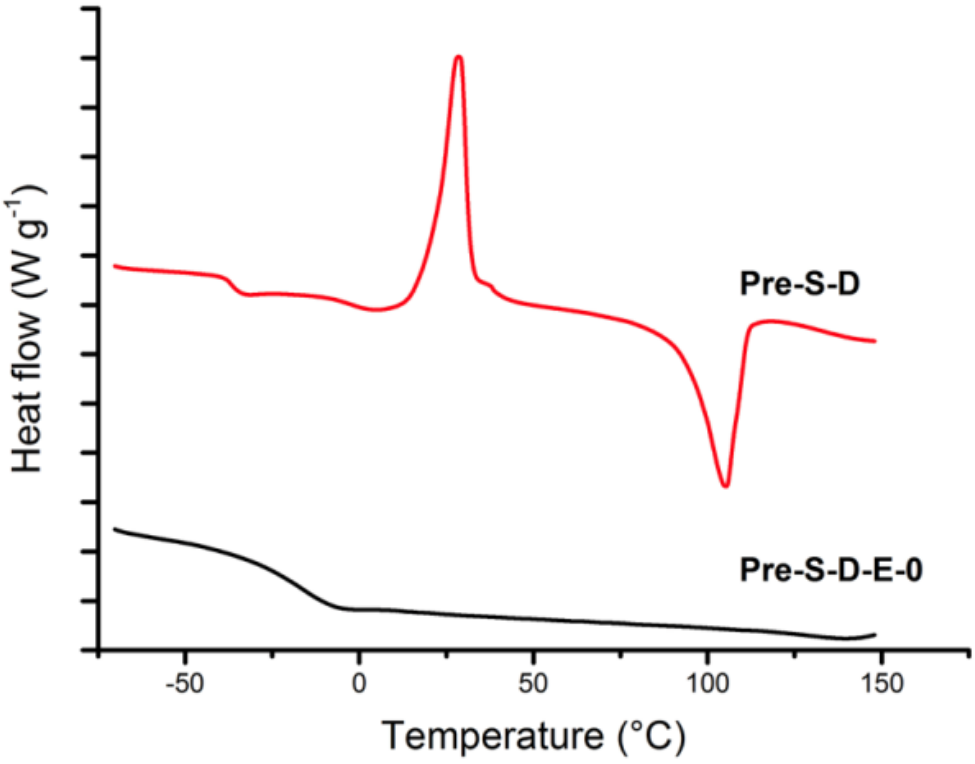

Figure 2.7 DSC traces for prepolymer Pre-S-D and ternary system prepolymer Pre-S-E-0. Crystallisation and melting temperature of sulfur were detected from trace of Pre-S-D; only glass transition temperature was observed in prepolymer Pre-S-D-E-0.

Differential Scanning Calorimetry (DSC), the traces shown in Figure 2.7 demonstrate the glass transition temperatures of both Pre-S-D and Pre-S-D-E-0: -40 °C and -25°C respectively, demonstrating oligomer formation. However, sulfur crystallisation and melting temperature of sulfur can be observed from Pre-S-D, indicating precipitation of crystalline sulfur, whereas there is no more first order transition presented in Pre-S-D-E-0, demonstrating there is no crystalline sulfur. The kinetics of the ternary system was monitored by nuclear magnetic resonance spectroscopy (NMR) during the initial reaction and curing stage, shown from Figure 2.8 to Figure 2.11. However, as crosslink density increased the solubility of the polymer decreased. Initially individual peaks indicative of both DCPD and EGDMA are detected. Compared with the reference of pure DCPD and EGDMA (shown in Figure 2.12), in 3 minutes, small peaks at 3.5 ppm were identified as S-C-H protons. More importantly, from 3 minutes to 7 minutes,

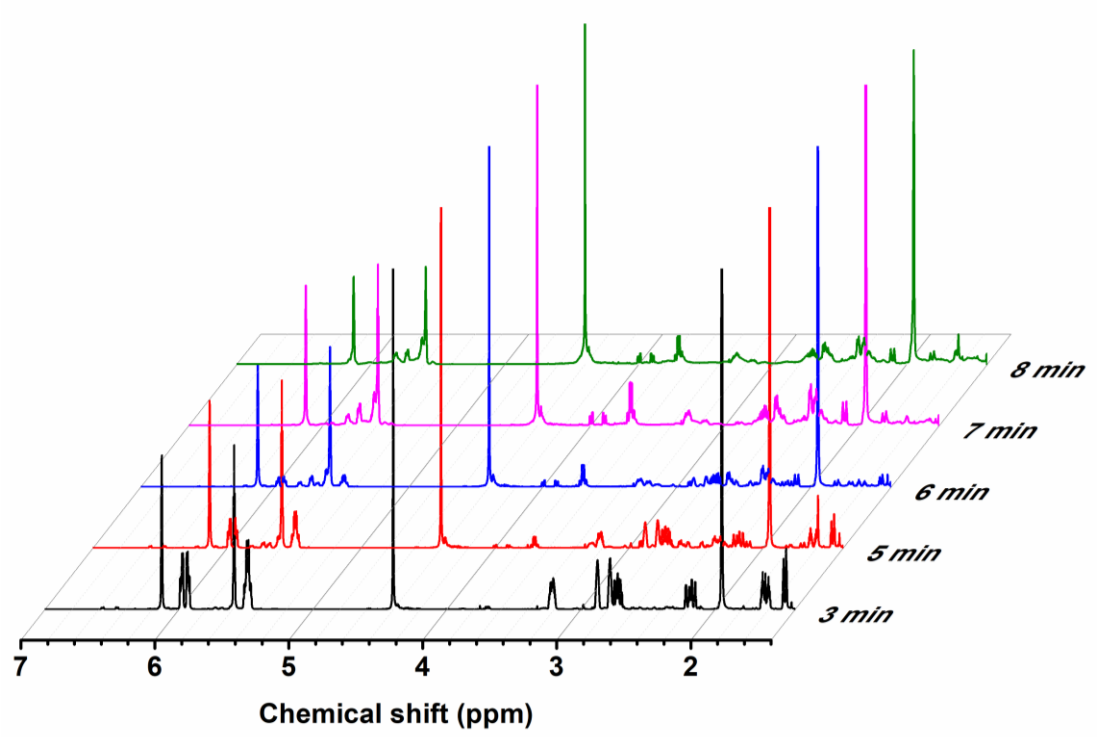

Figure 2.8 Spectra taken in the stirred reaction stage. From bottom to top, the spectra are reaction at 3 min, 5 min, 6 min, 7min, and 8min.

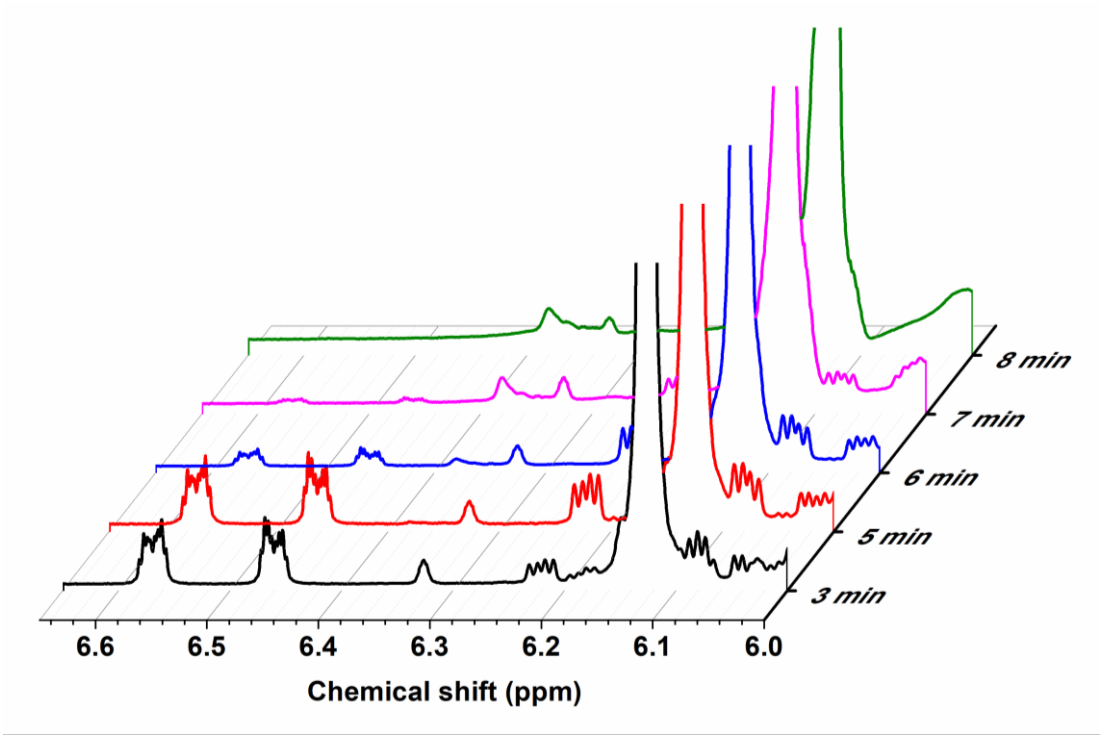

Figure 2.9 Spectra taken in the stirred reaction stage. From bottom to top, the spectra are reaction at 3 min, 5 min, 6 min, 7min, and 8min.

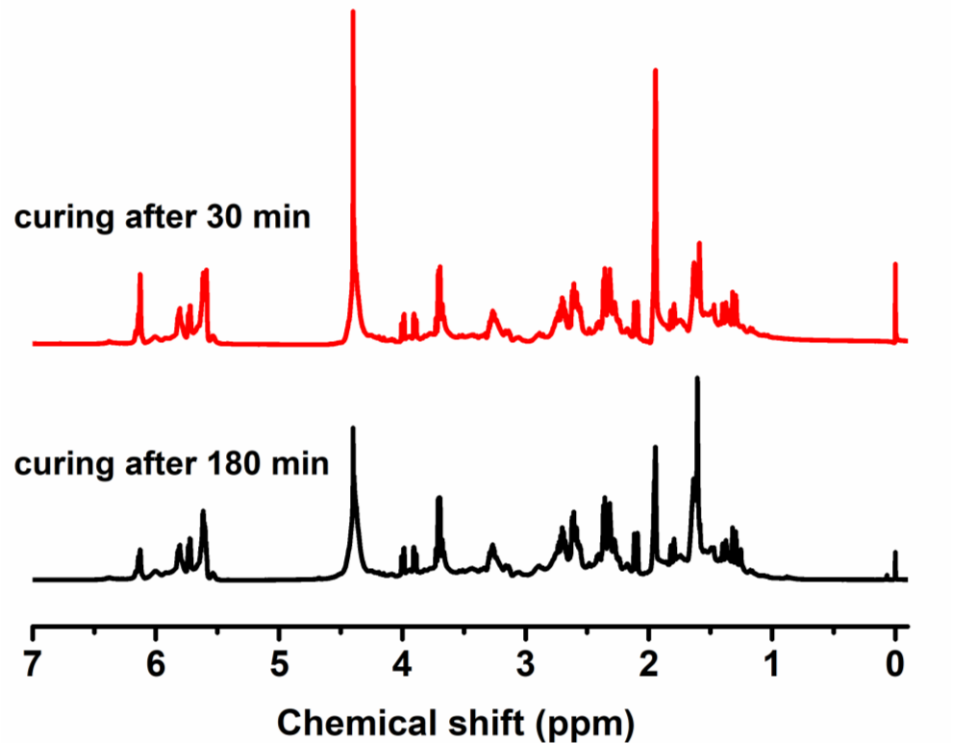

Figure 2.10 Spectra taken during the curing stage. From top to bottom, the spectra are polymers cured for 30 minutes and further cured after 3 hours.

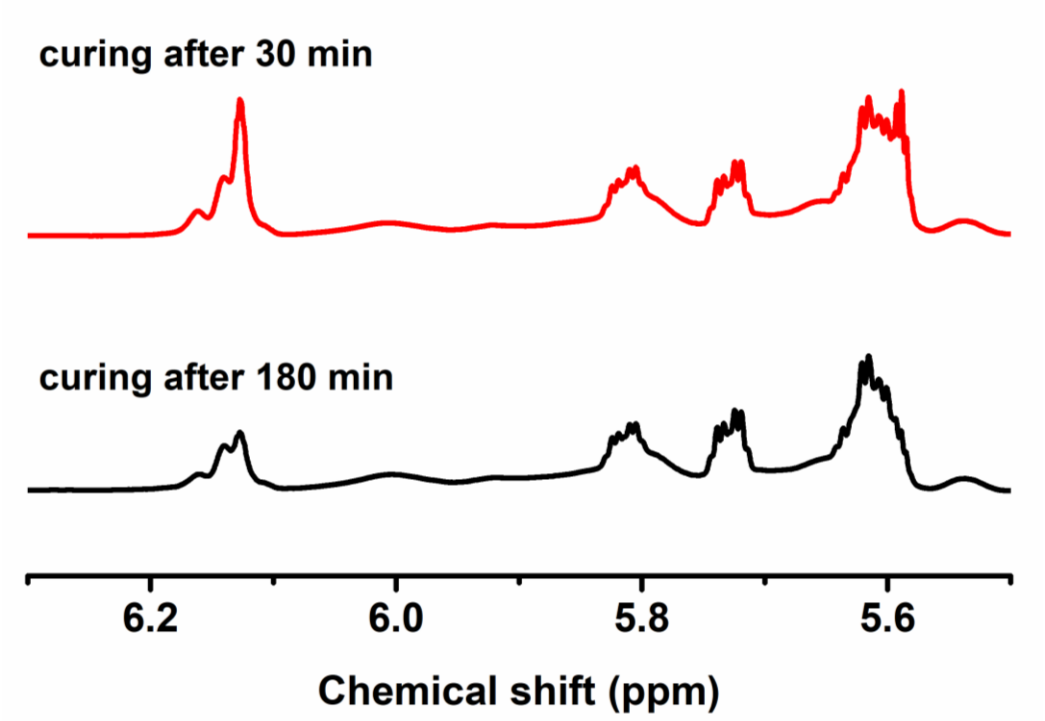

Figure 2.11 Spectra taken during the curing stage. From top to bottom, the spectra are polymers cured for 30 minutes and further cured after 3 hours.

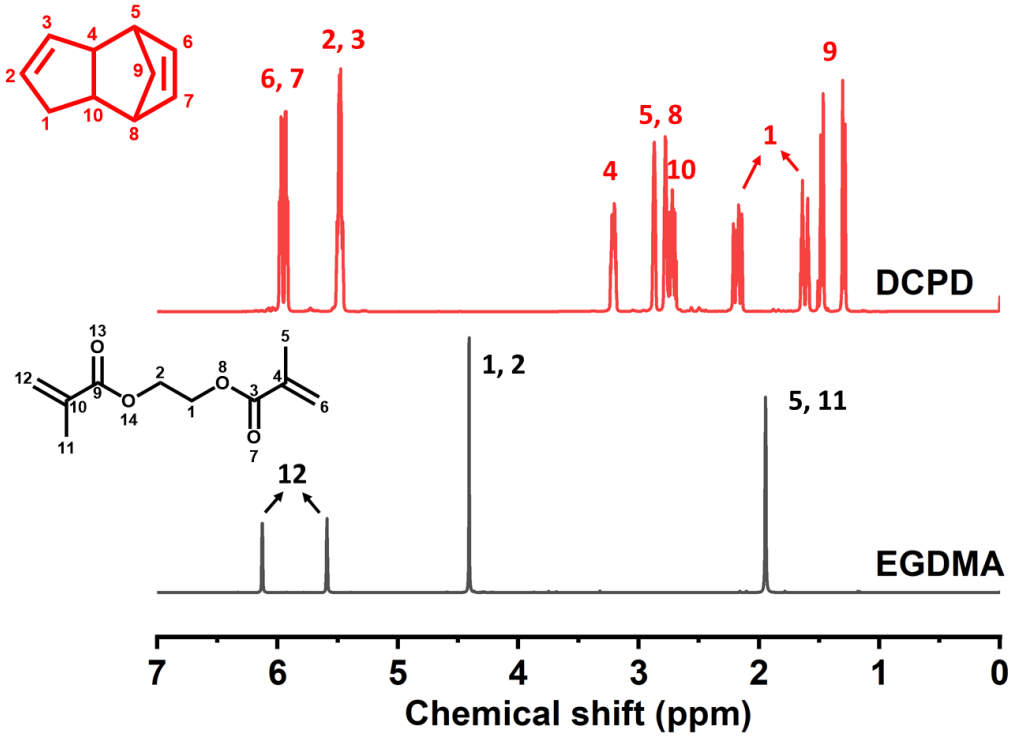

Figure 2.12 ^{1}H NMR spectrum of standard DCPD and EGDMA. All peaks were assigned in corresponding numbers.

peaks at 6.5 ppm were evidential of an α-proton sulfur substitution reaction on the DCPD, as the peak was shifted downfield. It was found that the EGDMA had not reacted at this point. During the reaction it was observed that the peaks (at 5.5 ppm and 5.9 ppm) corresponding to the C=C-H protons of DCPD decreased and, finally, disappeared. The spectra showed that peaks in the 3.5–4 ppm region increased, showing an increase of S-C-H protons. Furthermore, because of the substitution of sulfur, peaks corresponding to the initial CH_2 decreased and shifted downfield. By the end of the reaction, most previous sharp peaks belonging to DCPD became broad, suggesting generation of oligomers from the inverse vulcanisation of sulfur and DCPD. Further confirmation was conducted by gel permeation chromatography (GPC) that the molecular weight of prepolymer is M_w= 955 g mol^{-1} and M_w/M_n = 4.641 (shown in Figure 2.13). However, we suppose that the molecular weight of prepolymer could be higher than what was tested, because when the pre-polymer was dissolved in THF,

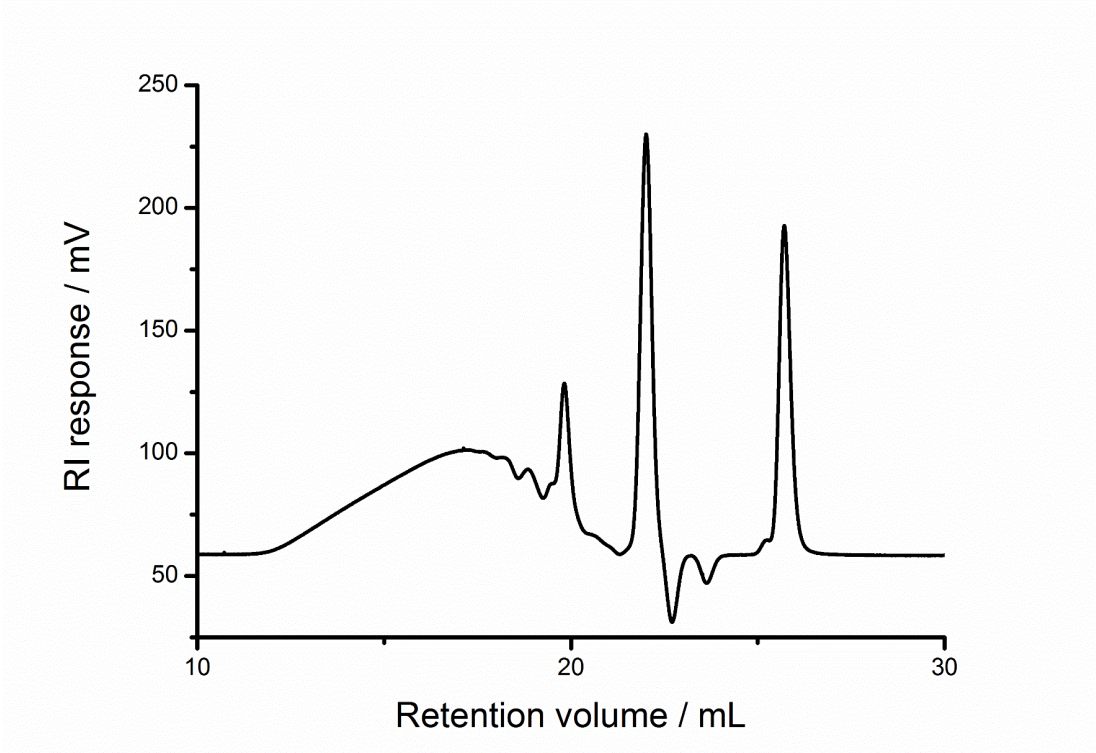

Figure 2.13 GPC trace for prepolymer Pre-S-D-E in THF. Oligomers could be observed with low molecular weight and broad polydispersity.

back-biting of long dangling sulfur chains may occur, generating elemental sulfur and dissolved in THF directly (shown in Figure 2.14). In contrast, four main peaks corresponding protons of EGDMA changed little, suggesting that EGDMA reacted little in this phase of the reaction. In the delayed curing stage, the change of EGDMA was evident when comparing the initial state of pre-polymer and after 3 hours of curing. First of all, the peaks at 5.6 and 6.3 ppm corresponding to C=C bonds of EGDMA decreased, indicating the reaction of double bonds. Additionally, the broadening of the peak at 4.4 ppm further indicated polymer formation.

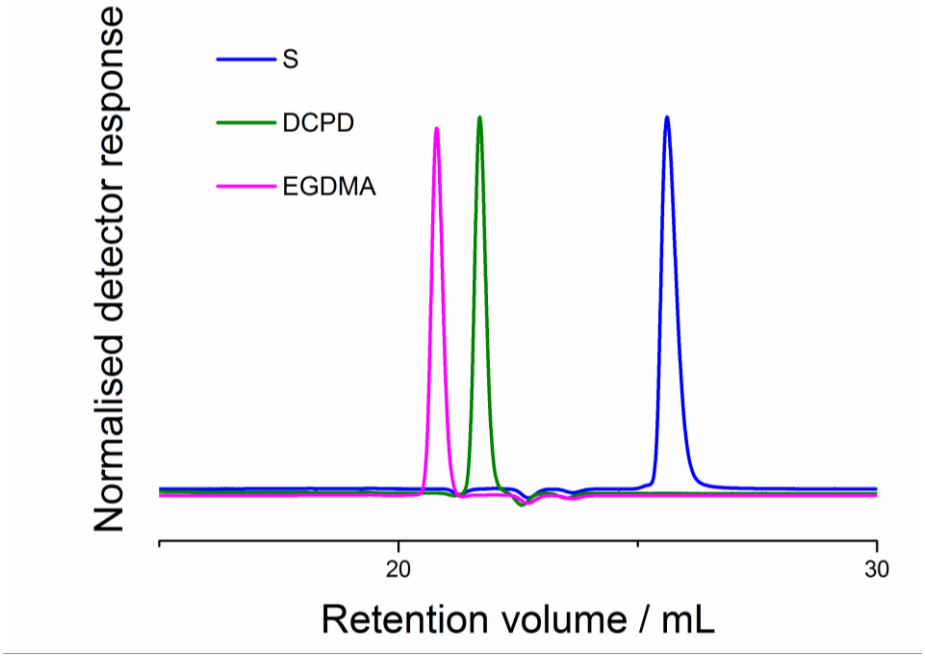

Figure 2.14 Crosslinkers and elemental sulfur were also tested through GPC to compare to the trace of the prepolymer. The organic crosslinker peaks do not directly match any of the peaks observed for the pre-polymer (Figure 2.13), though they could be slightly shifted due to the presence of the polymer. In comparison, the NMR shows no DCPD, but does show remaining EGDMA, therefore the sharp peaks in the GPC shown in Figure 2.13 could be due to unreacted crosslinkers or low molecular weight oligomers. The sulfur peak could be matched with the peak from prepolymer, suggesting that sulfur may precipitate from the THF solution due to back-biting of dangling sulfur chains.

All terpolymer samples cured from different delay phases exhibited homogeneous morphology, good shape persistence, full conversion, and had no evidence of phase separation (Figure 2.15). Surfaces of all cured samples were smooth without bubbling, indicating that during the curing step no auto-acceleration had occurred.

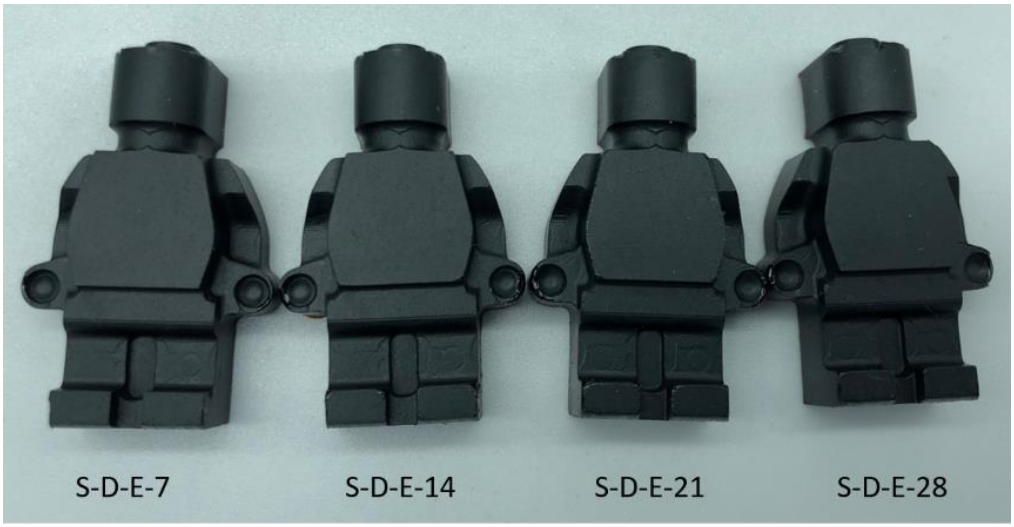

Figure 2.15 Moulded samples prepared from corresponding prepolymers after 7 days, 14 days, 21 days, and 28 days, from left to right. The dimension of the samples is 25 mm × 40 mm.

Auto-acceleration, also known as the Trommsdorff–Norrish effect or the gel effect, in inverse vulcanisation is a major challenge in upscaling in both the lab and industry. The auto-acceleration was alleviated effectively in the ternary system, because it could be supposed that unreacted EGDMA dispersed well in the thick polymer solution or pre-polymer, and acted as plasticizers as well. The small molecules increased the mobility of all the system so that greatly improved heat dissipation. To test this hypothesis, ethylene glycol diacetate (EGDA) was used to substitute EGDMA as a non-polymerisable counterpart. The EGDA was still able to prevent sulfur precipitation and auto-acceleration, though because of lower miscibility, some phase separation occurred after reaction (shown in Figure 2.16).

Figure 2.16 EGDMA was substituted by EGDA to test the role of plasticizers. From the testing, we found that no sulfur was precipitated and there was no autoacceleration during the reaction. However, a lower miscibility of the EGDA resulted in it separation out to a lighter surface layer.

In order to further confirm that all S_8 has reacted after curing and the stability of cured polymers, powder X-ray diffraction (PXRD) patterns were recorded of all delayed curing samples as shown in Figure 2.17. All delayed curing polymers showed no sharp peak that correspond to crystalline sulfur. Also, the broad peaks of different samples indicated the amorphous state of different fully cured polymers.

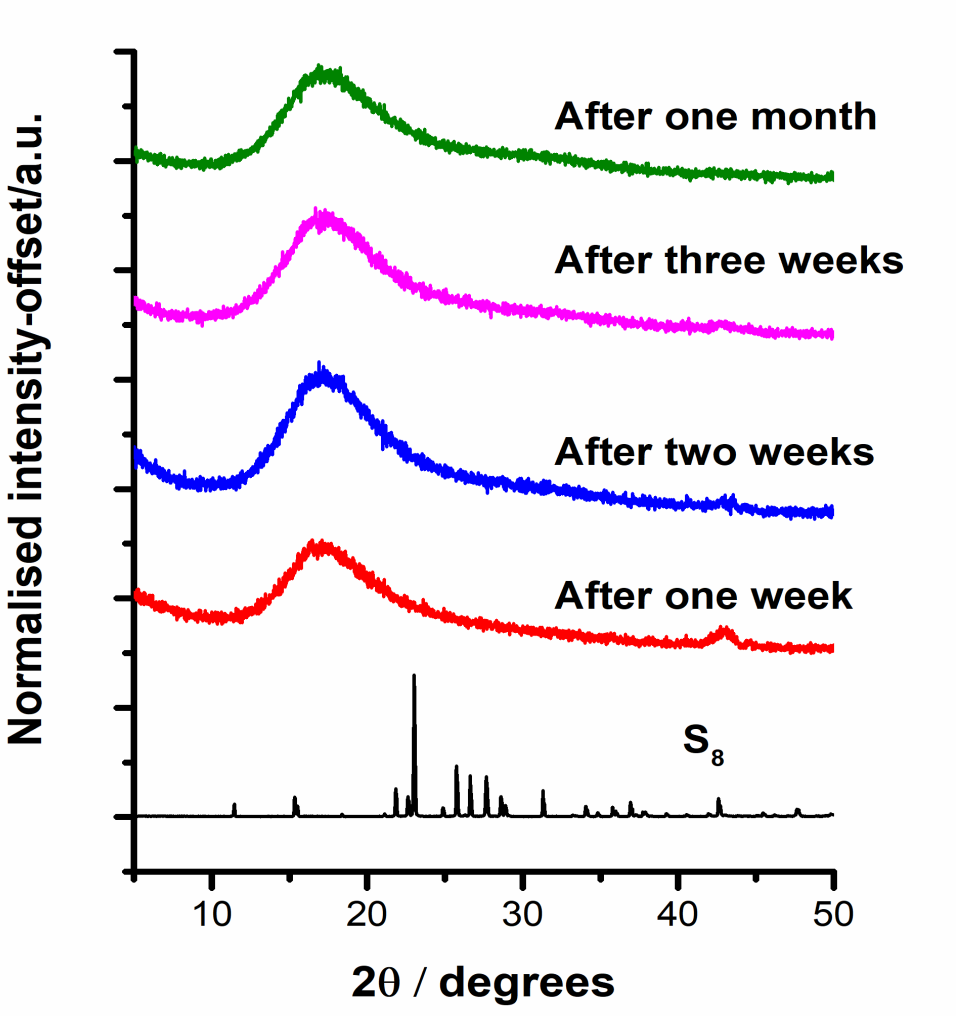

Figure 2.17 Offset PXRD patterns of samples cured from different delayed phases, S_8 crystal was not observed in any samples.

Moreover, DSC thermograms were performed on all cured samples, as shown in Figure 2.18. From the DSC traces, there was no first order transition identified, which is indicative of no S_8 crystals embedded in the produced polymers. Glass transition temperatures (T_g) of four samples cured at different delayed phases were also tested at same rate of increasing temperature.

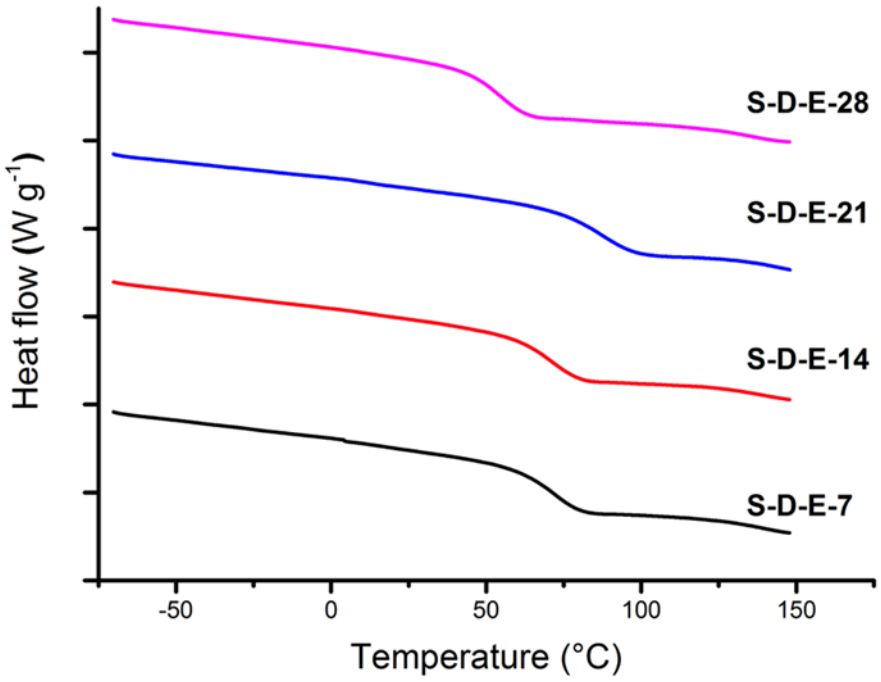

Figure 2.18 Offset DSC traces of samples cured from different delayed phases, no S8 crystal was observed and the glass transition temperature of polymers were stable at around 55 °C

The results of them were similar, in a range from 50 to 55°C, suggesting the stability of pre-polymers and cured polymers. Additionally, only one T_g was present, suggesting a homogeneous copolymer, and further confirmed by the visual morphology of the samples (Figure 2.4). Thermogravimetric analysis (Figure 2.19) of all of the final cured polymers showed similar char mass, and no decomposition below 200 °C. Elemental analysis (Table 2.1) of the cured polymers is close to the expected values, with a slight excess of sulfur, likely because differences in volatility of the organic and inorganic components during reaction and curing.

Table 2.1 Elemental analysis of delayed curing polymers

	Calc %			Analysis		
	% C	% H	% S	% C	% H	% S
S-D-E-7	37.80	4.00	50.00	36.25	3.93	53.90
S-D-E-14	37.80	4.00	50.00	36.34	3.91	53.46
S-D-E-21	37.80	4.00	50.00	36.45	3.94	53.30
S-D-E-28	37.80	4.00	50.00	36.25	3.90	53.55

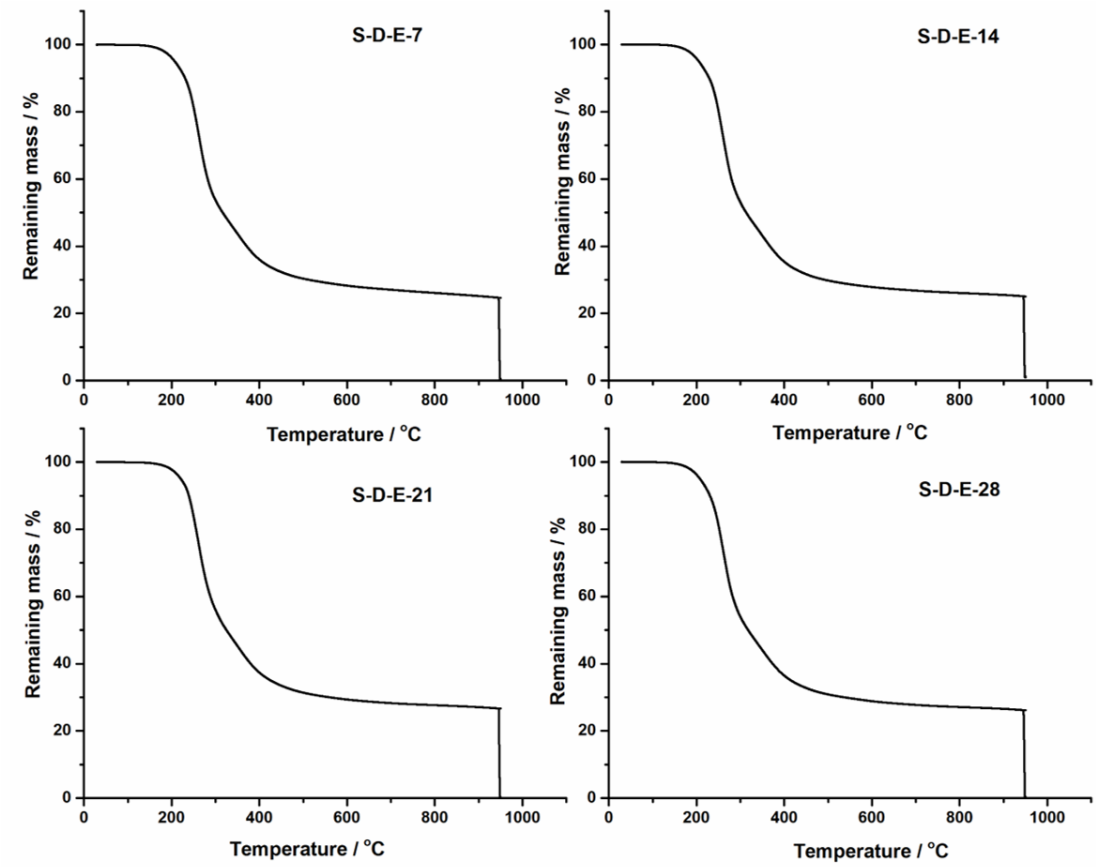

Figure 2.19 Thermogravimetric analysis of inverse vulcanisation polymers cured from corresponding pre-polymers. TGA thermograms showed all polymers had similar decomposition temperature and char mass remaining.

2.5 Conclusions

In summary, a ternary system was studied for the delayed curing of inverse vulcanised polymers. Because the reactivity of EGDMA is lower than DCPD in this reaction, EGDMA did not react until curing stage. EGDMA molecules appear to stabilise oligomers in the pre-polymer, and prohibit depolymerisation and precipitation of sulfur. In the curing stage, unreacted EGDMA acted as plasticizer, resulting in increasing the mobility of the system and as a heat sink. Therefore, this ternary system provided a solution to prevent exothermic auto-acceleration, and made it possible to preserve pre-polymer solution for more than one month with little change to produce highly crosslinked polymers. It is our hope that this process will help for the industrial scale up for inverse vulcanised polymers and provides some insight into a new area of research.

2.6 Experimental

2.6.1 Materials

Sulfur (S_8, sublimed powder, reagent grade, ⩾ 99.5%, Brenntag UK & Ireland. Purchased in 25 kg bags), ethylene glycol dimethylacrylate (EGDMA, 98%, Alfa Aesar), ethylene glycol diacetate (EGDA, 99% SigmaAldrich), dicyclopentadiene (DCPD >95%, TCI), chloroform-d ($CDCl_3$, Cambridge Isotope Laboratories Inc.)

2.6.2 Method

Synthesis of crosslinked polymers

Reactants (sulfur and crosslinkers (used as received), 10 g in total, as the weight ratio of 1:1:2 for DCPD: EGDMA:S) were mixed in 40 mL volume glass vials. The mixture was stirred at 170 °C in aluminium blocks and stirred by magnetic stirrer bars with stirring speed of 1000 rpm, and reacted for 8 mins. When the reaction had changed to thick dark brown liquid, the prepolymer was transferred into 5 different sample vials to be cured later. The first prepolymer was cured at 140 °C in the oven, and the rest samples were cured from different delay phases (7 days, 14 days, 21 days, and 28 days), individually, at 140 °C in the oven.

2.6.3 Characterisation methods

Powder X-ray Diffraction (PXRD). Data was measured using a PANalytical X'Pert PRO diffractometer with Cu-K_α radiation, operating in transmission geometry.

Differential Scanning Calorimetry (DSC). DSC were performed on a TA Instruments Q200 DSC, under nitrogen flow, and with heating and cooling rates of 5 °C min^{-1}.

Nuclear magnetic resonance (NMR). The reactions were monitor by solution NMR in deuterated chloroform, and recrystallized catalysts were performed by solution NMR in $CDCl_3$, using a Bruker Advance DRX (400 MHz) spectrometer.

Gel permeation chromatography (GPC): The molecular weight of the soluble fraction of the polymers was determined by gel permeation chromatography (GPC) using a Viscotek system comprising a GPCmax (degasser, eluent and sample delivery system), and a TDA302 detector array, using THF as eluent.

Thermal gravitational analysis (TGA): TGA was carried out in platinum pans using a Q5000IR analyzer (TA Instruments) with an automated vertical overhead thermobalance. The samples were heated at 10 °C min^{-1} to 950 °C under nitrogen.

2.7 References

(1) Schmidt, M. The Scientific Basis for Practical Applications of Elemental Sulfur. In *New Uses of Sulfur*; 1978; pp 1–12.

(2) Abdel-Mohsen Onsy, Mohamed; Maisa, E.-G. Sulfur Concrete for the Construction Industry– a Sustainable Development Approach. *J. Ross Publ.* **2010**.

(3) Hasell, T.; Parker, D. J.; Jones, H. A.; McAllister, T.; Howdle, S. M. Porous Inverse Vulcanised Polymers for Mercury Capture. *Chem. Commun.* **2016**, *52* (31), 5383–5386.

(4) Worthington, M. J. H.; Kucera, R. L.; Chalker, J. M. Green Chemistry and Polymers Made from Sulfur. *Green Chem.* **2017**, *19* (12), 2748–2761.

(5) Chung, W. J.; Griebel, J. J.; Kim, E. T.; Yoon, H.; Simmonds, A. G.; Ji, H. J.; Dirlam, P. T.; Glass, R. S.; Wie, J. J.; Nguyen, N. A.; Guralnick, B. W.; Park, J.; Somogyi, Á.; Theato, P.; Mackay, M. E.; Sung, Y.; Char, K.; Pyun, J. The Use of Elemental Sulfur as an Alternative Feedstock for Polymeric Materials. *Nat. Chem.* **2013**, *5* (6), 518–524.

(6) Crockett, M. P.; Evans, A. M.; Worthington, M. J. H.; Albuquerque, I. S.; Slattery, A. D.; Gibson, C. T.; Campbell, J. A.; Lewis, D. A.; Bernardes, G. J. L.; Chalker, J. M. Sulfur-Limonene Polysulfide: A Material Synthesized Entirely from Industrial By-Products and Its Use in Removing Toxic Metals from Water and Soil. *Angew. Chemie Int. Ed.* **2016**, *55* (5), 1714–1718.

(7) Griebel, J. J.; Glass, R. S.; Char, K.; Pyun, J. Polymerizations with Elemental Sulfur: A Novel Route to High Sulfur Content Polymers for Sustainability, Energy and Defense. *Prog. Polym. Sci.* **2016**, *58*, 90–125.

(8) Wu, X.; Smith, J. A.; Petcher, S.; Zhang, B.; Parker, D. J.; Griffin, J. M.; Hasell, T. Catalytic Inverse Vulcanization. *Nat. Commun.* **2019**, *10* (1), 647.

(9) Gomez, I.; Leonet, O.; Blazquez, J. A.; Mecerreyes, D. Inverse Vulcanization of Sulfur Using Natural Dienes as Sustainable Materials for Lithium–Sulfur Batteries. *ChemSusChem* **2016**, *9* (24), 3419–3425.

(10) Parker, D. J.; Jones, H. A.; Petcher, S.; Cervini, L.; Griffin, J. M.; Akhtar, R.; Hasell, T. Low Cost and Renewable Sulfur-Polymers by Inverse Vulcanisation, and Their Potential for Mercury Capture. *J. Mater. Chem. A* **2017**, *5* (23), 11682–11692.

(11) Parker, D. J.; Chong, S. T.; Hasell, T. Sustainable Inverse-Vulcanised Sulfur Polymers. *RSC Adv.* **2018**, *8* (49), 27892–27899.

(12) Smith, J. A.; Wu, X.; Berry, N. G.; Hasell, T. High Sulfur Content Polymers: The Effect of Crosslinker Structure on Inverse Vulcanization. *J. Polym. Sci. Part A Polym. Chem.* **2018**, *56* (16), 1777–1781.

(13) Zhang, Y.; Griebel, J. J.; Dirlam, P. T.; Nguyen, N. A.; Glass, R. S.; Mackay, M. E.; Char, K.; Pyun, J. Inverse Vulcanization of Elemental Sulfur and Styrene for Polymeric Cathodes in Li-S Batteries. *J. Polym. Sci. Part A Polym. Chem.* **2017**, *55* (1), 107–116.

(14) Boyd, D. A.; Baker, C. C.; Myers, J. D.; Nguyen, V. Q.; Drake, G. A.; McClain, C. C.; Kung, F. H.; Bowman, S. R.; Kim, W.; Sanghera, J. S. ORMOCHALCs: Organically Modified Chalcogenide Polymers for Infrared Optics. *Chem. Commun.* **2017**, *53* (1), 259–262.

(15) Anderson, L. E.; Kleine, T. S.; Zhang, Y.; Phan, D. D.; Namnabat, S.; LaVilla, E. A.; Konopka, K. M.; Ruiz Diaz, L.; Manchester, M. S.; Schwiegerling, J.; Glass, R. S.; Mackay, M. E.; Char, K.; Norwood, R. A.; Pyun, J. Chalcogenide Hybrid Inorganic/Organic Polymers: Ultrahigh Refractive Index Polymers for Infrared Imaging. *ACS Macro Lett.* **2017**, *6* (5), 500–504.

(16) Gupta, V.; Ghosh, S.; Phapale, V. Polymerization of Elemental Sulfur with Various Divinyl and Diallyl Monomers and Properties of the Copolymers. *Phosphorus. Sulfur. Silicon Relat. Elem.* **2018**, *193* (11), 752–758.

(17) Deng, Z.; Hoefling, A.; Théato, P.; Lienkamp, K. Surface Properties and Antimicrobial Activity of Poly(Sulfur- Co -1,3-Diisopropenylbenzene) Copolymers. *Macromol. Chem. Phys.* **2018**, *219* (5), 1700497.

(18) Mann, M.; Kruger, J. E.; Andari, F.; McErlean, J.; Gascooke, J. R.; Smith, J. A.; Worthington, M. J. H.; McKinley, C. C. C.; Campbell, J. A.; Lewis, D. A.;

Hasell, T.; Perkins, M. V.; Chalker, J. M. Sulfur Polymer Composites as Controlled-Release Fertilisers. *Org. Biomol. Chem.* **2019**, *17* (7), 1929–1936.

(19) Chung, W. J.; Simmonds, A. G.; Griebel, J. J.; Kim, E. T.; Suh, H. S.; Shim, I.-B.; Glass, R. S.; Loy, D. A.; Theato, P.; Sung, Y.-E.; Char, K.; Pyun, J. Elemental Sulfur as a Reactive Medium for Gold Nanoparticles and Nanocomposite Materials. *Angew. Chemie Int. Ed.* **2011**, *50* (48), 11409–11412.

(20) Worthington, M. J. H.; Shearer, C. J.; Esdaile, L. J.; Campbell, J. A.; Gibson, C. T.; Legg, S. K.; Yin, Y.; Lundquist, N. A.; Gascooke, J. R.; Albuquerque, I. S.; Shapter, J. G.; Andersson, G. G.; Lewis, D. A.; Bernardes, G. J. L.; Chalker, J. M. Sustainable Polysulfides for Oil Spill Remediation: Repurposing Industrial Waste for Environmental Benefit. *Adv. Sustain. Syst.* **2018**, *2* (6), 1800024.

(21) Thielke, M.; Bultema, L.; Brauer, D.; Richter, B.; Fischer, M.; Theato, P. Rapid Mercury(II) Removal by Electrospun Sulfur Copolymers. *Polymers (Basel).* **2016**, *8* (7), 266.

(22) Lundquist, N. A.; Worthington, M. J. H.; Adamson, N.; Gibson, C. T.; Johnston, M. R.; Ellis, A. V.; Chalker, J. M. Polysulfides Made from Re-Purposed Waste Are Sustainable Materials for Removing Iron from Water. *RSC Adv.* **2018**, *8* (3), 1232–1236.

(23) Akay, S.; Kayan, B.; Kalderis, D.; Arslan, M.; Yagci, Y.; Kiskan, B. Poly(Benzoxazine- Co -Sulfur): An Efficient Sorbent for Mercury Removal from Aqueous Solution. *J. Appl. Polym. Sci.* **2017**, *134* (38), 45306.

(24) Abraham, A. M.; Kumar, S. V.; Alhassan, S. M. Porous Sulphur Copolymer for Gas-Phase Mercury Removal and Thermal Insulation. *Chem. Eng. J.* **2018**, *332* (May 2017), 1–7.

(25) Lundquist, N. A.; Sweetman, M. J.; Scroggie, K. R.; Worthington, M. J. H.; Esdaile, L. J.; Alboaiji, S. F. K.; Plush, S. E.; Hayball, J. D.; Chalker, J. M. Polymer Supported Carbon for Safe and Effective Remediation of PFOA- and PFOS-Contaminated Water. *ACS Sustain. Chem. Eng.* **2019**, *7* (13), 11044–11049.

(26) Young, R. J.; Lovell, P. A. *Introduction to Polymers*; 2011.

(27) Smith, J. A.; Green, S. J.; Petcher, S.; Parker, D. J.; Zhang, B.; Worthington, M. J. H.; Wu, X.; Kelly, C. A.; Baker, T.; Gibson, C. T.; Campbell, J. A.; Lewis, D. A.; Jenkins, M. J.; Willcock, H.; Chalker, J. M.; Hasell, T. Crosslinker Co-Polymerisation for Property Control in Inverse Vulcanisation. *Chem. - A Eur. J.* **2019**.

(28) Zhang, Y.; Konopka, K. M.; Glass, R. S.; Char, K.; Pyun, J. Chalcogenide Hybrid Inorganic/Organic Polymers (CHIPs) via Inverse Vulcanization and Dynamic Covalent Polymerizations. *Polym. Chem.* **2017**, *8* (34), 5167–5173.

(29) Glass, R. S.; Zhang, Y.; Char, K.; Pavlopoulos, N. G.; Karayilan, M.; Kleine, T. S.; Pyun, J. Nucleophilic Activation of Elemental Sulfur for Inverse Vulcanization and Dynamic Covalent Polymerizations. *J. Polym. Sci. Part A Polym. Chem.* **2018**, *57* (1), 7–12.

(30) Griebel, J. J.; Nguyen, N. A.; Namnabat, S.; Anderson, L. E.; Glass, R. S.; Norwood, R. A.; Mackay, M. E.; Char, K.; Pyun, J. Dynamic Covalent Polymers via Inverse Vulcanization of Elemental Sulfur for Healable Infrared Optical Materials. *ACS Macro Lett.* **2015**, *4* (9), 862–866.

Chapter 3. Mercury capture with an inverse vulcanized polymer formed from garlic oil, a bioderived comonomer

3.1 Context

3.1.1 Abstract

The refining of petroleum feedstocks has produced a surplus of the by-product elemental sulfur that is currently underused and is therefore, extremely low cost. The combination of sulfur with organic crosslinking units by inverse vulcanisation polymerisation, provides a route to low cost materials with a wide array of potential applications. To fully exploit the availability of elemental sulfur and to allow the product polymers to align well with the principles of green chemistry, a renewable crosslinker is desirable. Reported here is a polymer formed from inverse vulcanisation, produced from industrial waste sulfur, and bio-derived garlic oil blend. This polymer has tuneable properties when blended with another industrial waste product, dicyclopentadiene. These polymers were found to have a high affinity to capture mercury, particularly for low mercury concentrations where other sorbents are often not effective. It is these low concentrations that are most industrially relevant and important for environmental and health concerns as even low concentrations of toxic mercury can have cumulative and severe consequences. Crucially, these ternary polymer systems are mechanically robust due to their increased glass transition temperatures and hardness values, making them viable for practical applications.

3.1.2 Publication

Bowen Zhang*, **Liam J. Dodd**, **Peiyao Yan**, **Tom Hasell***, Mercury capture with an inverse vulcanized polymer formed from garlic oil, a bioderived comonomer, *Reactive and Functional Polymers*. 161 (2021) 104865.

3.1.3 Author contributions

Bowen Zhang: Conceptualization; Data curation; Formal analysis; Investigation; Methodology; Validation; Visualization; Writing - original draft; Writing - review & editing. **Liam J. Dodd** and **Peiyao Yan**: Formal analysis; Writing - review & editing. **Tom Hasell**: Conceptualization; Funding acquisition; Project administration; Resources; Supervision; Writing - review & editing.

3.2 Introduction

As the awareness of human impact on the environment increases, not just in governments but also individuals, sustainable or renewable materials have been increasingly explored in order to reduce "plastic pollution".[1,2] Plastic pollution mainly refers to the negative effects on the environment by accumulation of conventional synthetic polymers, which are derived from petrochemicals and cannot be easily degraded. Therefore, a novel process, reducing the dependence on the limited petrochemicals, is desirable to replace conventional polymers synthesis and decrease the carbon footprint. Because of more than 50 wt% sulfur content, inversed vulcanised polymers were considered as a promising new material to decrease the usage of traditional petrochemical feedstocks. The background of sulfur productions and the applications of inversed vulcanised polymers have already been covered in more detail in the previous chapters, but to recap this briefly here.

Elemental sulfur is a by-product from the petrochemicals industry, however, the supply of sulfur outstrips the demand, leading to the surplus sulfur being stockpiled open to air next to fuel refineries.[3-7] Furthermore, as increasing amounts of fossil fuels are consumed, energy resources more heavily polluted with sulfur are exploited, such as tar sands and heavy oils, resulting in the surplus sulfur stockpiles growing at an increasingly rapid rate.[8] Admittedly, redundant sulfur appears to have limited effect on the environment, though this requires further study, but there is a potential safety issue of the often large, open air stockpiles of sulfur because it is flammable.[9] Considering sulfur is incredibly cheap and readily available to be used, therefore, an industrial process using large amounts of sulfur as a feedstock is desirable.[4,10]

Polymeric sulfur can be easily synthesized by heating elemental sulfur above 159 °C, as shown in Figure 1.4.[4,6,7] However, polymeric sulfur suffers from instability and depolymerizes back to S_8 monomers, even at room temperature. In order to synthesize stable high sulfur content polymers, recently, inverse vulcanization was studied and developed because of its facile reaction processing and high atom efficiency.[5,7,11,12] Depending upon the chemical and mechanical properties of these materials, inverse vulcanised polymers were applied in heavy metal uptake [4,10,13,14], IR transparent lenses,[15–17] fertilizer release,[18] adhesive application,[19,20] repairable materials,[20,21] Li-S

batteries,[22–25] oil–water separation,[26] sustainable and recyclable composites,[27,28] and antibacterial materials.[29]

In the early study, the new crosslinkers, which can be reacted to generate stable and functional thiopolymers, were the focus of inverse vulcanization. Therefore, a variety of crosslinkers have been studied since 2013 when the reaction of 1,3-diisopropenylbenzene (DIB) with sulfur was reported and first termed as inverse vulcanization.[7] Although, crosslinked by DIB, sulfur chains were stabilized and the product, , the DIB crosslinker is a synthetic chemical and not currently produced on large scales. Therefore, more economical or renewable crosslinkers were reported, including vegetable oils,[31] botryococcene,[25] terpinolene,[32] farnesene, farnesol, myrcene,[10] squalene, perillyl alcohol,[33] and diallyl disulfide (DADS).[19,22,34] DADS is major organosulfur compound found in Allium vegetables, like garlic and onion, and it can be prepared by the decomposition of allicin. Along with DADS, other garlic derived compounds, such as diallyl sulfide (DAS) and garlic essential oil (GEO), were studied as monomers in inverse vulcanization, because they are sustainable and increase the overall sulfur content because of the presence of disulfide bonds in their structures. However, unless under long term (24 hours) curing at high temperature (>160 °C), these polysulfides have sub-ambient glass transition temperatures (around 0 °C).[19,22,34] Dried garlic powder (DGP) was studied as a biosorbent of heavy metals, resulting from the high affinity of the sulfur bond for metal ions.[35] However, to apply garlic derived inverse vulcanized polymers in mercury capture, a high glass transition temperature (T_g) is desirable, to improve shape persistence and hardness at room temperature, and reduce the compaction of sorbent beds under pressure.

Here we report a ternary sulfur polymer synthesized though inverse vulcanization of sulfur, dicyclopentadiene (DCPD), and garlic oil blend (GOB). Sulfur is a by-product of the petrochemicals industry,[4,7] DCPD is a by-product of the steam cracking of naphtha to form ethylene[10], and GOB is plant based in origin.[19,22,34] Hence, all chemicals employed in the reaction were industrial byproducts or bioderived compounds. With the addition of the comonomer, DCPD, the product poly(S-DCPD-GOB) had higher T_g and much higher hardness than the sulfur polymer prepared by

sulfur and GOB only. Additionally, even with a lower fraction of elemental sulfur involved in the reaction, poly(S-DCPD-GOB) presented a higher mercury uptake capability than poly(S-DCPD).

3.3 Aims

4. Investigate ternary system, consisting of S_8, DCPD, and garlic oil blend, in inverse vulcanisation reaction.
5. Investigate the mechanical properties of binary and ternary thiopolymers
6. To study the application of thiopolymers, synthesized by S_8, DCPD, and garlic oil blend, in mercury capture.

3.4 Results and discussion

3.4.1 Thiopolymers

Garlic oil blend is produced by using steam distillation to extract a variety of volatile organosulfur compounds from garlic and then condensing them. GOB composes of three major compounds, DADS, diallyl trisulfide (DATS), and DAS. Compared with its compositions, GOB is economical and ready to be reacted without any purification. Inverse vulcanization of sulfur and GOB, as shown in Scheme 3.1 with different ratios was conducted first. The final products, poly(S-GOB), were named as SG-X-Y, where X and Y are the percentages of sulfur and GOB respectively. For example, SG5050 represents a 50 : 50 w/w % of sulfur to GOB. From visual appearance (Figure 3.1), all sulfur polymers were black homogeneous solids, however, as the content of sulfur increased, the final products become softer, which was demonstrated by hardness testing and T_g's. In order to uptake mercury from solution, the material should be ground into fine powder, however, poly (S-GOB) couldn't be ground by hand with a mortar and pestle at room temperature, as it is too rubbery, as shown in Figure 3.2. In

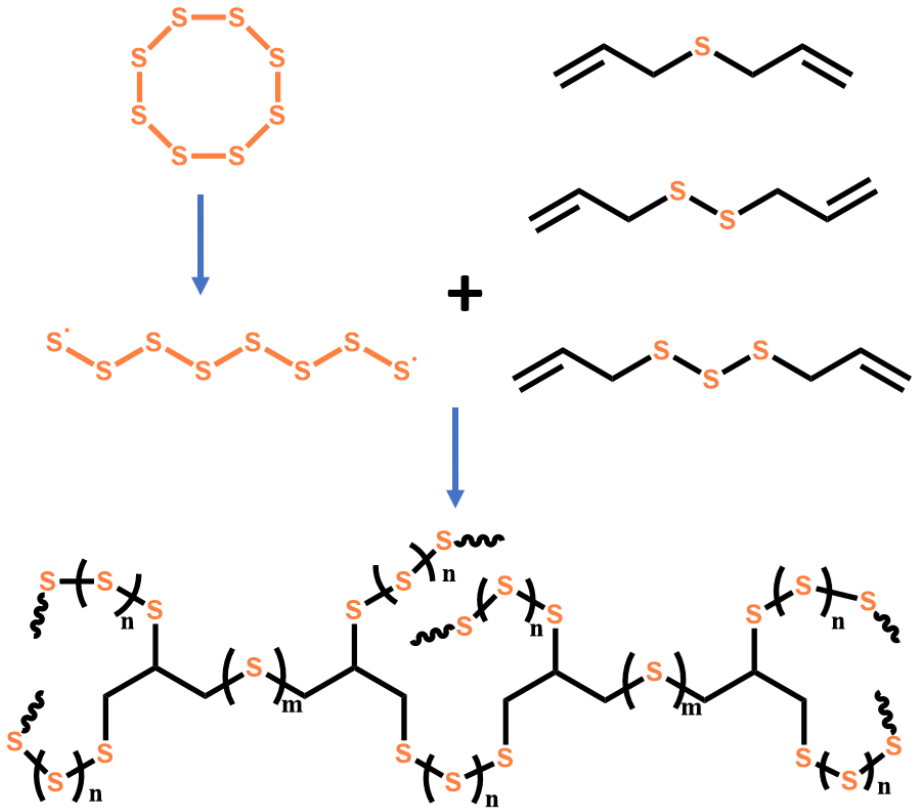

Scheme 3.1 Scheme for inverse vulcanization of sulfur and GOB, where n depends on the ratio of sulfur and m is 1, 2, or 3.

Figure 3.1 Photographs of final molded products of different polysulfides after curing. The dimension of the samples is 25 mm × 40 mm.

a previous report, DCPD was found to readily co-polymerize with other crosslinkers in inverse vulcanization systems, and enhanced the T_g of the product polymers.[32] Poly(S-GOB-DCPD) was synthesized under the same conditions as poly(S-GOB). Two sections of preparation were conducted, which were 50 w/w % of sulfur with varied ratio of co-crosslinker and a 1 : 1 weight ratio of co-crosslinker with varied sulfur from 50-80 w/w %. Like the naming system of poly(S-GOB), DCPD blended sulfur polymers were named as SGD-X-Y-Z, such as SGD504010, for the polysulfide prepared from 50 : 40 : 10 w/w % of sulfur, GOB, and DCPD respectively. Unlike poly(S-GOB), especially SG7030, SG8020, and SG9010, all poly(S-GOB-DCPD)

materials exhibited rigidity, easily grinding into fine powder with particle sizes smaller than 170 mesh (0.090 mm), as shown in Figure 3.2. Initially, the reactions of SG5050,

Figure 3.2 Comparison between ground representative samples, from left to right, SG9010, SG5050, SGD504010, and SGD502525.

SGD504010, and SGD502525 were selected as representative examples of reaction sets and were screened through ^{1}H NMR. SG5050, SGD504010, and SGD502525were chosen to test respectively our binary system, ternary system with varied GOB/DCPD ratio, and ternary system with varied sulfur/crosslinker ratio, respectively (see Figure 3.2 and later discussions). All ^{1}H NMR spectroscopies were based on the soluble fraction of the products. As GOB is a mixture, the ^{1}H NMR spectroscopy of its major component, DADS, was analyzed to further confirm the identity of the peak of allyl group, as shown in Figure 3.3. The peaks at 3.3 ppm were assigned as the methylene

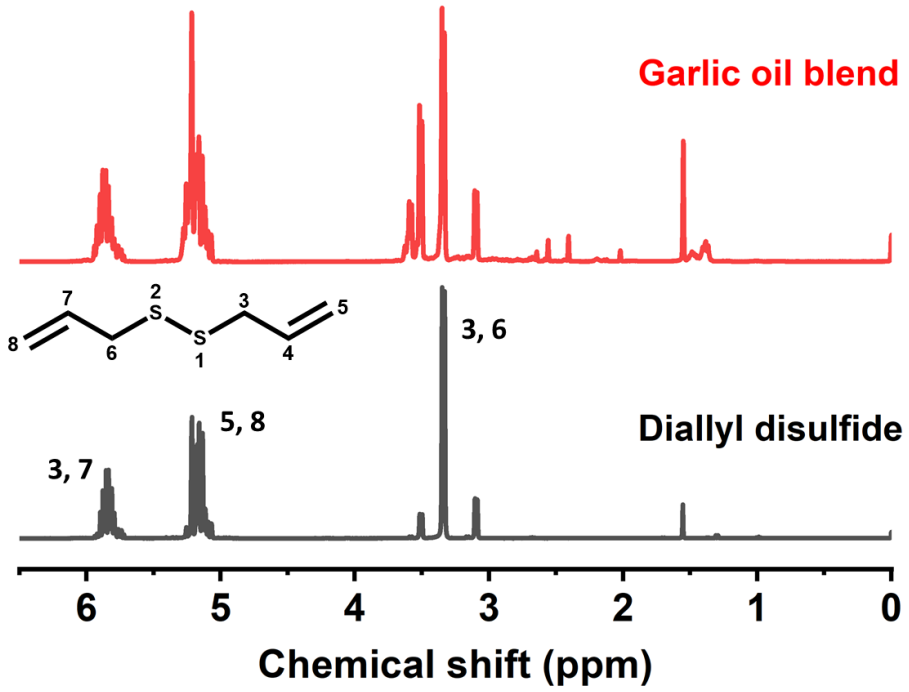

Figure 3.3 ^{1}H NMR spectroscopy of garlic oil blend and pure diallyl disulfide. All peaks of pure diallyl disulfide were assigned in corresponding figures.

protons of DADS, the peaks at 3.1 ppm were assigned as the methylene protons of DAS, and the peaks from 5.0 ppm to 6.0 ppm are assigned as ethylene protons. For SG5050, the lack of allyl peaks in the Figure 3.4, confirms the reaction of C=C double bonds of GOB. Additionally, from the apparent decrease in the intensity of the methylene proton peaks of DADS, the breakage of C=C double can also be confirmed. The broad peaks from 2.6 to 4.0 ppm in Figure 3.4 are identified as the protons on the newly generated S-C-H, protons on the original methylene group of all GOB components, and, protons, probably, due to α-proton sulfur substitution. Different from Figure 3.4, both Figure 3.5 and Figure 3.6 show peaks from 5.5 ppm to 5.8 ppm, which are generated from inverse vulcanization of sulfur and DCPD, as shown in Figure 3.7. All ^{1}H NMR spectroscopies (Figure 3.4, Figure 3.5, Figure 3.6, Figure 3.7, Figure 3.8, and Figure 3.9) of polymers show broad peaks from 1.0 ppm to 1.6 ppm, indicating the presence of a polymer structure.

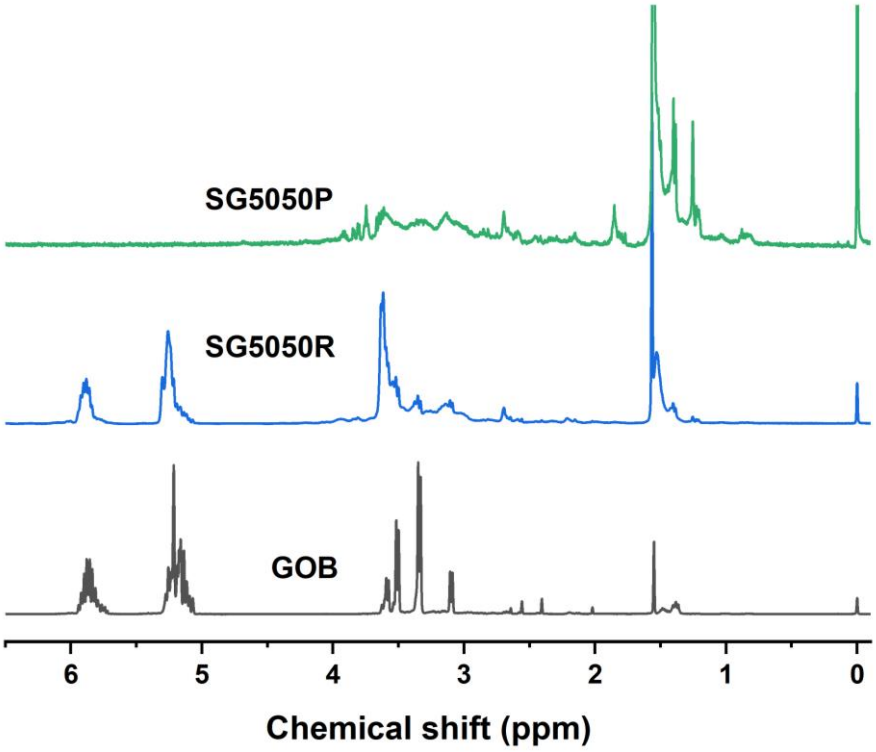

Figure 3.4 ^{1}H NMR spectroscopy of SG5050 in CDCl3. From top to bottom, the spectra are the soluble part of cured polymer, named as SG5050P, soluble part of pre-polymer after fully reacting, named as SG5050R, and GOB.

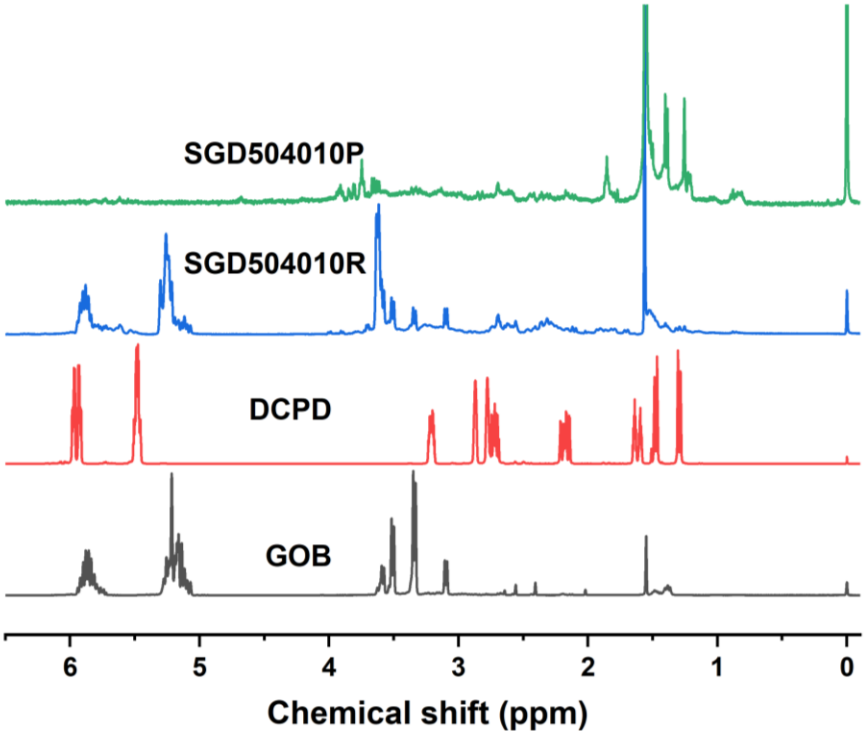

Figure 3.5 ^{1}H NMR spectroscopy of SG504010 in CDCl3. From top to bottom, the spectra are the soluble part of cured polymer, named as SG504010P, soluble part of pre-polymer after fully reacting, named as SG504010R, DCPD and GOB.

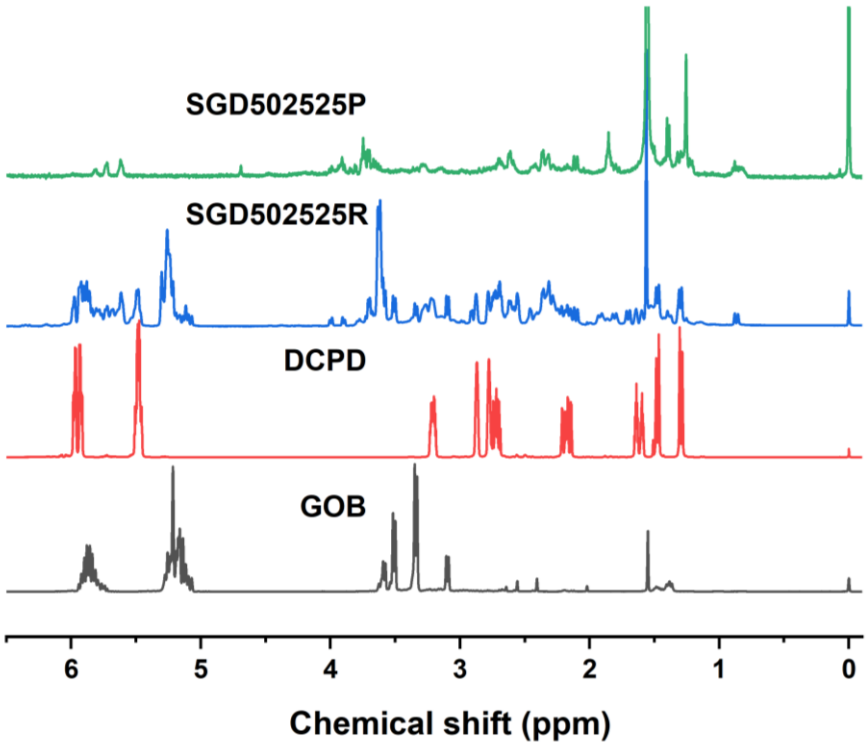

Figure 3.6 ^{1}H NMR spectroscopy of SG502525 in CDCl3. From top to bottom, the spectra are the soluble part of cured polymer, named as SG502525P, soluble part of pre-polymer after fully reacting, named as SG502525R, DCPD and GOB.

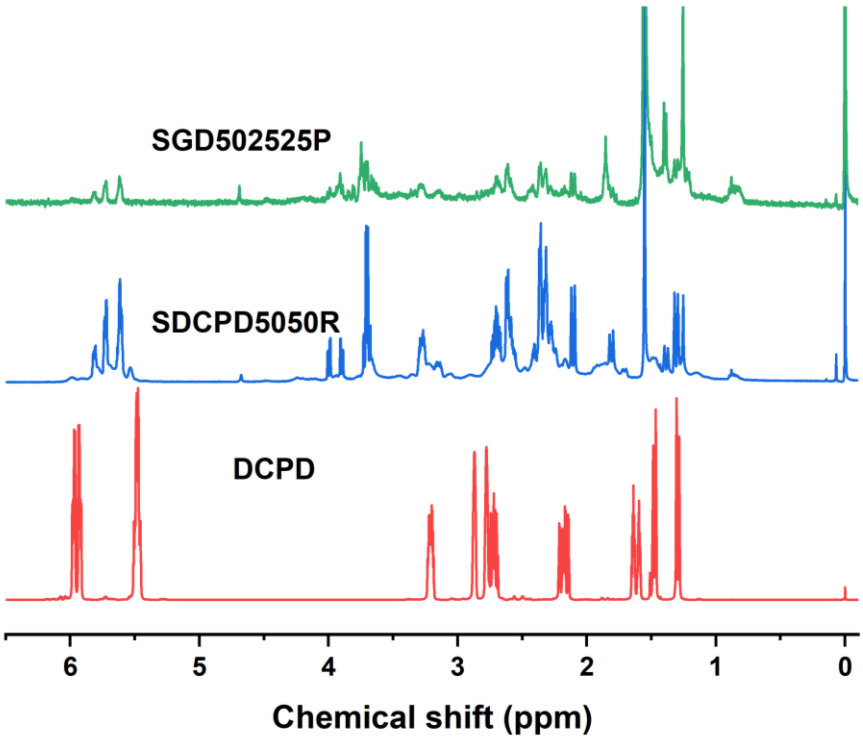

Figure 3.7 ^{1}H NMR spectroscopy of SG502525, poly (S-DCPD) (SDCPD5050R), and DCPD

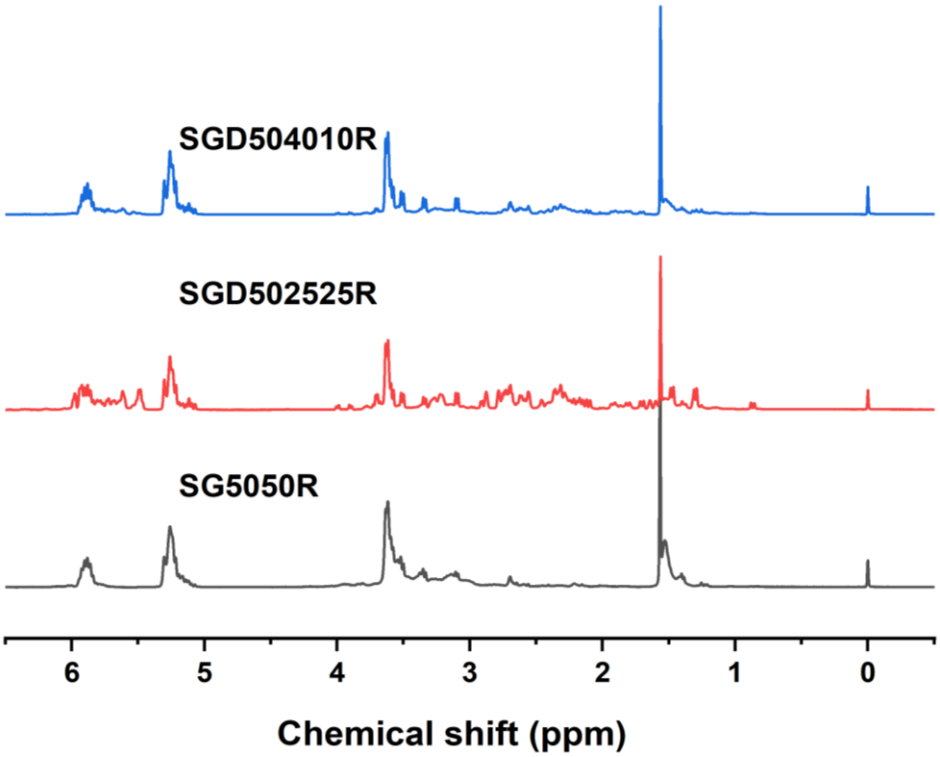

Figure 3.8 Stacked ^{1}H NMR spectroscopy of representative polymers' soluble part of pre-polymer after fully reacting, named as SGD-X-Y-Z-R.

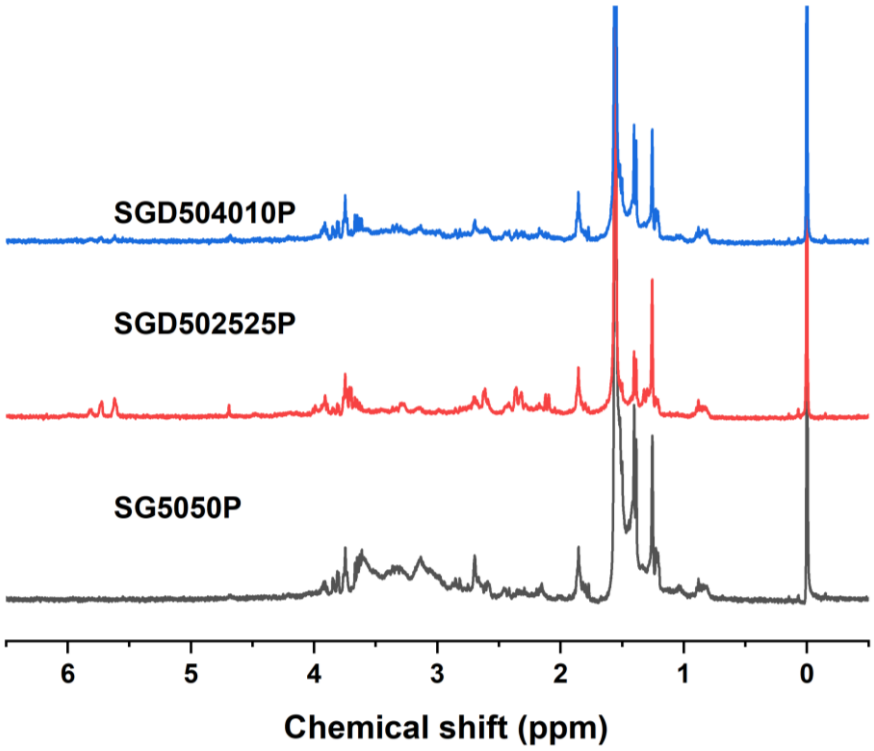

Figure 3.9 Stacked 1H NMR spectroscopy of representative polymers' soluble part of cured polymer, named as SGD-X-Y-Z-P

Polymerization and the presence of a crosslinked structure could be further confirmed from the solubility of the products, as shown in Figure 3.10 and Figure 3.11. The maximum of soluble fractions was less than 15 w/w % from 500 mg sample in 10 mL solvent, and none of the samples were fully soluble in $CHCl_3$. For the binary polymers of sulfur and GOB, the solubility of polymer decreased with increasing of sulfur content, which could be explained by the properties of polymer trending closer to that of elemental sulfur, as the proportion of sulfur increased. A similar conclusion could be found in the ternary system. Additionally, the ratio of DCPD negatively affected the solubility of product, aligned with the literature that poly(S-DCPD) is insoluble. [10] The insoluble fraction corresponds to the higher molecular weight and fully crosslinked component, the majority product, as opposed to lower molecular weight oligomers.

Figure 3.10 Solubility study of polysulfides. (top) and soluble fractions in $CHCl_3$ (bottom). From left to right, they are SG5050, SG6040, SG7030, SG8020, SG9010, SGD504010, SGD503020, SGD502030, SGD501040, SGD502525, SGD602020, SGD701515, and SGD801010.

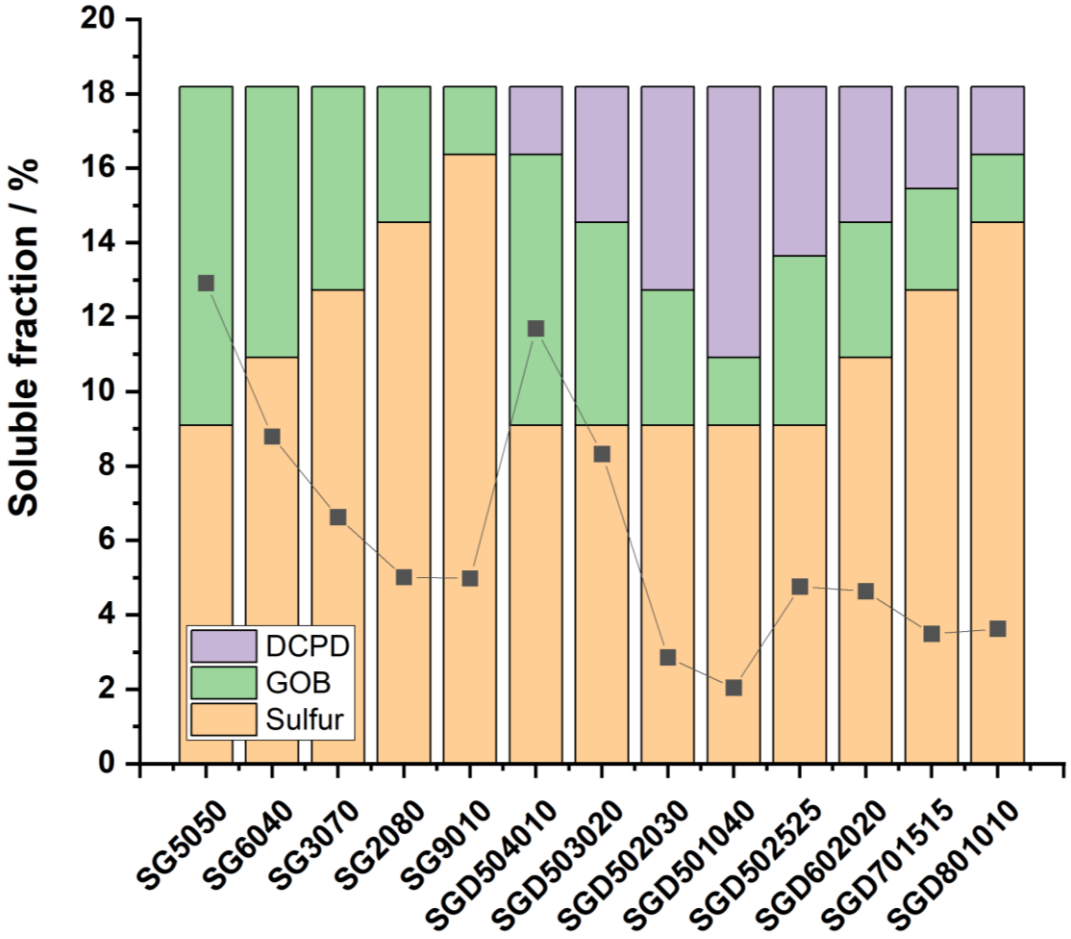

Figure 3.11 Solubility study of polysulfides. Bar chart indicated the component ratio of designed reactant.

From the ATR-FTIR patterns of sulfur-DCPD-GOB, as shown in Figure 3.12 and Figure 3.13, reaction of C=C bonds and sulfur can be confirmed as well. The signals at 3080 and 1633 cm^{-1} corresponded to the C=C-H stretching and C=C stretching modes, and after reaction, all polymers demonstrated a clear reduction in those two signals. Additionally, reduction of signals at 995 and 915 cm^{-1}, indicating monosubstituted alkene, could be observed. Moreover, a more intense signal was formed at 669 cm^{-1}, assigned as C-S stretching, further confirming inverse vulcanization.[36] Like ternary system reaction, similar signal changing could be detected in binary system, as shown in Figure 3.14.

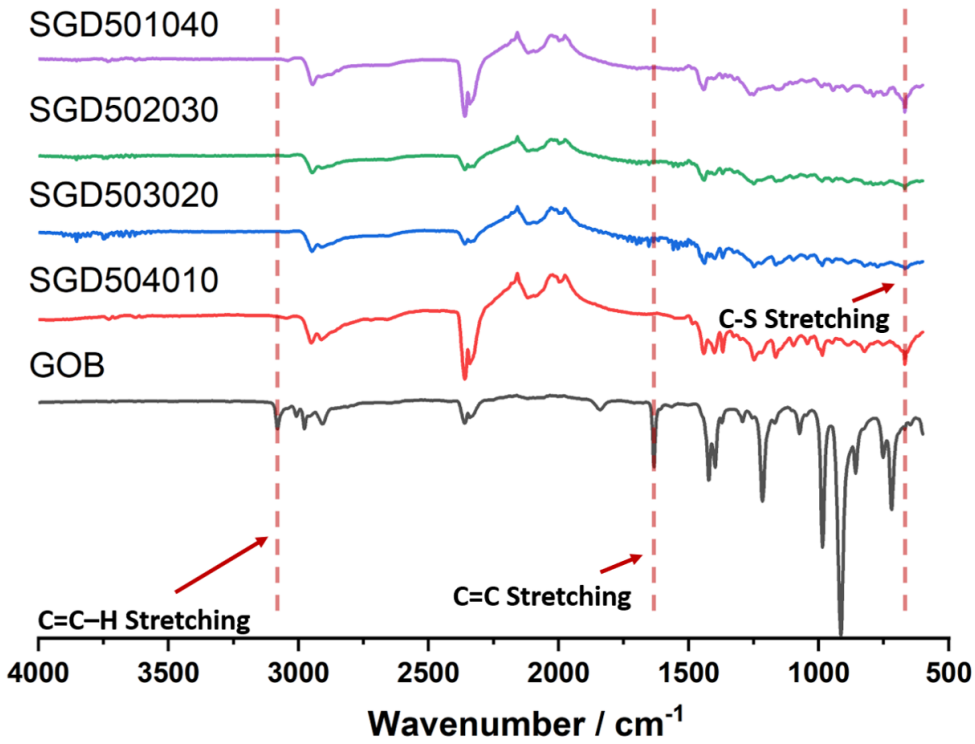

Figure 3.12 FT-IR spectroscopy of polysulfides with varied ratio of GOB to DCPD.

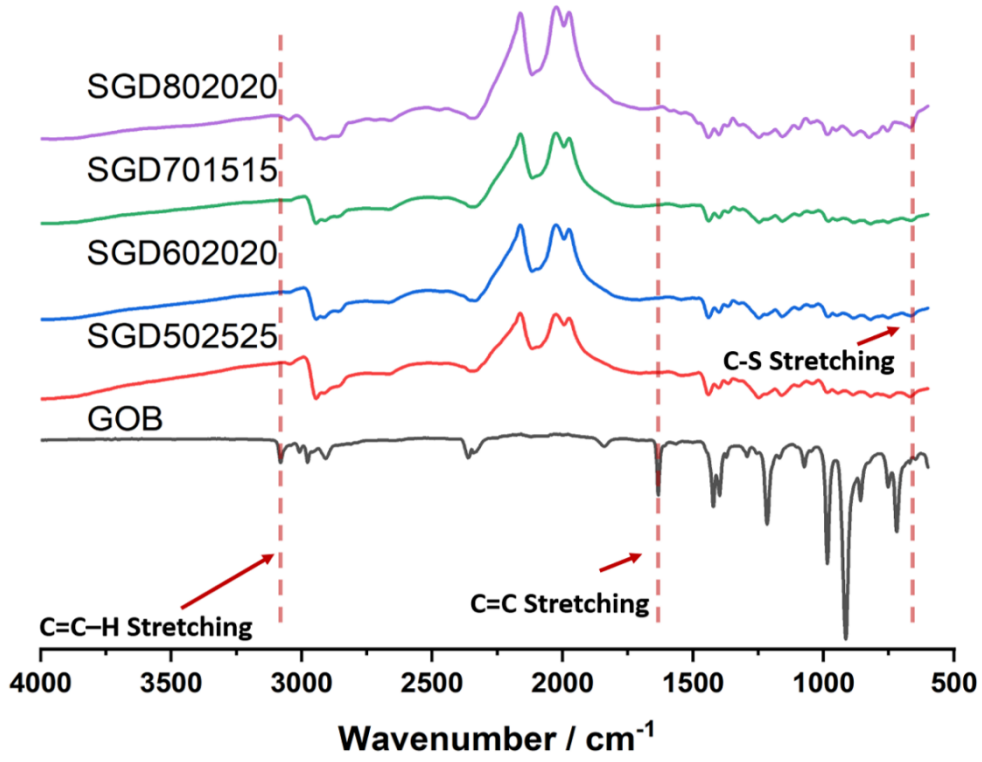

Figure 3.13 FT-IR spectroscopy of polysulfides synthesized by ternary system with same weight ratio of DCPD and GOB.

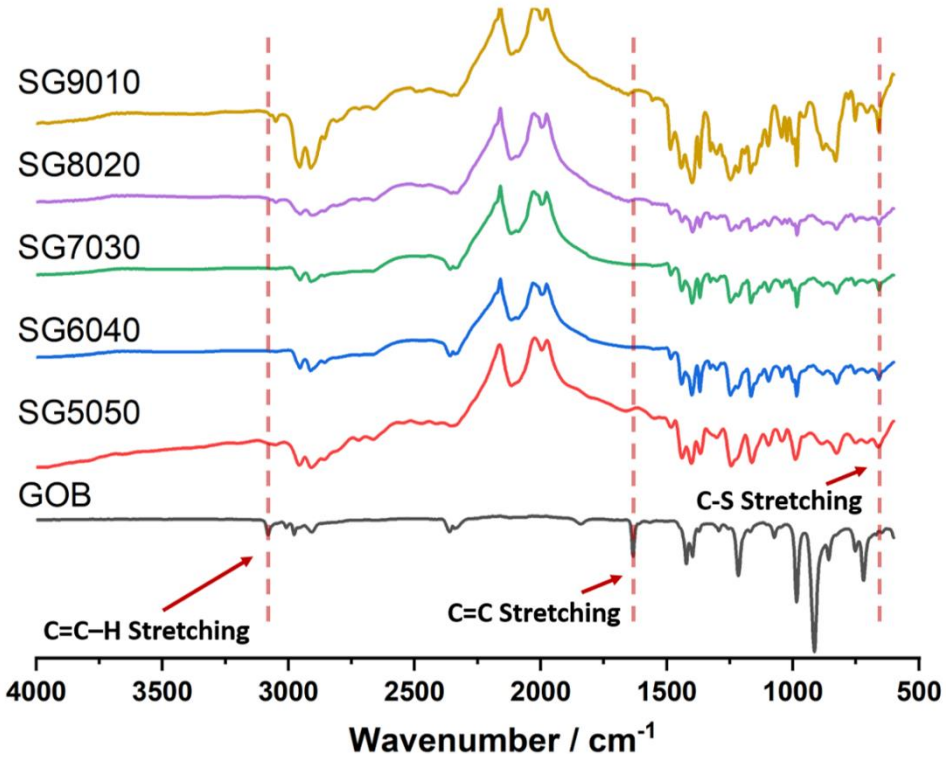

Figure 3.14 FT-IR spectroscopy of polysulfides synthesized by binary system.

Powder X-ray diffraction (PXRD) was applied to detect residual sulfur crystals within all polymer samples. Identical sharp peaks from sulfur crystals could be observed in the PXRD pattern of SG9010 and SG8020 (Figure 3.15), which indicates that a high ratio of sulfur (≥ 80 w/w %) cannot be stabilized by GOB through inverse vulcanization. Only amorphous polymer was observed from other PXRD patterns for both binary and ternary system, as shown in Figure 3.16 and Figure 3.17.

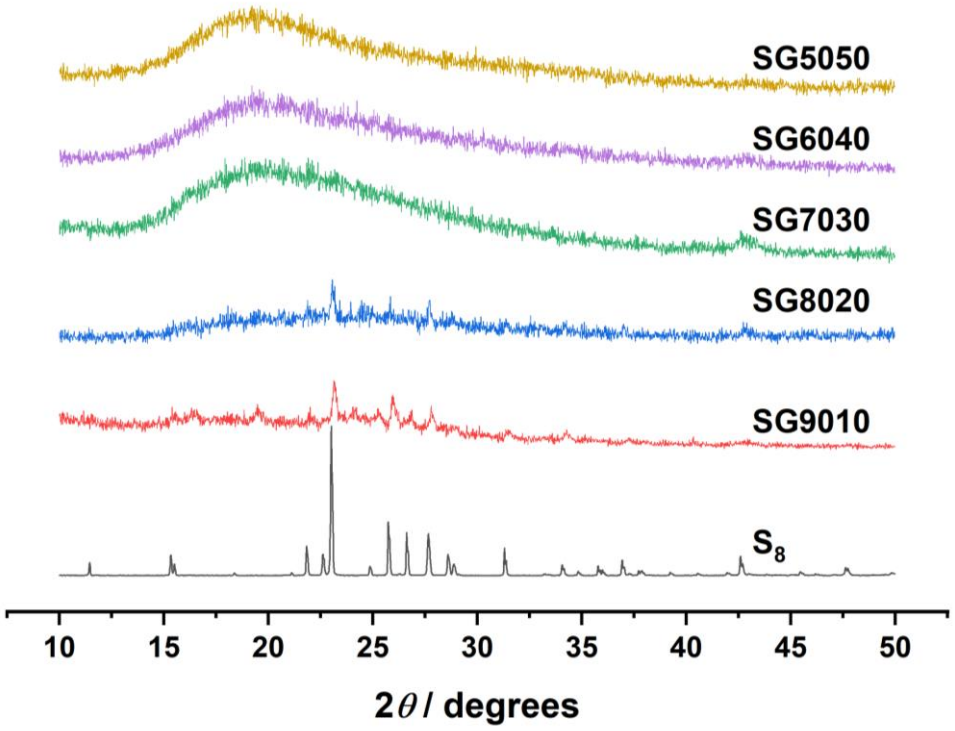

Figure 3.15 Offset PXRD patterns for polysulfides synthesized by binary system

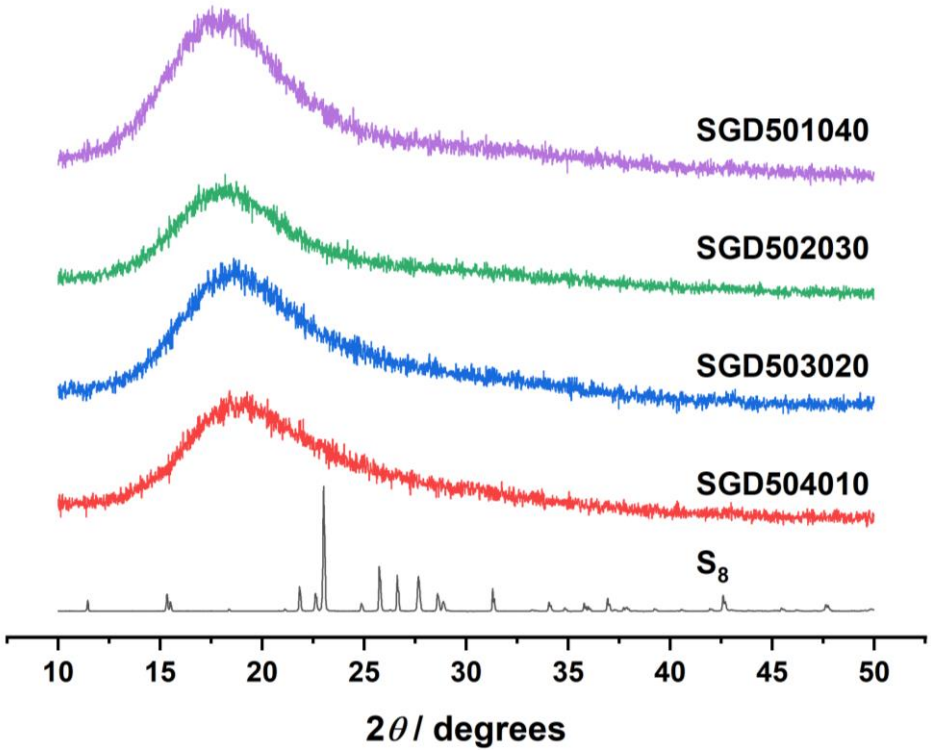

Figure 3.16 Offset PXRD patterns for polysulfides with varied ratio of GOB to DCPD.

Differential Scanning Calorimetry (DSC) was performed to investigate the thermal properties of the samples. Sulfur crystal melting peaks could be observed from the DSC trace of SG9010, further confirming SG9010 that either this amount of sulfur could not be reacted fully, or it rapidly depolymerized upon cooling. From the second heating cycle traces, it could be found that glass transition temperatures (T_g) of sulfur-GOB polymers, from -20 to 0 °C, are all below room temperature, as shown in Figure 3.18. Thus, the materials do not maintain their shapes well at room temperature and are too soft to be ground into fine power to apply as Hg absorbents. However, the T_g of GOB derived polymer could be increased dramatically through copolymerizing with DCPD. When a mixture of GOB-DCPD (equal amount by weight) were used as crosslinkers instead of GOB alone, the T_g's of the sulfur polymers were increased to above 10 °C, as shown in Figure 3.19. More clearly, as shown in Figure 3.20 and Figure 3.21, keeping same amount of sulfur, increasing ratio of DCPD positively influences the T_g of copolymers.

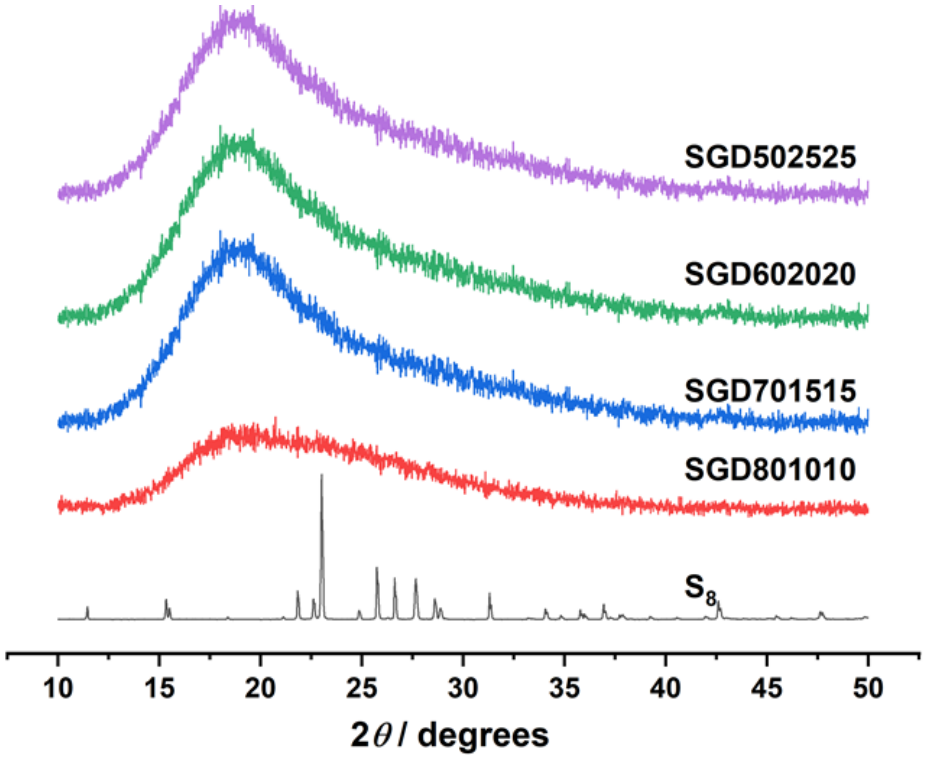

Figure 3.17 Offset PXRD patterns for polysulfides synthesized by ternary system with same weight ratio of DCPD and GOB.

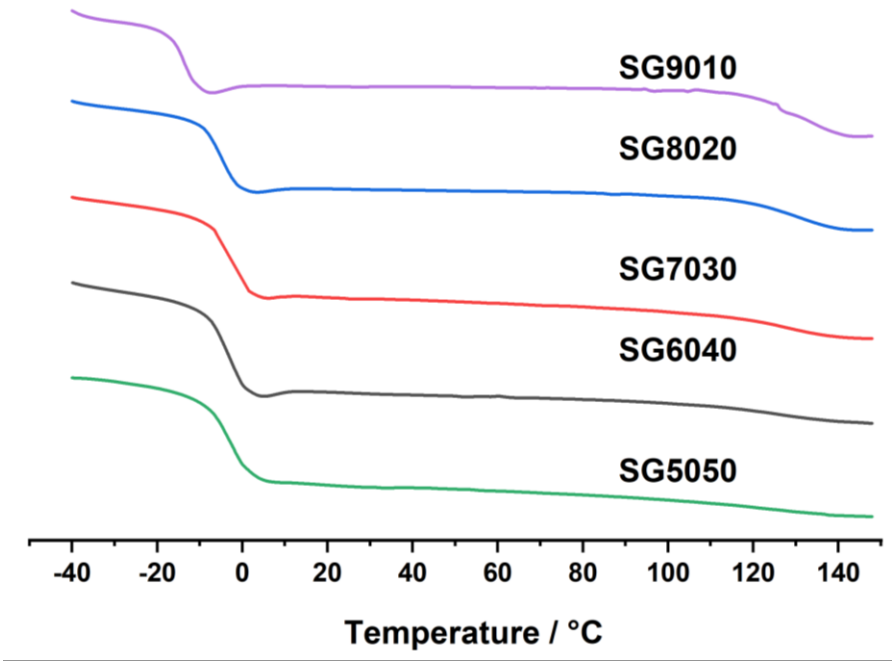

Figure 3.18 Offset DSC traces for polysulfides synthesized by binary system

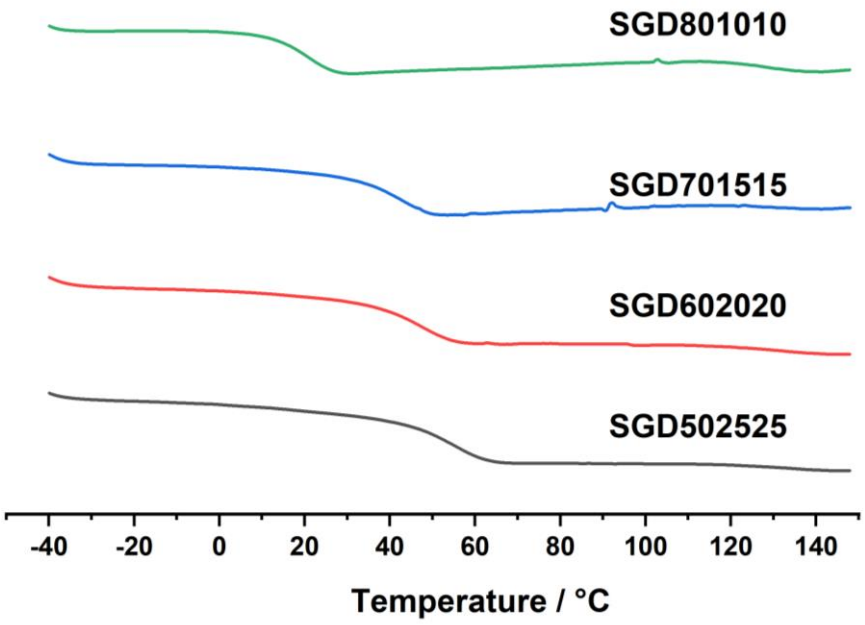

Figure 3.19 Offset DSC traces for polysulfides synthesized by ternary system with same weight ratio of DCPD and GOB.

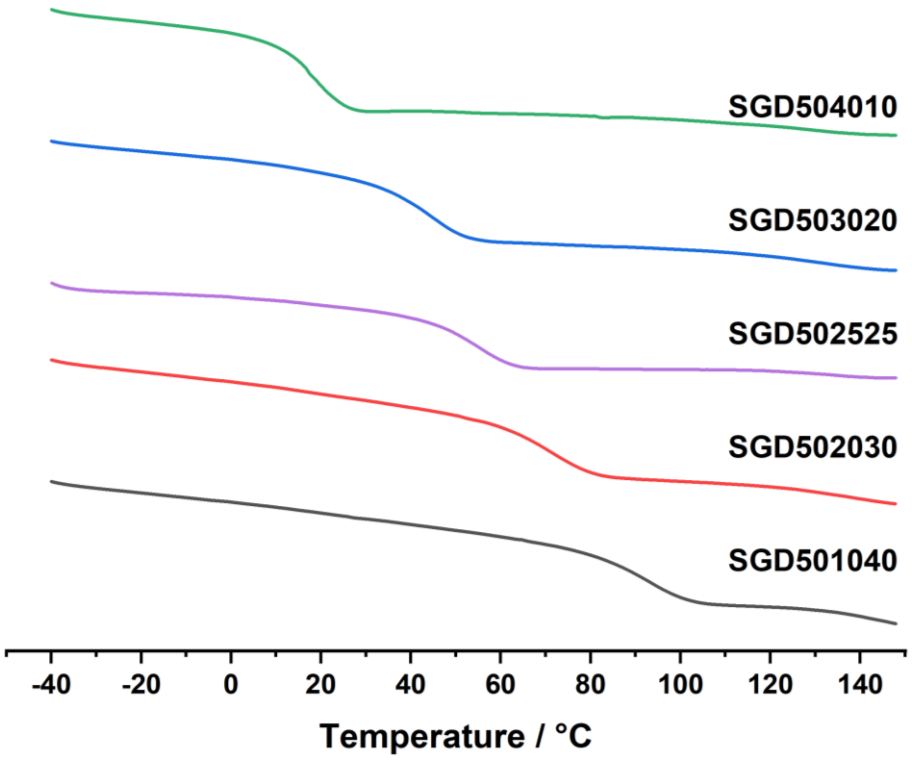

Figure 3.20 Offset DSC traces for polysulfides with varied ratio of GOB to DCPD.

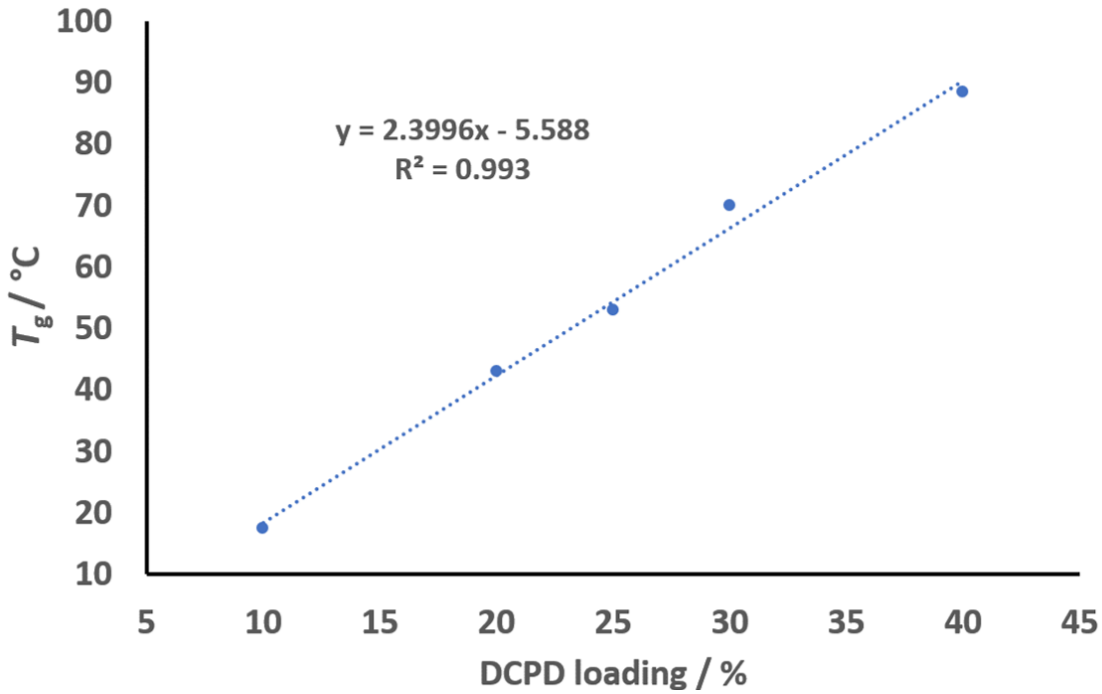

Figure 3.21 T_g trend with varied DCPD loading and liner fitting. It can be found that increasing amount to DCPD could directly increase the T_g of final products.

Unlike binary sulfur-GOB polymers, which were rubbery, sulfur-DOB-DCPD polymers were rigid and brittle at room temperature. This was probably because of the stable and rigid molecular structure of DCPD. At room temperature, the hardness of sulfur polymers crosslinked by GOB only was much lower than that of a ternary copolymer of GOB and DCPD as well. As shown in Figure 3.22, Figure 3.23, and Figure 3.24, blending with DCPD increased the hardness from scale A to scale D, which is a scale for harder materials. Although DCPD is a factor affecting hardness, the sulfur content must also be considered. The hardness of the polymers firstly increased with increasing sulfur loading, and then sharply decreased after a maximum, which occurred at SG3070 in Figure 3.22, and at SGD602020 in Figure 3.24.

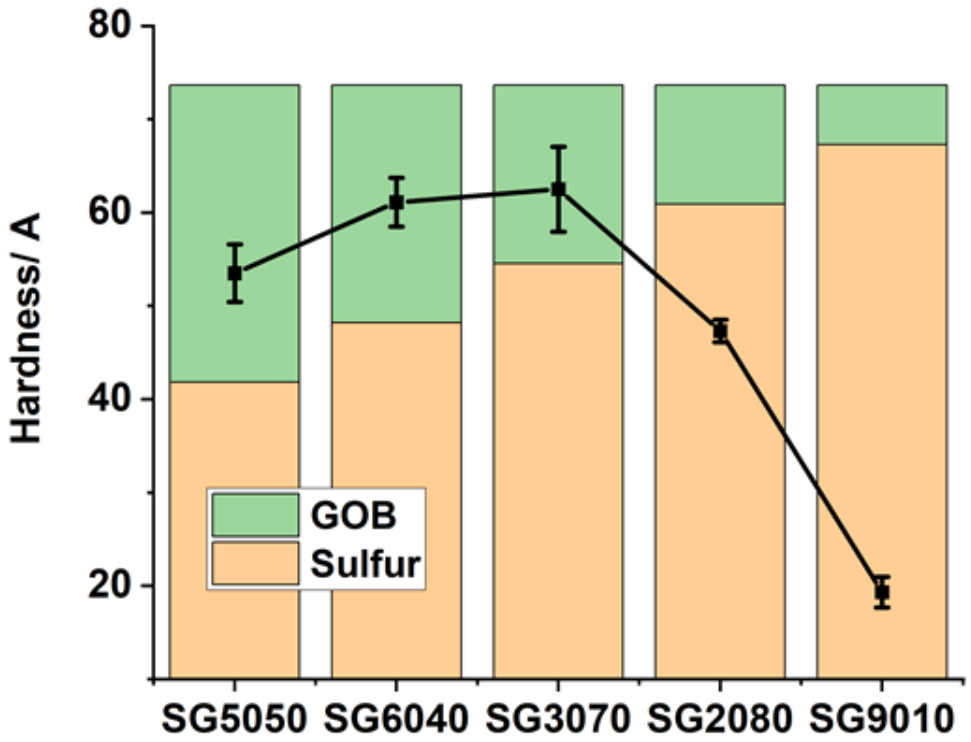

Figure 3.22 Hardness of polysulfides synthesized from sulfur and GOB by type A digital shore durometer.

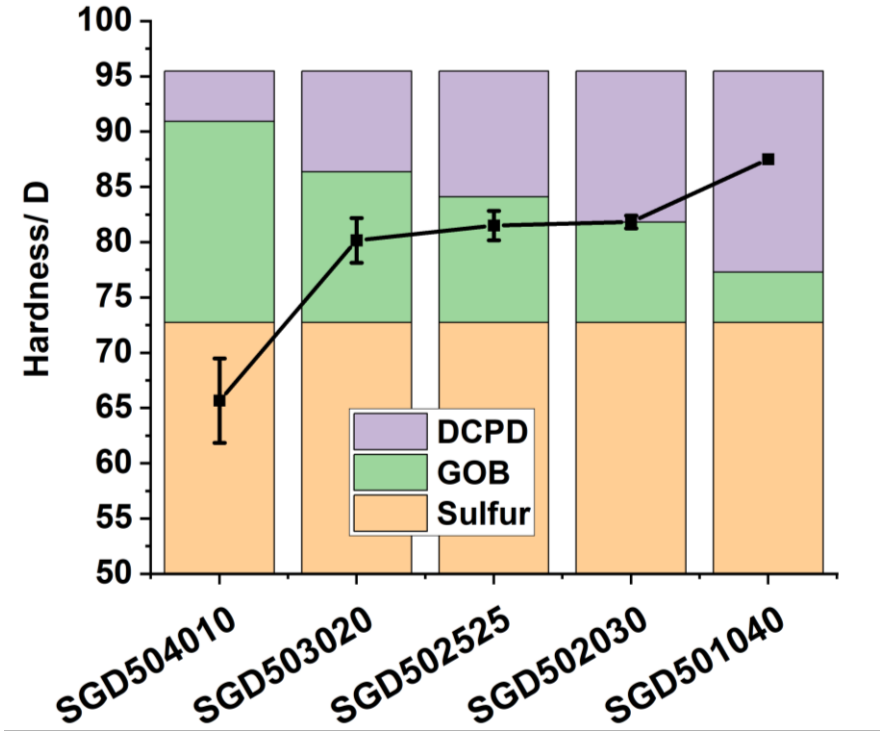

Figure 3.23 Hardness of polysulfides synthesized from sulfur, GOB, and DCPD by type D digital shore durometer. Bar chart indicated the component ratio of designed reactant.

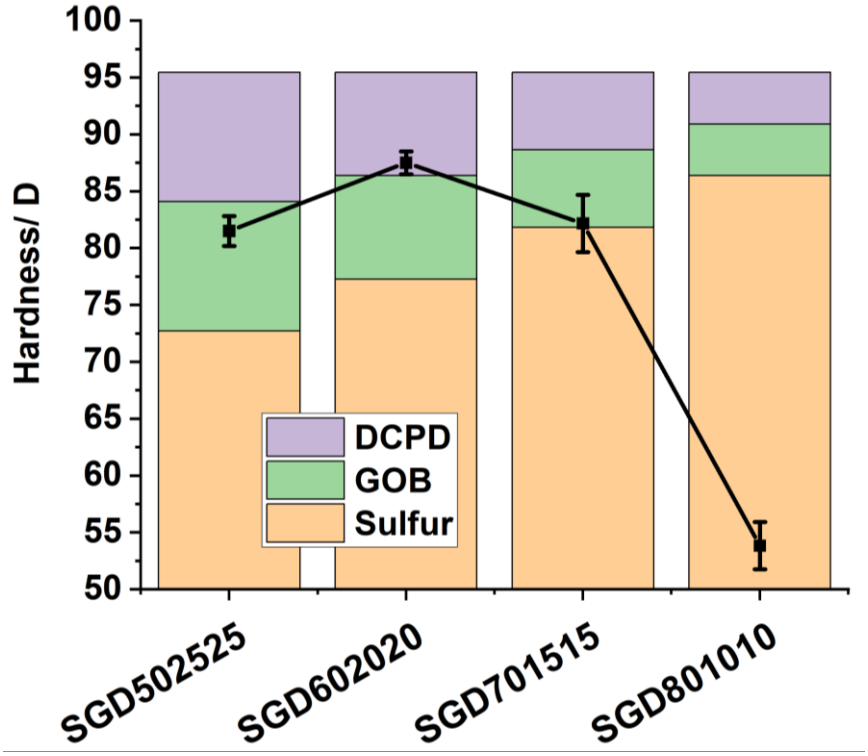

Figure 3.24 Hardness of polysulfides synthesized from sulfur, GOB, and DCPD by type D digital shore durometer. Bar chart indicated the component ratio of designed reactant.

3.4.2 Mercury uptake studies

Because of the presence of sulfur, which has high affinity for Hg^{2+}, polysulfides are applied as mercury absorbents. Poly(S-limonene) was the first reported inverse vulcanized polymer to detect mercury from aqueous solution. However, suffering from low T_g and molecular weight, poly(S-limonene) would creep at room temperature, therefore, it could only be used as a detector or coating, rather than a freestanding absorbent. Following this, more crosslinkers were explored in the synthesis of sulfur polymers for mercury sequestration, such as, DCPD, myrcene, farnesene, farnesol, perillyl alcohol, squalene, and 2-carboxyethyl acrylate (CEA). Meanwhile, different physical configurations of materials have been reported to improve the mercury uptake capacity of absorbents. The strategies were typically focused upon increasing the surface area of polysulfide materials, such as supercritical carbon dioxide ($scCO_2$) foaming polysulfides,[37] salt templating for porous polysulfides,[38] and coating/loading polysulfides on supports.[31,39] Thus, as both sulfur-GOB-DCPD polymers and sulfur-GOB polymers are bulk materials with no pores, a fine powder could efficiently increase the contact surface of absorbent. Very fine powders were successfully prepared by grinding sulfur-DOB-DCPD polymers, however, powders of sulfur-GOB polymers aggregated into clusters because of their sticky and elastomeric properties. All powder samples of sulfur-GOB-DCPD polymers were exposed to aqueous $HgCl_2$ solutions in order to examine their mercury uptake capability. From 2 ppm Hg^{2+} solution, SGD501040 absorbed 82 % mercury, SGD701515 took up 94 % mercury, and the other compositions of SGD removed ≥ 99 % mercury, as shown inTable 3.1. This is a significant result because even low concentrations of mercury in water can have very severe health effects, so it is important to have materials that are capable of removing all the mercury from a solution, rather than removing most of the mercury but leaving small but hazardous traces behind. Furthermore, the most common situation in practice, is to find low concentrations of mercury in water, rather than high concentrations. Therefore, what is required are materials that can remove as much mercury as possible from low concentrations, rather than having high capacity at high concentration, but low uptake at low concentration. Nevertheless, for completeness of the study, more concentrated solutions of Hg^{2+} were prepared (initial concentration 20 ppm). SGD504010 removed 37 % Hg^{2+} from aqueous solution, which was the highest

mercury uptake among sulfur-GOB-DCPD polymer. Therefore, the content of GOB is clearly beneficial to mercury affinity. These results were also aligned with the elemental analysis, which was shown in Table 3.2.

Table 3.1 Mercury ion uptake results[a]

	2 ppm Hg^{2+} solution		20 ppm Hg^{2+} solution	
	conc. / ppm	Removed / %	conc. / ppm	Removed / %
Blank[b]	0.04	N/A	0.03	N/A
SGD504010	0.01	100.0	6.67	37.0
SGD503020	0.00[b]	100.0	7.96	24.8
SGD502525	0.05	98.8	8.91	15.8
SGD502030	0.00[b]	100.0	9.07	14.2
SGD501040	0.19	81.9	9.11	13.9
SGD602020	-0.01[c]	100.0	8.63	18.4
SGD701515	0.09	94.0	8.95	15.4
SGD801010	-0.01[c]	100.0	7.53	28.8
Control[d]	0.87	N/A	10.57	N/A

a All values shown were original detected value by ICP-OES, which would be half of the pristine value, because of acid stabilisation and dilution (10 % of Nitric acid add and specific DI water add to dilute the concentration to half of pristine value, in order to follow the testing limitation of ICP-OES and calculate easily).
b Blank is the sample of pure DI water.
c – means testing results were negligible or below detected limitation of ICP-OES
d Control is the standard solution sample of specific concentration prepared by $HgCl_2$

As shown in Figure 3.25 and Figure 3.26, the mercury uptake positively correlates with the sulfur content in the polysulfides. The results could be explained though Pearson's hard-soft-acid- base (HSAB) principle, from which sulfur is a "soft" Lewis base and mercury is a "soft" Lewis acid. Samples SGD504010 and SGD701515 resulted in comparable sulfur contents to each other by elemental analysis, despite their different initial compositions: SGD504010 starting with more GOB, and a lower

amount of elemental sulfur (S_8), while SGD701515 starting with more elemental sulfur (S_8), and less GOB. That SGD504010 adsorbed the most Hg of the two samples therefore suggests that GOB is more beneficial for Hg uptake than elemental sulfur. SGD801010 composed of around 12.5 % more sulfur than SGD504010, nevertheless, the mercury uptake capacity of SGD801010 was still lower than that of SGD504010. Exposed to 20 ppm Hg^{2+}, the mercury uptake capacity of SGD504010 is 1.60 mg/g, which is much higher than the calculated maximum capacity of another reported garlic derived mercury absorbent, which is 0.6497 mg/g.[35] This mercury uptake capacity is lower than those inverse vulcanized polysulfides with post treatment, such as coated microbeads (527 mg/g),[13] coated silica gel (65.25 mg/g),[31] and electrospun nanofiber (328 mg/g).[40] However, it is still competitive to other bulk inverse vulcanized polysulfides, like poly(S-*r*-Canola) (1.81 mg/g),[41] poly(S-*r*-Rice Bran) (1.92 mg/g),[41] poly(S-*r*-Castor) (2.01 mg/g),[41] and even much higher than post-treated poly(S-DCPD), such as foamed S-DCPD (0.1mg/g).[10]

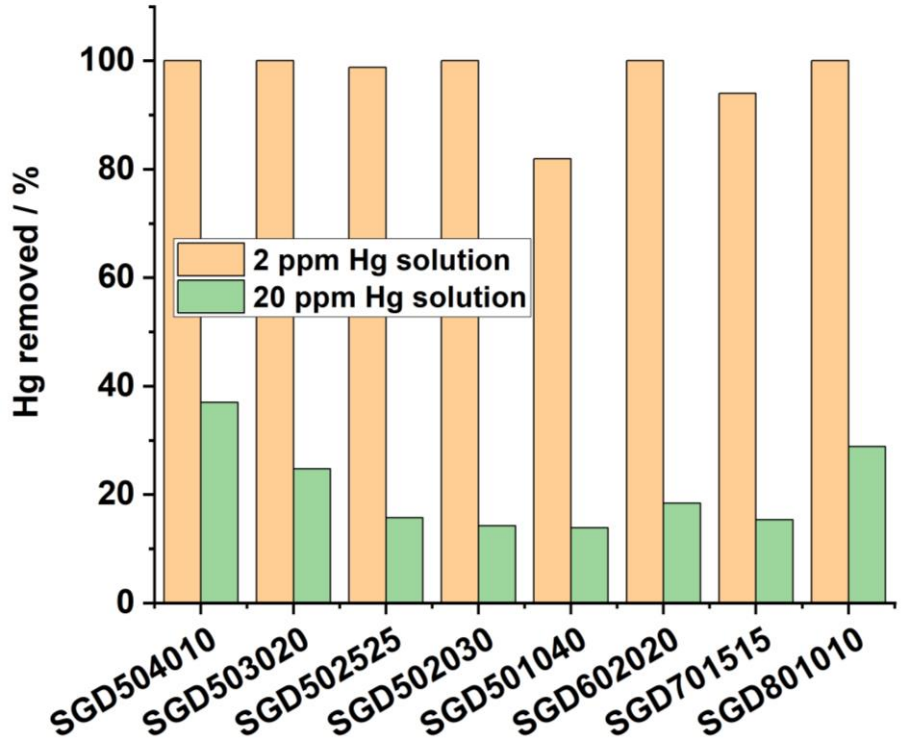

Figure 3.25 Static absorption study of polysulfides with different concentration $HgCl_2$ solution

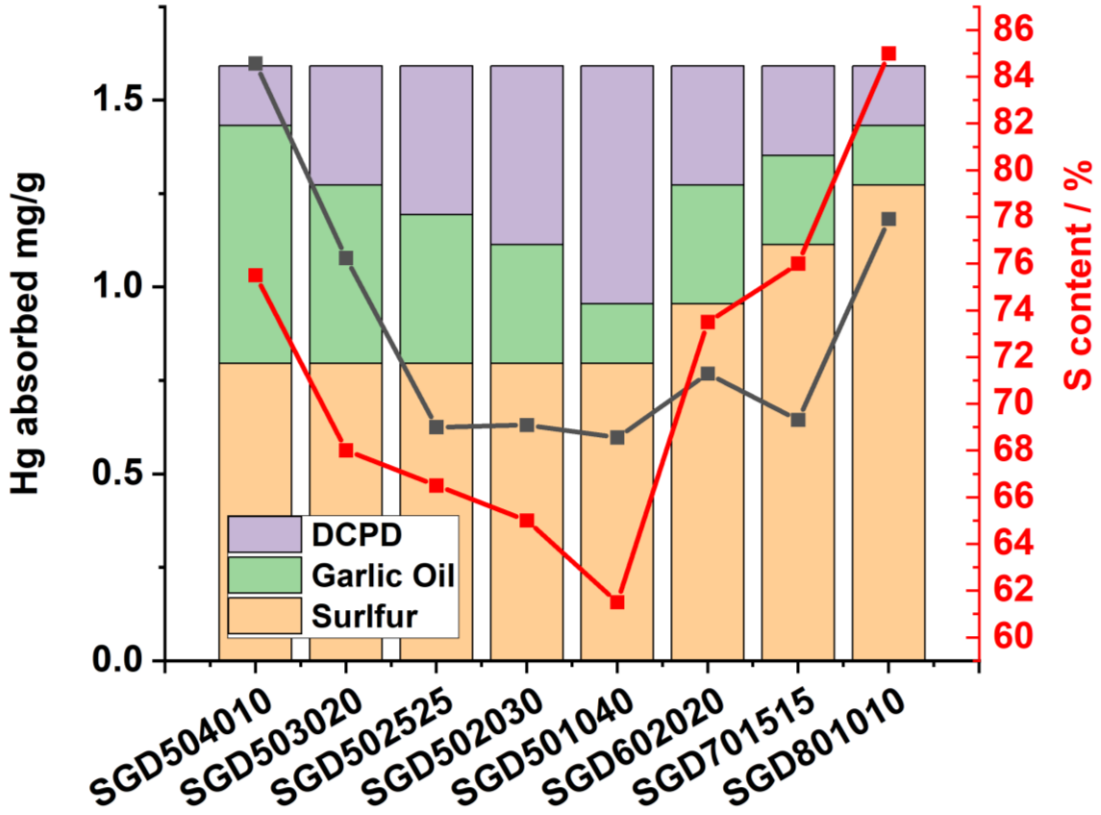

Figure 3.26 The relationship between mercury absorption, initial polymer component ratio, and surlfur content from elemental analysis.

3.5 Conclusions

In conclusion, we report the use of garlic oil blend, a renewable and bioderived compound, as a crosslinker in inverse vulcanization, as well as how the use of dicyclopentadiene as a comonomer alongside garlic oil blend can improve the properties of the final polymer. It was found that polymers containing only garlic oil as a comonomer lacked the structural rigidity not to agglomerate back together during grinding. However, the addition of dicyclopentadiene allows the resulting ter-polymers to form a fine free flowing powder, without agglomeration, and suitable for use in mercury capture. The addition of dicyclopentadiene alongside the garlic oil blend also allowed greater contents of sulfur to be stabilized. The resultant ternary system polymer of sulfur, garlic oil blend and dicyclopentadiene was found to be capable of removing more than a pure sulfur-DCPD polymer alone. The garlic oil blend provides the benefit to mercury uptake, and the DCPD provides the physical properties to allow its use. The most effective combination able to remove over 99 % of the mercury from solution; reducing the concentration of mercury in a 2 ppm solution down to below detection limits by ICP-OES. This is sufficient to make water with industrially relevant levels of contamination safe for use.

3.6 Experimental

3.6.1 Materials

Sulfur (S_8, sublimed powder, reagent grade, ⩾ 99.5%, Brenntag UK & Ireland), dicyclopentadiene (DCPD >96.0 %, Sigma-Aldrich), Garlic oil blend (GOB, Sigma-Aldrich), mercury (II) chloride (ACS, 99.5% MIN, Alfa Aesar UK), Chloroform-d (99.8 atom % D, Sigma Aldrich).

3.6.2 Method

Synthesis of crosslinked polymers

Reactants (sulfur and crosslinkers (used as received), 10 g in total, specific ratio for different samples are listed in Table 3.2) were mixed in 40 mL volume glass vials. The mixture was stirred at 175 °C in aluminium blocks and stirred by magnetic stirrer bars with stirring speed of 1000 rpm. The reaction time depended on both the ratio of sulfur to crosslinker and different type of crosslinkers. When the reaction had changed to thick dark brown liquid, the prepolymer was transferred into a silicone mould and moved into an oven at 140 °C for 18 hours.

Table 3.2 Designed crosslinking degree and detected element contents.[a]

Sample Name	Designed component / %			Expected element contents / %			Detected element contents / %		
	S_8	GOB	DCPD	C	H	S	C	H	S
SG5050	50.0	50.0	/	21.6	3.0	63.4	20.3	2.8	76.5
SG6040	60.0	40.0	/	17.3	2.4	70.7	16.8	2.2	81.0
SG7030	70.0	30.0	/	13.0	1.8	78.0	12.6	1.9	85.5
SG8020	80.0	20.0	/	8.6	1.2	85.3	9.4	1.5	90.0
SG9010	90.0	10.0	/	4.3	0.6	92.7	4.4	1.1	95.0
SGD504010	50.0	40.0	10.0	26.4	3.3	60.7	24.5	2.7	72.5
SGD503020	50.0	30.0	20.0	31.2	3.6	58.0	28.1	3.2	68.0
SGD502030	50.0	20.0	30.0	35.9	3.9	55.3	32.3	3.4	65.0
SGD501040	50.0	10.0	40.0	40.7	4.2	52.7	35.3	3.7	61.5
SGD502525	50.0	25.0	25.0	33.5	3.8	56.7	30.7	3.3	66.5
SGD602020	60.0	20.0	20.0	26.8	3.0	65.3	24.0	2.8	73.5
SGD701515	70.0	15.0	15.0	20.1	2.3	74.0	21.7	2.3	76.0
SGD801010	80.0	10.0	10.0	13.4	1.5	82.7	13.8	1.5	85.0

[a] Expacted value is calculated by known components from GOB.

The higher than expected sulfur content in the polymers is likely the result of the organic reactants having a higher volatility during the reaction, and hence being partially removed by evaporation before the reaction is complete.

Mercury uptake

To test the effect on mercury removal, 2 ppm and 20 ppm Hg^{2+} solutions were prepared. 50 mg of different polysulfides were individually placed into 10 mL solution in a 12 mL polypropylene centrifuge tube. After capping the tube, samples were left to agitate on a tube roller at 60 rpm for 24 hours. The subsequent mixtures were removed by using 0.45 μm nylon syringe filter. Stabilized with 1 mL HNO_3(aq), the filtrate was analysed via ICP-OES, using an Agilent 5110 ICP-OES spectrometer.

Solubility studies

To study the solubility of polysulfides, 0.5 g polymers were immersed in 10 mL of chloroform in the sample vials, individually. After 24 hours, the insoluble materials were separated by filter paper and dried in the vacuum oven at room temperature for 12 hours. After fully drying, the mass of samples was measured. The mass of all sample vials and filter paper was measured as well before and after using to calculate insoluble fraction.

3.6.3 Characterization

Nuclear magnetic resonance (NMR)

The reactions were monitor by solution NMR in deuterated chloroform, using a Bruker Advance DRX (400 MHz) spectrometer.

Powder X-ray Diffraction (PXRD)

Samples were analysed using a PANalytical Empyrean diffractometer with Cu-K_a radiation, operating in transmission geometry.

Differential scanning calorimetry (DSC). DSC were performed on a TA Instruments Q200 DSC, under nitrogen flow, and with heating and cooling rates of 10 °C/min from -50 to 150 °C in ‘heat-cool-heat’ program.

Attenuated total reflection Fourier transform infrared (ATR-FTIR)

FTIR spectra were measured between 4000 and 500 cm^{-1} on a Bruker Vertex 70 spectrometer, with a Platinum ATR module.

Hardness

Hardness of polymers were evaluated using type A digital shore durometer and type D digital shore durometer. Flat surface of all polymer block was tested by durometer above 5 times tests to obtain a reliable average value.

3.7 References

(1) Moore, C. J. Synthetic Polymers in the Marine Environment: A Rapidly Increasing, Long-Term Threat. *Environ. Res.* **2008**, *108* (2), 131–139.

(2) Anastas, P.; Eghbali, N. Green Chemistry: Principles and Practice. *Chem. Soc. Rev.* **2010**, *39* (1), 301–312.

(3) Griebel, J. J.; Glass, R. S.; Char, K.; Pyun, J. Polymerizations with Elemental Sulfur: A Novel Route to High Sulfur Content Polymers for Sustainability, Energy and Defense. *Prog. Polym. Sci.* **2016**, *58*, 90–125.

(4) Crockett, M. P.; Evans, A. M.; Worthington, M. J. H.; Albuquerque, I. S.; Slattery, A. D.; Gibson, C. T.; Campbell, J. A.; Lewis, D. A.; Bernardes, G. J. L.; Chalker, J. M. Sulfur-Limonene Polysulfide: A Material Synthesized Entirely from Industrial By-Products and Its Use in Removing Toxic Metals from Water and Soil. *Angew. Chemie Int. Ed.* **2016**, *55* (5), 1714–1718.

(5) Worthington, M. J. H.; Kucera, R. L.; Chalker, J. M. Green Chemistry and Polymers Made from Sulfur. *Green Chem.* **2017**, *19* (12), 2748–2761.

(6) Boyd, D. A. Sulfur and Its Role In Modern Materials Science. *Angew. Chemie Int. Ed.* **2016**, *55* (50), 15486–15502.

(7) Chung, W. J.; Griebel, J. J.; Kim, E. T.; Yoon, H.; Simmonds, A. G.; Ji, H. J.; Dirlam, P. T.; Glass, R. S.; Wie, J. J.; Nguyen, N. A.; Guralnick, B. W.; Park, J.; Somogyi, Á.; Theato, P.; Mackay, M. E.; Sung, Y.; Char, K.; Pyun, J. The Use of Elemental Sulfur as an Alternative Feedstock for Polymeric Materials. *Nat. Chem.* **2013**, *5* (6), 518–524.

(8) O Mohamed, A. M.; El Gamal, M. M.; Onsy, A.-M. *SULFUR CONCRETE FOR THE CONSTRUCTION INDUSTRY A Sustainable Development Approach*; 2010; Vol. 1.

(9) Carn, S. A.; Krueger, A. J.; Krotkov, N. A.; Gray, M. A. Fire at Iraqi Sulfur Plant Emits SO2 Clouds Detected by Earth Probe TOMS. *Geophys. Res. Lett.* **2004**, *31* (19), 2–5.

(10) Parker, D. J.; Jones, H. A.; Petcher, S.; Cervini, L.; Griffin, J. M.; Akhtar, R.;

Hasell, T. Low Cost and Renewable Sulfur-Polymers by Inverse Vulcanisation, and Their Potential for Mercury Capture. *J. Mater. Chem. A* **2017**, *5* (23), 11682–11692.

(11) Chalker, J. M.; Worthington, M. J. H.; Lundquist, N. A.; Esdaile, L. J. Synthesis and Applications of Polymers Made by Inverse Vulcanization. *Top. Curr. Chem.* **2019**, *377* (3), 1–27.

(12) Zhang, Y.; Glass, R. S.; Char, K.; Pyun, J. Recent Advances in the Polymerization of Elemental Sulphur, Inverse Vulcanization and Methods to Obtain Functional Chalcogenide Hybrid Inorganic/Organic Polymers (CHIPs). *Polym. Chem.* **2019**, *10* (30), 4078–4105.

(13) Limjuco, L. A.; Fissaha, H. T.; Kim, H.; Nisola, G. M.; Chung, W.-J. Sulfur Copolymerization with Hydrophilic Comonomers as Polysulfides in Microbeads for Highly Efficient Hg 2+ Removal from Wastewater . *ACS Appl. Polym. Mater.* **2020**.

(14) Lin, H. K.; Lai, Y. S.; Liu, Y. L. Cross-Linkable and Self-Foaming Polysulfide Materials for Repairable and Mercury Capture Applications. *ACS Sustain. Chem. Eng.* **2019**, *7* (4), 4515–4522.

(15) Kleine, T. S.; Lee, T.; Carothers, K. J.; Hamilton, M. O.; Anderson, L. E.; Ruiz Diaz, L.; Lyons, N. P.; Coasey, K. R.; Parker, W. O.; Borghi, L.; Mackay, M. E.; Char, K.; Glass, R. S.; Lichtenberger, D. L.; Norwood, R. A.; Pyun, J. Infrared Fingerprint Engineering: A Molecular-Design Approach to Long-Wave Infrared Transparency with Polymeric Materials. *Angew. Chemie - Int. Ed.* **2019**, *58* (49), 17656–17660.

(16) Griebel, J. J.; Nguyen, N. A.; Namnabat, S.; Anderson, L. E.; Glass, R. S.; Norwood, R. A.; Mackay, M. E.; Char, K.; Pyun, J. Dynamic Covalent Polymers via Inverse Vulcanization of Elemental Sulfur for Healable Infrared Optical Materials. *ACS Macro Lett.* **2015**, *4* (9), 862–866.

(17) Anderson, L. E.; Kleine, T. S.; Zhang, Y.; Phan, D. D.; Namnabat, S.; LaVilla, E. A.; Konopka, K. M.; Ruiz Diaz, L.; Manchester, M. S.; Schwiegerling, J.; Glass, R. S.; Mackay, M. E.; Char, K.; Norwood, R. A.; Pyun, J. Chalcogenide

Hybrid Inorganic/Organic Polymers: Ultrahigh Refractive Index Polymers for Infrared Imaging. *ACS Macro Lett.* **2017**, *6* (5), 500–504.

(18) Mann, M.; Kruger, J. E.; Andari, F.; McErlean, J.; Gascooke, J. R.; Smith, J. A.; Worthington, M. J. H.; McKinley, C. C. C.; Campbell, J. A.; Lewis, D. A.; Hasell, T.; Perkins, M. V.; Chalker, J. M. Sulfur Polymer Composites as Controlled-Release Fertilisers. *Org. Biomol. Chem.* **2019**, *17* (7), 1929–1936.

(19) Herrera, C.; Ysinga, K. J.; Jenkins, C. L. Polysulfides Synthesized from Renewable Garlic Components and Repurposed Sulfur Form Environmentally Friendly Adhesives. *ACS Appl. Mater. Interfaces* **2019**, *11* (38), 35312–35318.

(20) Tonkin, S. J.; Gibson, C. T.; Campbell, J. A.; Lewis, D. A.; Karton, A.; Hasell, T.; Chalker, J. M. Chemically Induced Repair, Adhesion, and Recycling of Polymers Made by Inverse Vulcanization. *Chem. Sci.* **2020**, *11* (21), 5537–5546.

(21) Zhang, B.; Gao, H.; Yan, P.; Petcher, S.; Hasell, T. Inverse Vulcanization below the Melting Point of Sulfur. *Mater. Chem. Front.* **2020**, *4* (2), 669–675.

(22) Gomez, I.; Leonet, O.; Blazquez, J. A.; Mecerreyes, D. Inverse Vulcanization of Sulfur Using Natural Dienes as Sustainable Materials for Lithium–Sulfur Batteries. *ChemSusChem* **2016**, *9* (24), 3419–3425.

(23) Wu, F.; Chen, S.; Srot, V.; Huang, Y.; Sinha, S. K.; van Aken, P. A.; Maier, J.; Yu, Y. A Sulfur-Limonene-Based Electrode for Lithium-Sulfur Batteries: High-Performance by Self-Protection. *Adv. Mater.* **2017**, *1706643*, 1–8.

(24) Zhang, Y.; Griebel, J. J.; Dirlam, P. T.; Nguyen, N. A.; Glass, R. S.; Mackay, M. E.; Char, K.; Pyun, J. Inverse Vulcanization of Elemental Sulfur and Styrene for Polymeric Cathodes in Li-S Batteries. *J. Polym. Sci. Part A Polym. Chem.* **2017**, *55* (1), 107–116.

(25) Oishi, S.; Oi, K.; Kuwabara, J.; Omoda, R.; Aihara, Y.; Fukuda, T.; Takahashi, T.; Choi, J.-C.; Watanabe, M.; Kanbara, T. Synthesis and Characterization of Sulfur-Based Polymers from Elemental Sulfur and Algae Oil. *ACS Appl. Polym. Mater.* **2019**, *1* (5), 1195–1202.

(26) Worthington, M. J. H.; Shearer, C. J.; Esdaile, L. J.; Campbell, J. A.; Gibson,

C. T.; Legg, S. K.; Yin, Y.; Lundquist, N. A.; Gascooke, J. R.; Albuquerque, I. S.; Shapter, J. G.; Andersson, G. G.; Lewis, D. A.; Bernardes, G. J. L.; Chalker, J. M. Sustainable Polysulfides for Oil Spill Remediation: Repurposing Industrial Waste for Environmental Benefit. *Adv. Sustain. Syst.* **2018**, *2* (6), 1800024.

(27) Karunarathna, M. S.; Lauer, M. K.; Thiounn, T.; Smith, R. C.; Tennyson, A. G. Valorisation of Waste to Yield Recyclable Composites of Elemental Sulfur and Lignin. *J. Mater. Chem. A* **2019**, *7* (26), 15683–15690.

(28) Lundquist, N. A.; Tikoalu, A. D.; Worthington, M. J. H.; Shapter, R.; Tonkin, S. J.; Stojcevski, F.; Mann, M.; Gibson, C. T.; Gascooke, J. R.; Karton, A.; Henderson, L. C.; Esdaile, L. J.; Chalker, J. M. Reactive Compression Molding Post-Inverse Vulcanization: A Method to Assemble, Recycle, and Repurpose Sulfur Polymers and Composites. *Chem. - A Eur. J.* **2020**, *26* (44), 10035–10044.

(29) Deng, Z.; Hoefling, A.; Théato, P.; Lienkamp, K. Surface Properties and Antimicrobial Activity of Poly(Sulfur- Co -1,3-Diisopropenylbenzene) Copolymers. *Macromol. Chem. Phys.* **2018**, *219* (5), 1700497.

(30) Zhang, B.; Petcher, S.; Hasell, T. A Ternary System for Delayed Curing Inverse Vulcanisation. *Chem. Commun.* **2019**, *55* (72), 10681–10684.

(31) Wu, X.; Smith, J. A.; Petcher, S.; Zhang, B.; Parker, D. J.; Griffin, J. M.; Hasell, T. Catalytic Inverse Vulcanization. *Nat. Commun.* **2019**, *10* (1), 647.

(32) Smith, J. A.; Green, S. J.; Petcher, S.; Parker, D. J.; Zhang, B.; Worthington, M. J. H.; Wu, X.; Kelly, C. A.; Baker, T.; Gibson, C. T.; Campbell, J. A.; Lewis, D. A.; Jenkins, M. J.; Willcock, H.; Chalker, J. M.; Hasell, T. Crosslinker Copolymerization for Property Control in Inverse Vulcanization. *Chem. - A Eur. J.* **2019**, 10433–10440.

(33) Parker, D. J.; Chong, S. T.; Hasell, T. Sustainable Inverse-Vulcanised Sulfur Polymers. *RSC Adv.* **2018**, *8* (49), 27892–27899.

(34) Khawaja, S. Z.; Vijay Kumar, S.; Jena, K. K.; Alhassan, S. M. Flexible Sulfur Film from Inverse Vulcanization Technique. *Mater. Lett.* **2017**, *203*, 58–61.

(35) Eom, Y.; Won, J. H.; Ryu, J. Y.; Lee, T. G. Biosorption of Mercury(II) Ions from Aqueous Solution by Garlic (Allium Sativum L.) Powder. *Korean J. Chem. Eng.* **2011**, *28* (6), 1439–1443.

(36) Coates, J. Interpretation of Infrared Spectra, A Practical Approach. In *Encyclopedia of Analytical Chemistry*; John Wiley & Sons, Ltd: Chichester, UK, 2006; pp 1–23.

(37) Hasell, T.; Parker, D. J.; Jones, H. A.; McAllister, T.; Howdle, S. M. Porous Inverse Vulcanised Polymers for Mercury Capture. *Chem. Commun.* **2016**, *52* (31), 5383–5386.

(38) Petcher, S.; Parker, D. J.; Hasell, T. Macroporous Sulfur Polymers from a Sodium Chloride Porogen - A Low Cost, Versatile Remediation Material. *Environ. Sci. Water Res. Technol.* **2019**, *5* (12), 2142–2149.

(39) Scheiger, J. M.; Direksilp, C.; Falkenstein, P.; Welle, A.; Koenig, M.; Heissler, S.; Matysik, J.; Levkin, P. A.; Theato, P. Inverse Vulcanization of Styrylethyltrimethoxysilane–Coated Surfaces, Particles, and Crosslinked Materials. *Angew. Chemie - Int. Ed.* **2020**, *59* (42), 18639–18645.

(40) Thielke, M.; Bultema, L.; Brauer, D.; Richter, B.; Fischer, M.; Theato, P. Rapid Mercury(II) Removal by Electrospun Sulfur Copolymers. *Polymers (Basel).* **2016**, *8* (7), 266.

(41) Tikoalu, A. D.; Lundquist, N. A.; Chalker, J. M. Mercury Sorbents Made By Inverse Vulcanization of Sustainable Triglycerides: The Plant Oil Structure Influences the Rate of Mercury Removal from Water. *Adv. Sustain. Syst.* **2020**, *4* (3), 1–9.

Chapter 4. Inverse vulcanisation in mild condition

4.1 Context

4.1.1 Abstract

Elemental sulfur is an abundant by-product of the petrochemicals industry, but polymeric sulfur cannot be used because they are not stable and depolymerize to the monomer, S_8. Inverse vulcanization reported recently uses vinylic monomers as crosslinkers to stabilize polymers made from elemental sulfur. Herein we report that the catalyst sodium diethyldithiocarbamate trihydrate allows inverse vulcanization to be conducted at low temperatures (110 °C), even below the melting point of sulfur (120 °C). Lower reaction temperatures are beneficial for not only energy economy, but also in preventing dangerous auto-acceleration, hydrogen sulfide generation, and allowing low boiling point monomers to be used. Excess catalyst can be recovered from the polymers, and despite a crosslinked structure, the reversibility of the S-S bonds allows the polymers to be recycled.

4.1.2 Publication

Bowen Zhang, **Hui Gao**, **Peiyao Yan**, **Samuel Petcher**, **Tom Hasell***, Inverse vulcanization below the melting point of sulfur, *Materials. Chemistry. Frontiers.* 4 (2020) 669–675.

4.1.3 Author contributions

Bowen Zhang: Conceptualization, Methodology, Investigation, Formal analysis, Writing - original draft, Writing - review & editing. **Hui Gao**: Investigation. **Peiyao Yan**: Investigation. **Samuel Petcher**: Investigation, Formal analysis, Writing - review & editing **Tom Hasell**: Resources, Writing - review & editing, Supervision, Project administration, Funding acquisition.

4.2 Introduction

As discussed in previous chapters, sulfur polymers synthesized by inverse vulcanisation have attracted attention in recent years, because of their potential to reduce reliance on ecologically damaging conventional synthetic polymers, and alleviating the "excess sulfur problem".[1–3]

Sulfur polymers have been studied for a variety of applications,[4–6] however, widespread practical applications to be realised, scaling the reaction up and simplifying the processing are two key challenges. In previous chapters, by involving blend crosslinkers, a ternary system could synthesize a reservable pre-polymer solution, effectively avoiding auto-acceleration and elongating the periods of time before curing, however, the reaction was still conducted at high temperature (> 140 °C). According to the principle of green chemistry,[5,7] the design for reactions should consider energy efficiency and renewability as well. Therefore, in order to achieve a lower reaction temperature (< 140 °C) for inverse vulcanization, several different systems have been investigated. Dynamic Covalent Polymerizations were termed to prepare sulfur polymers at mild temperature, even as low as 60 °C, but required the synthesis of oligomers or prepolymers at higher temperatures first to generate activated sulfur radicals.[8,9] Dynamic sulfur bonds were vital to this strategy, because of acting as an accelerator to reduce the reaction energy of the whole system. Thus, the disadvantage of complex operation cannot be overlooked. However, this modification made it possible to incorporate crosslinkers with lower boiling points into inverse vulcanization.[8,9] Another main approach is applying catalyst in the system, a better way also aligned with green chemistry. But, to date, the temperature limitation was still fixed to 135 °C, a temperature required to melt sulfur then to generate sulfur radicals.[10]

Herein is reported a mild condition catalytic inverse vulcanization, in which the temperature is below 119 °C, at which sulfur remains in the solid state, to prepare stable sulfur polymers (Figure 4.1). In this process any excess catalyst could be collected and recycled. It was supposed that the catalyst may lower the energy of reactions, likely acting as an initiator attacking and opening S_8 at low temperature, allowing the activated sulfur chains to propagate in the whole system. Additionally,

after leaching catalyst in the products, sulfur polymers could be remoulded into alternative shapes at 110 °C because of the S-S dynamic covalent bonds.

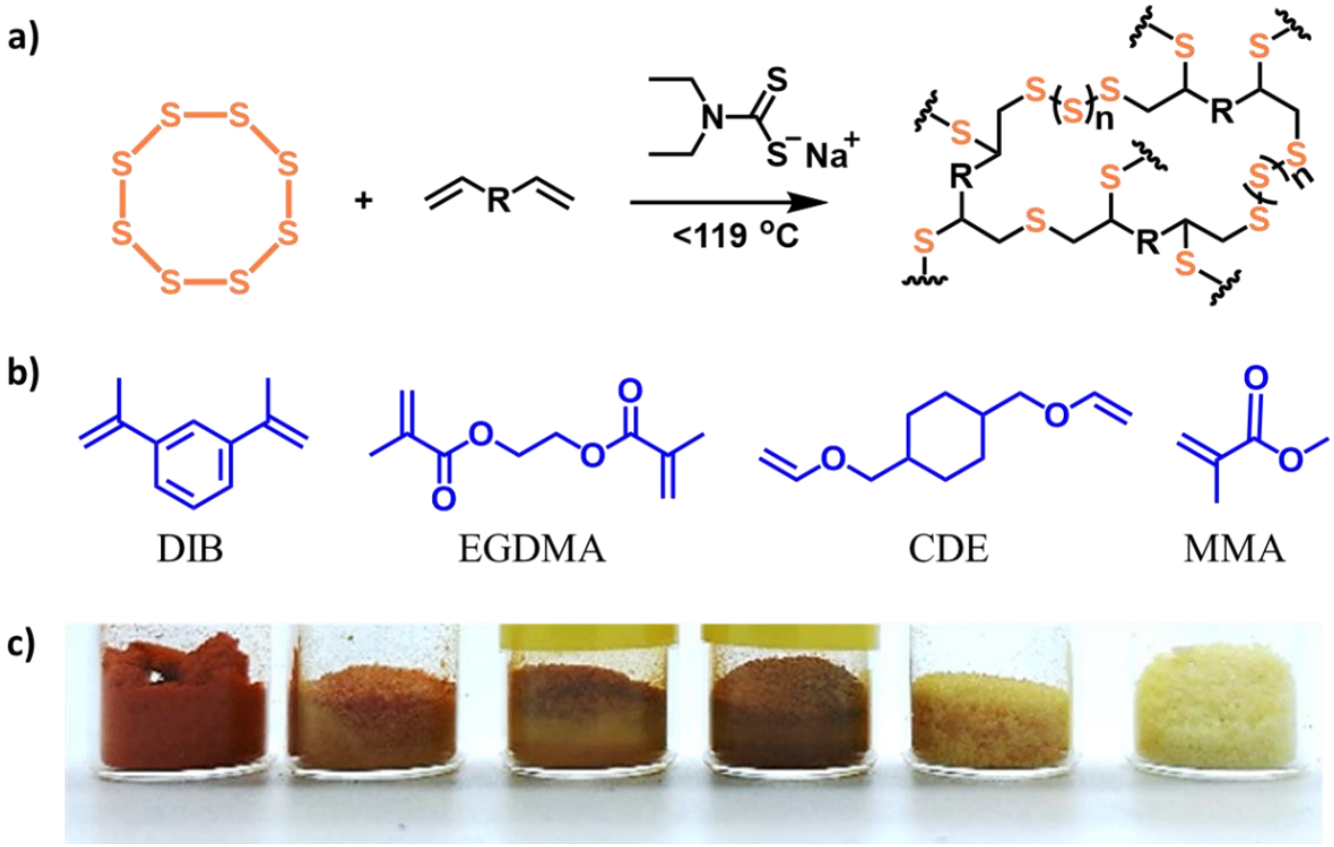

Figure 4.1 (a) General reaction scheme for the inverse vulcanization below sulfur melting point with catalyst NaDTC. (b) Structure of crosslinkers for inverse vulcanization reported, from left to right, 1,3-diisopropenylbenzene (DIB), ethylene glycol dimethylacrylate (EGDMA), Cyclohexanedimethanol divinyl ether (CDE) and methy methacrylate (MMA). (c) Stable solid state products generated from inverse vulcanization below 119 °C. From left to right, ground sulfur polymers of SDIBC0T180, SDIBC1T110, SDIBC5T110, SDIBC10T110, SEGDMAC1T110, and SEGD- MAC1T100 (see footnote of Table 3.1 for naming system).

4.3 Aims

1. Investigate the possibility of inverse vulcanisation reaction at low temperature (110 °C).
2. Investigate the role of catalyst in inverse vulcanisation.
3. Investigate the potential of recycling of any excess catalyst and the remould of thiopolymer powder at low temperature because of dynamic covalent bonds.

4.4 Results and discussion

4.4.1 Sulfur polymers

Sodium diethyldithiocarbamate trihydrate (NaDTC) has been used as a rubber accelerator in industry,[11] and this inspired us to apply this chemical into inverse vulcanisations. However, for some reactions, it reacted too quickly and generated inhomogeneous products, or even resulted in auto-acceleration from the Trommsdorff-Norrish effect at the standard heating temperature (higher than 135 °C) of inverse vulcanizations.[10] Therefore, this phenomenon encouraged us to trial this chemical to initiate and accelerate inverse vulcanization at low temperature. Moreover, it was noticed that the organic ligand of NaDTC seemed to benefit the miscibility of the system compared with inorganic catalysts, such as Na_2S. Conventionally, inverse vulcanization has been performed at a temperature higher than 135 °C to induce cleavage of sulfur rings and generate disulfur radicals. But in the reaction at lower temperature, sulfur rings were possibly opened heterogeneously by nucleophilic activation.[8] Considering that sulfur is solid at below 120 °C, the reaction is conducted in two phases, thus the ratio of sulfur to crosslinkers is important as too much sulfur (such as Sample SDIB30C1T110, see Table 4.1 footnote for naming system) decreases mobility of the system, resulting in inhomogeneous products, as shown Figure 4.2 Sulfur polymers were prepared as stable solids at low temperature with different colours as shown in Figure 4.1 (a). The difference in colour appears to depend on the degree of reaction and the length of sulfur chain, as the more catalyst applied the darker product is.

Figure 4.2 It can be observed that sample SDIB30C1T110 is inhomogeneous with bubbles, which is because of low mobility of the system followed by triggering auto acceleration.

Table 4.1 Samples trialed with different components and under different conditions.

Sample name*	Crosslinker /%	NaDTC /%	Temperature/°C	Reacting time and curing time
SEGDMAC1T100	EGDMA 50%	1	100	20 min; overnight (>12 hours)
SEGDMAC1T110	EGDMA 50%	1	110	10 min; overnight (>12 hours)
SDIB30C1T110	DIB 30%	1	110	Incomplete reaction of sulfur
SDIBC1T110	DIB 50%	1	110	>12 hours, <24 hours; overnight (>12 hours)
SDIBC5T110	DIB 50%	5	110	>12 hours, <24 hours; overnight (>12 hours)
SDIBC10T110	DIB 50%	10	110	12 hours; overnight (>12 hours)
SDIBC0T180	DIB 50%	0	180	10min; no curing
SMMAC10T95	MMA 50%	10	95	>12 hours, <24 hours; 96 hours (curing temperature raised from 95 °C to 110 °C gradually)
SEGDMAC0T110	EGDMA 50%	0	110	No reaction
SDIBC0T110	DIB 50%	0	110	>40 hours; overnight (>12 hours)
SMMAC0T95	MMA 50%	0	110	No reaction

Naming system: sulfur polymers are referred to as S–Crosslinker-P-C-n-T-n, where P is the percentage of crosslinkers used in the experiments, if the ratio of sulfur to crosslinker is 1:1, P will be omitted, C-n refers to weight percentage of catalyst, and T-n shows the temperature reactions were conducted.

4.4.1.1 Poly(S-DIB)

The reactions (*e.g.* SDIBC0T110) without catalyst at low temperature were conducted as control experiments. Surprisingly, it was found that even with no catalyst DIB could react with solid sulfur but prohibitively slowly. From the ^{1}H NMR (Figure 4.3) performed at 18 hours, there were some new peaks appearing between 3.0 and 4.0, indicating the generation of S-C bonds. This is the first time inverse vulcanization has been observed below the sulfur melting temperature as shown in Figure 4.4. However, because it took more than 40 hours for the reaction to reach completion without catalyst, this would be problematic for practical use. The reactions of sulfur and DIB with catalyst are initially heterogeneous. After 2 hours, all visible solid sulfur was either dissolved or reacted with no more solid remaining (Figure 4.5), but the reaction still remained heterogeneous in that two distinct liquid layers could be seen. Around 7 hours, the degree of reaction determined by NMR was similar to that of SDIBC0T110 at 18 hours, as shown in Figure 4.3.

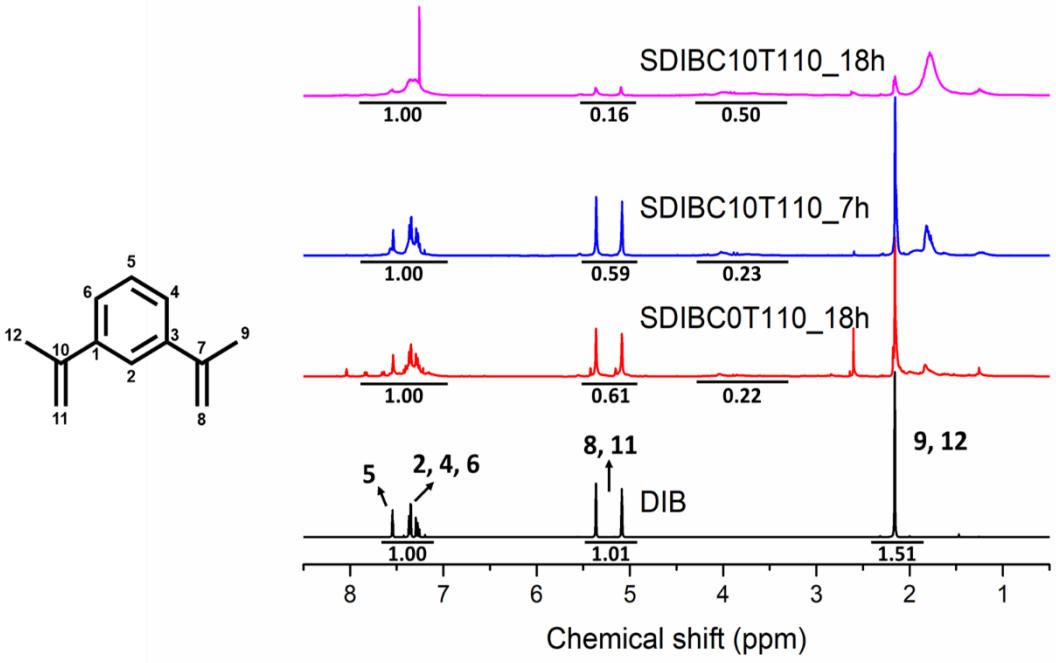

Figure 4.3 ^{1}H NMR spectra for SDIBC0T110 followed at 18 hours, SDIBC10T110 followed at 7 hours and 18 hours, and DIB standard. For SDIBC0T110, clearly, compared with pure DIB, the integral ratio of the peaks at 7.0 to 7.5 to the peak at 5.0 to 5.5 decreased, demonstrating the reduction of C=C bonds. And new peaks at 3.0 to 4.0 suggested the apparence of S-C-H generatted. For SDIBC10T110, followed at 7 hours, the integral of the peaks at this stage is similar to that of SDIBC0T110 at 18 hours, indicating that the degree of reactions is similar. After 18 hours, spectra of SDIBC10T110 was performed from the dissolved part of sulfur polymers. Only a small signal of C=C bonds remains compared with the reaction without catalyst assuming same time. The peaks are also broader, indicative of polymerisation.

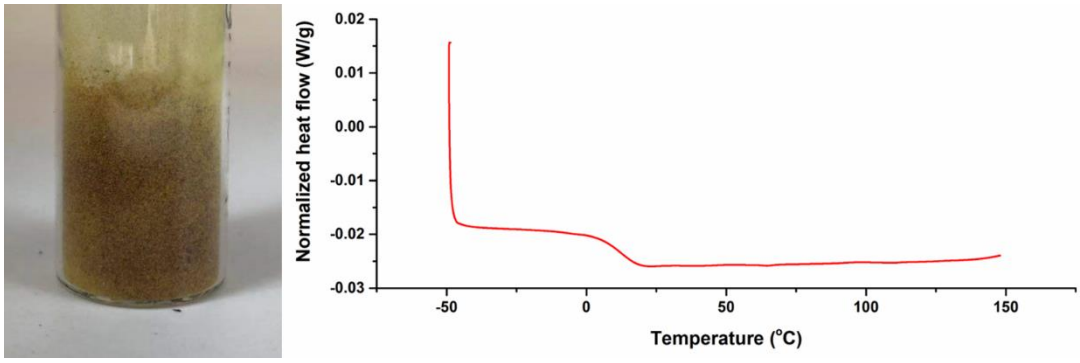

Figure 4.4 Inverse vulcanisation of sulfur and DIB at 110 °C without catalyst. Left is ground SDIBC0T110 samples and the right is DCS trace of SDIBC0T110, showing that T_g is around 10 °C and no peaks of melting sulfur.

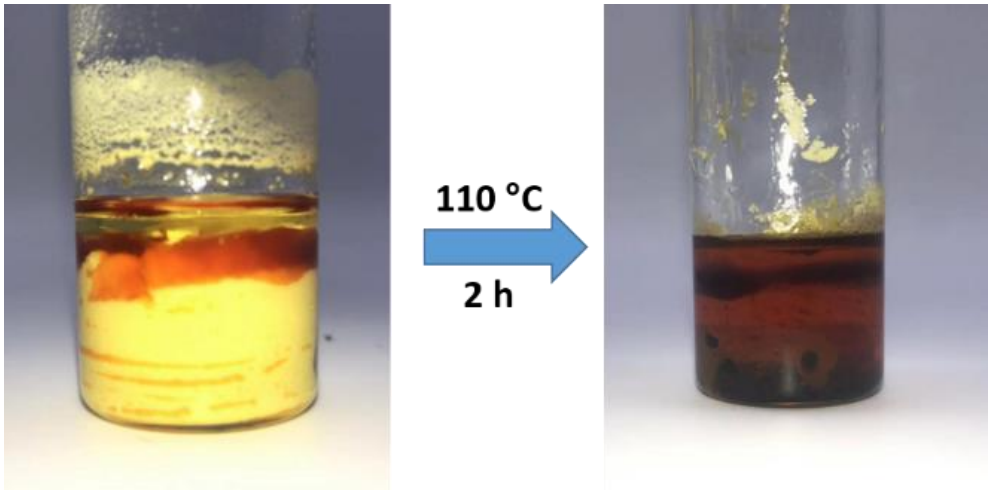

Figure 4.5 Images of reaction of SDIBC10T110: left is the beginning of the reaction with solid sulfur, and right is, after 2 hours, the two phases of reaction but no solid sulfur observed.

We also compared the ^{1}H NMR of SDIBC10T110 assumed same time with SDIBC0T110, indicating that the reaction with NaDTC is much more complete at same temperature (Figure 4.3). Sulfur polymers made at low temperature were from light yellow to dark brown, changing with the amount of catalyst. These colours are similar in appearance to these of conventionally produced sulfur polymers. Increased catalyst content in the reaction is likely to lead to increased C=C double bond reaction, and shorter S-S chains between crosslinkers.

The ATR-FTIR patterns, as shown in Figure 4.6, of Poly(S-DIB) further confirmed this assumption. As the amount of catalyst is increased, reductions of signals were shown at 3080, 3041, and 1640 cm^{-1}, corresponding to the stretching and symmetric stretching vibrations of C=C-H and stretching vibration of C=C respectively. Moreover, the clear decrease of signals at 887 cm^{-1}, of the CH_2 out-of-plane deformation, verified more C=C double bounds are consumed in the reaction with increased catalyst content. According to the result of elemental analysis, the actual sulfur content of SDIBC1T110 was found to be higher than that calculated in theory, probably because of the evaporation of monomers during the reaction processing (as shown in Table 4.2).

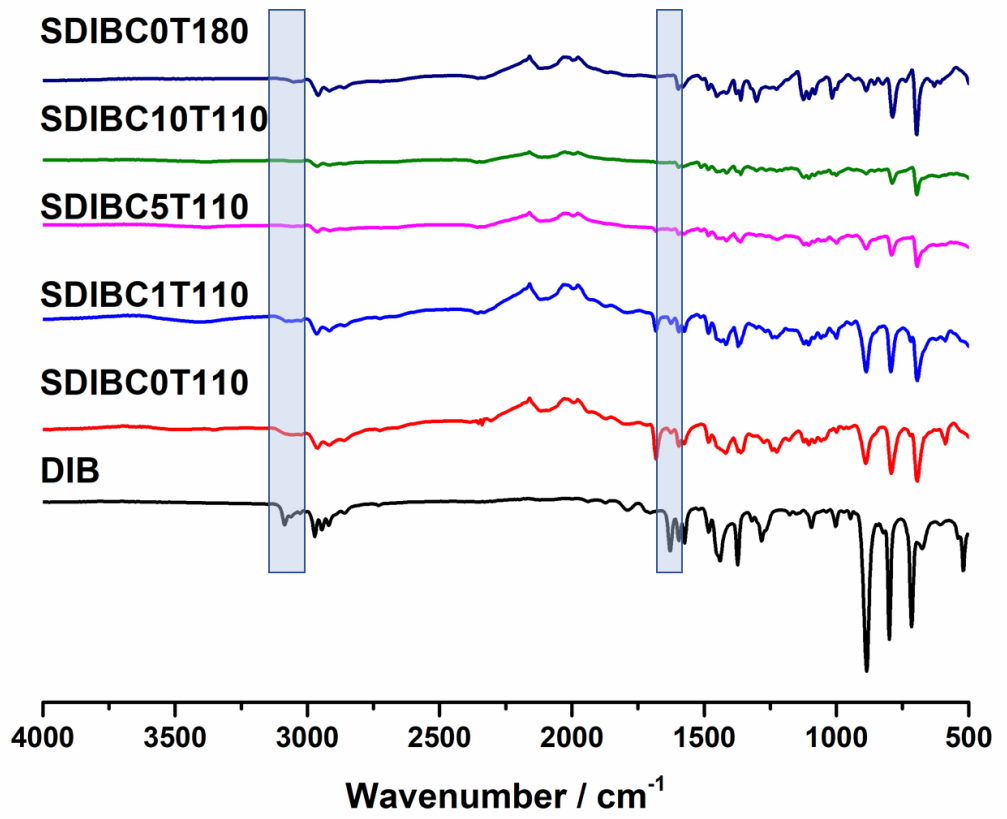

Figure 4.6 FT-IR spectroscopy of sulfur polymers with different amount catalyst. As the amount of catalyst is increased, reductions of signals were seen at 3080, 3041, and 1640 cm^{-1}, corresponding to the stretching and symmetric stretching vibrations of C=C-H and stretching vibration of C=C respectively.

Table 4.2 Elemental analysis of sulfur polymers with different component and prepared under different conditions.

	Calc %			Analysis %		
	% C	% H	% S	% C	% H	% S
SEGDMAC1T100	30.75	3.61	50.48	30.18	3.56	50.91
SEGDMAC1T110	30.75	3.61	50.48	30.51	3.61	50.43
SDIBC1T110	44.45	5.57	49.98	39.25	3.90	55.48
SDIBC5T110	46.22	5.87	51.87	42.17	4.15	52.74
SDIBC10T110	48.44	6.23	54.24	43.20	4.36	50.43
SDIBC0T180	44.44	5.56	50.00	45.34	4.44	51.02

From the DSC traces, as shown in Figure 4.7 and Figure A4.1, T_g increased with the amount of catalyst. In comparison with the thiopolymer produced from S and DIB without catalyst (but at the higher temperature of 180 °C), sulfur polymers generated from the reaction with 1% catalyst had lower T_g, however the products of both reactions with 5% and 10% catalyst had higher T_g. There is no sulfur melting peak observed from all sulfur polymers.

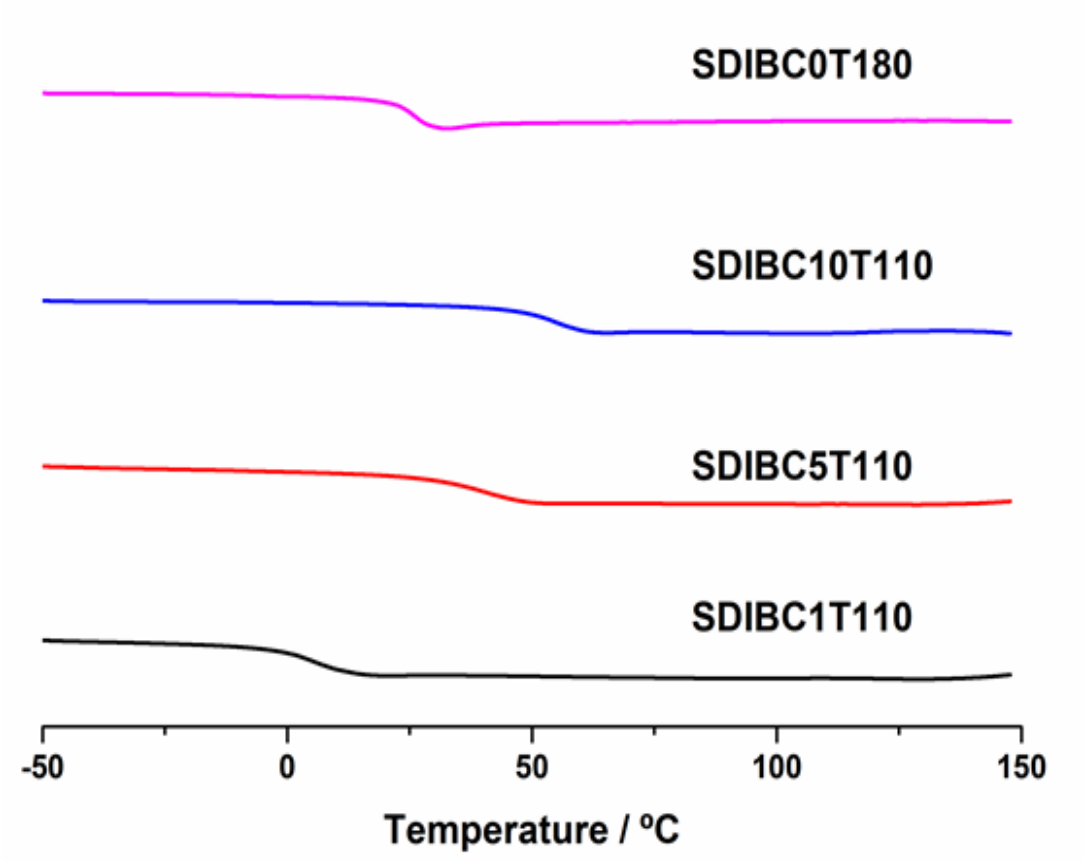

Figure 4.7 Offset DSC traces for different percentage NaDTC of poly(S-DIB).

Powder X-ray diffraction (PXRD) was also used to detect if residual sulfur crystals are present in the amorphous copolymers. Interestingly, from powder X-ray diffraction patterns of all poly(S-DIB), as shown in Figure 4.8 and Figure 4.9, different sharp peaks could be observed, some of which do not match the pattern of any sulfur polymorph. After further study, the patterns observed in SDIBC5T110 and SDIBC10T110 were identified as that of NaDTC, indicating the presence of residual catalyst in the polymers.

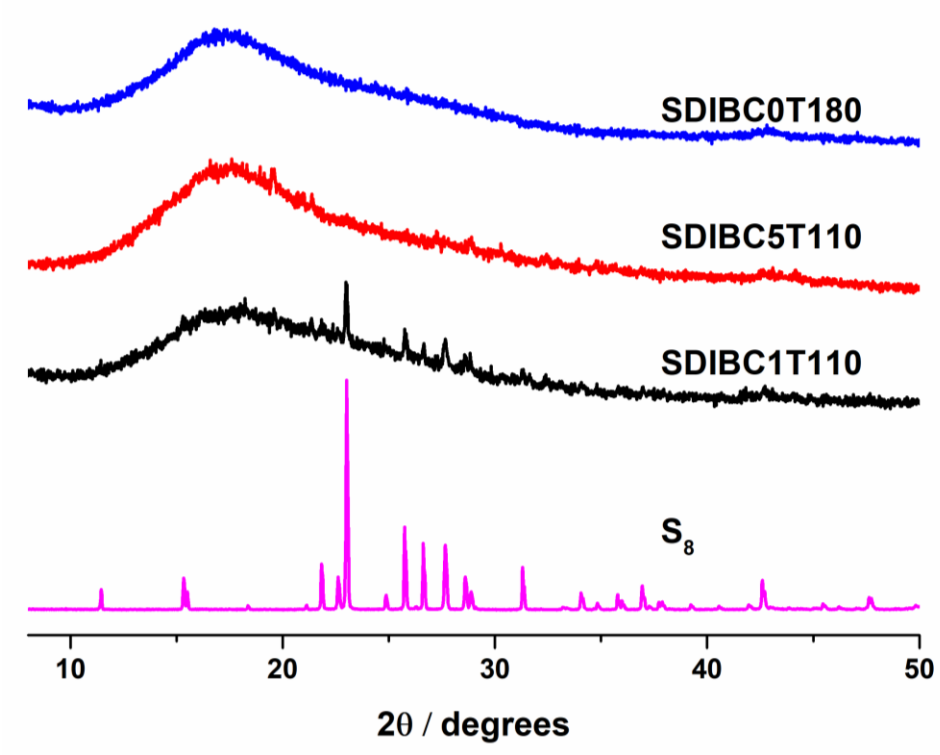

Figure 4.8 Offset PXRD patterns for different percentage NaDTC of poly(S-DIB).

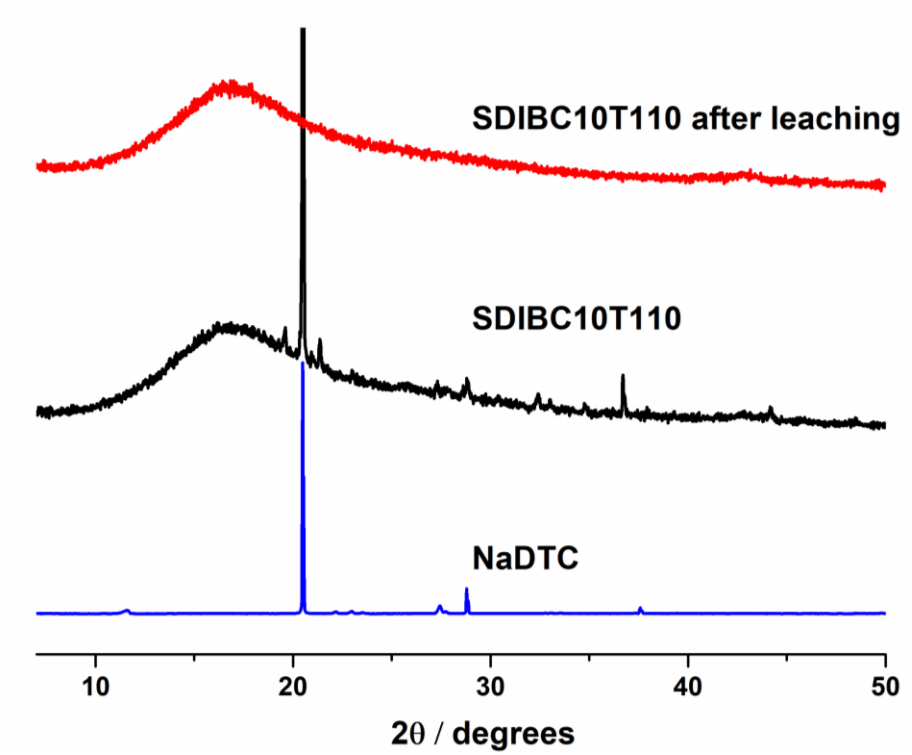

Figure 4.9 Offset PXRD patterns for SDIBC10T110 and corresponding residual solid after leaching, and NaDTC.

Additionally, to test the degree of the reaction and the stability of product, any amorphous sulfur imbedded in the polymers synthesized after 3 months was detected by thin layer chromatography (TLC). The result (Figure 4.10) shown no sulfur could be detected from SDIBC10T110, suggesting the totally consumption of elemental

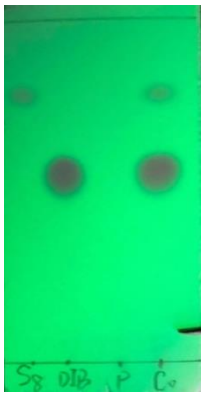

Figure 4.10 Detection of elemental sulfur by TLC. Spots on the baseline from left to right are elemental sulfur, DIB, poly(S-DIB), and mixture of sulfur, DIB, and poly(S-DIB). Neither sulfur or DIB was detected in the polymer after 3 months since being synthesized, proving the high completion of reaction and good stability of the final product.

sulfur and the stability of S-S bonds. The reaction was increased from 10 g to 100 g to demonstrate the potential for scaling up (Figure 4.11), benefiting industrial processing.

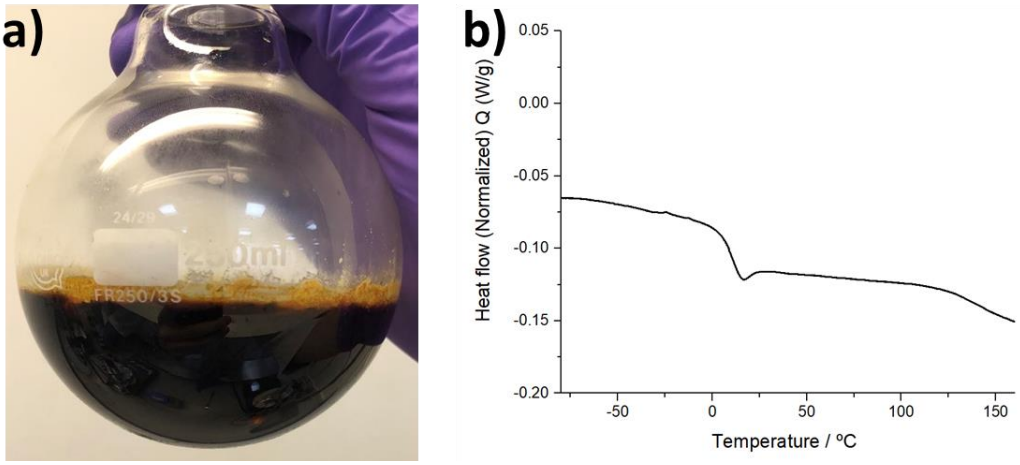

Figure 4.11 a) Scale up testing of reaction of sulfur and DIB from 10 g to 100 g. b) DCS trace of large-scale products, showing comparable T_g to SDIBC10T110.

4.4.1.2 Poly(S-EGDMA) and poly(S-MMA)

Similar to the control experiments of sulfur and DIB, SEGDMAC0T110 and SMMAC0T95 were performed, as shown in Figure 4.12. However, unlike SDIBC0T110, sulfur did not react with either EGDMA or MMA at low temperature for more than 18 hours, which were confirmed by 1H NMR (Figure 4.13 and Figure 4.14). Involved NaDTC, EGDMA reacted heterogeneous with sulfur initially at mild temperature and became homogeneous at last (Figure 4.15).

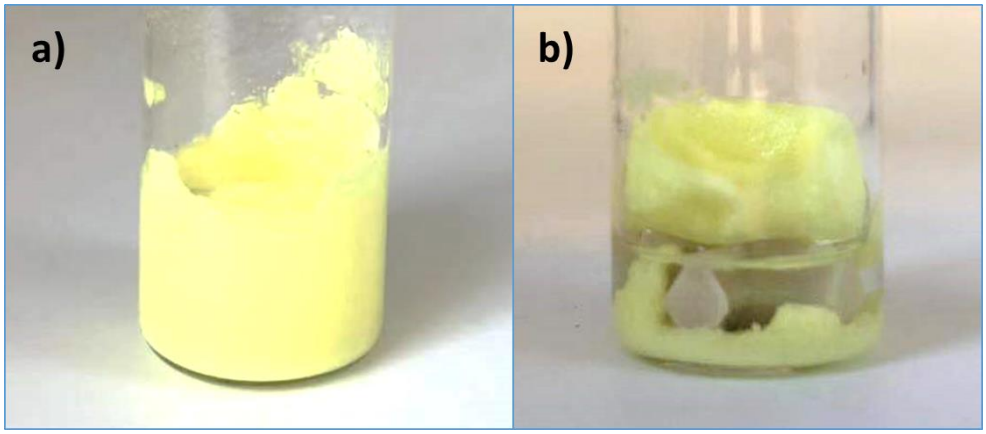

Figure 4.12 a) The reaction of SEGDMAC0T110, b) the reaction of SMMAC0T95

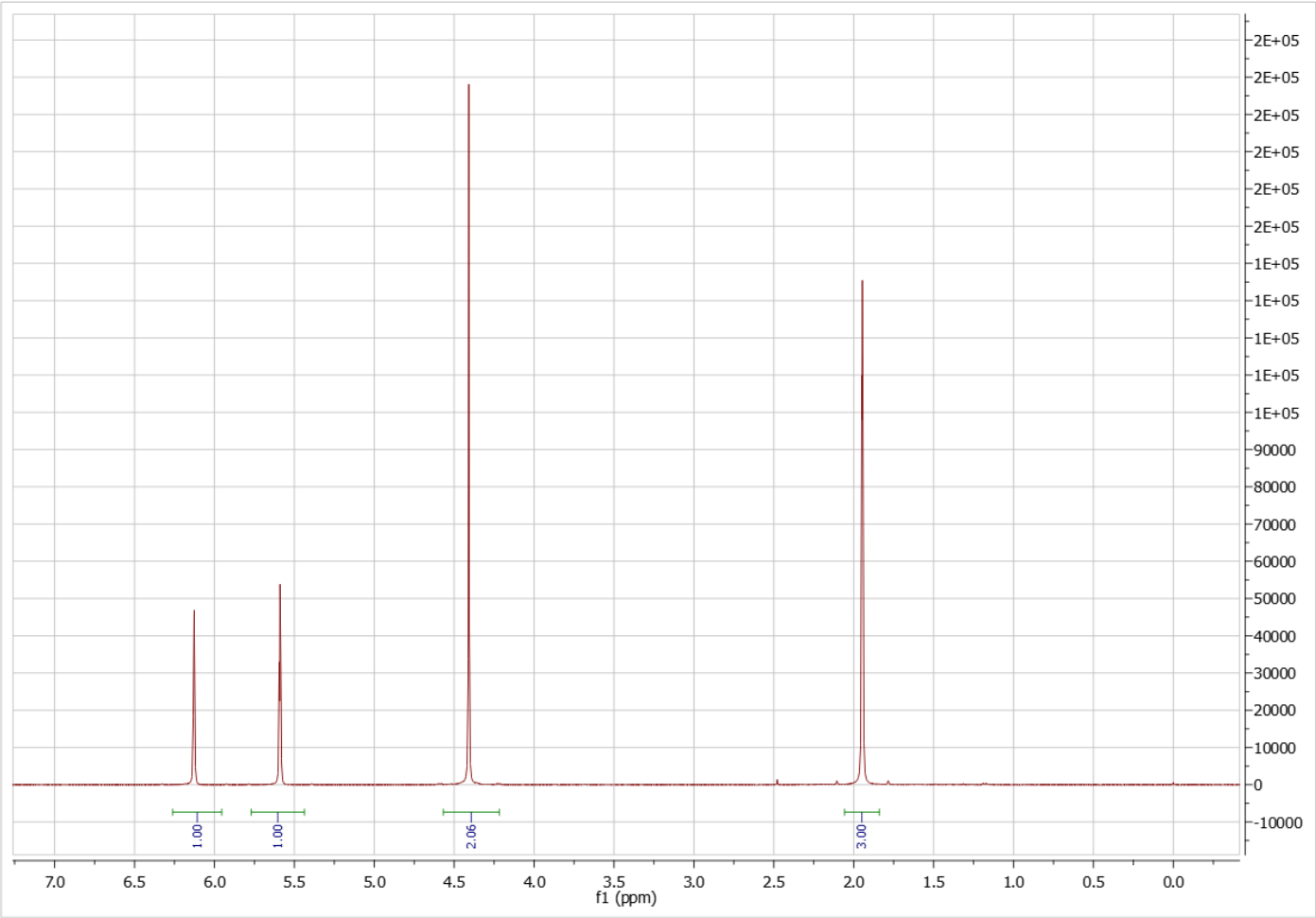

Figure 4.13 ^{1}H NMR spectra for SEGDMAC0T110. Apparently, C=C bonds in EGDMA were not reacted. Assignment of each peak can be found in Figure 2.12.

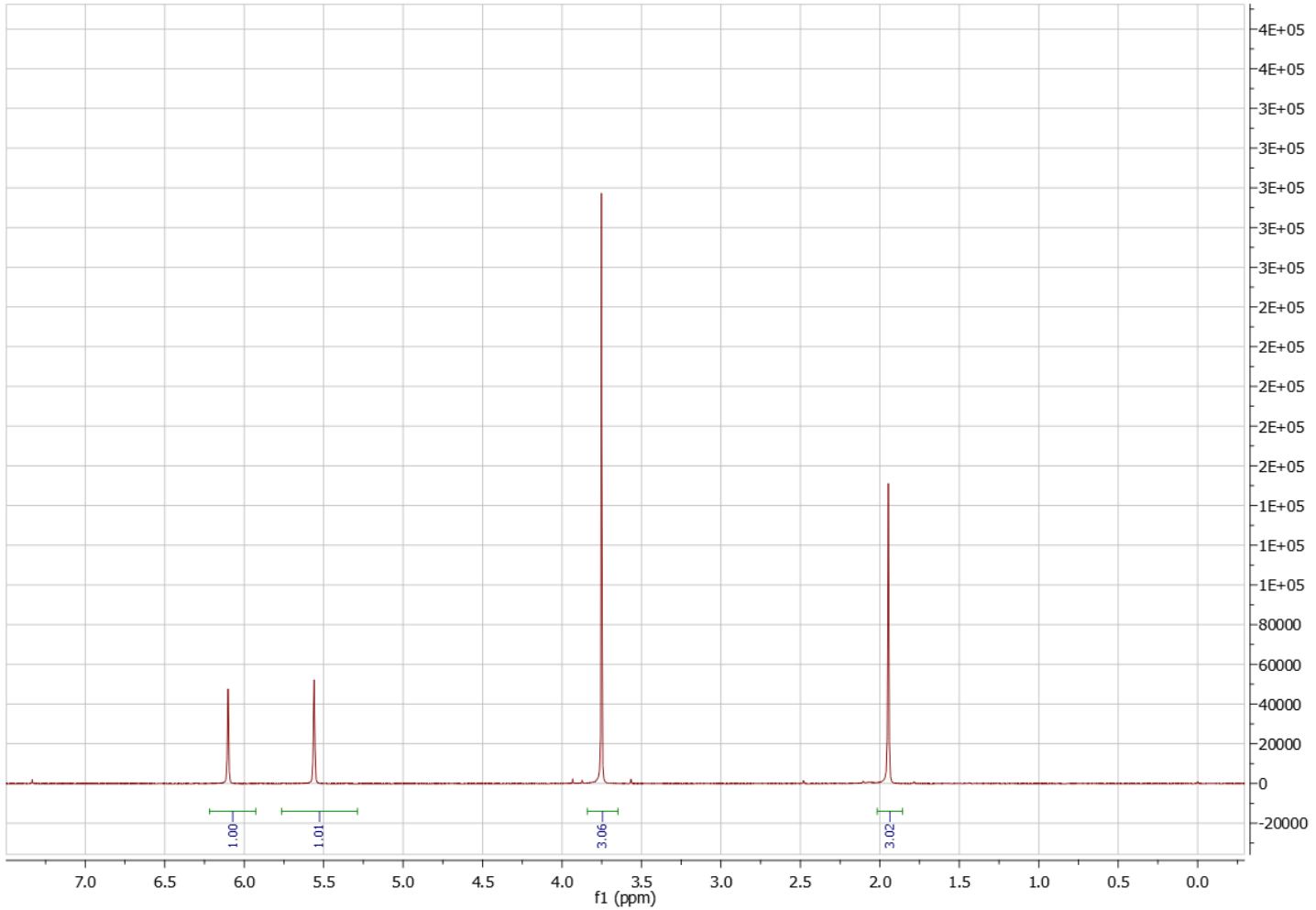

Figure 4.14 ^{1}H NMR spectra for SMMAC0T95. Same with the reaction of SEGDMAC0T110, without NaDTC, MMA cannot react with sulfur. Assignment of each peak can be found in Figure 4.22.

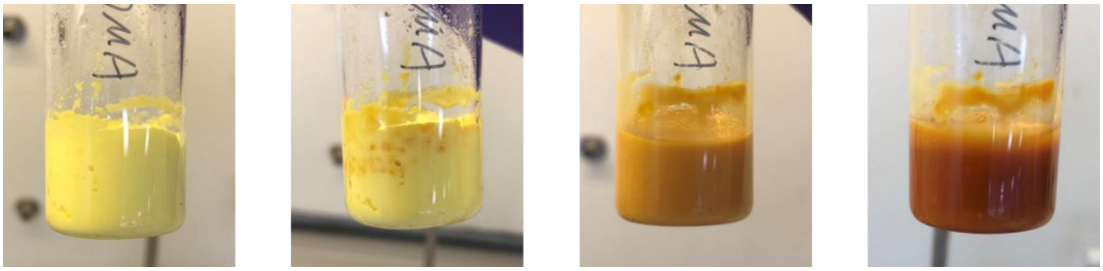

Figure 4.15 Images of processing to produce Poly(S-EGDMA) at 110 °C, showing heterogeneity initially and homogeneity as time progresses.

From the DSC traces (see Figure 4.16 and Figure A 4.2), sulfur polymers prepared from EGDMA at different temperature (100 or 110 °C) have clear glass transition temperatures, indicating the generation of homogenous copolymers. There is no significant difference the T_g, suggesting that the reacting temperature did not affect reaction processing very much. In both situations, no S_8 crystals were detected.

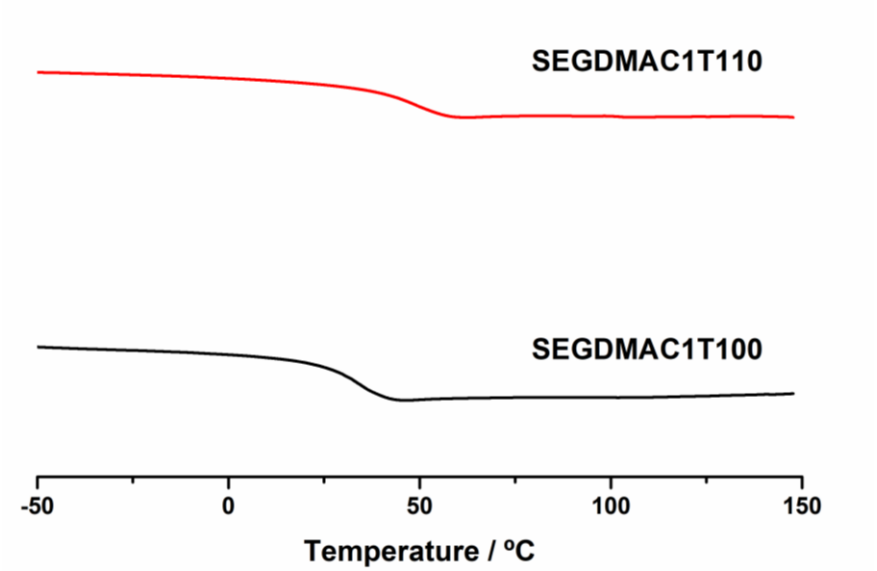

Figure 4.16 Offset DSC traces for different temperatures of poly(S-EGDMA) with NaDTC.

A higher ratio of catalyst added to the reaction of sulfur and EGDMA further increased the rate, but also trigged auto-acceleration, introducing heterogeneity (Figure 4.17). From the diffraction patterns of poly(S-EGDMA) (Figure 4.18), a small signal of crystalline elemental sulfur could be detected from the sample made at 100 °C, but there was no sharp peak observed from the sample made at 110°C.

Figure 4.17 5% NaDTC led to Trommsdorff-Norrish effect driven auto-acceleration in the reaction of sulfur and EGDMA, resulting in heterogeneity.

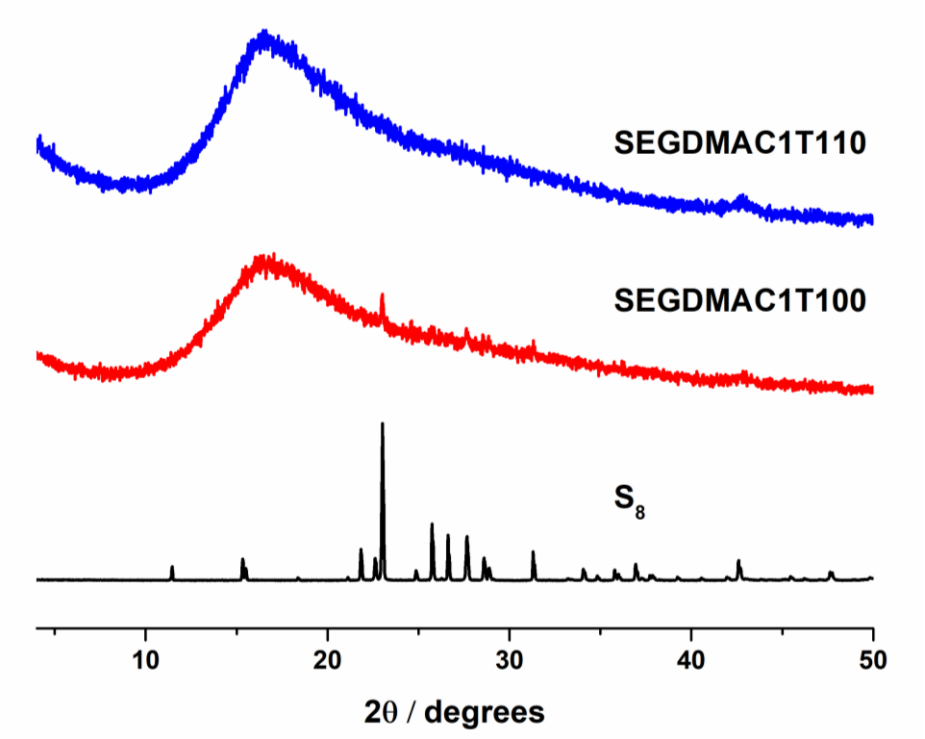

Figure 4.18 Offset PXRD patterns for poly(S-EGDMA) synthesized at different temperatures with NaDTC

With the same amount of catalyst, the reaction time of S and EGDMA was much shorter than that of S and DIB, giving an opportunity to screen the reaction through ^{1}H NMR in the early stage of polymerisation. As the reaction proceeds (Figure 4.19), the integral ratio of the peaks at 5.6 and 6.1 to the peak at 4.4 reduced, indicating the decreasing of C=C double bonds. Interestingly, new peaks appeared next to both peaks assigned as C=C bond protons, and also the ratio of the new shifted peaks to the original peaks increased, as shown in Figure 4.20. We speculate that new peaks are shifted from the original positions because of polymerization of sulfur onto the double bond at the other end of the molecule. However, we have to point out that hydrogen substitution is also a possibility.

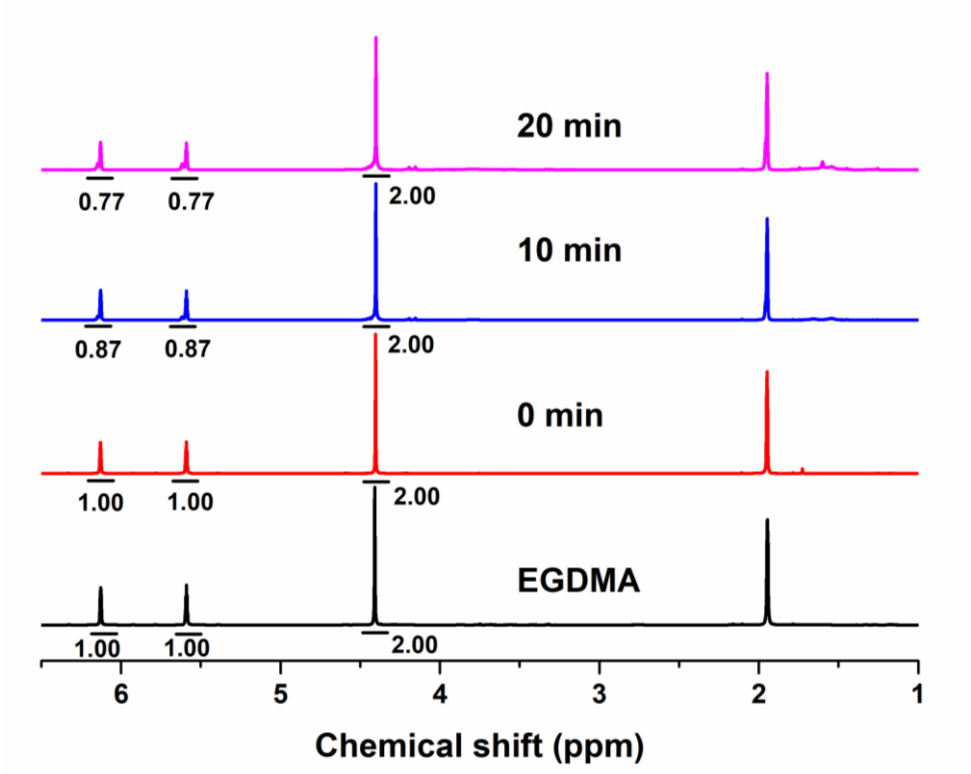

Figure 4.19 ^{1}H NMR spectra for the reaction of sulfur-EGDMA from 0 min to 20 min, and the integral of vinyl protons reduced.

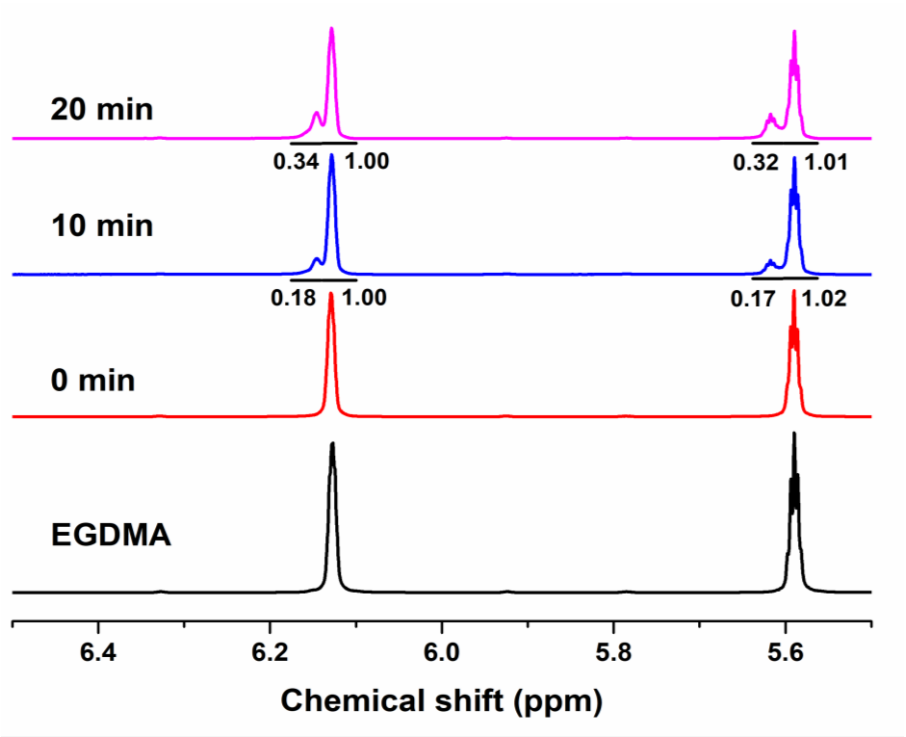

Figure 4.20 Peaks of vinyl protons shifted to downfield.

The product prepared from S and MMA is more like oligomer or low molecular weight branched polysulfide than a thiopolymer, and unlike poly(S-DIB) and poly(S-EGDMA), all products of S-MMA could be dissolved in deuterated chloroform. Gel permeation chromatography (GPC) was used to test the molecular weight of S-MMA, showing results of M_w= 740 g mol^{-1} and M_w/M_n = 1.22 (Figure 4.21). After curing and removing from the oven, the product was a homogeneous wax-like material, however, cooling to room temperature, 30 min later, phase separation could be observed, and sulfur crystals were precipitated. This was probably because with only one C=C bond in MMA, it was difficult to stabilize too much sulfur. The reaction was followed by ^{1}H NMR as well, as shown in Figure 4.22. Two peaks indicating alkenyl hydrogens reduced and finally disappeared after long term curing. However, it is hard to say there is no homopolymerisation by MMA, but, from the peaks around 3, the reaction between sulfur and MMA could be confirmed. However, from the comparison between 1H NMR spectra for S-MMA-96h and PMMA, it could be concluded that copolymerization of sulfur is dominant reaction instead of homopolymerization of MMA (Figure 4.23).

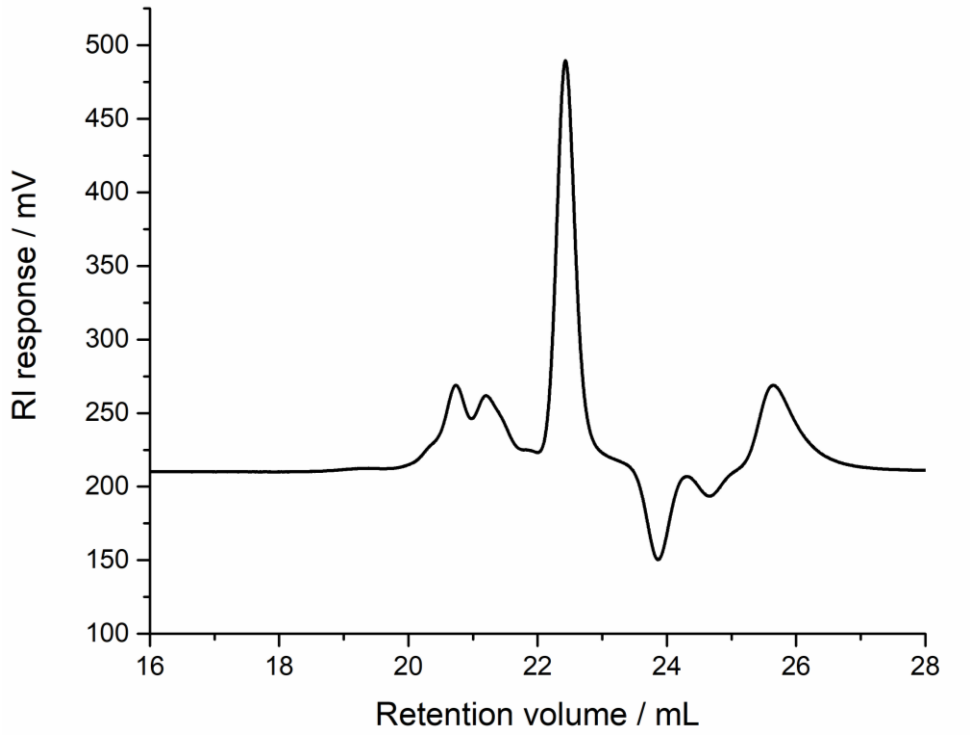

Figure 4.21 GPC trace for SMMAC10T95 in THF. Oligomers could be observed with low molecular weight and broad polydispersity.

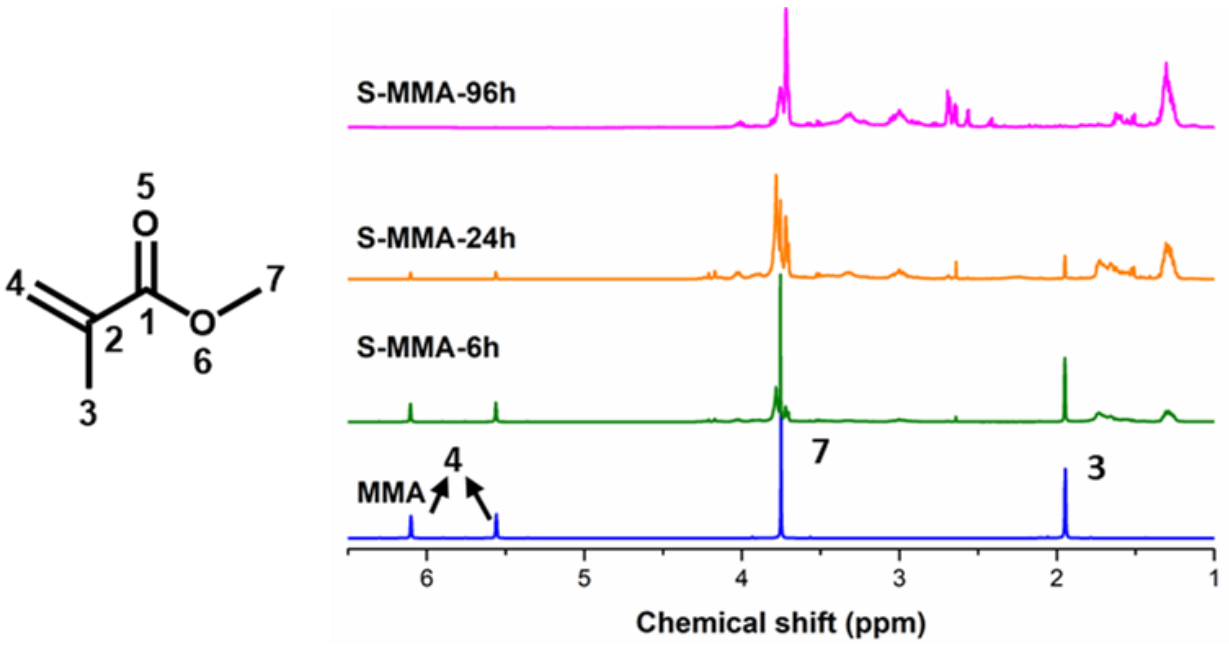

Figure 4.22 ^{1}H NMR spectra for the reaction of sulfur and MMA at different time. Apparently, after further curing, vinyl groups were totally reacted.

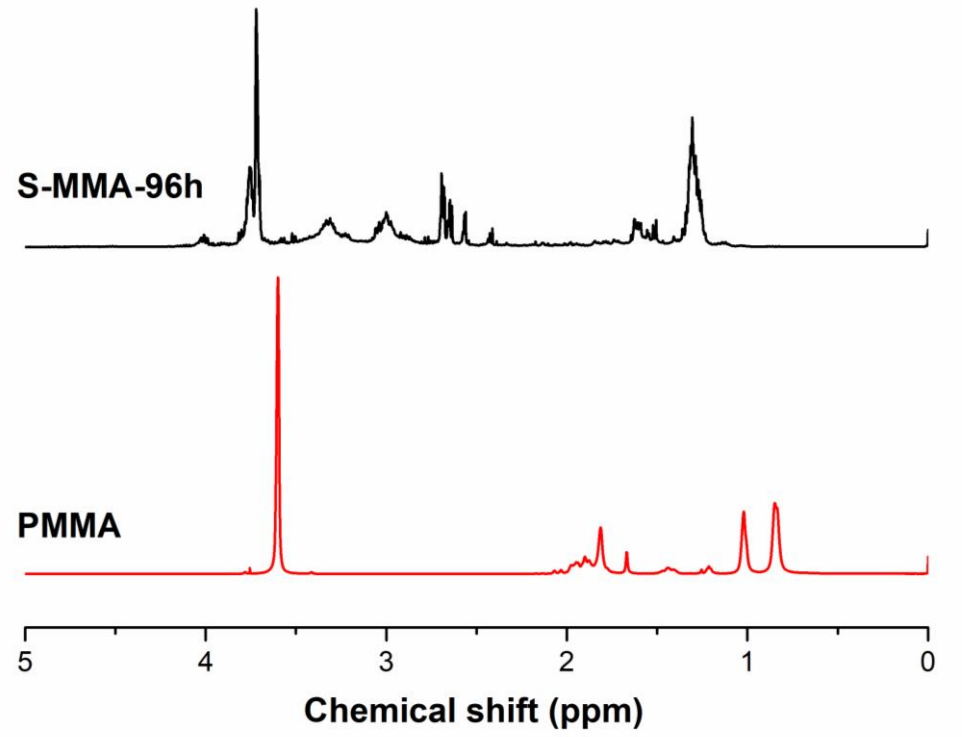

Figure 4.23 ^{1}H NMR spectra for S-MMA-96h and PMMA. Chemical shifts of main peaks of PMMA and those of S-MMA-96h are different, suggesting the reaction is mainly copolymerisation of sulfur and MMA instead of homopolymer of MMA.

4.4.1.3 Poly(S-CDE)

In order to further prove the catalyst could be used in inverse vulcanization at mild temperature, benefiting crosslinkers with low boiling point, 1,4-cyclohexanedimethanol divinyl ether (CDE) was induced to react with elemental sulfur directly, as shown in Figure 4.24. CDE was previously used as a crosslinker in mild temperature reported by Jenkins and co-authors. However, in their report they found that CDE could not be reacted directly with sulfur below its boiling point, rather a prepolymer made by reacting sulfur with another crosslinker at high temperature was needed to generate dynamic sulfur bonds which then activate the low temperature reaction of the mixed crosslinker system. For the direct sulfur-CDE system, catalyzed by NaDTC, several characterizations confirmed that CDE reacted with S_8 completely at 110 °C in only one step.

Figure 4.24 Photo of poly(S-CDE) made with and without catalyst. Left sample is the product without catalyst (lighter in colour) and right one is poly(S-CDE) made adding 10% NaDTC (darker)

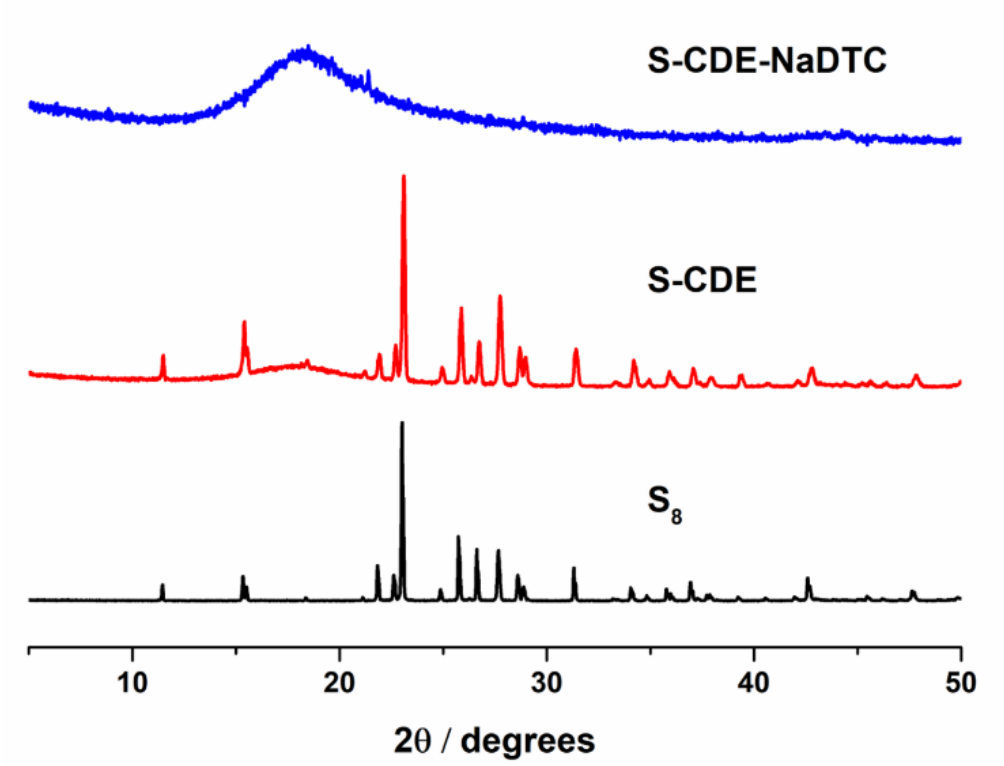

Figure 4.25 PXRD patterns of poly(S-CDE), the product made absence catalyst, and elemental sulfur. Apparently, sulfur crystals still could be detected from the product prepared without catalyst, however, poly(S-CDE) is amorphous.

Like DIB, CDE surprisingly could react sparingly with sulfur at 110 °C, but free sulfur, either crystal or amorphous, could still be detected from the products by PXRD, as shown in Figure 4.25. However, no sulfur could be detected from poly(S-CDE) made involving catalyst. Final poly(S-CDE) is insoluble in $CDCl_3$, as shown in figure Figure 4.26, suggesting the polymer crosslinked and only the low molecular weight oligomer was tested in NMR. Kinetic studies (as shown in Figure 4.27) for the S-CDE proved reactions between sulfur and C=C bonds, because of the decrease of the integral of vinyl protons, and new peaks appeared at 4, and between 5 and 6. Finally, TLC results, as shown in Figure 4.28, demonstrated no detectable sulfur in poly(S-CDE).

Figure 4.26 S-CDE-NaDTC is insoluble in $CDCl_3$, suggesting generation of crosslinked polymer.

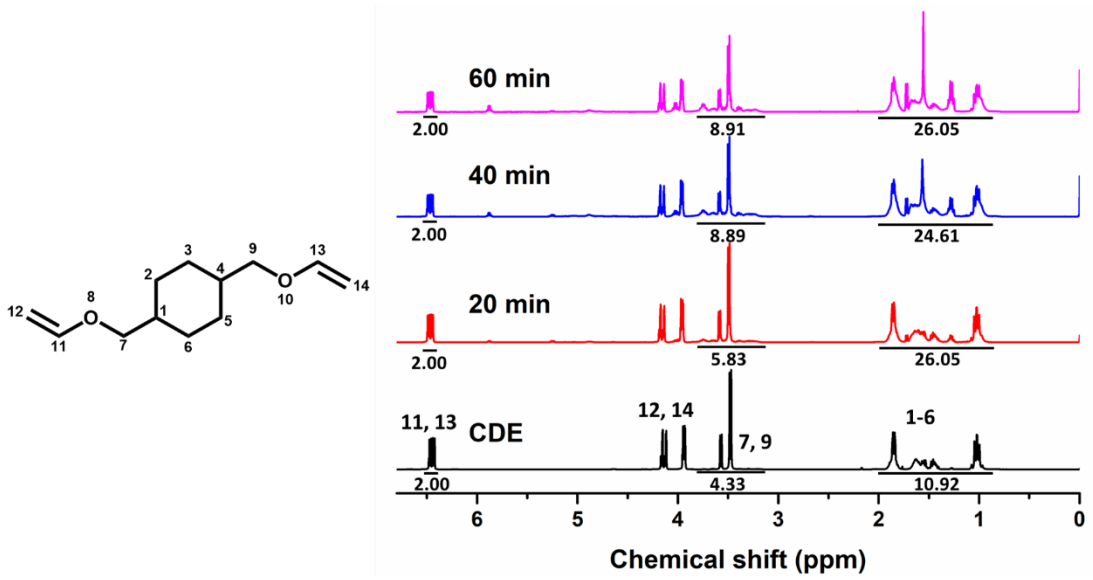

Figure 4.27 Kinetic studies of S-CDE by ^{1}H NMR, proving reactions between sulfur and C=C bonds

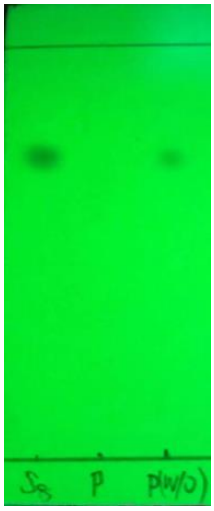

Figure 4.28 TLC results of detecting free elemental sulfur in poly(S-CDE) Spots on baseline are sulfur, poly(S-CDE), and the product made absence catalyst.

4.4.2 Leaching and remoulding

As residual catalyst was detected by PXRD, the sulfur polymers was ground into fine powder and washed with water, attempting to separate the polymer and catalyst. After washing and centrifugation, the supernatant was evaporated to crystalize residual catalyst. The yield of recrystallisation was only 7.9%, mainly because some catalyst is likely still trapped in the sulfur polymers. From NMR results, as shown in Figure 4.29,

the crystalized products have the same pattern as pure NaDTC along with other impurity peaks. This indicates there is the potential for recycling of any excess catalyst used. In the rubber industry, the term catalyst is often used for additives included to increase the rate of vulcanization, largely because it is not possible to separate them back out of the material and reuse them. As such, the term catalyst may not be technically appropriate. In this report, NaDTC has been termed as a catalyst instead of accelerator because it is a more broadly recognized term. After drying, the washed polymers were retested by PXRD. The pattern showed no crystallinity remained. After reheating in the oven, the fine powder could be remolded into different shapes (Figure 4.30). In the reforming processing, with residual catalyst trapped in the sulfur polymers, the S-S bonds were activated as dynamic covalent bonds, even at the low temperature of 110 °C

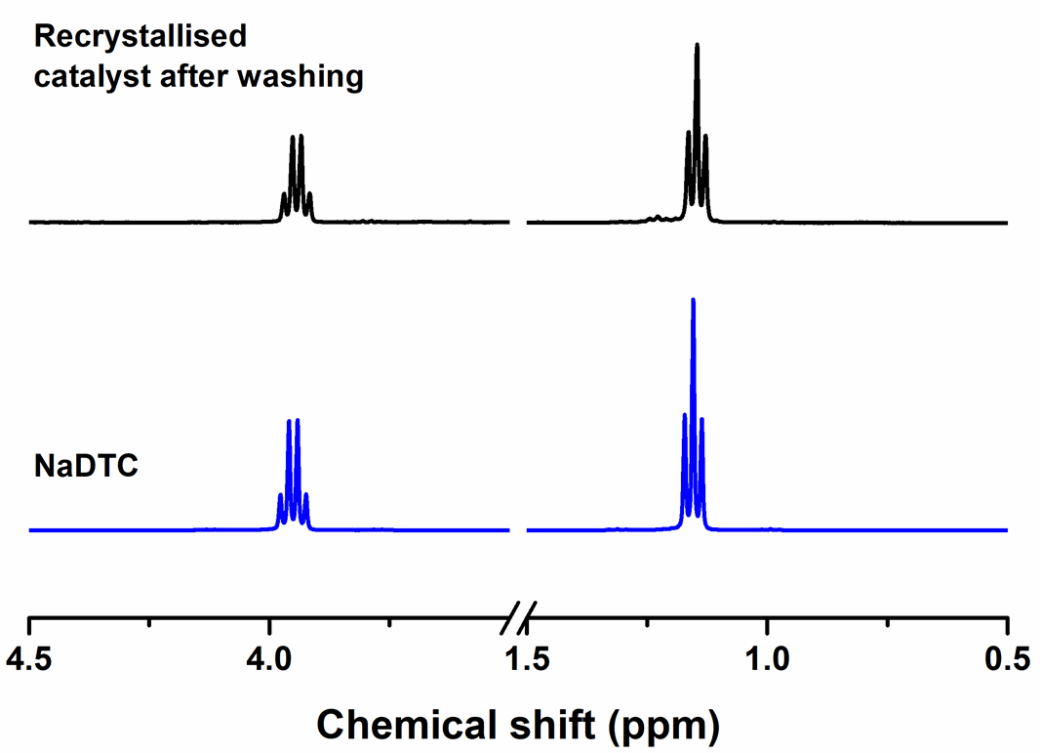

Figure 4.29 ^{1}H NMR spectra for residual solid crystallised after leaching and standard NaDTC

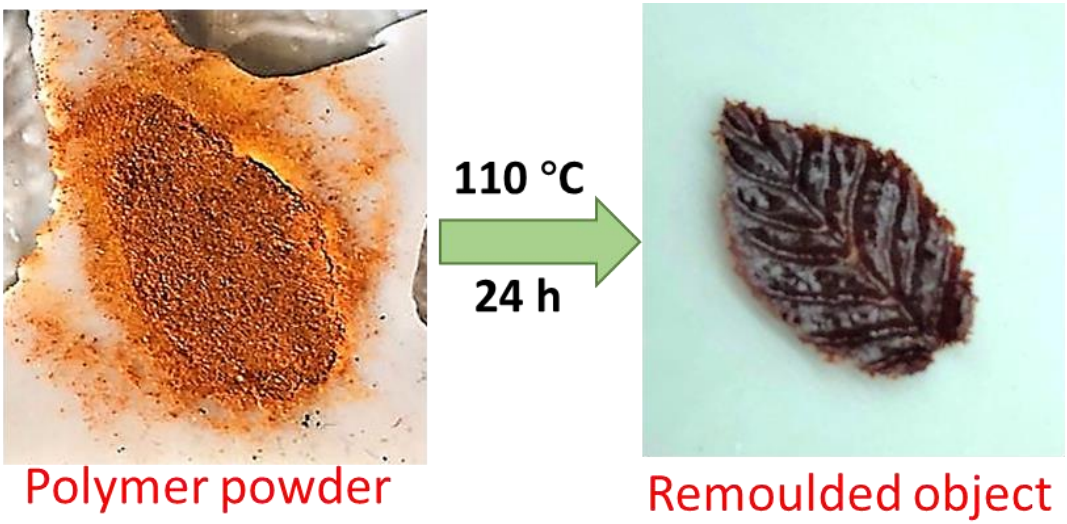

Figure 4.30 Washed powder was transferred in silicone mould and remoulded sample from reprocessing in the oven at 110 °C.

4.5 Conclusions

Different sulfur polymers were successfully synthesized by inverse vulcanization below the sulfur melting temperature, with NaDTC as a catalyst. Chemically stable and shape-persistent high-sulfur-content copolymers could be generated. Through this method, no solvents or pre-reacted species were required, and residual catalyst could also be recovered, aligned with the principles of green chemistry. It should be considered that the time taken for the reaction will also contribute to the energy costs, as well as the temperature itself. That noted, this catalytic route allows lower temperatures to be used, or shorter reaction times for a given temperature. Lower temperatures allow lower boiling crosslinkers to be more easily incorporated, and may be required if sulfur polymers are to be combined with other temperature sensitive materials. Additionally, after washing, the sulfur polymers could be reprocessed at mild temperature, allowing recycling. Thus, a new route to inverse vulcanize at low temperature is provided.

4.6 Experimental

4.6.1 Materials

Sulfur (S8, sublimed powder, reagent grade, ≥99.5%, Brenntag UK & Ireland. Purchased in 25 kg bags), ethylene glycol dimethylacrylate (EGDMA, 98%, Alfa Aesar), sodium diethyldithiocarbamate trihydrate (Alfa Aesar), 1,3-diisopropenylbenzene (DIB, 97%, TCI), and methyl methacrylate (MMA, 99%, Sigma Aldrich) were commercially available and used as received. Cyclohexanedimethanol divinyl ether (CDE, 98%, Sigma Aldrich), Poly(methyl methacrylate) (PMMA, Sigma Aldrich), and Chloroform-d (99.8 atom % D, Sigma Aldrich), hexane (≥95%, Sigma Aldrich)

4.6.2 Method

Polymerisations

Reactants (5 g sulfur, 5 g crosslinker, and the associated amount of catalyst) were mixed in 40 mL volume glass vials by vortex, before being heated at the specified temperatures in aluminium blocks and stirred by magnetic stirrer bars for polymerisations. For DIB, heating in the aluminium block was required for a minimum of 12 hours in order to generate fully solid products, which were then further cured in an oven at 110 °C for 12 hours. For EGDMA, the reaction finished in 20 minutes to generate fully solid products, and further curing was conducted in the oven at 110 °C for 12 hours. For MMA, the reaction was conducted at 95 °C for more than 12 hours, and moved into an oven for further curing for 96 hours. Specific conditions and components for different samples are listed in Table 1. For CDE, 5 g sulfur, 5 g CDE, and 10% NaDTC were mixed in 40 mL volume glass vials by vortex, before being heated at 110 °C in aluminium blocks and stirred by magnetic stirrer bars for polymerisations for 1 hour. Reaction absence of catalyst in same scale and same conditions was conducted as well.

4.6.3 Characterisation

Leaching and remoulding

Sulfur polymer SDIBC10T110 was ground into fine powder and washed by water. Supernatant was evaporated after centrifugation to recrystallize the catalyst. Residual

solid powder was dried and transferred into a silicone mould and reheated at 110 °C in the oven for 48 hours to remould.

Powder X-ray Diffraction (PXRD)

Data were measured using a PANalytical X'Pert PRO diffractometer with Cu-Kα radiation, operating in transmission geometry. And all data were measured over the range 5-50° 2θ in 0.013° steps over 60 minutes.

Differential Scanning Calorimetry (DSC)

DSC were performed on a TA Instruments Q200 DSC, under nitrogen flow, and with heating and cooling rates of 5 °C min^{-1} from -50 to 150°C in 'heat-cool-heat' program.

Nuclear magnetic resonance (NMR)

The reactions were monitor by solution NMR in deuterated chloroform, and recrystallized catalysts were performed by solution NMR in D_2O, using a Bruker Advance DRX (400 MHz) spectrometer.

Attenuated total reflection fourier transform infra-red (ATR-FTIR).

Fourier Transform Infrared (FTIR) spectra were measured between 4000 and 500 cm^{-1} on a Bruker Vertex 70 spectrometer, with a Platinum ATR module.

Elemental Analysis

CHNS elemental analysis was conducted on a Thermo Flash EA 1112.

Gel permeation chromatography (GPC)

The molecular weight of the soluble fraction of the polymers was determined by gel permeation chromatography (GPC) using a Viscotek system comprising a GPCmax (degasser, eluent and sample delivery system), and a TDA302 detector array, using THF as eluent.

Thin layer chromatography (TLC)

10 mg polymer or sulfur was added into 10 mL dichloromethane (DCM), and 1 mL DIB was dissolved into 10 mL DCM. Solutions were spotted individually on the traditional silica TLC plates with hexane eluent.

4.7 Appendix

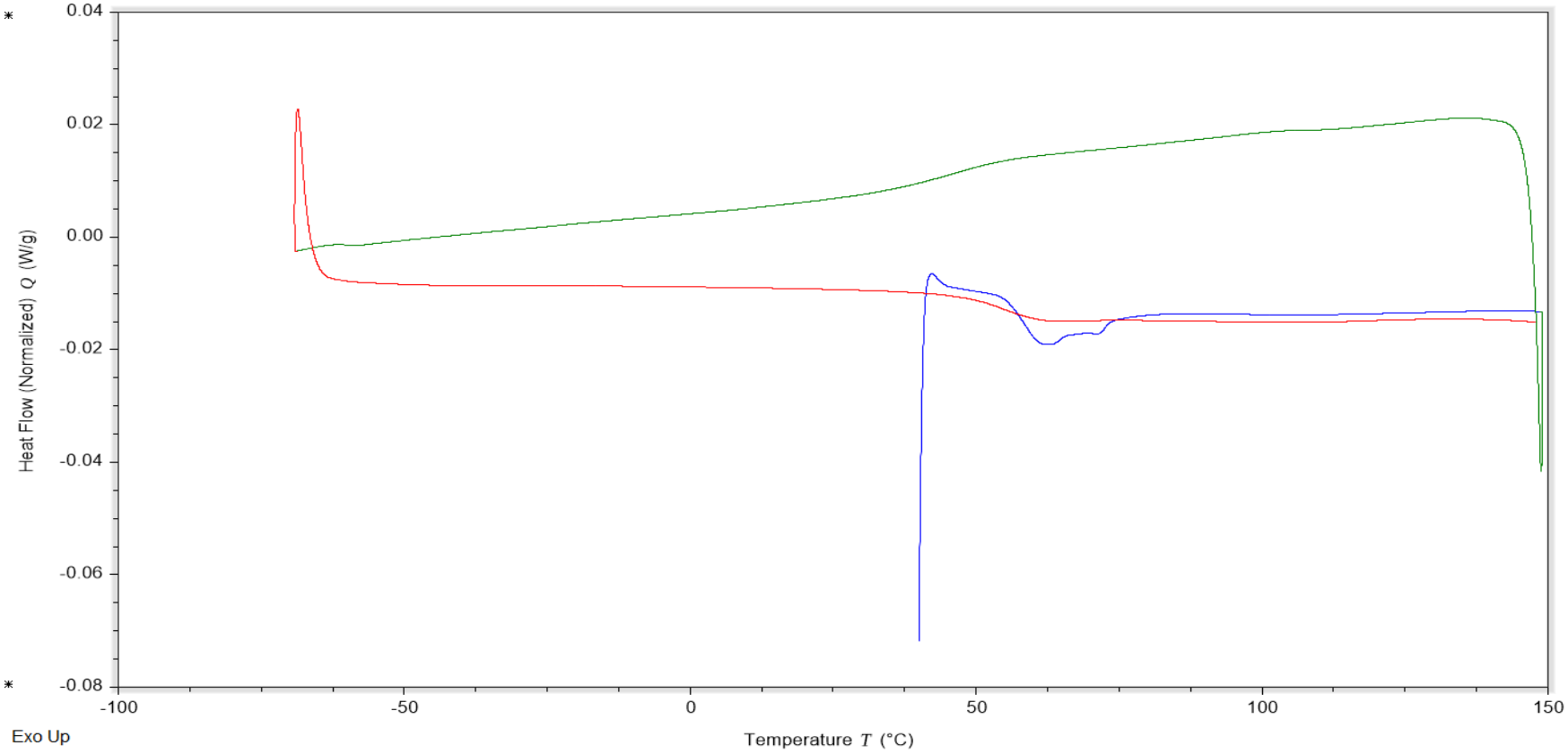

Figure A4.1 Full DSC traces of SDIBC10T110 scanned by heating-cooling-heating program showed no sulfur crystals remain and there is a glass transition temperature of 53 °C.

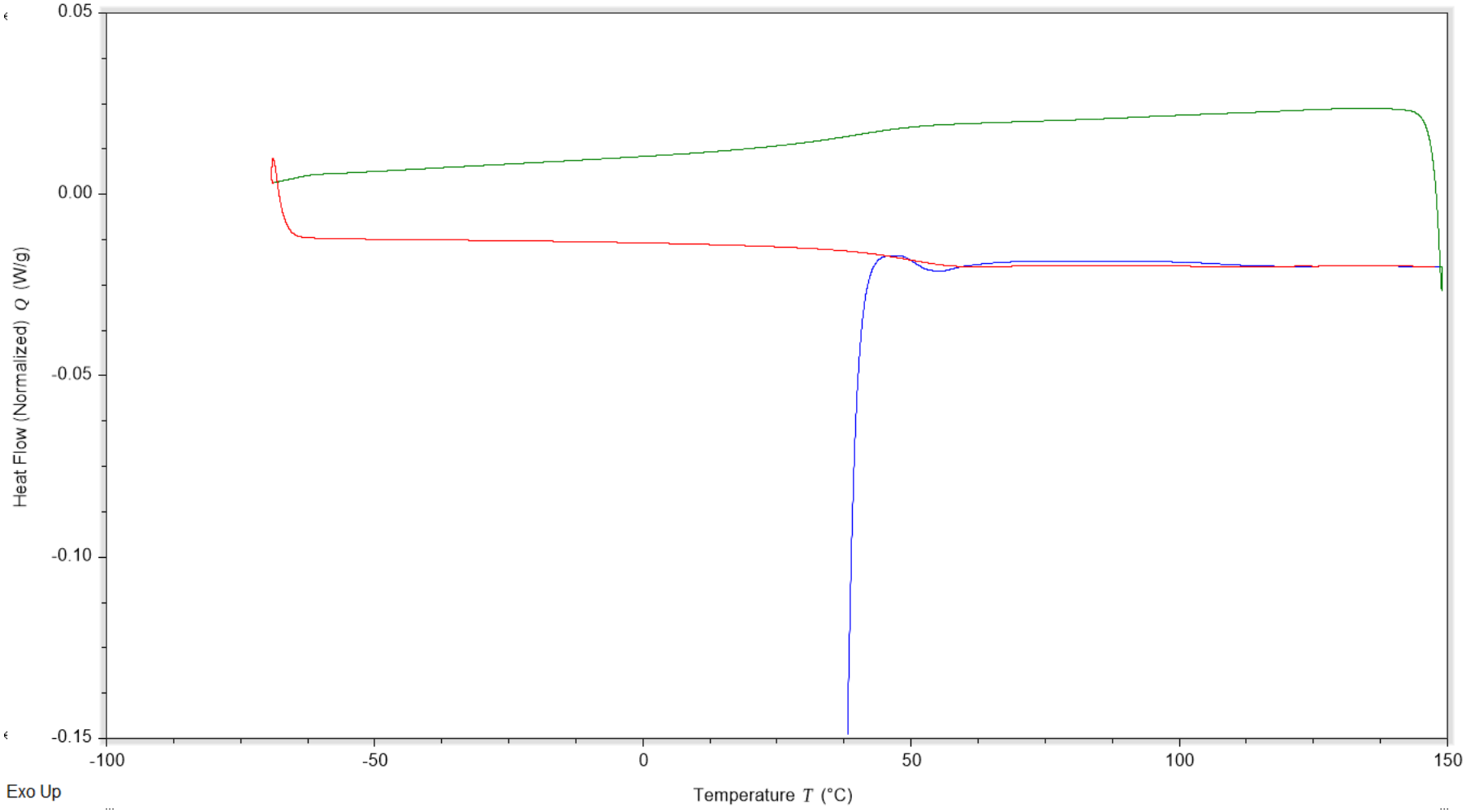

Figure A 4.2 Full DSC traces of SEGDMAC1T110 scanned by heating-cooling-heating program showed no sulfur crystals remaining and a glass transition temperature of 57 °C.

4.8 References

(1) Schmidt, M. The Scientific Basis for Practical Applications of Elemental Sulfur. In *New Uses of Sulfur*; 1978; pp 1–12.

(2) Abdel-Mohsen Onsy, Mohamed; Maisa, E.-G. Sulfur Concrete for the Construction Industry– a Sustainable Development Approach. *J. Ross Publ.* **2010**.

(3) Hasell, T.; Parker, D. J.; Jones, H. A.; McAllister, T.; Howdle, S. M. Porous Inverse Vulcanised Polymers for Mercury Capture. *Chem. Commun.* **2016**, *52* (31), 5383–5386.

(4) Boyd, D. A. Sulfur and Its Role In Modern Materials Science. *Angew. Chemie Int. Ed.* **2016**, *55* (50), 15486–15502.

(5) Worthington, M. J. H.; Kucera, R. L.; Chalker, J. M. Green Chemistry and Polymers Made from Sulfur. *Green Chem.* **2017**, *19* (12), 2748–2761.

(6) Park, K. W.; Leitao, E. M. The Link to Polysulfides and Their Applications. *Chem. Commun.* **2021**, *57* (26), 3190–3202.

(7) Anastas, P.; Eghbali, N. Green Chemistry: Principles and Practice. *Chem. Soc. Rev.* **2010**, *39* (1), 301–312.

(8) Zhang, Y.; Pavlopoulos, N. G.; Kleine, T. S.; Karayilan, M.; Glass, R. S.; Char, K.; Pyun, J. Nucleophilic Activation of Elemental Sulfur for Inverse Vulcanization and Dynamic Covalent Polymerizations. *J. Polym. Sci. Part A Polym. Chem.* **2019**, *57* (1), 7–12.

(9) Westerman, C. R.; Jenkins, C. L. Dynamic Sulfur Bonds Initiate Polymerization of Vinyl and Allyl Ethers at Mild Temperatures. *Macromolecules* **2018**, *51* (18), 7233–7238.

(10) Wu, X.; Smith, J. A.; Petcher, S.; Zhang, B.; Parker, D. J.; Griffin, J. M.; Hasell, T. Catalytic Inverse Vulcanization. *Nat. Commun.* **2019**, *10* (1), 647.

(11) Halls, D. J. The Properties of Dithiocarbamates A Review. *Mikrochim. Acta* **1969**, *57* (1), 62–77.

Chapter 5. Magnetic sulfur-doped carbons for mercury adsorption

5.1 Context

5.1.1 Abstract

Mercury pollution is a significant threat to the environment and health worldwide. Therefore, effective and low-cost absorbents that are easily scalable are needed for real-world applications. Enlarging the surface area of the materials and doping with heteroatoms are two of the most common strategies to cope with this problem. Sulfur-doped activated carbon synthesized from the carbonization of inverse vulcanized thiopolymers makes it possible to combine both large specific surface area and doping of heteroatoms, resulting in outperformance in mercury uptake against commercial activated carbons. Convenient recovery of mercury absorbents after treatment should be beneficial in mercury collecting and recycling. Therefore, magnetic sulfur-doped carbons (MSCs) were prepared by functionalizing sulfur doped carbons through chemical precipitation with magnetic iron oxides. Besides the characterisations of materials, mercury uptake experiments, such as stactic test, capacity test, impact of solution pH, and mixed ions interferences were performed. These MSCs exhibit high specific surface area (1,329 m^2/g), high sulfur content (up to 14.8 wt%), porous structure, low cost, and are convenient for retrieval. MSCs are demonstrated high uptake capacity (187 mg g^{-1}) and efficiency in mercury solution and multifunctional absorption in mixed ions solution, showing their potential to be applied in water purification and environmental remediation.

5.1.2 Publication

Bowen Zhang, Samuel Petcher, Hui Gao, Peiyao Yan, Diana Cai, George Fleming, **Douglas J. Parker, Samantha Y. Chong Tom Hasell**. Magnetic sulfur-doped carbons for mercury adsorption, *Journal of Colloid and Interface Science.* 603 (2021) 728–737.

5.1.3 Author contributions

Bowen Zhang: Conceptualization, Methodology, Investigation, Formal analysis, Writing - original draft, Writing - review & editing. **Samuel Petcher**: Investigation, Formal analysis, Writing - review & editing. **Hui Gao**: Investigation. **Peiyao Yan**: Investigation. **Diana Cai**: Investigation. **George Fleming**: Writing - review & editing. **Douglas J. Parker**: Writing - review & editing. **Samantha Y. Chong**: Formal analysis.

Tom Hasell: Resources, Writing - review & editing, Supervision, Project administration, Funding acquisition.

5.2 Introduction

With the advantage of high specific surface areas and hierarchical porous structure, porous materials have attracted increasingly interests in recent year.[1–5] Studies about porous materials were conducted by different research groups not only in preparation, characterisation, but in more and more applications, such as carbon dioxide capture[6] , gas separation,[5,7] catalysis,[8,9] supercapacitor electrodes,[10] removal of hazardous materials,[2,11–14] and energy conversion.[15] Various of novel porous materials, for example Metal Organic Frameworks (MOFs) [2,8,9,16], Covalent Organic Frameworks (COFs) [1,4], and Polymers of Intrinsic Microporosities (PIMs) [3,7,12], have been reported, however, high cost or low productive capacity hindered their application in a real-world. However, porous carbonaceous materials exhibit advantages over those porous materials in high cost effectiveness and industrial scale production, showing highly potential application in many different areas.[17] Activated carbons are very common and play an important role in industry, due in part to the variety of natural and synthetic materials that can be used as precursors, with preparation processes that are simple and scalable. In order to optimize the application of activated carbon, as well as increasing the specific surface area of materials, incorporation of functional groups onto the carbon surface is another strategy.[18–20] Considering the improvement of adsorbative abilities and unique electronic features, heteroatom dopants were one of the most effective approaches incorporated into activated carbons.[18,21] Sulfur-doped carbonaceous materials with firmly and covalently bound sulfur-carbon structures were synthesized from carbonizing thienyl-contained block polymers by Schmidt *et al.* [22,23] In this method, sulfur content varied from 5–23 wt%. These materials showed high specific surface area up to 711 m^2/g. However, complexity of synthesizing precursors and the associated cost hindered its application. Therefore, discovery of a cheap and abundant sulfur content precursor is vital to sulfur doped carbon.

Inverse vulcanization was first coined by Pyun in 2013.[24–26] After that, high sulfur-content polymers have been synthesized and applied into different areas, which were covered from the previous chapters.[24-34] Thiopolymers generated via inverse vulcanization with high sulfur content (normally higher than 50 wt%), find use as precursors for sulfur-doped carbon. However, there have only been a few reports of their use as precursors for sulfur containing composites, such as sulfur-doped carbons.

Poly(S-diisopropenyl benzene) and poly(S-limonene) were first reported as precursors in carbonisation of inversed vulcanised polymers, producing high specific surface areas microporous materials that could be applied in gas and liquid phase separations.[28] However, with a narrow pore size distribution, solely in the microporous range and lacking in larger transport pores, these materials are not suitable for metal adsorption. Carbonized poly(S-DCPD) has been reported with high sulfur content (~ 15 wt%), hierarchical porous structure and much higher specific surface areas (up to 2200 $m^2 g^{-1}$), which could be used for gas adsorption, mercury capture, and water purification.[5] Mercury pollution is an urgent global health concern.[29] Therefore, 128 countries signed a joint agreement, Minamata Convention, to reduce mercury through anthropogenic emissions, such as fossil fuel combustion, small-scale gold mining, cement industry, etc.[26,30,31]

Magnetic absorbents have been applied to take up different hazardous materials from solution or aquatic waste because of their retrievability.[14,32–35] Since 1973, the first time magnetic particles has been reported as separation method by Robinson *et al.* ,[36] relevant studies developed fast and broadly. The preparation of magnetic absorbents was normally from two approaches: functionalisation the surface of magnetic materials to generate a core-shell structure magnetic absorbents and generation magnetic materials on the surface of absorbents material.[14,36] The core-shell structure

Figure 5.1 Schematic of synthesis procedure of magnetic sulfur-doped carbons and the application of magnetic sulfur-doped carbons for mercury absorption. Step 1. Functionalization of sulfur-doped carbons from precipitation of iron oxides onto sulfur-doped carbons surface. Step 2. Removal mercury from mercury chloride solution. Step 3. Retrieval of sorbents after adsorption via a magnet.

could protect the inner magnetic material, but the synthesis is more complex than another method, because it was always needed a shell and functionalize the shell to make it have affinity to specific adsorbate.[34,37] Whereas, the processing of generation magnetic materials on the surface is facile, but the generated magnetic materials could may influence the capture ability and capacity of absorbent.[14] However, both methods prepared magnetic absorbents that could be quickly and conveniently separated by external magnetic field, providing significant advantage over conventional absorbents in circumventing of column packing problem, which is always time-consuming step in filtration or separation. With the advantages of high surface area and porous structure, magnetic carbon composites are one of the most attractive and cost-effective material types for hazardous material uptake and water purification in real-life. Here we demonstrate treated sulfur-doped carbons with magnetic properties, and their convenient retrieval of sorbents under an external magnetic field for real-world applications (as shown in Figure 5.1). The composites are shown to have varied specific surface areas, magnetic response and mercury uptake depending on the ratio of sulfur-doped carbon to iron oxides. Moreover, beneficial from iron oxides, magnetic sulfur-doped carbons (MSCs) are presented as a multifunctional adsorbent in mixed ions solution. The carbonisation feedstocks used, sulfur and DCPD, both have the advantage of being industrial by-products, available cheaply and at large scale. Crucially, considering the low-cost and simple processing, MSCs are promising materials for environmental remediation. Magnetic porous material formed from inverse vulcanised polymers has not been previously reported.

5.3 Aims

1. Synthesize magnetic sulfur-doped carbons by precursors of thiopolymers
2. Investigate how the variation of ratio of iron oxide to sulfur-doped carbons influence the properties of composite.
3. Study the application of magnetic sulfur-doped carbons in mercury uptake
4. To compare magnetic sulfur-doped carbons with reported materials in mercury capture.

5.4 Results and discussion

5.4.1 Design and characterization of magnetic sulfur-doped activated carbons

Poly(S-DCPD) was initially synthesized as previously reported [38], as shown in Scheme 5.1, and as set out in the methods. These sulfur polymers were then carbonized and chemically activated by potassium hydroxide (KOH) under nitrogen atmosphere at 750 °C for 2 hours to form sulfur-doped activated carbons with hierarchical structure and high specific surface areas (Figure 5.2 and Table 5.1), the resultant product was denoted as SC1M0. As a precursor of magnetic sulfur-doped carbons, SC1M0 was characterized by elemental analysis (EA) and contained 74.24 wt% carbon, 1.22 wt% hydrogen, and 14.80 wt% sulfur. X-ray photoelectron spectroscopy of similarly inverse-vulcanised-polymer derived activated carbons have shown that though sulfur is lost from the more extended polysulfides through the reversibility of the S-S bonds at elevated temperature, mono- or di-sulfide linkages are retained; the majority of the signal for retained sulfur being consistent with thioethers and disulfides [28].

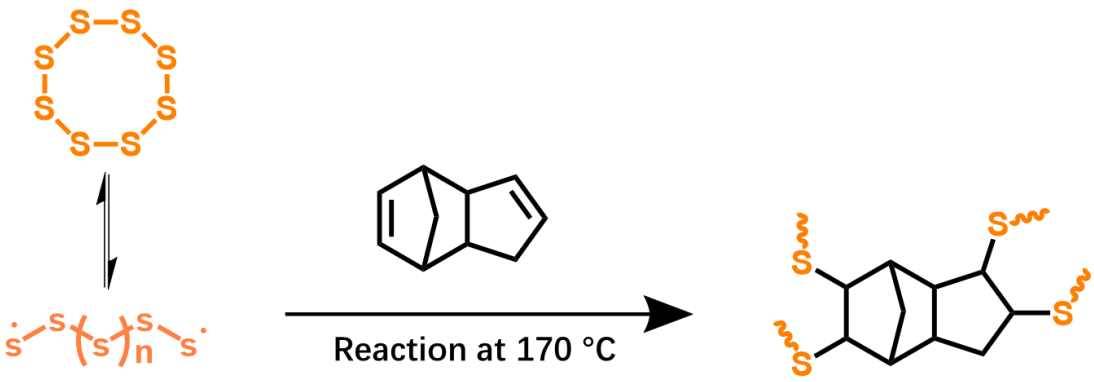

Scheme 5.1 Synthetic scheme for inverse vulcanization of sulfur and DCPD.

Table 5.1 Physical properties of MSCs

Sample	BET surface area (m^2 g^{-1})	Total pore volume [a] (cm^3 g^{-1})
SC1M0	1801	0.91
SC2M1	1329	0.75
SC1M1	1038	0.67
SC1M2	668	0.56
SC0M1	80	0.23

Magnetic composites were synthesized with varying weight ratios of sulfur-doped activated carbons to iron oxides, from 1:2, 1:1, to 2:1, and the composites were denoted as SC1M2, SC1M1, and SC2M1, respectively. Additionally, iron oxides synthesized in the same conditions was prepared as a blank sample, denoted as SC0M1. Nitrogen adsorption of all the samples, as shown in Figure 5.2, were applied to investigate the surface area, porous structure and diameter distribution information. The isotherm of pristine sulfur-doped carbon SC1M0 presented a type I(b) isotherm indicating that the material is a microporous solid with relatively broad pore size distributions including wider micropores and possibly narrow mesopores [39]. Calculated by the BET model, SC1M0 had the highest specific surface areas (SA_{BET} = 1,801 m^2/g). The relatively broad pore size distributions could be confirmed through calculation by non-local density functional theory (NL-DFT) as well (Figure 5.3). It was found that the pore sizes of SC1M0 are mainly in the micropore range (< 2 nm) with a small amount of narrow mesopores with widths not exceeding about 4 nm.

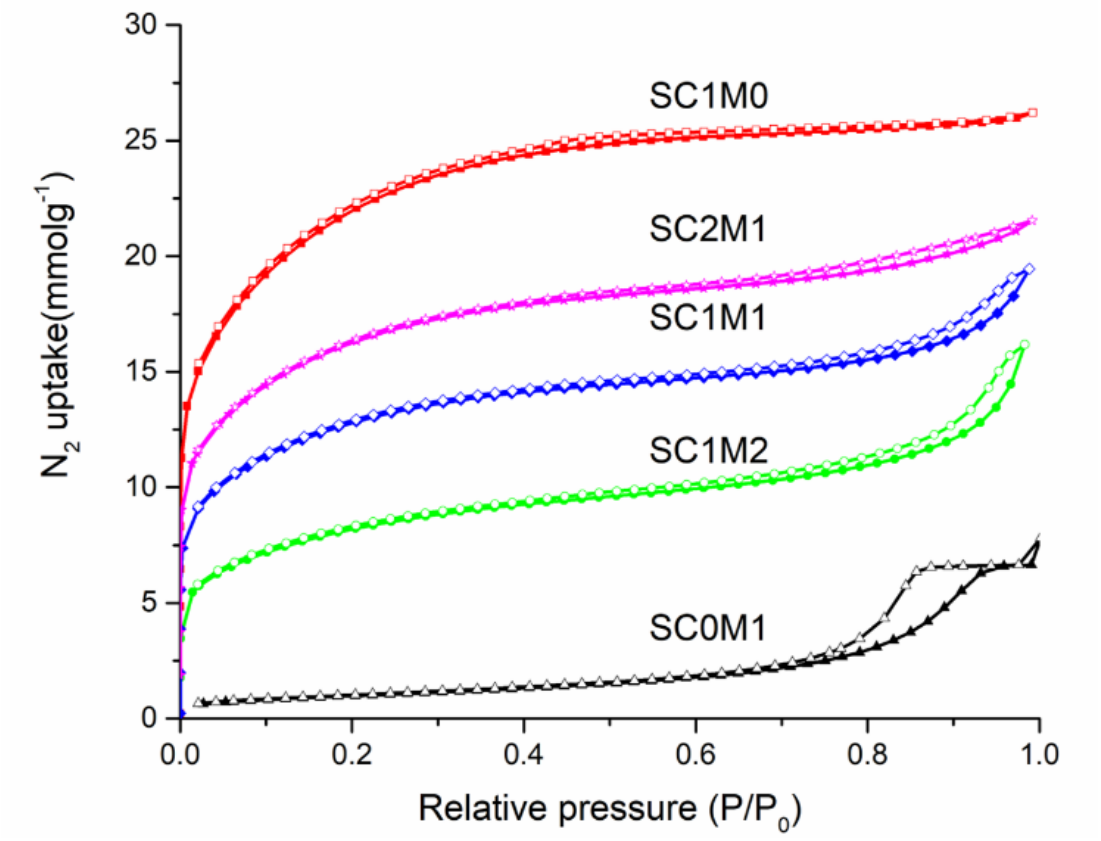

Figure 5.2 Nitrogen adsorption–desorption isotherms, at 77 K, of magnetic sulfur-doped activated carbons. Sample names indicate the ratio of sulfur-carbon (SC) to magnetic iron oxide (M), from pure sulfur-carbon (SC1M0) through to pure iron oxide (SC0M1).

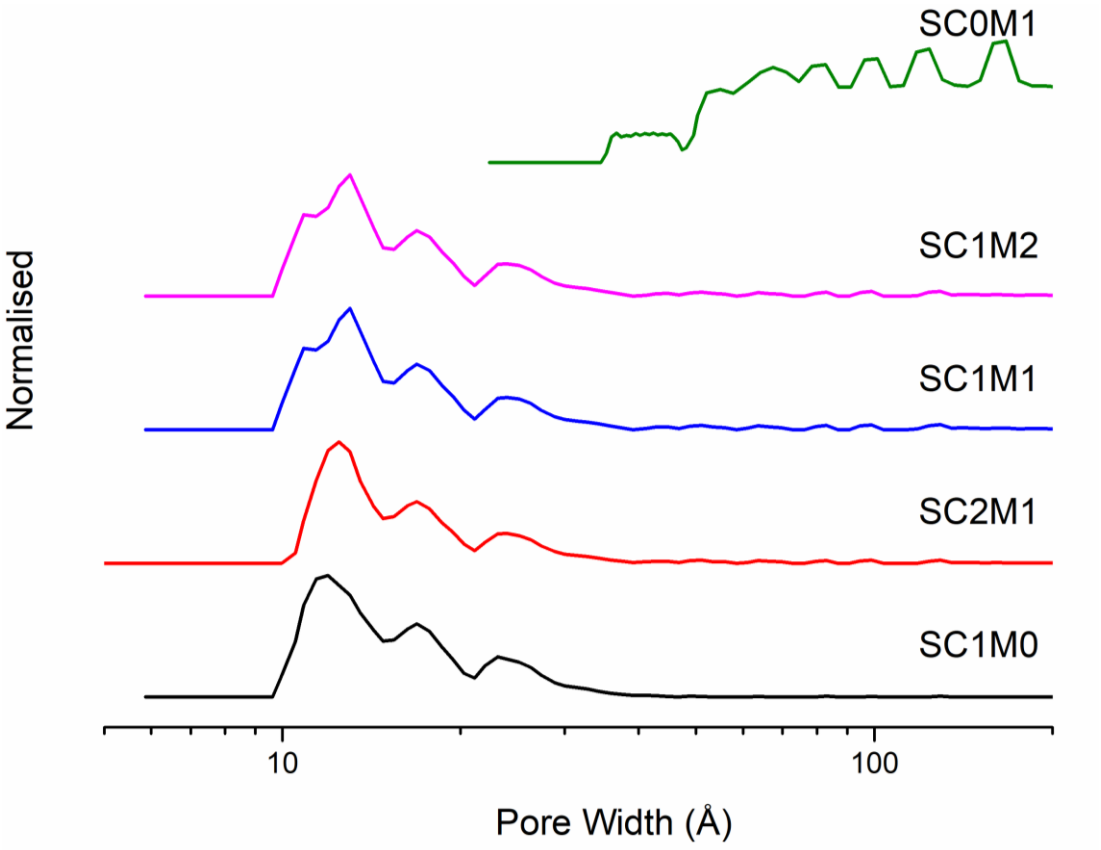

Figure 5.3 Pore size distributions of magnetic sulfur-doped carbon calculated by non-local density functional theory (NL-DFT), from the nitrogen sorption isotherms. It can be observed that micropores and small mesopores were generated from sulfur-doped carbon without iron oxides (SC1M0), and big mesopores and macropores were generated from synthesised iron oxides (SC0M1). However, the composites, with different ratiso of sulfur-doped carbon to iron oxides, could be found to possess hierarchical structure with all types of pore.

The isotherm shape of SC0M1 shows that this material is a nonporous or macroporous solid and the calculated SA_{BET} was 80 m^2/g. Hysteresis loop and the pore size distribution of SC0M1 indicated that synthesized iron oxides has few micropores but includes mesopores and more macropores, which were probably due to aggregation of generated iron oxides, and resultant inter-particle voids. Compared with SC0M1, all MSC composites had much higher surface areas and a more porous structure. As the ratio of iron oxides was increased in the composite, the SA_{BET} of materials decreased from 1,329 m^2/g to 668 m^2/g, however, normalized pore size distribution curves illustrated that the microporous structure of sulfur-doped carbon was not changed. Interestingly, after comparison of all normalized pore size distributions and the hysteresis loops of gas sorption isotherms of MSCs, it could be found that the

percentage of mesopores increased with the ratio of iron oxides to sulfur-doped carbon, although BET surface area and pore volume (as shown in Table 5.1) decreased dramatically. It could be speculated that the growth of pore size is because of generation of the iron oxides crystals on the pristine carbon backbone. The loss of surface area is approximately consistent with the combination of the theoretical composition. For instance, SC1M2, at two parts magnetite to one part sulfur doped carbon, would be expected to have a surface area of 654 m^2/g from direct combination ((2 x 80) +1801 / 3), which is very close to the value of 668 m^2/g observed during testing. Any significant blocking of pores caused by magnetite formation would lead to a deviation from this agreement.

The morphology of both precursor (SC1M0) and magnetic sulfur-doped activated carbons were studied through scanning electron microscopy (SEM). From Figure 5.4 and Figure 5.5, the irregular particulate structure of the precursor carbon could be seen, and only sulfur, carbon, and oxygen could be detected by energy-dispersive X-ray analysis (EDX), as expected.

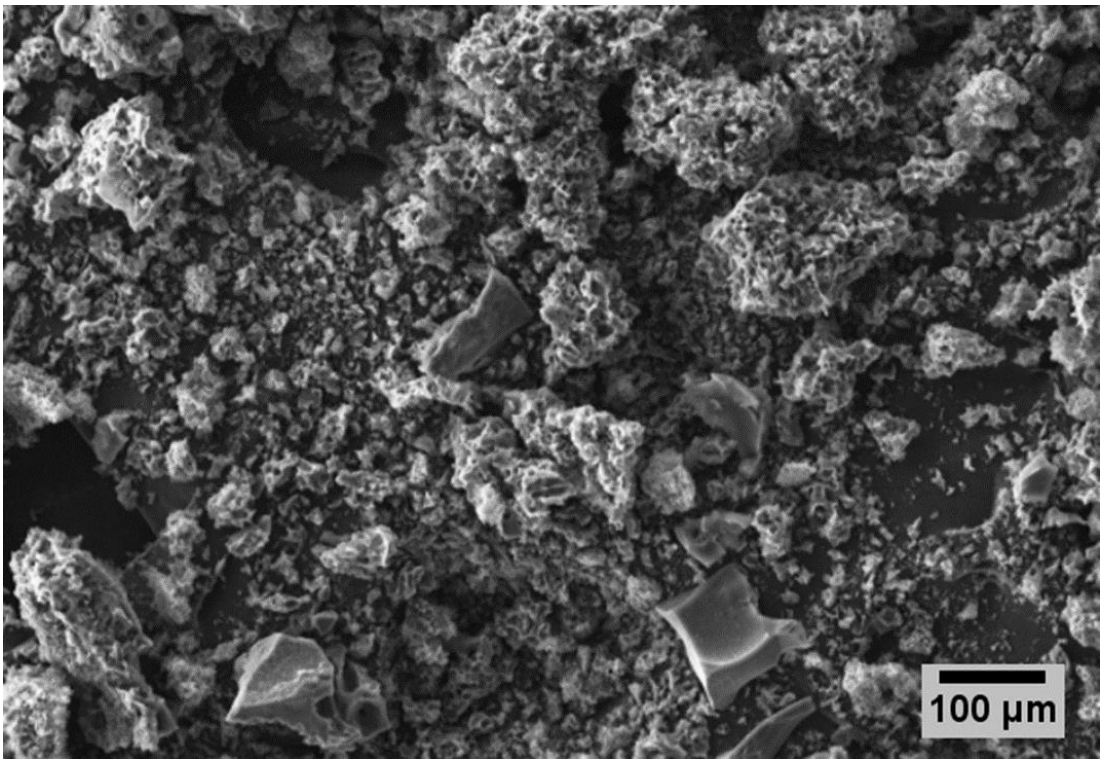

Figure 5.4 SEM images of SC1M0

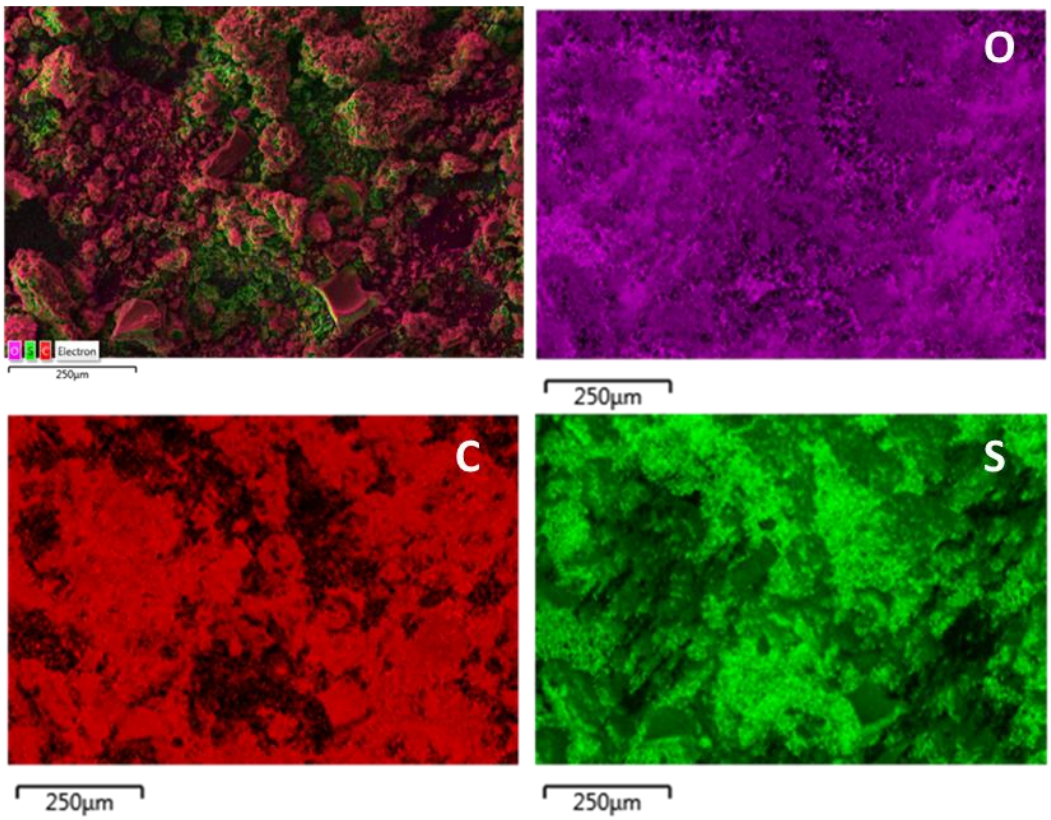

Figure 5.5 Energy- dispersive X-ray analysis (EDX) maps for SC1M0, showing combined elements, oxygen, carbon, and sulfur.

However, after functionalization, the presence of iron with a homogeneous distribution could be confirmed on the surface of MSCs in mapping images, as shown in Figure 5.6. Comparison between the EDX analysis results of SC1M1 (Figure 5.7 , Figure 5.8 and Figure 5.9), and SC1M2, confirmed more iron on the surface of SC1M2 (Figure 5.10), corroborating the calculated results.

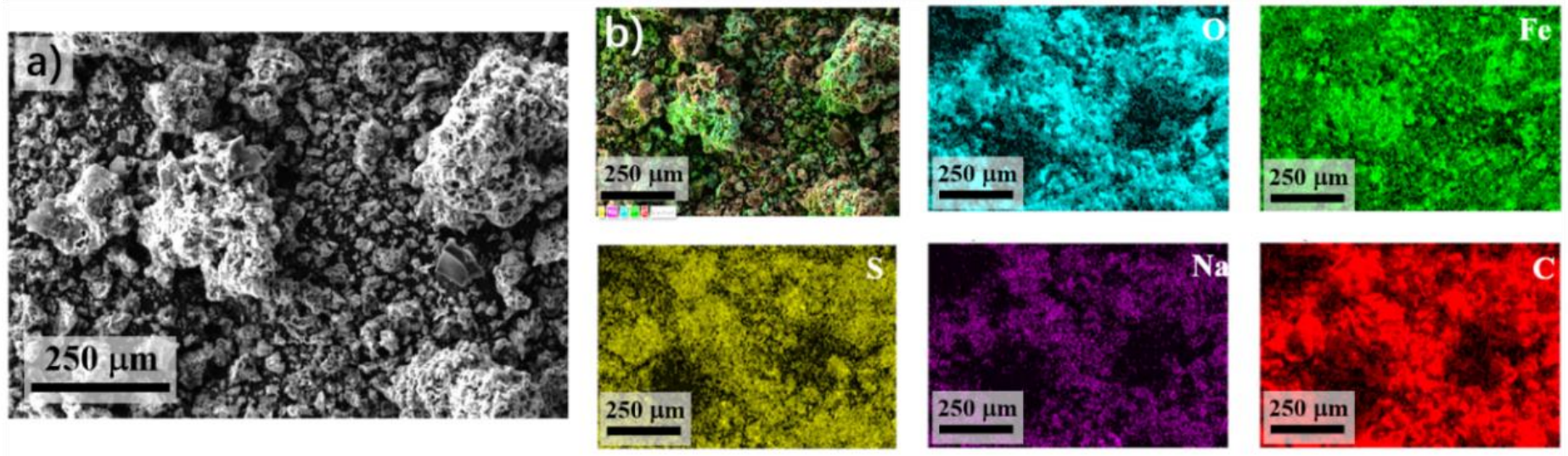

Figure 5.6 a) SEM image of SC1M2. b) Energy- dispersive X-ray analysis (EDX) maps showing, (clockwise from top left) combined elements, oxygen, iron, carbon, sodium, and sulfur.

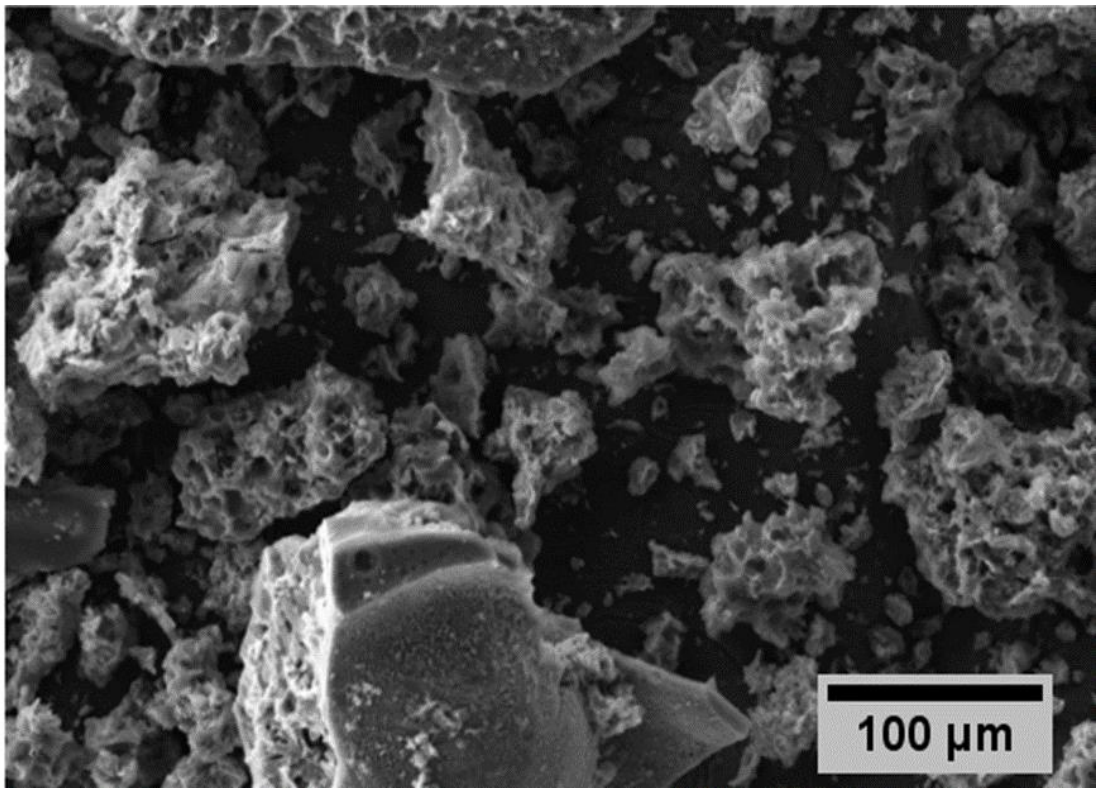

Figure 5.7 SEM images of SC1M1

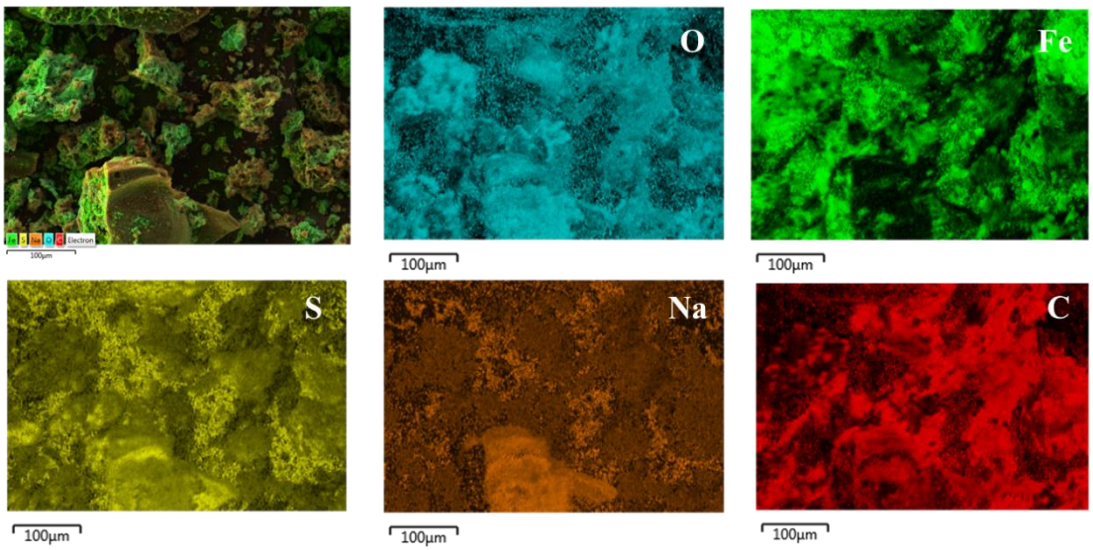

Figure 5.8 Energy- dispersive X-ray analysis (EDX) maps for SC1M1

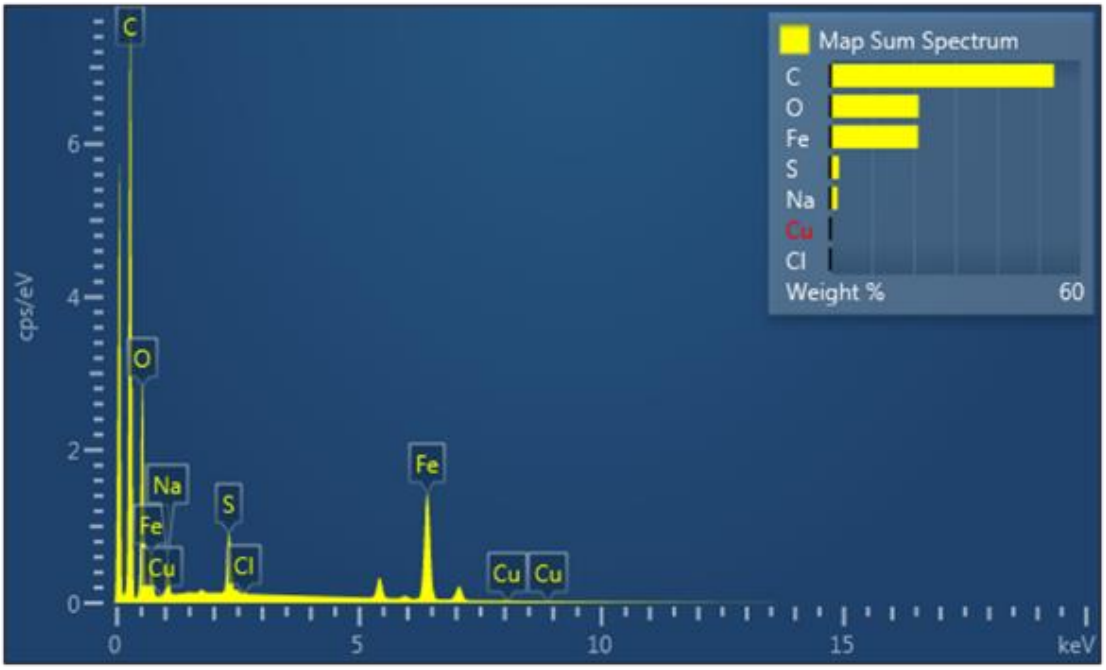

Figure 5.9 EDX peaks for SC1M1. Iron was confirmed on the surface of SC1M1 by EDX, and the weight percentage of iron was ~ 20%.

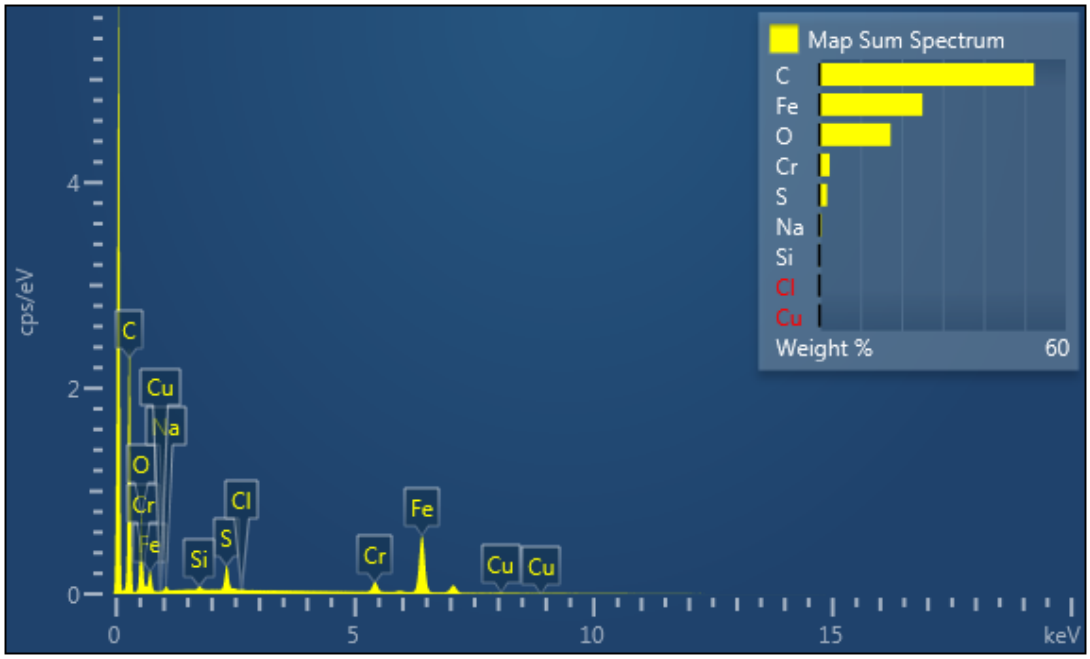

Figure 5.10 Energy- dispersive X-ray analysis (EDX) for SC1M2. The results show that more iron was detected on the surface of SC1M2 (higher than 20%) than that of SC1M1.

In order to study more accurately the compositions of all composites, thermogravimetric analysis (TGA) was conducted. Shown in Figure 5.11, SC0M1, composed primarily of iron oxides, is the most thermally stable material with negligible weight loss (<5%) up to 950 °C. In comparison, SC1M0 was almost completely combusted (> 99%) at 600 °C. Therefore, the difference in thermo-stability between iron oxides and sulfur-doped carbon could be applied to analyze the components in the composite. TGA curves of SC1M2, SC1M1, and SC2M1 demonstrated that the percentage of iron oxides is 67%, 50%, and 35%, respectively, in agreement with the theoretical loading. The porous structure and iron oxide nanoparticles in SC1M1 were further observed by transmission electron microscopy (TEM), as shown in Figure 5.12.

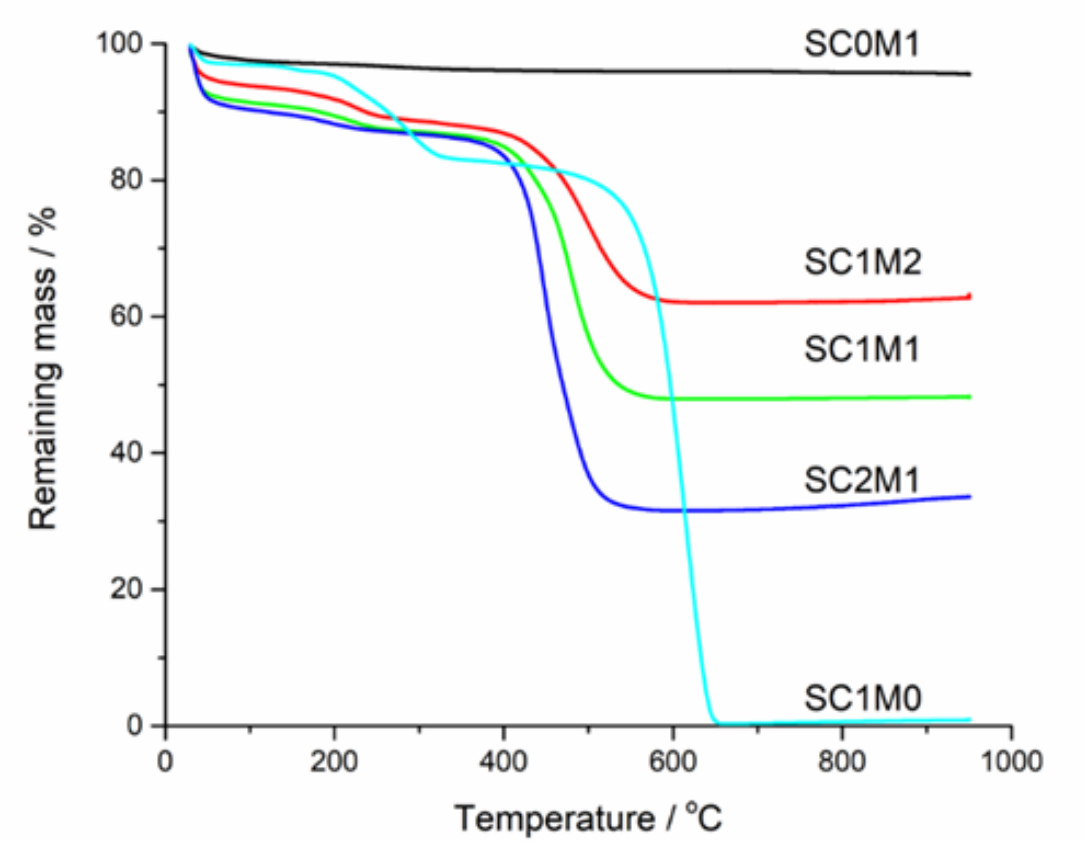

Figure 5.11 Thermogravimetric analysis (TGA) of all magnetic sulfur-doped carbons. The mass remaining at high temperature increases proportionally with the intended iron oxide loading.

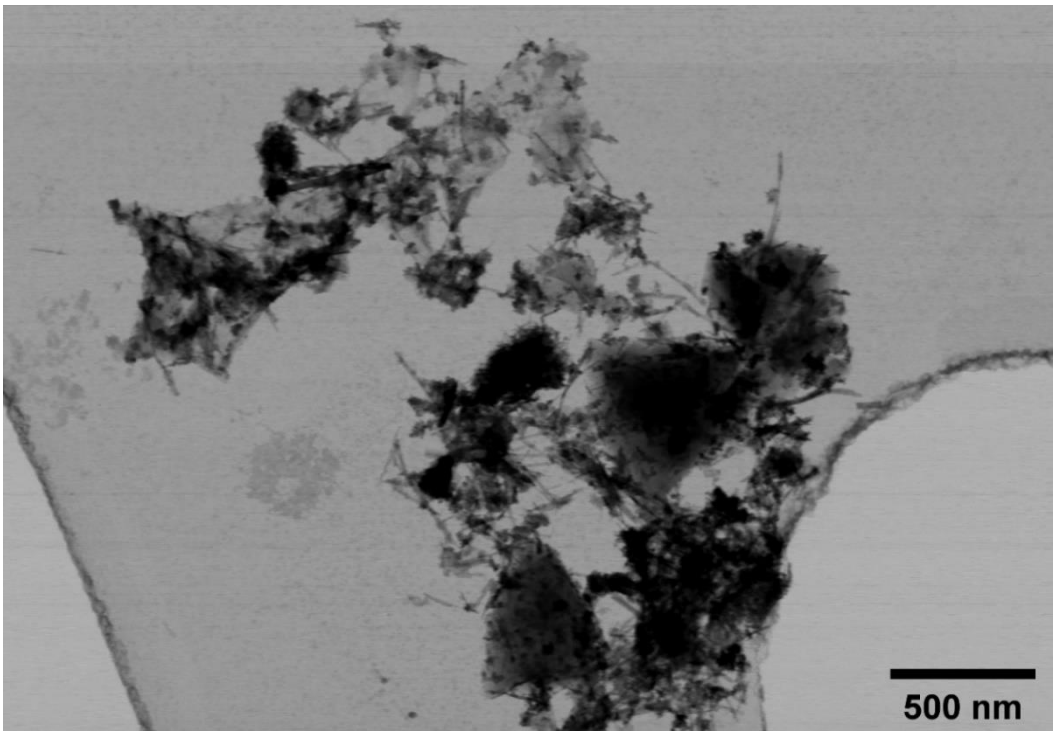

Figure 5.12 TEM images of SC1M1, from which porous structure and iron oxide nanoparticles could be observed

Powder X-ray Diffraction (PXRD) was conducted to investigate generation of iron oxide on the precursor (SC1M0). Commercial magnetite (Fe_3O_4) was also tested to compare with all synthesized composites. In Figure 5.13, diffraction peaks at $2\theta = 30.1°$ and 35.3° are observed in PXRD patterns of both SC0M1 and other MSC composites. These reflections are in agreement with the (220) and (311) reflections of Fe_3O_4 and the structurally related maghemite (γ-Fe2O3) [14,40,41]. The peaks at $2\theta = 21.2°$ of the magnetic sulfur-doped activated carbons was speculated to be goethite (α-FeO(OH)) (110) [14,41]. Considering that maghemite, magnetite and goethite are common products under this reaction condition, the magnetic precipitates synthesized are likely composites of all three types iron oxides [14,42]. A comparison of the diffraction patterns of SC1M1 to simulations of magnetite and maghemite is shown in Figure 5.14. The relatively low intensity, and broadening of the peaks in the case of the synthesized samples, in comparison to the commercial Fe_3O_4, is indicative of a small crystallite size, suggesting nanoscopic, rather than microscopic particles of oxide particles. This is consistent with the SEM and EDX data, which indicated that iron was present fairly

homogeneously throughout the material, but not in aggregates large enough to be individually detected as distinct brighter area

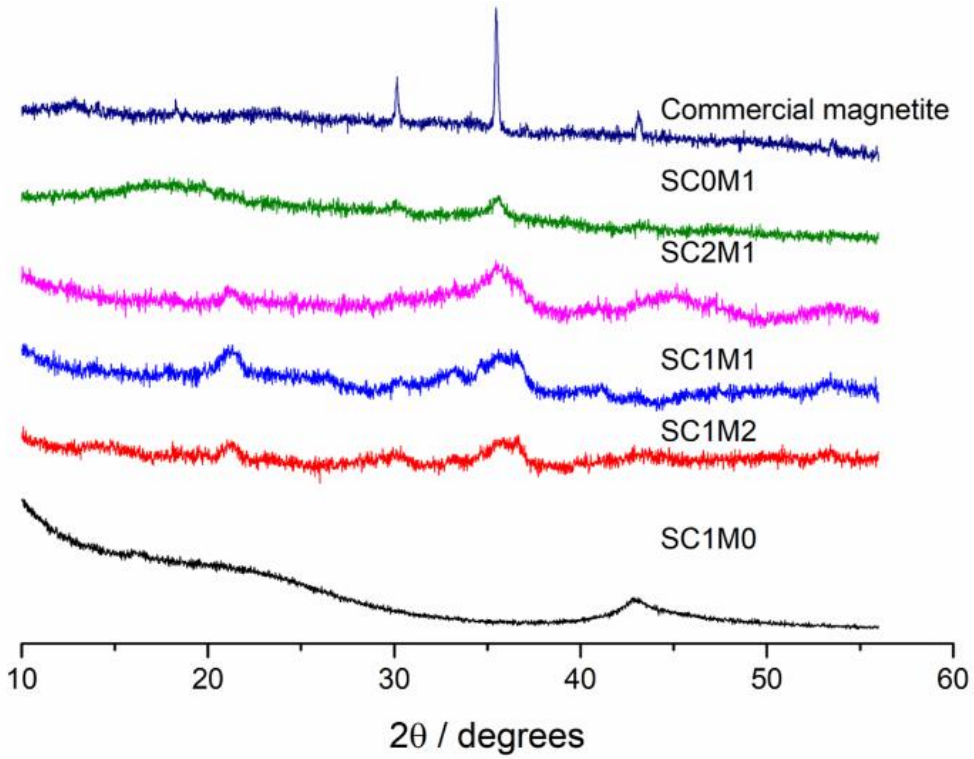

Figure 5.13 Offset PXRD patterns of MSC composite samples.

The magnetization curves of all MSC samples are shown in Figure 5.15. Unlike the pristine sulfur-doped carbon SC1M0, which is diamagnetic (Figure 5.16), all MSC samples show superparamagnetism with only slight hysteresis. The saturation magnetization values were 22.0, 13.9, 7.3 emu/g for SC1M2, SC1M1, SC2M1, respectively. As shown in Figure 5.17, this trend corresponds closely to the relative iron oxide content in the composites.

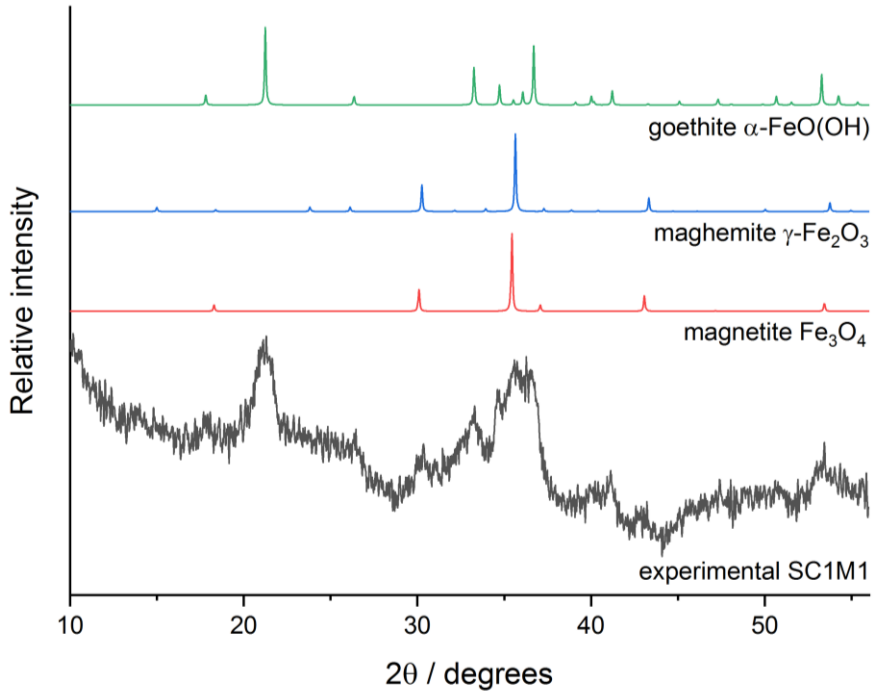

Figure 5.14 Experimental powder diffraction pattern of SC1M1 and patterns simulated from crystal structures (Inorganic Crystal Structure Database) for magnetite, cubic maghemite, and tetragonal maghemite. Offset.

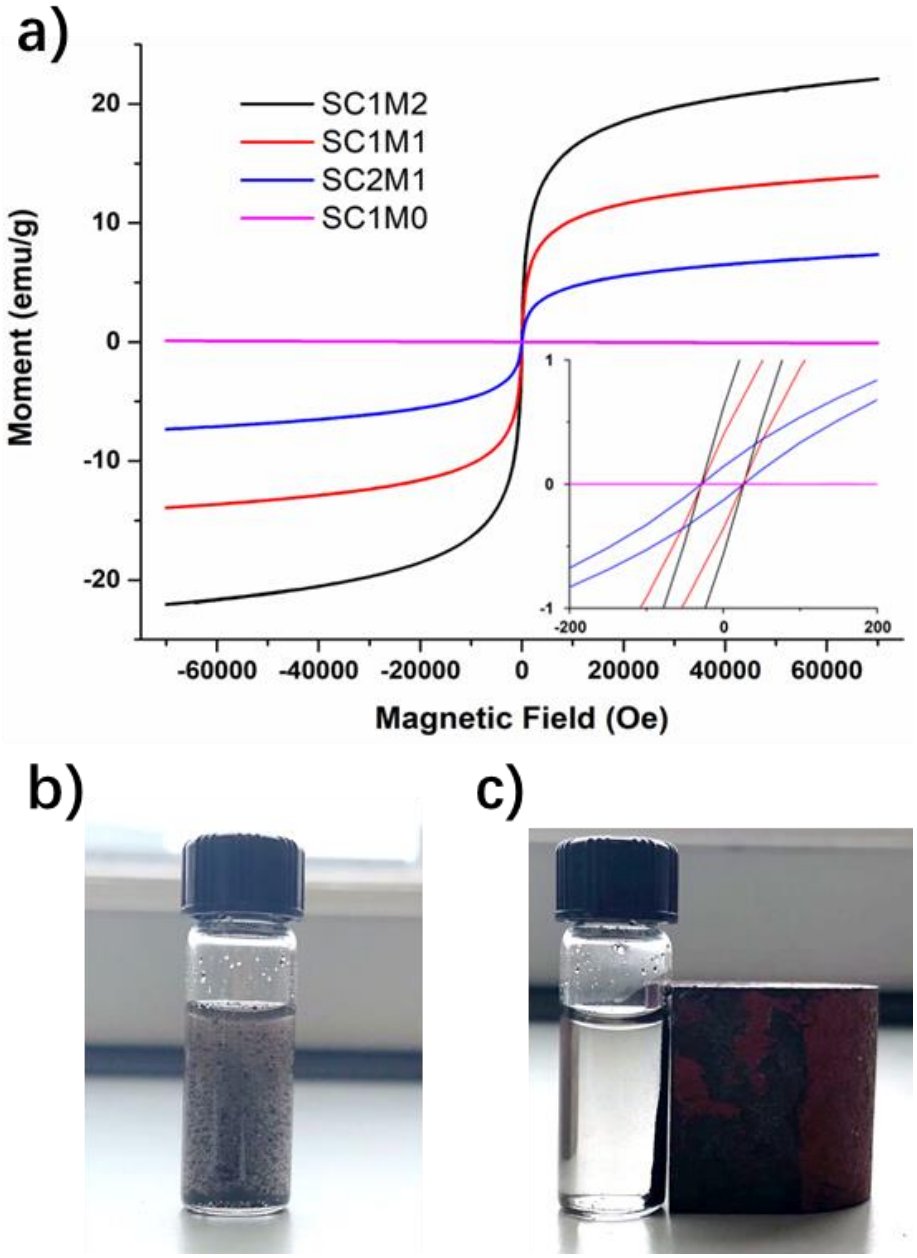

Figure 5.15 a) Magnetization measurement of MSC composites with applied field between −7 and 7 kOe at 293 K. The insets are the enlargement of the centre part of the curves. b) A suspension of MSCs in HgCl2 solution. c) Retrieval of sorbents through external magnetic field.

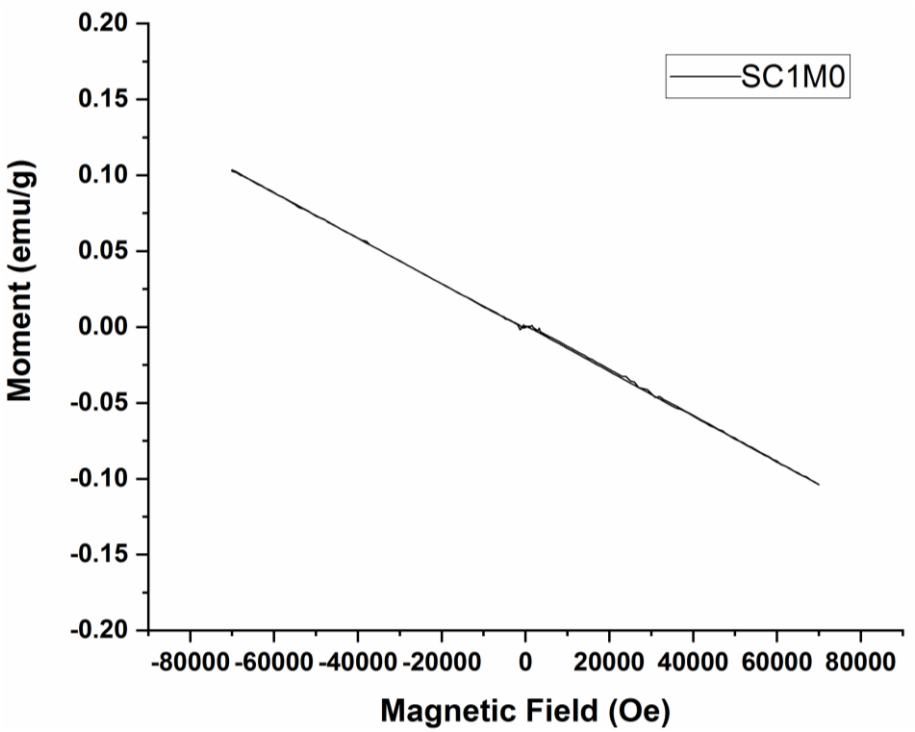

Figure 5.16 Magnetization measurement of SC1M0, showing its diamagnetism.

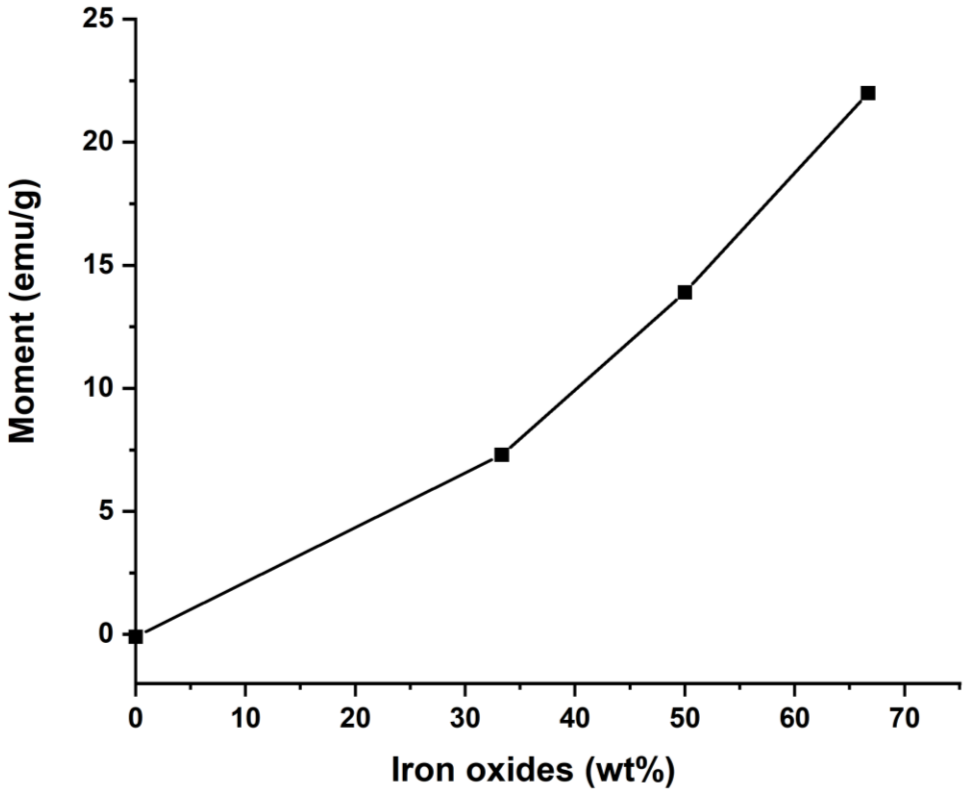

Figure 5.17 Magnetization (applied field at7 kOe) for different iron oxide content MSCs. Magnetization increases as the iron oxides percentage increasing.

5.4.2 Mercury capture studies

Materials produced in this study have potential application as remediation media for mercury contaminated water streams. Several key attributes of the materials make them potentially useful in this regard: high specific surface area, covalently bound sulfur and mesoporosity [5]. However, recovery of particulate media from solution remains a challenge in this regard, until now. By incorporation of magnetic FeO we demonstrate it is possible to sequester solid particulate material from solution, using only a magnetic field (Figure 5.15 (b) and (c)).

However, questions remain about the effect of the incorporation of iron oxides into the material, and the effect it has on the effectiveness of sequestration of the material. A series of static tests were performed in order to assess the viability of various formulations of the material for $HgCl_2$ sorption. The same amount of different MSCs were used to absorb mercury from constant concentration $HgCl_2$ solutions (500 ppm). It was found, as shown in Figure 5.18(a), that inclusion of iron oxides reduced the overall effectiveness of the material, in terms of the percentage of mercury removed. However, this is as would be expected because the measurements are based on the addition of an equal mass of material, and the iron oxide is not active. The unsupported iron oxide itself removed only negligible amounts of mercury (3.23%), indicating the importance of the substrate. The iron oxide is considerably denser than the sulfur-doped carbon, so contributes much of the mass, even if little of the volume. What is important to determine is not if the overall uptake is changed, but rather if the uptake of the sulfur-doped carbon component is changed. It is possible that the iron oxide particles could block pores thus reducing mercury uptake. To determine the effect of the iron oxide inclusion on the efficiency of the sulfur-doped carbon, the mercury uptake was plotted calculating the capacity based only on the mass of sulfur-doped carbon. The uptake does not appear to be detrimentally affected by the incorporation of magnetic material, rather the capacity was actually improved. However, there is likely also an influence on partitioning resulting from the changed Hg/substrate ratio.

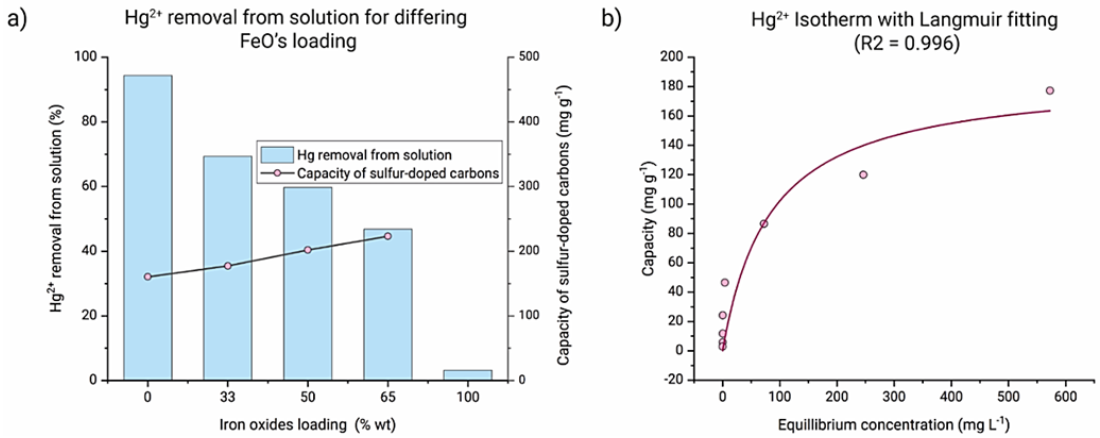

Figure 5.18 a) Static mercury uptake test of various formulations of MSCs, showing the proportion of Hg removed from a 500 ppm, 10 ml solution of HgCl2 by 30 mg of material (left Y axis), and the capacity for Hg of the sulfur-doped carbon (right Y axis). b) Absorption isotherm of Hg2+ onto the substrate, fitted to the Langmuir model.

Considering the results of static tests and the magnetization of MSCs, SC1M1 was selected to conduct further mercury capacity tests. A very steep uptake at low concentration is crucial for use industrially; desired concentrations to be purified are ~ 2 ppm, ideally being reduced to below 0.006 ppm, the level recommended safe for drinking water by the world health organization [43]. Figure 5.18(b) demonstrates this high affinity, removing almost all mercury from low concentration solutions. Fitting this data to a Langmuir isotherm allowed for deduction of the thermodynamic parameters Q_{max}, and K_L: the saturation capacity and affinity coefficient. Q_{max} was found to be 187.4 mg g^{-1} and K_L to be 0.01 L mg^{-1}. The capacity is comparable to many conventional activated carbons, and certainly high enough for practical application. The steep initial uptake, at low concentration makes this material gives superior performance in comparison to conventional activated carbon over an industrially relevant concentration range. For instance, at ~4 ppm concentration, SC1M1 shows an uptake of 47 mg g^{-1} compared to 3 mg g^{-1} for a conventional activated carbon at the same concentration (see Figure 5.19), an improvement of an order of magnitude. Additionally, the adsorption kinetics of mercury on MSCs were studied by fitting results with a pseudo-first order and pseudo-second order model, as shown in Figure 5.20. The results shown that pseudo-second order rate model is better to describe the mercury adsorption rate of MSCs, with q_e = 48.75 ± 1.40 mg g^{-1}, and k_2 = 0.0118 ± 0.0038 g mg^{-1} min^{-1}. This k_2 is lower than that of thiol-functionalized MOF (k_2= 1.30

$\times 10^{-1}$ g mg^{-1} min^{-1})[44], but higher than that of pS-CEA (k_2= 1.38 $\times 10^{-4}$ g mg^{-1} min^{-1})[45] and pS-CEA (2:1)/PAN microfiber (k_2= 2.25$\times 10^{-4}$ g mg^{-1} min^{-1})[46].

Nonlinear kinetic model pseudo- first order (**Equation 5-1**) and pseudo-second order rate equations (**Equation 5-2**) were employed to fit Hg^{2+} adsorption by SC1M1.

$$\boldsymbol{q_t = q_e(1 - e^{-k_1 t})} \qquad \textbf{Equation 5-1}$$

$$q_t = \frac{k_2 {q_e}^2 t}{1 + k_2 q_e t} \qquad \textbf{Equation 5-2}$$

Where,

q_t = mercury uptake by SC1M1 at time (mg mercury / g SC1M1)

q_e = mercury uptake by SC1M1 at equilibrium (mg mercury / g SC1M1)

k_1 = rate constant of pseudo-first order kinetic model (min^{-1})

k_2 = rate constant of pseudo-second order kinetic model (g mg^{-1} min^{-1})

Fitting results:

pseudo- first order

q_e= 47.15 ± 1.61 mg g^{-1} k_1 = 0.28 ± 0.07 min^{-1} r^2 = 0.96

pseudo-second order

q_e= 48.75 ± 1.40 mg g^{-1} k_2 = 0.0118 ± 0.0038 g mg^{-1} min^{-1} r^2 = 0.98

For metal ion removal, solution pH may affect adsorption, therefore, the initial pH of solution was adjusted to investigate the impact of pH on mercury uptake, as shown in Figure 5.21. It was found that, in terms of SC1M0, pH had little effect on Hg uptake in these conditions, which remained ~110 mg g^{-1}. However, in the same testing conditions, solution pH had a marked effect on mercury removal of SC1M1, which increased from 43% (pH=4), to 56% (pH=7), to 68% (pH=10), corresponding to q_e = 32 mg g^{-1} to, 49 mg g^{-1}, to final 69 mg g^{-1} in capacity.

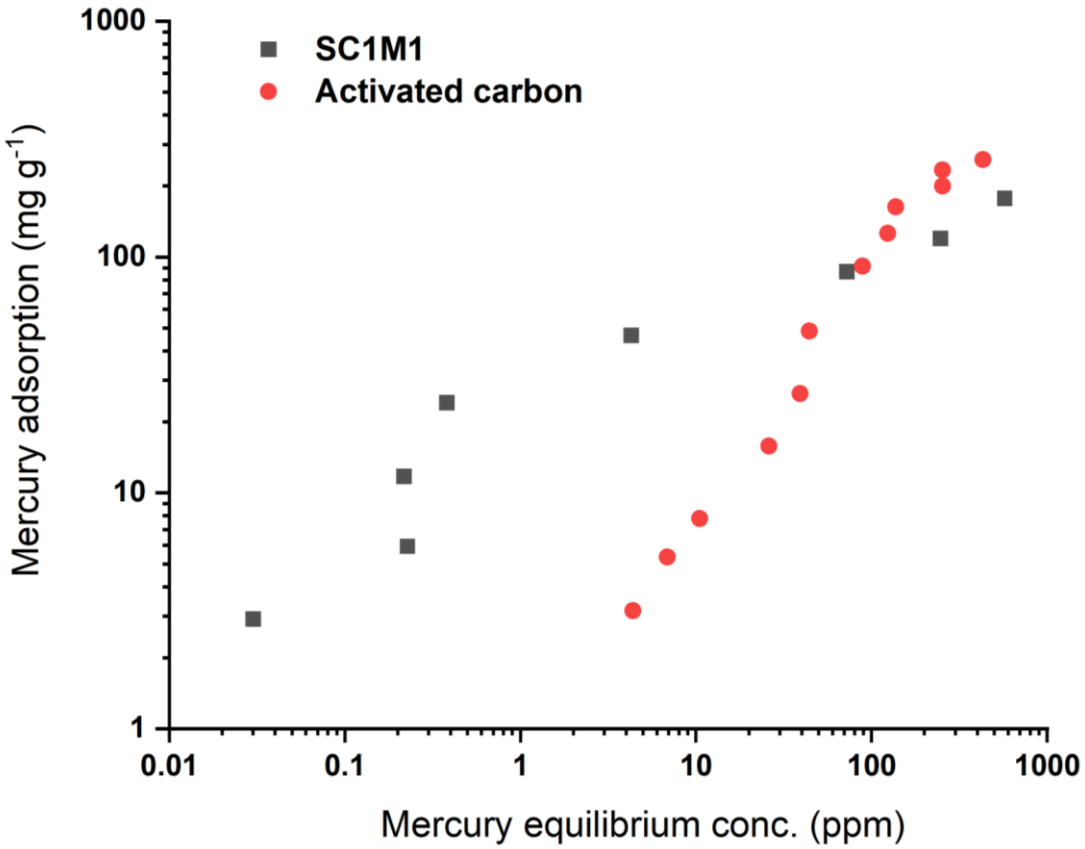

Figure 5.19 Comparison of mercury uptake between MSCs and conventional activated carbons. It is clear that activated carbons have high capacity in higher equilibrium concentration, but MSCs are much more sensitive at lower concertation. Activated carbon results taken from previous work.4

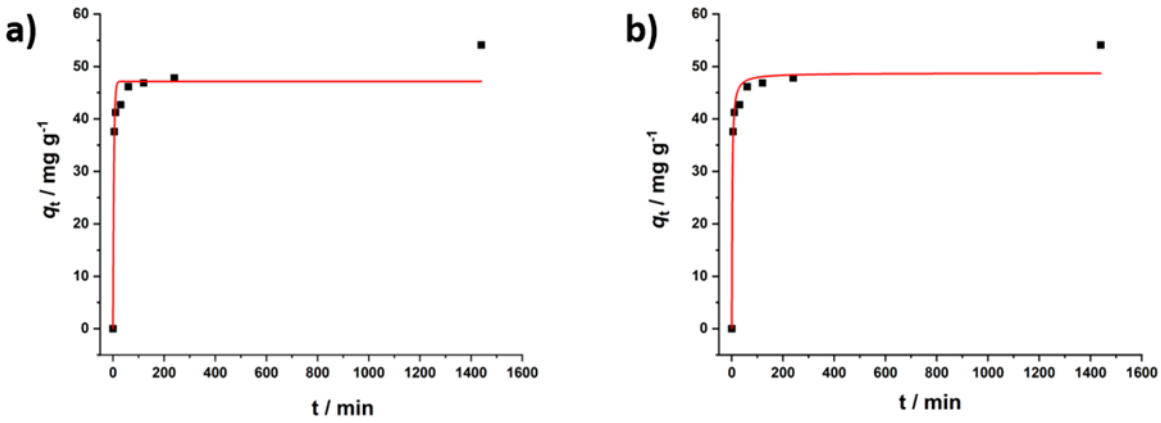

Figure 5.20 Kinetics fitting of mercury removal by SC1M1 using (a) pseudo-first and (b) pseudo-second models.

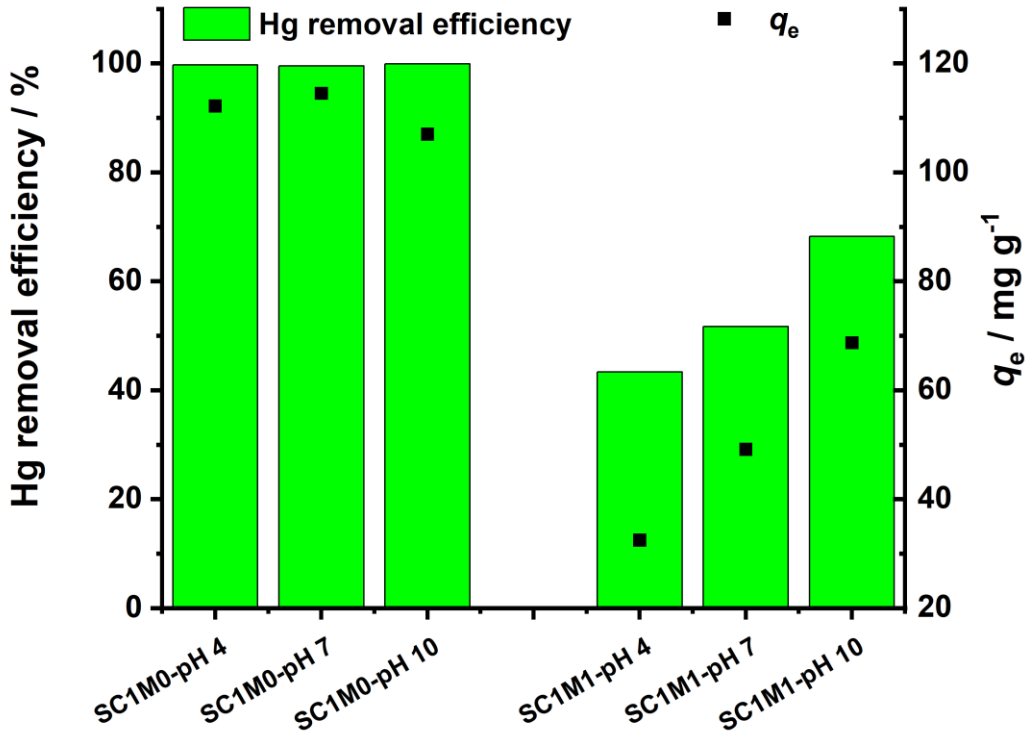

Figure 5.21 Effect of solution pH on mercury uptake. For SC1M0, pH value had little effect on mercury uptake, probably, resulting from high saturated capacity of SC1M0, however, for SC1M1, pH had a positive effect on mercury uptake, increasing qe from 32 mg g^{-1}, to 49 mg g^{-1}, final 69 mg g^{-1}.

MSCs were studied after mercury ($HgCl_2$ solution, C_0 = 10 ppm) uptake to understand their stability and recyclability. Although the state of Hg in MSCs is not clear, Hg can be observed on the surface of MSCs by EDX, as shown in Figure 5.22, Figure 5.23, and Figure 5.24. Magnetic nanoparticles are relatively stable on the surface of MSCs in mild conditions, as no iron was detected after mercury uptake (Hg residual concentration C_{e1} = 0.15 ppm, 99% mercury removed) by ICP-OES. However, magnetic nanoparticles were destroyed if harsh striping solution (0.5 M HCl + 1M thiourea) was used to remove the Hg. Leached by stripping solution, more than 50% Hg could be desorbed from MSCs, a result also suggested very high affinity of MSCs to mercury. Although iron was released by stripping agent, resulting in loss of magnetism, sulfur doped activated carbons were reusable in mercury uptake, removing more than 86 % Hg from 10 ppm $HgCl_2$ solution (C_{e2}= 1.38 ppm).

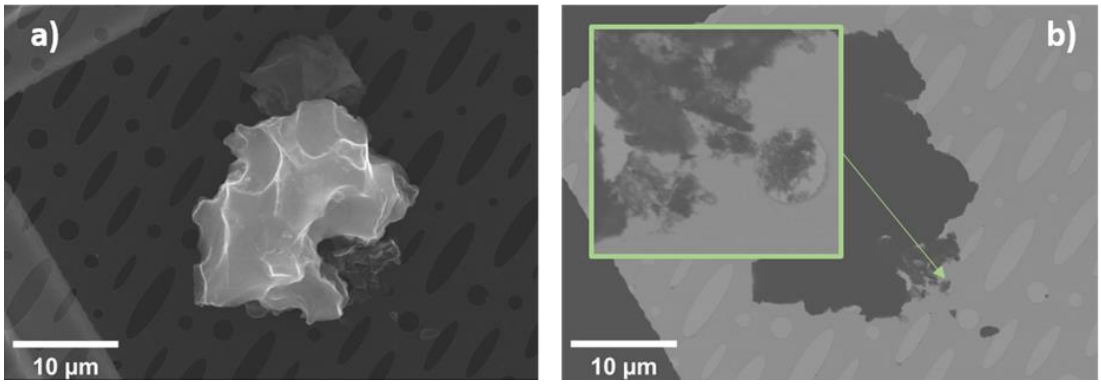

Figure 5.22 (a) SEM image of SC1M1 after mercury uptake. (b) TEM image of SC1M1 after mercury uptake

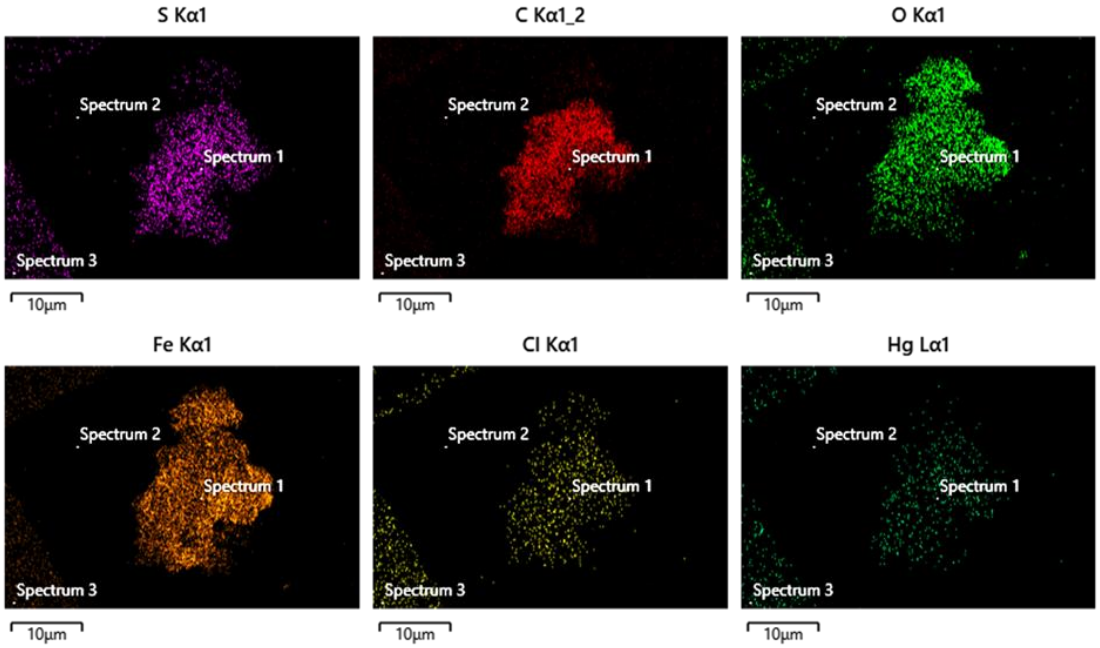

Figure 5.23 Energy- dispersive X-ray analysis (EDX) maps of SC1M1 after mercury uptake, showing, (clockwise from top left) sulfur, carbon, oxygen, iron, chloride, and mercury.

MSCs were compared with other reported mercury adsorbents (Table 5.2). Max capacity of mercury uptake is an effective parameter to evaluate. However, in practical terms these materials would often be unlikely to be exposed to the amounts and concentrations of Hg required to reach these saturation capacities. As long as the materials have an appreciable capacity (e.g. over 100 mg g^{-1}), and ideally a sharp uptake at low concentration this will allow effective use. Due to the scale and environments in which these materials would be used (industrial and remediation), the cost, stability, and ease of handling must also be considered. COF-based absorbents

have a relatively high maximum capacity compared with carbon-based materials, however, COF-based absorbents suffer from high cost and small scale, hindering the scope of applications. Magnetic mercury adsorbents are beneficial in ease of recovery, but normally possess lower max capacity mainly because the magnetic component in the material is denser than the adsorbing component. Sustainability, though sometimes overlooked, is relevant to consider in terms of potential mercury absorbents. Because MSCs are prepared using industrial by-products, sulfur and DCPD, as the feedstocks, rather than limited resources, they are desirable in environmental terms. Moreover, the low price of raw materials means the cost of MSCs would be highly competitive - estimated less than 0.5 $/g (Table 5.3), cheaper than many adsorbents. In comparison, the MNPC-T700-M3 carbon composite material, for example, is based upon synthesis from a costly and unsustainable metal-organic-framework feedstock. Similarly, synthesis of both the S-MAOP polymer and M-DAPS50-COF-SH COF magnetic sorbents require specialist and limited chemical resources, and complex synthesis. From Table1, it can be found that unlike more niche chemical products, MSCs could be produced in gram scale, showing potential for practical application. The MSCs reported here are therefore comparable in uptake to the related state of the art magnetic Hg sorbent materials reported in Table 1, but with the advantage of being lower in cost, more sustainable, and more suitable for production at scale.

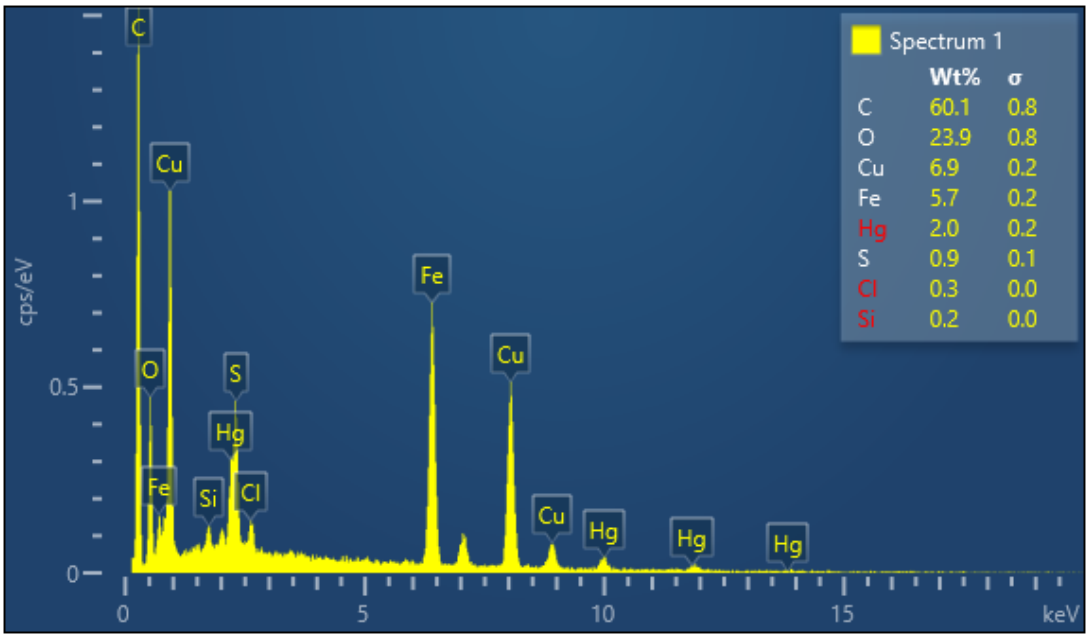

Figure 5.24 Energy- dispersive X-ray analysis (EDX) for SC1M1 after mercury uptake, showing mercury on the SC1M1.

Table 5.2 Comparison of different adsorbents for Hg^{2+} uptake

Adsorbents	Material type	Production scale	Max capacity (mg g^{-1})	Magnetic	Ref
CBAP-1	Porous Organic Polymer	grams	181-232	N	[47]
POFct-1	Porous Organic Framework	milligrams	167.19	N	[48]
S-MAOP	Organic polymer-based	milligrams	512	Y	[34]
COF-S-SH	Covalent Organic Framework	milligrams	1350	N	[49]
T-COF	Covalent Organic Framework	milligrams	1815	N	[50]
ACOF	Covalent Organic Framework	milligrams	175	N	[51]
MAC	Carbon	milligrams	119	N	[52]
M-DAPS50-COF-SH	Covalent Organic Framework-based	milligrams	383	Y	[37]
SWCNT-SH	Carbon	milligrams	131	N	[53]
Fe3O4-GS	Carbon composite	grams	23.03	Y	[54]
S-FMC	Carbon	grams	461-732	N	[55]
MNPC-T700-M3	Carbon composite	milligrams	182-476	Y	[56]
1K–S–DCPD-750	Carbon	grams	850	N	[5]
MSCs	Carbon composite	grams	187	Y	This work

Table 5.3 Price of the chemicals for MSCs

Chemicals	Pack Size	Price (£)
Sulfur	1kg	32.00
Dicyclopentadiene (DCPD)	1kg	53.00
KOH	1kg	35.20
$FeCl_3$	1kg	46.50
$FeSO_4{\cdot}7H_2O$	1kg	55.40
NaOH	1kg	66.20

Note: price quoted from Sigma-Aldrich UK. If produced at an industrial scale, this would be considerably lower, for example sulfur trades for approximately £100 / tonne, and DCPD for ~$600 / tonne at large scales.

Finally, although the high theoretical mercury uptake capacity is important, MSCs were studied in more realistic conditions, namely low mercury concentration with the presence of competing ions. The results are shown in Figure 5.25 and Table 5.4. CRM of trace metal aqueous solution was applied in this research to stimulate real industrial waste water. Blank testing was completed first to explore the stability of mercury solution in glass sample vials for one hour at room temperature. Apparently, the mercury concentration decreased from 7.518 to 6.059 ppb, around 20% losses of mercury from CRM solution. This result was aligned with literature that more than 20% losses was observed from mercury solution after 30 min from preparation, even stabilized by 2% HNO_3 [57]. Although the mechanism for mercury loss from solution is not clear, such as adsorption on the container walls, mercury volatilization, and conversion of mercury species, in this study, the loss of mercury was speculated because of adsorption on the sample vials wall, as exposure of solution is only within 1 hour. Hg concentrations of solution treated by SC1M0, SC2M1, and SC1M1 were all lower than the detection limitation of ICP-MS, significant reduction of mercury concentration from a level higher than WHO (6 ppb) guideline to negligible. Clearly, the competing ions do not adversely influence the mercury uptake at a low mercury concentration for the MSCs. Interestingly, the precursor of MSCs, SC1M0 showed very high selectivity to mercury. All mercury adsorbed was adsorbed, but only around 13 % of the Pb (original concentration: 226 ppb) was removed by SC1M0. However, the MSCs demonstrated more function in absorbing other hazard ions from aqueous solution, benefiting from the iron oxides [58,59]. More lead (Pb) was removed by MSCs as the content of iron oxides increased, and almost 50% of lead was removed from

CRM by SC1M1 to 126.74 ppb. Although this result is still much higher than the guideline of WHO, considering the pristine concentration of lead is relatively high, the lead capture capability of MSCs is acceptable and MSCs could be applied as pre-treatment material for high lead concentration waste water. More important, considerable arsenic (As) was removed by MSCs within one hour. More than 80 % of As from solution was absorbed by only 10 mg MSCs to around 40 ppb, which is lower than WHO maximum permissible limit of 50 ppb. Therefore, with no negative affect for mercury removal, MSCs could be applied as a multifunctional absorbent for different toxic metals in a mixed aqueous system.

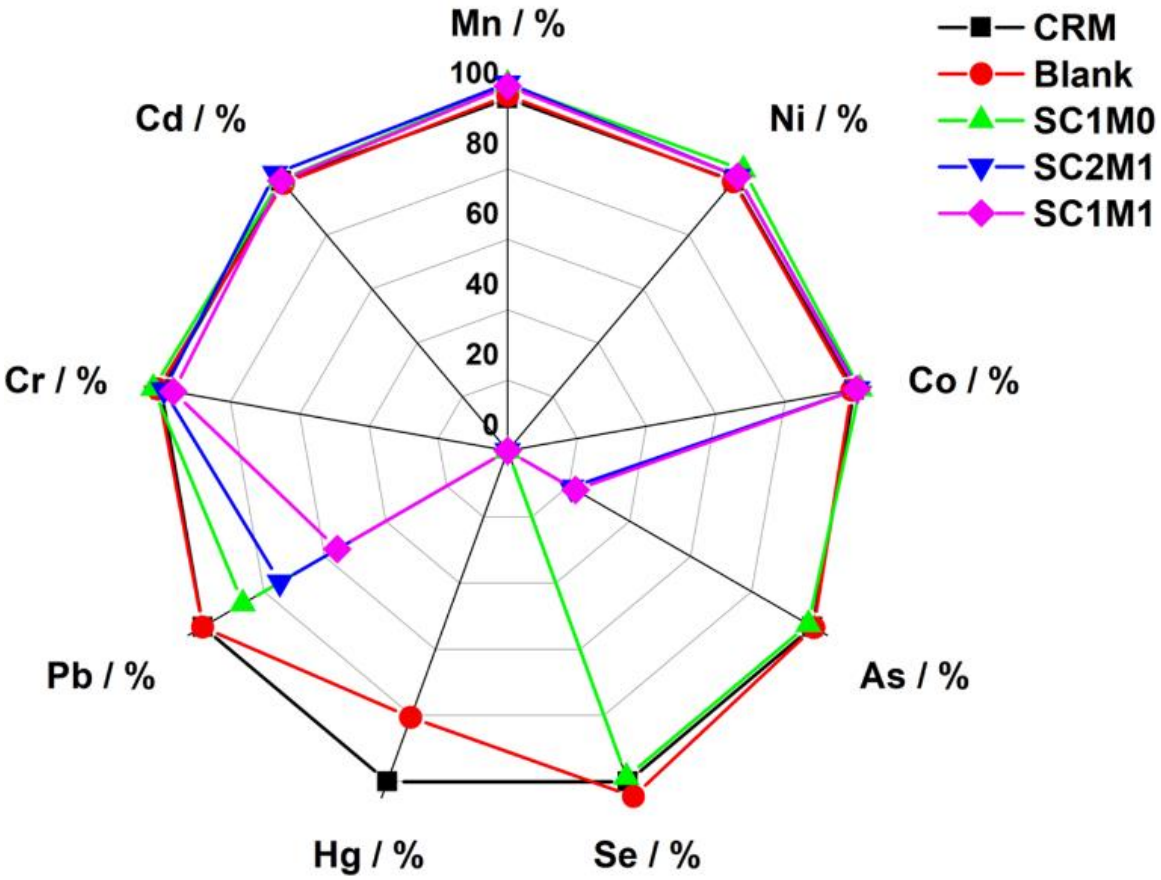

Figure 5.25 Selectivity test of MSCs using mixed ion solution, simulating waste water. Mercury could be removed to undetectable level by all sulfur-doped carbons. Arsenic was removed under WHO guideline by only MSCs materials.

Table 5.4 Selectivity test of MSCs from mixed ion solution

Sample	Cr / ppb	Mn / ppb	Ni / ppb	Co / ppb	As / ppb	Se / ppb	Cd / ppb	Hg / ppb	Pb / ppb
CRM	293.7	1018.2	1015.0	751.2	201.8	79.3	328.0	7.5	226.8
BLANK	296.5	1026.8	1012.0	746.0	202.7	82.9	325.0	6.1	227.0
SC1M0	300.2	1060.0	1056.9	763.2	199.1	78.2	329.2	-	197.0
SC2M1	291.3	1062.8	1031.6	757.9	42.0	-	337.0	-	169.5
SC1M1	283.4	1054.1	1032.0	756.2	45.0	-	328.2	-	126.7

Note: '-' means under detectable level of ICP-MS'

5.5 Conclusions

Magnetic sulfur-doped carbon composites were successfully synthesized by chemical precipitation of iron oxides onto the surface of sulfur-doped carbon. High specific surface area and porous structure of pristine carbon were observed in all synthesized MSCs, however, increasing the percentage of iron oxides decreased the BET surface area and broadened porous size distribution. Significant mercury capture performance of all samples shows a potential application of these composites in water purification and environmental remediation. More importantly, steep uptake at low concentration offers an advantage over conventional activated carbons, showing potential in industrial purification. Additionally, resulting from arsenic and lead adsorption by iron oxides, MSCs exhibited multifunction uptake capability in waste water. The magnetic properties of all MSCs make it possible that, after absorption of hazardous materials, the absorbents could be retrieved by external magnetic field. With low production cost, good adsorbing properties, and simple separation, magnetic sulfur-doped carbon composites can be considered as promising adsorbents in practical purification applications.

5.6 Experimental

5.6.1 Materials

Sulfur (S_8, sublimed powder, reagent grade, ⩾ 99.5%, Brenntag UK & Ireland. Purchased in 25 kg bags), dicyclopentadiene (DCPD >95%, TCI), iron (III) chloride ($FeCl_3$, reagent grade, 97%, Sigma-Aldrich), iron (II) sulfate heptahydrate ($FeSO_4 \cdot 7H_2O$, ACS reagent, Sigma-Aldrich), potassium hydroxide (KOH, Sigma-Aldrich), and sodium hydroxide (NaOH, Sigma-Aldrich), Trace Metal Certified Reference Material (QC3132-500ML, Lot LRAC5492, Sigma-Aldrich). pH buffer solutions (pH = 4.01, 7.00, 10.01, Thermo Scientific). All chemical precursors were used as received without any further purification. Deionized water was used in filtration and washing steps of the resultant materials.

5.6.2 Methods

Preparation of poly(S-DCPD)

Sulfur (10 g) was fully melted at 160 °C in 40 mL sample vials, and DCPD (10 g) added, before being stirred homogeneously by magnetic stirrer bar. After around 30 minutes, the whole system became a homogeneous black viscous liquid. These pre-polymers were then transferred into an oven for further curing at 140 °C overnight.

Preparation of sulfur-doped activated carbons

Carbonization was performed as previously reported. Typically, poly(S-DCPD) and KOH (weight ratio=1:1) were ground using a pestle and mortar, until homogeneous. The mixture was transferred into a ceramic boat and placed in a tube furnace. The furnace was purged with N_2 at 120 °C for 1 hour, then heated to 750 °C at a rate of 5 °C min^{-1} for 2 hours. When the furnace cooled to room temperature, the residue was removed and washed by 1 M HCl and deionized water. Final products were dried under vacuum overnight at 110 °C.

Preparation of magnetic sulfur-doped activated carbons

Sulfur-doped activated carbons were ground into fine powders, then suspended in the mixed solution of $FeCl_3$ and $FeSO_4$ for 2 hours. The amount of activated carbon was adjusted to synthesize composites with different ratios of activated carbon/iron oxides.

Then NaOH solution (5 mol L^{-1}) was dropped by pipette to precipitate the iron oxides. Precipitation was conducted at 70 °C for 2 hours. The resultant composites were filtered and dried at 70 °C for 8 hours in the oven.

5.6.3 Characterisation

Powder X-ray Diffraction (PXRD)

Samples were analysed using a PANalytical Empyrean diffractometer with Cu-K□ radiation, operating in transmission geometry.

Thermogravimetric Analysis (TGA)

TGA was carried out in platinum pans using a Q5000IR analyzer (TA Instruments) with an automated vertical overhead thermo balance. The samples were heated at 5 °C min^{-1} to 950 °C under air.

Pore Structure Analysis

Pore structure properties of the samples were determined via nitrogen adsorption and desorption at 77.3 K using a volumetric technique on an ASAP 2420 adsorption analyser (Micromeritics Instrument Corporation). Before analysis, the samples were degassed at 100 °C for 15 h under vacuum (10-5 bar). Brunauer-Emmett-Teller (BET) surface area was obtained in the relative pressure (P/P_0) range of 0.05–0.20.

Scanning electron microscopy (SEM)

Morphology images of the composite were achieved using a Hitachi S-4800 cold field emission scanning electron microscope (FE-SEM), with integrated energy- dispersive

X-ray analysis (EDX)

Magnetic Measurements. Magnetic measurements were carried out on powder samples using a commercial superconducting quantum interference device (SQUID) magnetometer MPMS3 (Quantum Design, USA). The magnetic field-dependent magnetization was measured at 293 K between −7 and 7 kOe.

5.6.4 Mercury uptake studies

Static mercury uptake capability

500 ppm $HgCl_2$ solution was prepared. 30 mg of different MSC composites were individually added into 10 mL solution in a 12 mL polypropylene centrifuge tube. Each solution was left to agitate on a tube roller at 60 rpm for 24 hours. The subsequent mixtures were separated by use of a Nylon 0.50 µm syringe filter. The filtrate was then stabilized with 1 mL HNO3(aq).

Capacity studies using mercury solution

A series of solutions of Hg^{2+} were prepared from $HgCl_2$ in the concentrations: 6.25, 12.5, 25, 50, 100, 250, 500, and 1000 ppm. 10 mL aliquots of these solutions were pipetted into 12 mL polypropylene centrifuge tubes. To each tube 20 mg of SC1M1 (see Results and Discussion for naming system) composite was added. Each solution was left to agitate on a tube roller at 60 rpm for 24 hours. The subsequent mixtures were separated by use of a Nylon 0.45 µm syringe filter. The filtrate was then stabilized with 1 mL HNO_3(aq).

Samples were then analyzed via inductively coupled plasma optical emission spectrometry (ICP-OES), using an Agilent 5110 ICP-OES spectrometer, equipped with an autosampler. Between each run the lines were rinsed with 10 % HNO3 solution for 60 seconds to prevent any potential carryover of Hg2+. To correct for any potential matrix effects an internal standard of Hafnium was employed.

The resultant isotherm was fitted to a Langmuir model, according to Eq. 1.

$$Q_e = \frac{Q_{max} K_L C_e}{1 + K_L C_e}$$

Langmuir model. where Q_e (mg g^{-1}) and C_e (mg L^{-1}) are the amount of equilibrium concentration of mercury solution and capacity of MCSs at equilibrium, respectively. Q_{max} (mg g^{-1}) and K_L (L mg^{-1}) are the saturation capacity of MCSs and affinity coefficient, respectively.

Reusability study of MSCs

10 mL $HgCl_2$ solution (C_0 = 10 ppm) were pipetted into a 12 mL polypropylene centrifuge tube. To the tube 20 mg of SC1M1 (see Results and Discussion for naming system) composite was added. The solution was left to agitate on a tube roller at 60

rpm for 24 hours. The subsequent mixtures were separated by magnet. The filtrate was then stabilized with 1 mL HNO3(aq).

Adsorbed materials were dried first and washed by 40 mL mixed stripping solution (1M thiourea/ 0.5 M HCl). The mixture was left to agitate on a tube roller at 60 rpm for 24 hours. The subsequent mixtures were separated by use of a Nylon 0.50 µm syringe filter. 9 mL of filtrate was transferred in to a 12 mL polypropylene centrifuge tube, and stabilized with 1 mL HNO3(aq). Left samples were rinsed with DI waster three times and dried for next adsorption testing.

Samples were then analyzed via inductively coupled plasma optical emission spectrometry (ICP-OES), using an Agilent 5110 ICP-OES spectrometer, equipped with an autosampler.

Effect of pH

100 ppm $HgCl_2$ solution was prepared by different pH buffer solutions (pH = 4.01, 7.00, 10.01). 10 mg of different MSC composites (SC1M0 and SC1M1) were individually added into 10 mL solution in a 12 mL polypropylene centrifuge tube. Each solution was left to agitate on a tube roller at 60 rpm for 24 hours. The subsequent mixtures were separated by use of a Nylon 0.50 µm syringe filter. The filtrate was then stabilized with 1 mL HNO_3(aq).

Selectivity test of MSCs

10 mL Certified reference material (CRM) were pipetted into 14 mL glass sample vials. To each tube 10 mg of SC1M0, SC2M1, and SC1M1 composite was added, respectively. Blank sample was prepared by adding no samples. Each solution was left to agitate on a tube roller at 60 rpm for 1 hour. The subsequent mixtures were separated by use of a Nylon 0.45 µm syringe filter. The filtrate was then stabilized with 1 mL HNO3(aq). Samples were then analyzed via inductively coupled plasma mass spectrometry (ICP-MS), using Perkin Elmer Nexion 2000 ICP-MS with a Meinhard nebuliser and cyclonic spray chamber.

5.7 References

(1) Cote, A. P. Porous, Crystalline, Covalent Organic Frameworks. *Science (80-.).* **2005**, *310* (5751), 1166–1170.

(2) Khan, N. A.; Hasan, Z.; Jhung, S. H. Adsorptive Removal of Hazardous Materials Using Metal-Organic Frameworks (MOFs): A Review. *J. Hazard. Mater.* **2013**, *244–245*, 444–456.

(3) McKeown, N. B.; Budd, P. M. Polymers of Intrinsic Microporosity (PIMs): Organic Materials for Membrane Separations, Heterogeneous Catalysis and Hydrogen Storage. *Chem. Soc. Rev.* **2006**, *35* (8), 675–683.

(4) Feng, X.; Ding, X.; Jiang, D. Covalent Organic Frameworks. *Chem. Soc. Rev.* **2012**, *41* (18), 6010.

(5) Lee, J. S. M.; Parker, D. J.; Cooper, A. I.; Hasell, T. High Surface Area Sulfur-Doped Microporous Carbons from Inverse Vulcanised Polymers. *J. Mater. Chem. A* **2017**, *5* (35), 18603–18609.

(6) Lee, J. S. M.; Briggs, M. E.; Hasell, T.; Cooper, A. I. Hyperporous Carbons from Hypercrosslinked Polymers. *Adv. Mater.* **2016**, *28* (44), 9804–9810.

(7) McKeown, N. B.; Budd, P. M.; Msayib, K. J.; Ghanem, B. S.; Kingston, H. J.; Tattershall, C. E.; Makhseed, S.; Reynolds, K. J.; Fritsch, D. Polymers of Intrinsic Microporosity (PIMs): Bridging the Void between Microporous and Polymeric Materials. *Chem. - A Eur. J.* **2005**, *11* (9), 2610–2620.

(8) Rogge, S. M. J.; Bavykina, A.; Hajek, J.; Garcia, H.; Olivos-Suarez, A. I.; Sepúlveda-Escribano, A.; Vimont, A.; Clet, G.; Bazin, P.; Kapteijn, F.; Daturi, M.; Ramos-Fernandez, E. V.; Llabrés Xamena, F. X. I.; Van Speybroeck, V.; Gascon, J. Metal-Organic and Covalent Organic Frameworks as Single-Site Catalysts. *Chem. Soc. Rev.* **2017**, *46* (11), 3134–3184.

(9) Yang, Q.; Xu, Q.; Jiang, H. L. Metal-Organic Frameworks Meet Metal Nanoparticles: Synergistic Effect for Enhanced Catalysis. *Chem. Soc. Rev.* **2017**, *46* (15), 4774–4808.

(10) Qie, L.; Chen, W.; Xu, H.; Xiong, X.; Jiang, Y.; Zou, F.; Hu, X.; Xin, Y.; Zhang,

Z.; Huang, Y. Synthesis of Functionalized 3D Hierarchical Porous Carbon for High-Performance Supercapacitors. *Energy Environ. Sci.* **2013**, *6* (8), 2497–2504.

(11) Crini, G. Non-Conventional Low-Cost Adsorbents for Dye Removal: A Review. *Bioresour. Technol.* **2006**, *97* (9), 1061–1085.

(12) Jimenez-Solomon, M. F.; Song, Q.; Jelfs, K. E.; Munoz-Ibanez, M.; Livingston, A. G. Polymer Nanofilms with Enhanced Microporosity by Interfacial Polymerization. *Nat. Mater.* **2016**, *15* (7), 760–767.

(13) Liu, P. S.; Chen, G. F. General Introduction to Porous Materials. In *Porous Materials*; Elsevier, 2014; pp 1–20.

(14) Oliveira, L. C. A.; Rios, R. V. R. A.; Fabris, J. D.; Garg, V.; Sapag, K.; Lago, R. M. Activated Carbon/Iron Oxide Magnetic Composites for the Adsorption of Contaminants in Water. *Carbon N. Y.* **2002**, *40* (12), 2177–2183.

(15) Wang, H.; Zhu, Q. L.; Zou, R.; Xu, Q. Metal-Organic Frameworks for Energy Applications. *Chem* **2017**, *2* (1), 52–80.

(16) Stock, N.; Biswas, S. Synthesis of Metal-Organic Frameworks (MOFs): Routes to Various MOF Topologies, Morphologies, and Composites. *Chem. Rev.* **2012**, *112* (2), 933–969.

(17) Stein, A.; Wang, Z.; Fierke, M. A. Functionalization of Porous Carbon Materials with Designed Pore Architecture. *Adv. Mater.* **2009**, *21* (3), 265–293.

(18) Xia, L.; Wu, X.; Wang, Y.; Niu, Z.; Liu, Q.; Li, T.; Shi, X.; Asiri, A. M.; Sun, X. S-Doped Carbon Nanospheres: An Efficient Electrocatalyst toward Artificial N2 Fixation to NH3. *Small Methods* **2019**, *3* (6), 2–6.

(19) Wu, T.; Li, X.; Zhu, X.; Mou, S.; Luo, Y.; Shi, X.; Asiri, A. M.; Zhang, Y.; Zheng, B.; Zhao, H.; Sun, X. P-Doped Graphene toward Enhanced Electrocatalytic N2 Reduction. *Chem. Commun.* **2020**, *56* (12), 1831–1834.

(20) Huang, H.; Xia, L.; Cao, R. R.; Niu, Z.; Chen, H.; Liu, Q.; Li, T.; Shi, X.; Asiri, A. M.; Sun, X. A Biomass-Derived Carbon-Based Electrocatalyst for Efficient N 2 Fixation to NH 3 under Ambient Conditions. *Chem. - A Eur. J.* **2019**, *25*

(8), 1914–1917.

(21) Guo, J.; Huo, J.; Liu, Y.; Wu, W.; Wang, Y.; Wu, M.; Liu, H.; Wang, G. Nitrogen-Doped Porous Carbon Supported Nonprecious Metal Single-Atom Electrocatalysts: From Synthesis to Application. *Small Methods* **2019**, *3* (9), 1–33.

(22) Schmidt, J.; Weber, J.; Epping, J. D.; Antonietti, M.; Thomas, A. Microporous Conjugated Poly(Thienylene Arylene) Networks. *Adv. Mater.* **2009**, *21* (6), 702–705.

(23) Paraknowitsch, J. P.; Thomas, A.; Schmidt, J. Microporous Sulfur-Doped Carbon from Thienyl-Based Polymer Network Precursors. *Chem. Commun.* **2011**, *47* (29), 8283–8285.

(24) Crockett, M. P.; Evans, A. M.; Worthington, M. J. H.; Albuquerque, I. S.; Slattery, A. D.; Gibson, C. T.; Campbell, J. A.; Lewis, D. A.; Bernardes, G. J. L.; Chalker, J. M. Sulfur-Limonene Polysulfide: A Material Synthesized Entirely from Industrial By-Products and Its Use in Removing Toxic Metals from Water and Soil. *Angew. Chemie Int. Ed.* **2016**, *55* (5), 1714–1718.

(25) Chung, W. J.; Griebel, J. J.; Kim, E. T.; Yoon, H.; Simmonds, A. G.; Ji, H. J.; Dirlam, P. T.; Glass, R. S.; Wie, J. J.; Nguyen, N. A.; Guralnick, B. W.; Park, J.; Somogyi, Á.; Theato, P.; Mackay, M. E.; Sung, Y.; Char, K.; Pyun, J. The Use of Elemental Sulfur as an Alternative Feedstock for Polymeric Materials. *Nat. Chem.* **2013**, *5* (6), 518–524.

(26) Worthington, M. J. H.; Kucera, R. L.; Chalker, J. M. Green Chemistry and Polymers Made from Sulfur. *Green Chem.* **2017**, *19* (12), 2748–2761.

(27) Anderson, L. E.; Kleine, T. S.; Zhang, Y.; Phan, D. D.; Namnabat, S.; LaVilla, E. A.; Konopka, K. M.; Ruiz Diaz, L.; Manchester, M. S.; Schwiegerling, J.; Glass, R. S.; Mackay, M. E.; Char, K.; Norwood, R. A.; Pyun, J. Chalcogenide Hybrid Inorganic/Organic Polymers: Ultrahigh Refractive Index Polymers for Infrared Imaging. *ACS Macro Lett.* **2017**, *6* (5), 500–504.

(28) Bear, J. C.; McGettrick, J. D.; Parkin, I. P.; Dunnill, C. W.; Hasell, T. Porous Carbons from Inverse Vulcanised Polymers. *Microporous Mesoporous Mater.*

2016, *232*, 189–195.

(29) WHO, W. H. O. Mercury in Drinking-Water, Background Document for Development of WHO Guidelines for Drinking-Water Quality. *WHO* **2005**, *WHO/SDE/WS*, WHO/SDE/WSH/05.08/10.

(30) Mann, M.; Luo, X.; Tikoalu, A.; Gibson, C. T.; Yin, Y.; Al-attabi, R.; Andersson, G. G.; Raston, C. L.; Henderson, L. C.; Pring, A.; Hasell, T.; Chalker, J. M. Carbonisation of a Polymer Made from Sulfur and Canola Oil. *Chem. Commun.* **2021**.

(31) Esdaile, L. J.; Chalker, J. M. The Mercury Problem in Artisanal and Small-Scale Gold Mining. *Chem. - A Eur. J.* **2018**, *24* (27), 6905–6916.

(32) Feng, L.; Cao, M.; Ma, X.; Zhu, Y.; Hu, C. Superparamagnetic High-Surface-Area Fe 3O 4 Nanoparticles as Adsorbents for Arsenic Removal. *J. Hazard. Mater.* **2012**, *217–218*, 439–446.

(33) Hao, W.; Björnerbäck, F.; Trushkina, Y.; Salazar-Alvarez, G.; Hedin, N.; Oregui Bengoechea, M.; Barth, T. High-Performance Magnetic Activated Carbon from Solid Waste from Lignin Conversion Processes. 1. Their Use As Adsorbents for CO2. *ACS Sustain. Chem. Eng.* **2017**, *5* (4), 3087–3095.

(34) Huang, L.; Shuai, Q. Facile Approach to Prepare Sulfur-Functionalized Magnetic Amide-Linked Organic Polymers for Enhanced Hg(II) Removal from Water. *ACS Sustain. Chem. Eng.* **2019**, *7* (Ii), 9957–9965.

(35) Park, H. S.; Koduru, J. R.; Choo, K. H.; Lee, B. Activated Carbons Impregnated with Iron Oxide Nanoparticles for Enhanced Removal of Bisphenol A and Natural Organic Matter. *J. Hazard. Mater.* **2015**, *286*, 315–324.

(36) Giakisikli, G.; Anthemidis, A. N. Magnetic Materials as Sorbents for Metal/Metalloid Preconcentration and/or Separation. A Review. *Analytica Chimica Acta*. July 30, 2013, pp 1–16.

(37) Huang, L.; Shen, R.; Liu, R.; Shuai, Q. Thiol-Functionalized Magnetic Covalent Organic Frameworks by a Cutting Strategy for Efficient Removal of Hg2+ from Water. *J. Hazard. Mater.* **2020**, *392* (December 2019), 122320.

(38) Parker, D. J.; Jones, H. A.; Petcher, S.; Cervini, L.; Griffin, J. M.; Akhtar, R.; Hasell, T. Low Cost and Renewable Sulfur-Polymers by Inverse Vulcanisation, and Their Potential for Mercury Capture. *J. Mater. Chem. A* **2017**, *5* (23), 11682–11692.

(39) Thommes, M.; Kaneko, K.; Neimark, A. V.; Olivier, J. P.; Rodriguez-Reinoso, F.; Rouquerol, J.; Sing, K. S. W. Physisorption of Gases, with Special Reference to the Evaluation of Surface Area and Pore Size Distribution (IUPAC Technical Report). *Pure Appl. Chem.* **2015**, *87* (9–10), 1051–1069.

(40) Wu, W.; Xiao, X. H.; Zhang, S. F.; Peng, T. C.; Zhou, J.; Ren, F.; Jiang, C. Z. Synthesis and Magnetic Properties of Maghemite (γ-Fe 2O 3) Short-Nanotubes. *Nanoscale Res. Lett.* **2010**, *5* (9), 1474–1479.

(41) Chen, Y. H. Thermal Properties of Nanocrystalline Goethite, Magnetite, and Maghemite. *J. Alloys Compd.* **2013**, *553*, 194–198.

(42) Perales Perez, O.; Umetsu, Y.; Sasaki, H. Precipitation and Densification of Magnetic Iron Compounds from Aqueous Solutions at Room Temperature. *Hydrometallurgy* **1998**, *50* (3), 223–242.

(43) WHO. *A Global Overview of National Regulations and Standards for Drinking-Water Quality*; 2018.

(44) Ke, F.; Qiu, L. G.; Yuan, Y. P.; Peng, F. M.; Jiang, X.; Xie, A. J.; Shen, Y. H.; Zhu, J. F. Thiol-Functionalization of Metal-Organic Framework by a Facile Coordination-Based Postsynthetic Strategy and Enhanced Removal of Hg 2+ from Water. *J. Hazard. Mater.* **2011**, *196*, 36–43.

(45) Limjuco, L. A.; Fissaha, H. T.; Kim, H.; Nisola, G. M.; Chung, W.-J. Sulfur Copolymerization with Hydrophilic Comonomers as Polysulfides in Microbeads for Highly Efficient Hg 2+ Removal from Wastewater . *ACS Appl. Polym. Mater.* **2020**.

(46) Limjuco, L. A.; Nisola, G. M.; Parohinog, K. J.; Valdehuesa, K. N. G.; Lee, S. P.; Kim, H.; Chung, W. J. Water-Insoluble Hydrophilic Polysulfides as Microfibrous Composites towards Highly Effective and Practical Hg2+ Capture. *Chem. Eng. J.* **2019**, *378* (June), 122216.

(47) Ravi, S.; Puthiaraj, P.; Row, K. H.; Park, D.-W.; Ahn, W.-S. Aminoethanethiol-Grafted Porous Organic Polymer for Hg 2+ Removal in Aqueous Solution. *Ind. Eng. Chem. Res.* **2017**, *56* (36), 10174–10182.

(48) Li, W.-T.; Zhuang, Y.-T.; Wang, J.-Y.; Yang, T.; Yu, Y.-L.; Chen, M.-L.; Wang, J.-H. A Three-Dimensional Porous Organic Framework for Highly Selective Capture of Mercury and Copper Ions. *ACS Appl. Polym. Mater.* **2019**, *1* (10), 2797–2806.

(49) Sun, Q.; Aguila, B.; Perman, J.; Earl, L. D.; Abney, C. W.; Cheng, Y.; Wei, H.; Nguyen, N.; Wojtas, L.; Ma, S. Postsynthetically Modified Covalent Organic Frameworks for Efficient and Effective Mercury Removal. *J. Am. Chem. Soc.* **2017**, *139* (7), 2786–2793.

(50) Afshari, M.; Dinari, M.; Zargoosh, K.; Moradi, H. Novel Triazine-Based Covalent Organic Framework as a Superadsorbent for the Removal of Mercury(II) from Aqueous Solutions. *Ind. Eng. Chem. Res.* **2020**, *59* (19), 9116–9126.

(51) Li, X.; Qi, Y.; Yue, G.; Wu, Q.; Li, Y.; Zhang, M.; Guo, X.; Li, X.; Ma, L.; Li, S. Solvent- and Catalyst-Free Synthesis of an Azine-Linked Covalent Organic Framework and the Induced Tautomerization in the Adsorption of U(vi) and Hg(Ii). *Green Chem.* **2019**, *21* (3), 649–657.

(52) Zhu, J.; Yang, J.; Deng, B. Enhanced Mercury Ion Adsorption by Amine-Modified Activated Carbon. *J. Hazard. Mater.* **2009**, *166* (2–3), 866–872.

(53) Bandaru, N. M.; Reta, N.; Dalal, H.; Ellis, A. V.; Shapter, J.; Voelcker, N. H. Enhanced Adsorption of Mercury Ions on Thiol Derivatized Single Wall Carbon Nanotubes. *J. Hazard. Mater.* **2013**, *261*, 534–541.

(54) Guo, X.; Du, B.; Wei, Q.; Yang, J.; Hu, L.; Yan, L.; Xu, W. Synthesis of Amino Functionalized Magnetic Graphenes Composite Material and Its Application to Remove Cr(VI), Pb(II), Hg(II), Cd(II) and Ni(II) from Contaminated Water. *J. Hazard. Mater.* **2014**, *278*, 211–220.

(55) Shin, Y.; Fryxell, G. E.; Um, W.; Parker, K.; Mattigod, S. V.; Skaggs, R. Sulfur-Functionalized Mesoporous Carbon. *Adv. Funct. Mater.* **2007**, *17* (15), 2897–

2901.

(56) Huang, L.; He, M.; Chen, B. B.; Cheng, Q.; Hu, B. Highly Efficient Magnetic Nitrogen-Doped Porous Carbon Prepared by One-Step Carbonization Strategy for Hg2+ Removal from Water. *ACS Appl. Mater. Interfaces* **2017**, *9* (3), 2550–2559.

(57) Zhang, J.; Chao, J.; Tang, Y.; Wan, P.; Yang, X. J.; Wong, C.; Bruce, M.; Hu, Q. Quantification of Trace Mercury in Water: Solving the Problem of Adsorption, Sample Preservation, and Cross-Contamination. *Glob. Challenges* **2020**, *4* (1), 1900061.

(58) Ratnaike, R. N. Acute and Chronic Arsenic Toxicity. *Postgrad. Med. J.* **2003**, *79* (933), 391–396.

(59) Siddiqui, S. I.; Chaudhry, S. A. Iron Oxide and Its Modified Forms as an Adsorbent for Arsenic Removal: A Comprehensive Recent Advancement. *Process Saf. Environ. Prot.* **2017**, *111*, 592–626.

Chapter 6. Conclusions

In the introductory chapter, the physical and chemical properties of elemental sulfur were showed first, followed by a novel conception, inverse vulcanisation, to synthesize high sulfur content polymers. The processing and applications of inverse vulcanisation were explained further. At last, basic background of porous materials was outlined, which will be used to discuss the project in later chapter.

In Chapter 2, a representative ternary system, consisting of elemental sulfur, DCPD, and EGDMA was studied for the delayed curing of inverse vulcanised polymers. It was found EGDMA react negligible at the initial stage, stabilising the oligomers in the pre-polymer, then it acted as plasticizer in curing stage, making the cured polymer homogeneously. It also found that pre-polymer could be stored at room temperature for more than one month with little change, which will provide a potential way for the industrial scale up of high sulfur content polymers.

In Chapter 3, a bio-derived crosslinker, garlic oil blend, was reacted with elemental sulfur via inverse vulcanisation to generate stable high sulfur content polymers. In order to increase the physical property of this polymer, DCPD was blend as co-monomer, resulting in a more rigid sulfur polymer, poly(S-DCPD-GOB), which can form a fine free flowing powder. Poly(S-DCPD-GOB) was demonstrated better performance than poly(S-DCPD) in mercury uptake. It could effectively remove mercury ion from a 2 ppm solution to negligible level by ICP-OES.

In first two chapters, an optimised processing and a new crosslinker were studied, however, after 9 years since inverse vulcanisation first time reported, it appeared several shortage of research novelties: the process of synthesis was only conducted by heating and the crosslinkers used in inverse vulcanisation were still focused on dienes. More synthesis methods, such as photo-initiation, microwave irradiation, and sonication, should be explored in the future. In terms of crosslinkers, alkynes were one of candidates in inverse vulcanisation, however, considering the higher bonding energy of the C≡C triple bonds, a proper catalyst was probably needed.

NaDTC was studied as catalyst in inverse vulcanisation in Chapter 4 initially. It was demonstrated that unreacted monomer, in conventional inverse vulcanisation, could

react with elemental sulfur with NaDTC as a catalyst, even at lower temperature, below the sulfur melting temperature. Compared with all reported low temperature inverse vulcanisation reaction, this novel approach was a one-step reaction, with no requirement to synthesize prepolymers. It was also found synthesized high sulfur content polymer could be reprocessed at low temperature because of dynamic covalent bond, showing a vitrimer like property. Catalysts should be a research focus in the future, because from the status quo, catalysts are the most promising way to decrease the reaction temperature and scale the reaction up. In the future work, binary catalysts would also be studied to increase the effectiveness of catalyst.

Magnetic sulfur-doped carbon composites, a derivative of inverse vulcanised polymer, were successfully synthesized. This magnetic sulfur-doped carbon kept the high surface area and porous structure from pristine sulfur-doped carbon, and exhibit magnetic property, which is convenient to be retrieved by external magnetic field. It was found this magnetic sulfur-doped carbon exhibiting high affinity to mercury ion from the solution. Especially, at low Hg concentration region, it captured take mercury steeply over conventional activated carbon. Because of functionalisation on the surface of this carbon, it also showed multifunction uptake capability in waste water, from which arsenic and lead could also be removed efficiently. Need to point out, derivatives of bulk inverse vulcanised polymer, not only sulfur-doped activated carbons but also coated particles, electrospun blend nanofibers, and polysulfide nanoparticles, may have more applications and better performance in the future because of relatively large surface area and more activity sites. Functionalisation of the inverse vulcanised polymer would be one of the future works in heavy metal uptake studies. Ideally, different functional groups could be attached on the inverse vulcanisation polymers so that more different heavy metals or precious metals could be captured selectively.

In summary, this thesis has described synthesis, new processing and application of inverse vulcanised polymers and derivative composites. These researches may help for the further study of this new material conception and the industrial scale up in the future.